MONASH University

Victorian brown coal char generation and reactivity for advanced utilisation technologies

Anthony William De Girolamo

BEng (Hons), BPharmSc

A thesis submitted for the degree of Doctor of Philosophy at

Monash University in 2017

Department of Chemical Engineering

Copyright notice

Table of Contents

Abstract

Brown coal is an abundant and low cost resource; however, it is currently almost exclusively used for power generation and power plants adjacent to the mine. This is due to its high moisture content and difficulty with handling. On the other hand, brown coal is a promising feedstock due to its low ash content and high reactivity. This thesis aims to investigate a process (pyrolysis) of upgrading the brown coal, alleviating these problems and creating an export-grade product. The product could replace bituminous coal currently used in applications such as energy generation and pulverised coal injection (PCI) in a blast furnace for iron generation. This is achieved by firstly considering the pyrolysis process for a briquette, and then evaluating the formed products.

To assist in the study of the pyrolysis process, a one-dimensional model was created of a brown coal briquette to evaluate the interaction between the intrinsic chemical and structural changes with the heat transfer and pressure distribution variations within the briquette. This modelling approach was coupled with an experimental investigation in a vertical fixed-bed furnace. Compared to smaller pulverised coal particles, it was found that pyrolysis of the larger briquette was limited by heat transfer, both by diffusion to the inner core, and from the evaporation of remaining moisture and the heat-absorbing nature of pyrolysis itself. Subsequently, the pyrolysis products were evaluated for their pyrolysis condition dependent properties. The increases in heating value with increased pyrolysis temperature and time were observed, which was eventually capable of generating a brown coal char product of similar heating value to coal that is commercially used in the PCI process. Further pyrolysis resulted in additional increases in the solid matrix density with lowered the reactivity of the char. However, the char samples nevertheless displayed greater reactivity compare to the PCI coal.

Two samples of industrially produced brown coal char were evaluated in further detail for their suitability to the PCI process, as a complete replacement for PCI coal and as a blend. Although only two products were received, the samples showed a range of properties dependent on their particle size. These size segregated groups were analysed in terms of meeting the requirements for a PCI fuel and their combustion performance in a drop tube furnace (DTF) that could replicate a similar environment to the injection point in a blast furnace. A relationship was established between volatile content burnout and minimum volatile content for the char was established. It was observed that specific size fractions of the brown coal char could meet the blast furnace requirements and even exceed the performance of PCI coal. A specific fraction of both chars was blended with the currently used PCI coal and the interactions were observed. In terms of ignition, a synergistic relationship between the two fuels was observed, increasing the fraction of fraction of brown coal char that could be blended beyond that which would be normally estimated based on the individual fuel properties.

Declaration

This thesis contains no material which has been accepted for the award of any other degree or diploma at any university or equivalent institution and that, to the best of my knowledge and belief, this thesis contains no material previously published or written by another person, except where due reference is made in the text of the thesis.

Signature: ADeGirolamo

Print Name: Anthony De Girolamo

Date: 28 Apr 2017

Publications during enrolment

De Girolamo, A., Grufas, A., Lyamin, I., Nishio, I., Ninomiya, Y., Zhang, L., Ignitability and combustibility of Yallourn pyrolysis char blended with PCI coal under simulated blast furnace conditions. *Energy & Fuels* **2015,** 30, (3), 1858-1868.

De Girolamo, A., Lameu, N. K., Zhang, L., Ninomiya, Y., Ignitability and combustibility of Yallourn pyrolysis char under simulated blast furnace conditions. *Fuel Processing Technology* **2017,** 156, 113-123.

Dai, B.Q., Low, F., De Girolamo, A., Wu, X., Zhang, L., Characteristics of ash deposits in a pulverized lignite coal-fired boiler and the mass flow of major ash-forming inorganic elements. *Energy & Fuels* **2013**.

Low, F., De Girolamo, A., Dai, B.Q., Zhang, L., Emission of Organically Bound Elements during the Pyrolysis and Char Oxidation of Lignites in Air and Oxyfuel Combustion Mode. *Energy & Fuels* **2014,** 28, (6), 4167-4176.

Dai, B. Q., Wu, X., De Girolamo, A., Cashion, J., Zhang, L., Inhibition of lignite ash slagging and fouling upon the use of a silica-based additive in an industrial pulverised coal-fired boiler: Part 2. Speciation of iron in ash deposits and separation of magnetite and ferrite. *Fuel* **2015,** 139, 733-745.

Low, F.; De Girolamo, A.; Wu, X.; Dai, B.; Zhang, L., Inhibition of lignite ash slagging and fouling upon the use of a silica-based additive in an industrial pulverised coal-fired boiler: Part 3–Partitioning of trace elements. *Fuel* **2015,** 139, 746-756.

Thesis including published works declaration

I hereby declare that this thesis contains no material which has been accepted for the award of any other degree or diploma at any university or equivalent institution and that, to the best of my knowledge and belief, this thesis contains no material previously published or written by another person, except where due reference is made in the text of the thesis.

This thesis includes two original papers published in peer reviewed journals and one submitted publications. The core theme of the thesis is low-rank coal upgrading and combustion. The ideas,

development and writing up of all the papers in the thesis were the principal responsibility of myself, the student, working within the Department of Chemical Engineering under the supervision of Lian Zhang.

The inclusion of co-authors reflects the fact that the work came from active collaboration between researchers and acknowledges input into team-based research

In the case of Chapters 4, 6 and 7, my contribution to the work involved the following:

Thesis Chapter	Publication Title	Status	Nature and % of student contribution	Co-author name(s) Nature and % of Co-author's contribution	Co-author(s), Monash student
4	Pyrolysis of Lignite Briquette – Experimental Investigation and 1-Dimensional Modelling Approach	Submitted	90% Concept, experimental work, writing	1) Vincent Tan, experimental work 5% 2) Zhenyu Liu, experimental work, paper revisions 5% 3) Lian Zhang, supervisor	Yes No No
6	Ignitability and combustibility of Yallourn pyrolysis char under simulated blast furnace conditions	Published	95% Concept, experimental work, writing	1) Natalia Lameu, experimental work 5% 2) Lian Zhang, supervisor 3) Yoshihiko Ninomiya, supervisor	No No No
7	Ignitability and Combustibility of Yallourn Pyrolysis Char Blended with Pulverized Coal Injection Coal	Published	85% Concept, experimental work, writing	1) Alexander Grufas, experimental work 5% 2) Ilia Lyamin, experimental work 5% 3) Iori Nishio, experimental work 5%	Yes Yes No No

	under Simulated Blast Furnace Conditions			4) Yoshihiko Ninomiya, supervisor 5) Lian Zhang, supervisor	No

I have renumbered sections of submitted or published papers in order to generate a consistent presentation within the thesis.

Student signature: ADeGirolamo **Date:** 28/04/17

The undersigned hereby certify that the above declaration correctly reflects the nature and extent of the student's and co-authors' contributions to this work. In instances where I am not the responsible author I have consulted with the responsible author to agree on the respective contributions of the authors.

Main Supervisor signature: x **Date:** 28/04/17

Acknowledgements

Firstly, I would like to express my gratitude to my supervisor, Lian Zhang for his continued support and encouragement throughout the length of my candidature. I would also like to thank my friends and colleagues in our research group, Bai Qian, Fiona, Iman, Janson, Jia, Jian, John, Miriam, Niken, Song, Tahereh, Teck Kwang, Vincent, and Wirhan.

Thank you to all the Chemical Engineering department staff, particularly Harry Bouwmeester, Jill Crisfield Kim Phu, Lilyanne Price, Paurnami Chandran, and Ross Ellingham.

For research funding and the top up scholarship I am grateful to Brown Coal Innovation Australia (BCIA). Australian Government are acknowledged for the Australian Postgraduate Award (APA) scholarship and Research Training Program (RTP). For additional research funding, thank you to the Australian Research Council (ARC) and Coal Energy Australia (CEA).

This research was supported in part by the Monash eResearch Centre and eSolutions-Research Support Services through the use of the Monash Campus HPC Cluster.

Finally, thank you to my family for their continuous motivation. Michelle, thank you for your understanding and patience and staying by my side through these difficult times.

List of Figures

Chapter 1

Chapter 2

Chapter 3

Chapter 4

Chapter 5

Chapter 6

Chapter 7

Chapter 8

List of Tables

Chapter 2

Chapter 3

Chapter 4

Chapter 5

Chapter 6

Chapter 7

Chapter 8

This page is intentionally left blank

Chapter 1 – Introduction

This page is intentionally left blank

1.1 Overview

Low-rank coal is an abundant resource, which is projected to last until the year 2100 at current growth rates [1]. Compared to higher-rank coals, it is characterised by having a high moisture content and a low heating value [2]. Consequently, it is used almost exclusively for power generation at adjacent power plants [3], owing to the cost of transport and spontaneous combustion risk. In its crude form, it combusts relatively inefficiently and has the highest greenhouse gas emissions per unit of electricity produced of common sources [4]. Low-rank coals are inexpensive, owing to their low cost of extraction [5]. This cost difference, as well as a secure feedstock supply presents an opportunity to more effectively utilise low-rank coal by upgrading through a pyrolysis process that will produce a beneficiated solid product, char, as well as value-added gas and liquid tar products.

In this PhD project, we have for the first time examined the plausibility of using a brown coal char product for advanced applications including pulverised coal injection (PCI), and discover the influence of the conditions under which the coal is pyrolysed. Such a research target is different from previous pyrolysis-related studies which have mainly focused on the production of liquid tar and fuel from pyrolysis, whereas the solid char has been rarely examined for its properties and utilisation in a value-added manner such as the PCI process in a blast furnace. The primary goal of this PhD research project is to optimise the pyrolysis conditions for Victorian brown coal so as to produce a final char product that will possess a high energy density, as well as can be handled and transported economically. In particular, the pyrolysis of Victorian brown coal in briquette form has been examined extensively. To the best knowledge of the author, this has yet to be addressed in the literature. Moreover, this research project aims to clarify the ignition and reactivity (including C-O_2, C-CO_2 and C-H_2O) of the brown coal char as well as to optimise the combustion conditions for an efficient burnout under the typical combustion conditions encountered in both blast furnaces and coal-fired power plants. The heterogeneous properties and reactivity of brown coal char has been examined for the first time. The key hypothesis for this study is that, a high-energy density char could be produced by prior palletisation of brown coal, and the low-volatile brown coal char could burn efficiently and even more rapidly than bituminous coal. Our study is expected to provide feedback to the engineering design of the brown coal pyrolyser and utilisation of the resultant char in blast furnaces and coal-fired power plants. In addition, the results from this study are expected to

shed new insights on the understanding of the science underpinning the pyrolysis and combustion of Victorian brown coal char.

It has been well known that the pyrolysis process will increase the value of the brown coal by increasing its energy density and transportability. However, eliminating part of the volatile matter and heat treatment of the coal is expected to lower combustion performance by decreasing oxidation reactivity [6]. Therefore, it is critical to find an optimum volatile content in the final char as well as to optimise the pyrolysis conditions. The pyrolysis process will induce both physical and chemical changes during the conversion to char [7]. Changes include the spread of pores throughout the coal and the subsequent change in surface area caused by this. The conditions under which the char is created, including temperature and heating rate, will have an impact on the final char product [8-12]. Particle size will also have an impact due to the slower heat transfer to within the particle.

Pulverised coal injection (PCI) technology involves directly injecting coal into the blast furnace, increasing productivity, and replacing a part of coke that is used for the process of making iron [13]. PCI coal has strict requirements in terms of ash content and composition, volatile content, moisture content and grindability [14]. To date, high-rank bituminous coal with low volatile content and anthracite are the only source for PCI fuel, which have diminishing reserves. The application of low-rank brown coal char as a PCI fuel to blend with other coals has yet to be tested. Since the PCI coal has a much higher market price than the power generation coal, it is critical to clarify the applicability of brown coal char as a PCI fuel in the blast furnace. Understanding this is also essential to optimise the coal pyrolysis conditions.

1.2 Research aims

The overall aim of this research is to understand whether Victorian brown coal can be upgraded to a fuel that can satisfy the needs of advanced applications such as PCI combustion in the blast furnace. Several key areas need to be examined individually to fully satisfy this work's hypothesis. Firstly, the method of upgrading needs to be established and understood. Secondly, the upgraded product needs to be evaluated by means of testing against industry standards and by analysing combustion performance. A realistic method of introducing a solid fuel product into a market is by blending with the existing fuel, therefore the interactions with a higher rank coal should be known. Lastly, it is of interest to recognize how the differences in the altered combustion environment compared to regular coal combustion will interplay with the decreased coal rank compared to the conventionally used bituminous coal.

In order to achieve this overall goal, the following specific objectives will be investigated:

1. To understand the brown coal pyrolysis mechanism for a larger scale briquette including heat transfer and structural changes through lab-scale experiments and a 1-D modelling approach.

2. To optimise the pyrolysis conditions for Victorian brown coal to produce a final char product that will possess a raised energy density, as well as can be handled and transported economically.

3. To examine the potential for Yallourn brown coal char to be used as a pulverized coal injection (PCI) fuel, its size-dependent properties, ignitability and combustibility under the simulated conditions of the blowpipe-tuyere section in a blast furnace.

4. To clarify both ignition and burnout rate for coal–char blends, which are critical for the combustion of PCI coal in the tuyere/blowpipe of a blast furnace.

5. To clarify the ignition and reactivity (including $C\text{-}O_2$, $C\text{-}CO_2$ and $C\text{-}H_2O$) of the brown coal char during conditions that prevail during PCI coal combustion.

1.3 Thesis outline

Chapter 1 gives an overview of the thesis, highlights the research aims and presents the outline.

Chapter 2 reviews the current state of knowledge for pyrolysis of brown coal and the application of upgraded brown coal to advanced applications.

Chapter 3 is a summary of the experimental facilities, modelling approaches and sample characterisation methods used in this thesis.

Chapter 4 explores the mechanism for the pyrolysis process of a lignite briquette. A 1-D model is created for the process and the predicted structural changes and tar emissions are explored and compared to the experimental results.

Chapter 5 compares the Yallourn coal pyrolysis products created under different conditions and their predicted combustion performance.

Chapter 6 examines the possibility of using Yallourn char as a replacement fuel for PCI coal in terms of required properties and combustion performance.

Chapter 7 evaluates the combustion performance of six different blending ratios with two industrially created Yallourn chars.

Chapter 8 analyses the combustion of brown coal char under conditions where high CO_2 or H_2O conditions are prevalent.

Chapter 9 gives the conclusions for this PhD project and makes future recommendations related to the utilisation of upgraded brown coal and understanding of the upgrading process.

Figure 1.1 shows a representation of the interaction of the different components of the thesis. Chapters 4 and 5 concentrate on the generation of the brown coal char. Chapter 6 uses char produced in an industrial scale shaft furnace in a PCI combustion scenario. This concept is extended in Chapter 7 when PCI coal is blended. Chapter 8 evaluates the brown coal reactivity in combustion reactivity in high CO_2/H_2O environments.

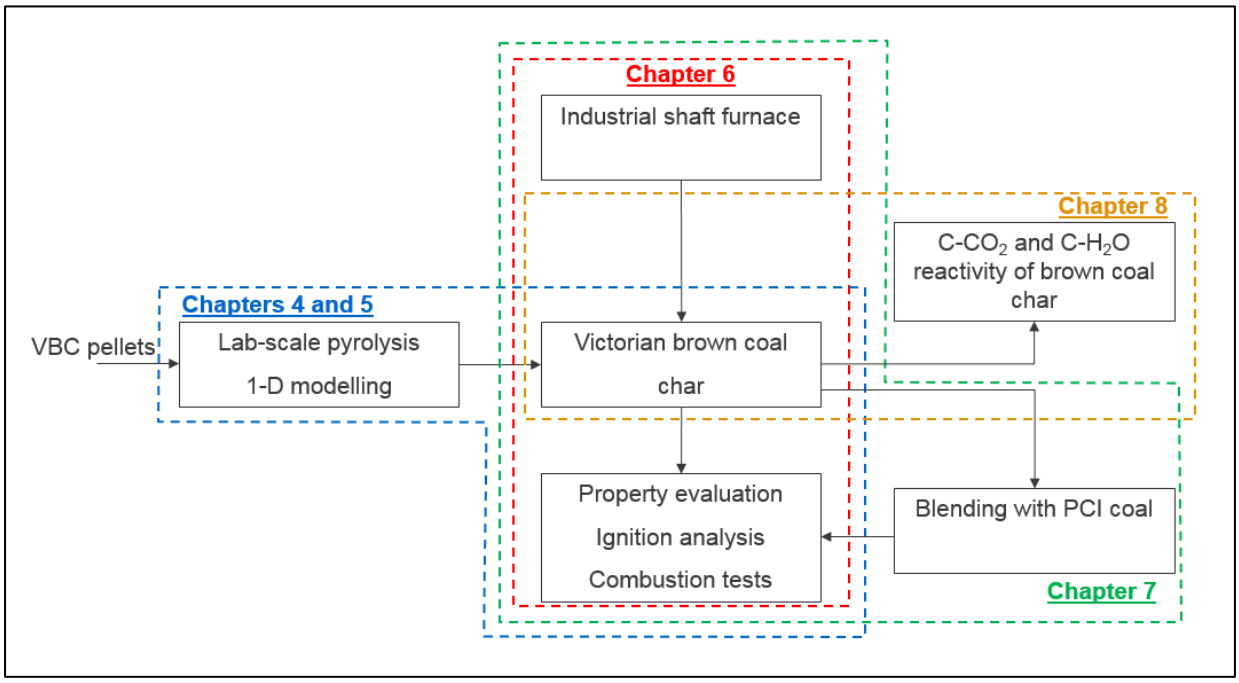

Figure 1.1 Thesis outline summary

References

1. Thielemann, T.; Schmidt, S.; Peter Gerling, J., Lignite and hard coal: Energy suppliers for world needs until the year 2100 — An outlook. *International Journal of Coal Geology* **2007,** 72, (1), 1-14.
2. Durie, R. A., *The Science of Victorian brown coal : structure, properties, and consequences for utilization*. Butterworth-Heinemann: Oxford, 1991; p xvi, 750 p.
3. Traa, Y., Is a renaissance of coal imminent?—challenges for catalysis. *Chemical Communications* **2010,** 46, (13), 2175-2187.
4. Weisser, D., A guide to life-cycle greenhouse gas (GHG) emissions from electric supply technologies. *Energy* **2007,** 32, (9), 1543-1559.
5. Mills, S. J., Global perspective on the use of low quality coals. *IEA Clean Coal Centre* **2011**.
6. Chan, M. L.; Jones, J. M.; Pourkashanian, M.; Williams, A., The oxidative reactivity of coal chars in relation to their structure. *Fuel* **1999,** 78, (13), 1539-1552.
7. Tillman, D., *The Combustion of Solid Fuels and Wastes*. Elsevier Science: 2012.
8. Wang, Q.; Zhang, R.; Luo, Z.; Fang, M.; Cen, K., Effects of Pyrolysis Atmosphere and Temperature on Coal Char Characteristics and Gasification Reactivity. *Energy Technology* **2016,** 4, (4), 543-550.
9. Park, S.-W.; Jang, C.-H., Effects of pyrolysis temperature on changes in fuel characteristics of biomass char. *Energy* **2012,** 39, (1), 187-195.
10. Cai, H. Y.; Güell, A. J.; Chatzakis, I. N.; Lim, J. Y.; Dugwell, D. R.; Kandiyoti, R., Combustion reactivity and morphological change in coal chars: Effect of pyrolysis temperature, heating rate and pressure. *Fuel* **1996,** 75, (1), 15-24.
11. Gale, T. K.; Bartholomew, C. H.; Fletcher, T. H., Effects of Pyrolysis Heating Rate on Intrinsic Reactivities of Coal Chars. *Energy & Fuels* **1996,** 10, (3), 766-775.
12. Cetin, E.; Moghtaderi, B.; Gupta, R.; Wall, T. F., Influence of pyrolysis conditions on the structure and gasification reactivity of biomass chars. *Fuel* **2004,** 83, (16), 2139-2150.
13. Carpenter, A. M., *Use of PCI in blast furnaces*. IEA Clean Coal Centre: 2006.
14. Chinese Standards, Specifications of coal used in pulverized coal injection (PCI). In 2008; Vol. GB/T 18512-2008.

This page is intentionally left blank

Chapter 2 – Literature review

This page is intentionally left blank

Scope of literature review

This literature review covers the motivation for upgrading low-rank coal, specifically via pyrolysis to form a high value product that can subsequently be used in advanced applications. It will be discussed how this method has been used and how the process can be modelled. Next, pulverised coal injection (PCI) is discussed and its potential to be used with an upgraded brown coal fuel.

2.1 Brown coal upgrading

2.1.1 Motive for upgrading

While brown coal (also known as lignite) is abundant and is relatively simple to extract in open-cut mines close to the surface, it contains a more than 60% moisture [1], leading to a very low heating value compared to higher rank coals. Oxygen content is also very high [2], meaning energy containing compounds rich in carbon are lower. On top of this, brown coal is vulnerable to spontaneous combustion, especially when moisture is low [3]. This makes safe transport and storage difficult. Consequently, brown coal use is typically limited to power generation at power plants adjacent to the mine. In Victoria, Australia, power generation accounts for 95% of brown coal consumed and brown coal supplies 85% of the state's electricity [4].

If these problems could be rectified, other potential uses of brown coal include gasification, liquefaction, and combustion in a blast furnace for steel production and in applications where black coal is currently used such as PCI. Table 2.1 compares some properties of brown coal and black coal. The first noticeable difference is the price. Victorian brown coal is as low as AU$ 2-7. Since brown coal is relatively younger than black coal it can be found closer to the surface making extraction cheaper. The black coal price is more than an order of magnitude higher, beginning at AU $110 and will depend on the quality of the coal including ash and sulphur concentration [5]. Coals that can be used for pulverised coal injection (PCI) can reach AU$ 230 [5]. Unlike black coal, there is not a free market for brown coal to be traded since it is uneconomic and difficult to transport, therefore is primarily used at an adjacent power plant. One of the reasons the transport is uneconomical is the high moisture content, up to 70% compared to black coal which has around 10% moisture. This will significantly lower its heating value. Additionally, dried Victorian brown coal has a high propensity to spontaneous combustion [6]. Density is also lower which means there will be a lower energy per unit volume.

Some advantages of Victorian brown coal are the relatively lower ash content and high reactivity [7].

Table 2.1 Comparison of Victorian brown coal with bituminous coals found in Australia

Property	Victorian brown coal (lignite)	Australian bituminous coals
Cost per tonne ($ AUD)	AU$ 2-7 [8]	AU$ 110-230 [5]
Moisture content *ar*	48-70% [9]	3.5-10% [10, 11]
Volatile matter content *db*	48.4-62.7% [12]	11-36.2% [10, 11, 13]
Ash content *db*	0.6-4.4% [12]	8-20% [10, 11]
Energy value (net wet)	5.8 to 11.5 MJ/kg [9]	22-29 MJ/kg [10, 11]
Energy value (gross dry)	25-29 MJ/kg [9]	28-32 MJ/kg [10, 11]
Sulphur content	<1% [9]	0.5-0.7% [10, 11]
Mining method	Open Cut	Open Cut & Underground
Bulk density	650-670 kg/m^3 [14]	770-930 kg/m^3 [14]

Based on the above analysis, it is evident that there is a significant opportunity for upgrading brown coal based on the cost difference and lack of current brown coal utilisation. If the cost of upgrading was lower than this price difference than it would be financially viable. Several methods have a large potential to raise the brown coal properties such as density, moisture and energy to a similar value to bituminous coal. Two of these methods that will be examined in more detail are briquetting and pyrolysis.

2.1.2 Methods of upgrading

2.1.2.1 Briquetting

Brown coal can be made into a briquette without the use of a binder through the assistance of oxygen containing functional groups and the remaining moisture. The briquettes have the advantage of reduced dust during transport and handling. The compression during briquetting will increase the volumetric energy density. Briquetting/pelletising lignite will create a low moisture product that is stable during transportation and storage [15]. In recent years, a brown coal drying and pelleting method has been utilised that increases density and removes moisture down to around 12% while also eliminating spontaneous combustion potential using a low temperature (60 °C) and a low pressure process [16]. Pelletised lignite could be further upgraded

into char for chemical production or power generation, while other products such as tar, pyrolysis oil and coal gas. Since the particle size distribution of char will be dependent on the size of the parent coal, pyrolysis of larger particle sizes including pellets is of interest to generate a product that is more suitable for transport. A particle as large as 1 *mm* will minimise the likelihood of becoming airborne. In addition, pelletised coal will have a higher density that could produce a char with a higher volumetric energy density. Briquetting could reduce the potential for spontaneous combustion since self-heating is reduced with increased particle size [17, 18].

2.1.2.2 Pyrolysis

2.1.2.2.1 Pyrolysis Overview

Compared to others methods, pyrolysis requires higher temperatures (>500 °C) and an oxygen free environment. The product, char will by dry and have a higher energy density due to the removal of volatile compounds, especially oxygen containing compounds. The propensity to spontaneously combust is largely removed. Much of the mass is lost, although it can be recovered as tar or coal gas.

Pyrolysis is a chemical degradation reaction caused by heat alone [19]. When describing the pyrolysis of carbonous compounds it may also be referred to as 'devolatilisation', i.e. the removal of volatile components from a material. Although pyrolysis occurs in the absence of oxygen, it is a principle step in the combustion process, after drying. The products of pyrolysis include the original solid mass which will become char while vapours generated may be condensable, known as tar or light gasses that are usually flammable. In the absence of oxygen, these products can be recovered.

Changes include the spread of pores throughout the coal and the subsequent change in surface area caused by this. Chemical processes include breaking of weaker bonds (-C-C- and -C-O-), resulting in formation of gasses that are released from the particle including methane, H_2O, CO, CO_2 and tar. Additional pyrolysis results in further evolution of gases as well as repolymerisation (cross-linking) of the char matrix. Compared to higher rank coals, lignite shows cross-linking behaviour at lower temperatures (~500 °C) [20].

2.1.2.2.2 The pyrolysis process in industry

Possible pyrolysis feedstocks include low-rank coal, biomass, waste tyres, refuse, and sewage sludge [21]. One of the earliest and most popular processes in industry for pyrolysis is the vertical shaft furnace [22]. The feedstock enters the side of the furnace near the top. The heat for pyrolysis can either be provided by direct or indirect heating. Possible sources of heat include combustion of natural gas or coal gas derived from the pyrolysis process. The hot gas providing heat to the process will usually flow counter-current to the feedstock. In the indirect heating mode, heat is transferred from the wall while in direct heating mode the hot gas will pass through the feedstock. Indirect heating will provide a higher calorific coal gas since flue gasses from the combustion process will not be mixed with the coal gas. An alternative method of direct heating is supply only oxygen or air will react with a portion of the char that is formed. Using oxygen will provide a higher heating value coal gas due to the absence of nitrogen.

2.1.2.2.3 Upgrading of brown coal via pyrolysis

Compared to biomass pyrolysis, there is a significant lack of resources concerning the upgrading of low-rank coals through pyrolysis. However, with recent commercial interest in upgrading of brown coal, and government investment in Victoria, through the Advanced Lignite Demonstration Program (ALDP) [23], there is much need for research and development of this technology before commercial deployment. Chu et al. studied the pyrolysis of lignite briquettes from Inner Mongolia, China at 450-900 °C in a fixed-bed reactor with a heating rate of 10-15 °C/min and measured the properties of the solid, liquid and gaseous products [24]. They found that with increased temperature during pyrolysis, both the briquette's falling strength and compressive strength were increased. The oxygen content in the char fell was reduced quickly and disappeared once 650 °C was reached. At 550 °C, the yield of tar was maximised, while gas yield kept increasing with temperature. Another study focused on upgrading of North Dakota lignite through rapid and slow pyrolysis where it is held for different residence times [25]. Their research showed a decrease in char reactivity in air with increased residence time, although a direct comparison between fast and slow heating at the same residence time was not made. It was also discovered that calcium was the dominant species in catalysis of the conversion process. Quyn et al. also examined the reactivity of a Victorian brown coal under pyrolysis at different temperatures made with a fluidised-bed/fixed-bed reactor [26]. The reactivity of the char in air increased in the range of 500-700 °C while decreasing at temperatures above this. The authors concluded that this was due to the changes in the relative

distribution of Na in the char matrix and pore surface. Rather than analysing char product reactivity, Suuberg et al. focused on char product composition at different heating rates, residence times and peak temperatures in a batch reactor [27]. Oxygen in the char product was reduced remarkably, particularly in the range of 650-700 °C and was eliminated at 1100 °C. Sulphur was had a linear reduction in concentration compared to peak temperature and carbon and nitrogen were mostly retained in the char. This reduction or elimination of oxygen is well correlated with an increase in heating value of the char [28].

Although the product properties have been studied, to date, the brown coal pyrolysis process has not been studied with the objective of producing a fuel for the PCI process. In contrast, the application of a previous study's results on Norway Spruce [29] to a blast furnace injection study was performed [30]. In the original study, pyrolysis temperature was varied between 150 – 800 °C and reported the increasing energy content with temperature as well as the changes in ultimate analysis properties and solid product yield. A partial pyrolysis at 250 °C was found to be optimal in decreasing the coke rate.

2.1.2.2.4 Modelling pyrolysis

A variety of models have been developed to describe the pyrolysis process and each is designed with a different end-use in mind. Table 2.2 shows a comparison of a selection of models. In the most simple of models, pyrolysis is modelled as a first-order decomposition reaction, with the kinetic rate is controlled by an Arrhenius expression (Equation 2.1 and Equation 2.2) [31].

$$\frac{dV}{dt} = k * (V^* - V) \qquad \text{Equation 2.1}$$

$$k = A \times e^{-E/RT} \qquad \text{Equation 2.2}$$

Where V* is the limit of V, typically the value determined by the proximate analysis or experimentally. At high temperatures or heating rates, the volatile yield can be 1.3 to 1.8 times higher than that predicted by the proximate analysis [31].

This approach is most commonly used in combustion models where it shows a satisfactory agreement with results and is not computationally expensive [32]. Due to the relatively short time for devolatilisation (0.14-0.16 s) compared to char burnout (0.7-0.85 s) [4], the results may not

be sensitive to the devolatilisation kinetics during combustion modelling. It has been reported that using a different heating rate for the same coal can result in a grossly different Arrhenius plot (Figure 2.1) [33]. This is because coal is not a homogenous entity and in fact would be better characterized by multiple first order reactions. Such a model exists and is known as the distributed activation energy model (DAEM) where the coal devolatilisation process is represented by an infinite set of first-order reactions where the activation energy is modelled by a distribution function [34]. Typically, the activation energy distribution is generally assumed to be a Gaussian distribution, while the pre-exponential factor is either a fixed value or a function of the activation energy. One of the main drawbacks of these types of models is that the volatile yield must be pre-determined and will not be affected by heating rate or temperature. Furthermore, these models do not consider the thermal history of the coal, e.g. a coal with devolatilisation 50% complete that is produced at 600 °C will be identical one produced at 800 °C. It should be expected that parts of the coal with different activation energies would be consumed in different proportions to each other at different temperatures. This is conflicting with the notion that DAEM is representing multiple first-order reactions. Instead, DAEM has the advantage of more accurately representing the devolatilisation compared to the first-order model for a diverse range of linear heating rates.

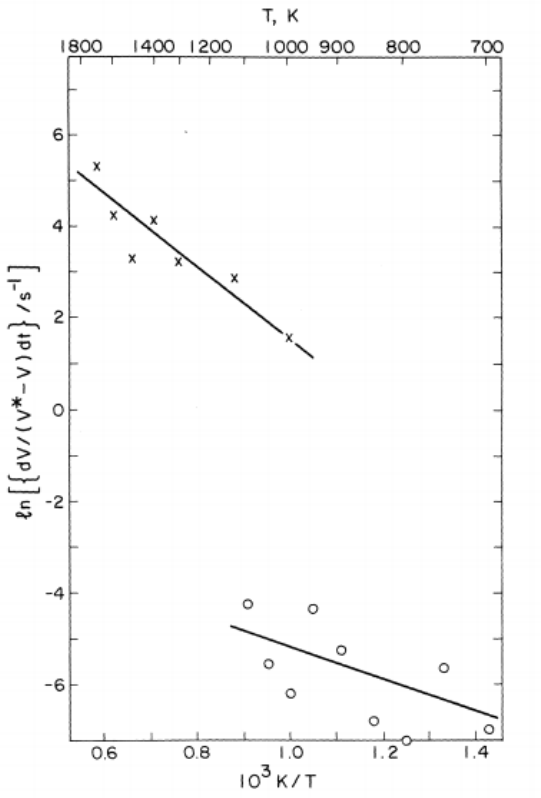

Figure 2.1 Arrhenius Plot of Global First-Order Single-Reaction Rate Coefficient for Devolatilization of a Given Coal. Heating rate: (x) 10^4 K/s; (o) 1 K/s. [33]

In reality, coal will be subjected to non-linear heating rates. During air-firing or oxy-firing pulverised coal combustion, a particle temperature/time graph has been shown to be somewhat sigmoidal in shape [32], while during pyrolysis of a wood slab the particle temperature/time graph with increasing temperature can be concave up or concave down depending on the location within the slab [35]. An early attempt at accounting for non-linear heating rates was made by Anthony et al. in 1975 by implementation of a secondary reaction system to describe repolymerisation and char forming reactions [36]. Through this mechanism it was possible to explain the increased volatile yield at higher heating rates, smaller particle sizes, and low pressures. This concept was expanded for the treatment of biomass pyrolysis by Koufopanos et al whereby the pyrolysis is described by a system of first-order reactions [37]. The virgin material will initially be converted to an intermediate in a reaction that is not associated with any mass loss. Following this, the intermediate material can either form gasses and volatiles in one reaction are char in a separate reaction. Miller and Bellan point out that the char formation must be accompanied by the simultaneous release of gas [38]. Therefore, instead of the

intermediate material forming char and gas separately, one reaction will describe the concurrent gas and char formation (at a fixed gas/char ratio) while a separate reaction describes formation of tar. An additional reaction will describe the vaporisation of this tar. This system is shown in Figure 2.2.

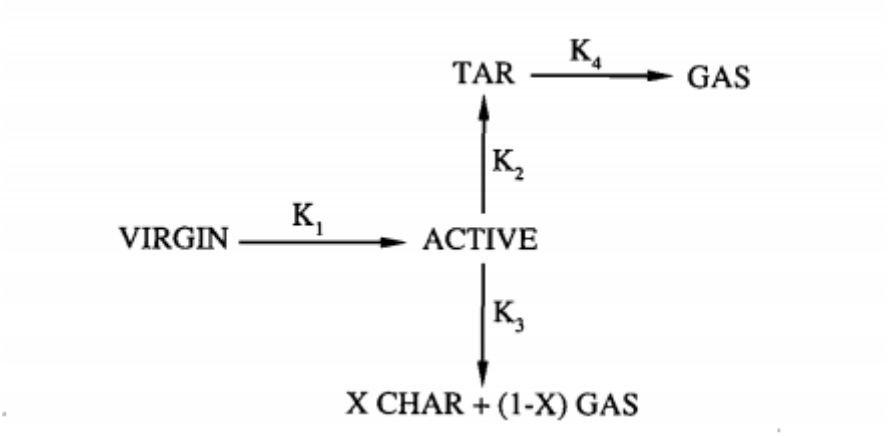

Figure 2.2 General reaction scheme used to model cellulose, hemicellulose and lignin kinetics [38].

With the more recent advances in understanding of coal structure, in the 1980s, several models were presented that consider the changes in coal structure. These are known as chemical percolation devolatilisation (CPD) [39], FG-FVC [40], and FLASHCHAIN [41]. These models consider bond breaking reactions, evaporation of low molecular weight compounds, and repolymerisation of the metaplast with the char matrix. By knowing the properties of the raw coal through ^{13}C, NMR experiments, through these models it is possible to predict the yield of char, tar and gasses, as well as formation of the metaplast and some properties of the tar and gasses. The CPD model, which shows high promise for use in this work due to its code availability and wide implementation, including integration into CFD software Ansys Fluent [42].

Table 2.2 Summary of commonly used pyrolysis models

Name	Summary	Products	Computational expense
Single rate kinetic model [31]	Devolatilization is first-order, dependent on the fraction of volatiles remaining in the particle.	Char, gas	Very low
Distributed activation energy model (DAEM) [34]	Reactions are an infinite set of irreversible first-order reactions and activation energy is a distribution function.	Char, gas	Low
First-order pathway model [37, 38]	The pyrolysis feedstock forms char, tar, gas by number of possible pathways	Char, tar, gas	Medium
Structure based network models [39-41]	Chemical percolation devolatilisation (CPD), FG-FVC and FLASHCHAIN methods include depolymerisation, light gas formation, cross-linking, and tar vaporisation.	Char, tar gas	High

Grant et al. proposed the CPD model in 1989 which uses percolation theory and a three-dimensional Bethe lattice [43]. The model was later further improved to include vapour-liquid equilibrium and a cross-linking mechanism [39]. Figure 2.3 shows the reaction sequence of the CPD model. Two types of bridges exist between aromatic clusters, known as labile bridges and char bridges (c). Bridges initially present as labile bridges, $\mathcal{L}$, will decompose to form an active intermediate $\mathcal{L}$*. This intermediate bridge is unstable so will react immediately via one of two competitive reactions. In the first, the labile bond is cleaved and two side chains are formed, δ. This can then undergo a cracking reaction to form a light gas g_1. In the second reaction, the reactive labile bond will form a stable char bridge with the concurrent formation of a light gas g_2. The rate of labile bridge breaking, k_b, and rate of gas release from side chains, k_g are both determined by Arrhenius expressions whereby the activation energy is given a standard deviation. The ratio of bridge breaking to char bridge formation (k_δ/k_c) is fixed at 0.9 based on experimental data.

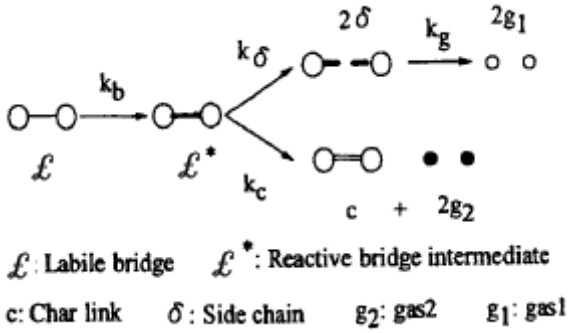

Figure 2.3 Reaction sequence for the CPD model [39].

As bridges are cleaved, clusters are completely detached from the lattice network, and form tar precursor fragments, also known as the metaplast. Depending on the temperature, pressure and molecular weight of the metaplast it may be vaporised by means of a flash vaporization scheme which uses vapour/liquid phase equilibration. Lower molecular weight compounds such as benzene and naphthalene will have a higher vapour pressure and are more readily vaporised. Higher molecular weight compound's vapour pressure is predicted based on a simple form of Raoult's Law. A simple cross-linking mechanism was implemented into the model which describes the repolymerisation of the metaplast with the coal matrix and is based on a first-order Arrhenius expression.

The input for the CPD model relies on four chemical structure parameters determined by ^{13}C NMR and one empirically determined parameter. Besides these five parameters, other parameters used in the data such as the vapour pressure correlation, and rates of gas formation, labile bridge breaking, cross-linking, should theoretically be independent of coal type. The four parameters determined by NMR measurements are: $\sigma+1$ - the coordination number which is the total number of attachments per cluster; p_0 - the initial fraction of intact bridges which are made up of the previously mentioned labile and char bridges; M_{clust} – the molecular weight of each cluster; and m_δ – the average molecular weight of a side chain. The empirically determined parameter is c_0, the initial fraction of char bridges and is determined by comparing char yields with predictions. Genetti showed that it may be possible to determine these parameters without the use of ^{13}C NMR, by relying on a correlation with the elemental composition and volatile matter content [44].

While it was previously mentioned that other parameters within the model are independent of coal type, several researchers have found that these parameters could be modified to better fit experimental data. Yan et al. found that the CPD model was overestimating the release of volatile matter from Chinese bituminous coal compared to TGA experiments [45]. This difference was negated by modification of the kinetic parameters for both labile bridge breaking and gas formation from side chains. The fitted parameters showed a better agreement with TGA experiments and better predicted the total yield of light gasses for a range of different coals compared to the original CPD model. Similarly Fletcher et al. was able to model the pyrolysis of biomass [46], black liquor [47], and oil shale [48] by modification of internal parameters within the CPD model.

2.2 Advanced utilisation technologies

2.2.1 Pulverised coal injection (PCI)

2.2.1.1 Operation

The majority of iron ore is converted into iron through smelting in a blast furnace. The main raw materials fed into the blast furnace are iron oxides (mostly hematite and magnetite), a carbon source (metallurgical coke) and flux (limestone), as well as hot blast air. Though oxidation of the carbon source by the air, carbon monoxide is produced (Equation 2.3).

$$C + \frac{1}{2}O_2 \rightarrow CO \qquad \text{Equation 2.3}$$

An alternative mechanism is also available, represented by Equation 2.4 and Equation 2.5.

$$C + O_2 \rightarrow CO_2 \qquad \text{Equation 2.4}$$

$$C + CO_2 \rightarrow 2CO \qquad \text{Equation 2.5}$$

Carbon monoxide is a reducing agent that can reduce iron oxide into iron metal (Equation 2.6).

$$Fe_2O_3 + 3CO \rightarrow 2Fe + 3CO_2 \qquad \text{Equation 2.6}$$

The interior of the blast furnace is filled with alternating layers of coke and iron ore. The product of the blast furnace is known as pig iron, which can be subsequently refined to produce steel. Another method of iron production is direct reduction, however less than 5% of iron is produced this way.

An improvement to this process is known as pulverised coal injection (PCI) which provides numerous benefits over the traditional blast furnace operation. This method involves injecting pulverised coal through a lance into a stream of pre-heated air in the tuyere that enters towards the bottom of the furnace. The PCI coal can replace a portion of the coke. Figure 2.4 shows a diagram of the PCI process. A lance is used to inject coal into a stream of hot pre-heated air. The stream can also be enriched with oxygen i.e. the oxygen concentration may be above 21%, but will not contain excess oxygen. Since the heated blast air is heated from 1000 °C to 1200 °C, the coal will react in a very short residence time in the raceway region.

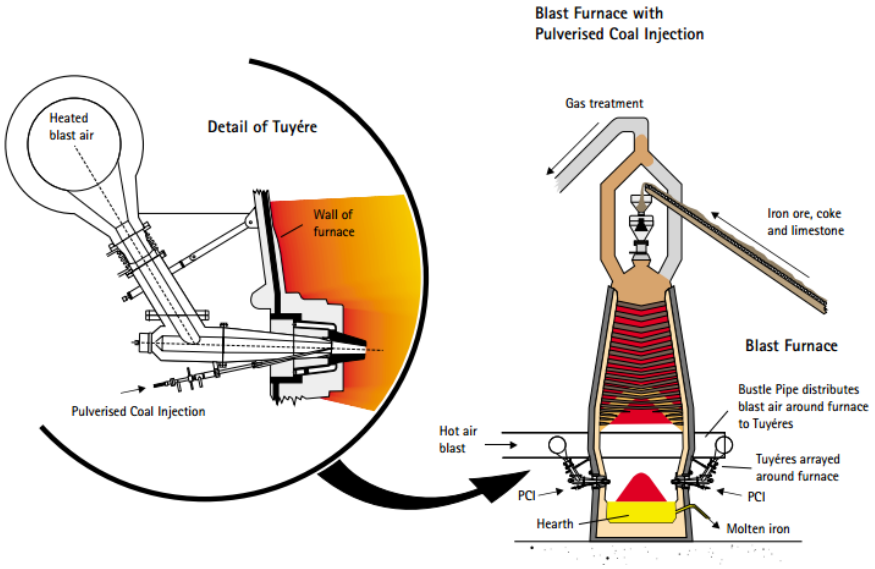

Figure 2.4 Diagram of pulverised coal injection (PCI) process. [49]

Besides providing heat for the furnace, the use of PCI also contributes towards the reducing of the iron oxide through the reactions in Equations 2.1-2.4. Additionally, steam produced by evaporation of moisture or by oxidation of hydrogen in the PCI coal may also assist in the production of carbon monoxide through the steam gasification reaction (Equation 2.7). Figure 2.5 provides an overview of the changing gas conditions in the raceway and subsequent changes in the coal reactions.

$$C + H_2O \rightarrow CO + H_2$$ Equation 2.7

The benefits of PCI technology include:

- Lower coke consumption rate
- Higher productivity
- Reduced emissions

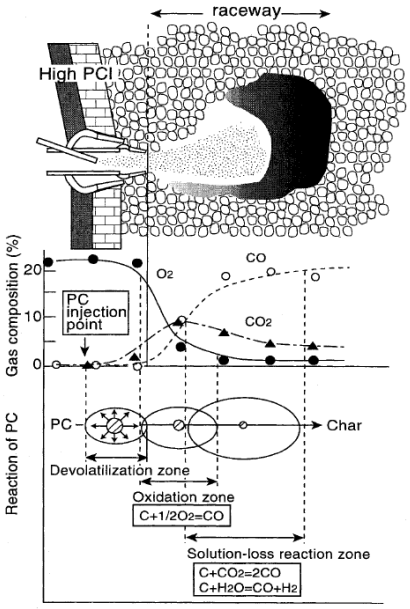

Figure 2.5 Schematic drawing of pulverised coal reaction in the raceway [50].

2.2.1.2 Requirements for a PCI fuel

A coal must meet certain requirements to be used as a PCI coal. This means that PCI coal is costlier compared to thermal coal. However, compared to coking coal, a wider range of higher rank coals are suitable. PCI coals are normally evaluated by properties including: Volatile matter, moisture, calorific value, alkali and sulfur content, and grindability.

Table 2.3 Chinese specifications of coal used in pulverized coal injection (PCI) [51]

Property	Grade	Standard
Ash, wt%	Grade 1	≤8.00
	Grade 2	8.00-10.00
	Grade 3	10.00-12.00
	Grade 4	12.00-14.00
Total sulfur, wt%	Grade 1	≤0.30
	Grade 2	0.30-0.50
	Grade 3	0.50-1.00
Hardgrove Grindability Index (HGI)	Grade 1	>70
	Grade 2	50-70
	Grade 3	40-50
Total phosphorus, wt%	Grade 1	<0.01
	Grade 2	0.01-0.03
	Grade 3	0.03-0.05
Total alkali (Na+K), wt%	Grade 1	<0.12
	Grade 2	0.12-0.2
Total moisture, wt%	Grade 1	<8.0
	Grade 2	8.0-10.0
	Grade 3	10.0-12.0

2.2.1.2.1 Coke replacement ratio

As previously stated, injecting coal into the blast furnace will replace a portion of the coke that enters the furnace, thus lowering coke requirements. The coke replacement ratio (CRR) refers to the mass of coke replaced per mass of coal injected and will fall between 0.8 and 1.0 kg coke/ kg coal [52]. There have been several indices created to predict the coke replacement ratio if the coal properties are known. Brouwer & Toxopeus determined such an index by analysing the operating performance of a PCI blast furnace [53].

$$CRR = \frac{-118.9 + 2.3\times C + 4.5\times H + 0.97\times ash}{100} \qquad \text{Equation 2.8}$$

Where C, H and ash are the amounts of carbon, hydrogen and ash respectively on a dry basis. On the other hand Hutny et al. developed a model based on a computer simulation that correlated replacement ratio with calorific value [54].

$$CRR = -0.6395 + 0.04 \times \Delta H_c \qquad \text{Equation 2.9}$$

Where ΔH_c is the calorific value of the fuel on a dry-ash-free basis. Likewise, Ishii also correlated the increasing coke replacement ratio with increasing calorific value, as well as with decreasing volatile matter contents [50].

2.2.1.2.2 Ash burden

Higher grade PCI coal favours lower ash content coal. There are several benefits to this including reduced energy required to melt the ash and reduced blockages in the lance and raceway. In addition to this, certain components of ash should be limited. Alkalis (sodium and potassium) can lead to degradation of the furnace lining [52]. Sulfur content also should be low. Flux that is added with coke for desulfurization into the furnace however increasing the sulfur input in the PCI coal will result in increased flux requirements and subsequently higher slag volumes and increased energy consumption to melt the slag. Chlorine has been shown to accumulate and cycle with the blast furnace shaft [55]. The gas at the top will be acidic and very corrosive. It is desired in the blast furnace that the ash fusion temperature is as high as possible in the blast furnace in order to reduce the risk of lance blockages caused by slag deposits [56]. Amounts of sulphur and phosphorous in the coal also need to be controlled as the will have a detrimental effect on steel quality [56].

2.2.1.2.3 Volatile matter

The amount of volatile matter present in the coal can have both positive and negative effects on the blast furnace performance. The volatile matter will release combustible gasses such as CO, H_2 and CH_4 as well as tar and incombustible gasses. The rapidly released gases will lead to increases in pressure and momentum in the raceway. Low volatile coals will generally have a higher calorific value [57], and consequently a higher coke replacement ratio. The lower volume of gas will lead to a lower pressure differential in the raceway [58]. On the other hand, high volatile matter coal will lead to increased coal burnout [59], as the chars produced from these

coals will have higher reactivity [60] and also because volatile matter release contributes to coal burnout. Another factor could be that the volatile flame will assist the ignition of char particles by increasing the flame temperature. Conversely, volatile oxidation will generate soot particles which are less reactive than char [61].

2.2.1.2.4 Reactivity

Increasing PCI rate is of interest to maximising productivity and reducing coke consumption, however one of the main limiting factors is unburnt char [62]. As previously mentioned, char can be converted to CO, CO_2, and H_2 through oxidation or by gasification with carbon dioxide and steam. Therefore, it is conceivable that char oxidation and gasification reactivity could be important parameters in the selection of a PCI fuel to maximise the PCI rate. On the other hand, under high temperatures experienced in the raceway, the reaction rate will be controlled by diffusion (Regime III), therefore the intrinsic reaction rate may be less relevant. However, Lu et al. [63] suggests that in the raceway, the highly turbulent environment and small particle size will mean that the overall rate of the combustion will be influenced by the intrinsic reactivity. Additionally, outside of the raceway, unburned char will combust under regime I or regime II conditions. [64].

2.2.1.3 PCI coal replacements

Due to the high cost of PCI coal, it has been proposed that biomass char (charcoal) could be used to fully replace the PCI coal [65], or as a blend [58, 66]. Wang et al. used a 1-D heat and mass balance model and concluded that charcoal could completely replace PCI coal, while torrefied material and wood pellets could only be injected in limited amounts [65]. Due to the lower S and ash content, an energy saving could be made as well as CO_2 emission reduction due to the renewable nature of biomass. Likewise, Mathieson et al. also considered a charcoal replacement, but instead used a combustion test apparatus that replicates the blast furnace tuyere and raceway conditions [58]. Under a fixed O/C ratio of 2.0 it was found that blending charcoal showed comparable or better burnout than a high-VM PCI coal. This could lead to higher coal injection rates in industrial practice which would subsequently increase productivity. Machado et al. also investigated the use of charcoal to replace PCI coal using a laboratory rig that simulated blast furnace conditions [66]. It was found that the higher CO_2 reactivity led to greater conversion compared to an imported coal used by a steel company.

One of the problems with charcoal utilisation is its low bulk (packing) density [58]. This can range from 0.1 g/cm^3 for sawdust [67], to 0.2 g/cm^3 for wood pellet waste [68], to 0.37 g/cm^3 for bark charcoal [69], although this could be increased to 0.56–0.63 g/cm^3 with a pelleting process [67]. In contrast, the bulk density of Victorian brown coal ranges between 0.65-0.67 g/cm^3 [14]. Feedstock cost and availability are also factors when considering a PCI replacement. The estimated cost of woody biomass in Australia was estimated to be $33.20 per tonne [70], with a large portion made up by the harvesting and chipping process. In contrast, the brown coal price mentioned earlier was $2-7 per tonne and contains more energy.

2.2.1.4 Blending of char with PCI coal

Solid fuel blending is the mixing of coals or other solid fuels to achieve the desirable qualities for the intended application [71]. The simplest approach to estimate the properties of a blend is to use a linear additive rule (Equation 2.10) [72].

$$M = (1 - x)M_a + xM_b \qquad \text{Equation 2.10}$$

Where M is the property being investigated, M_a and M_b are the values of property M in component a and b respectively, and x is the weight fraction of component b in the blend.

Studies have determined that some properties in the blend follow the linear additive rules while others do not. Riley et al. determined that the ultimate analysis (CHNS), moisture and lower calorific value are additive properties [73]. Ash and volatile matter had a slight variation from the calculated value, while Hardgrove grindability was non-additive. Hass et al. found that the proximate analysis volatile matter was additive, the rate of release of volatile matter and the high temperature volatile matter release in an isothermal plug flow reactor was non-additive [74]. In addition, the ash content, true density and lower calorific value were additive. They concluded that mineral compounds that vaporise could be responsible for the non-additive effects. In terms of combustion performance, it has been hypothesized that the brown coal or brown coal char could provide heat feedback to the bituminous coal to enhance its burnout [75]. Machado et al. al found non-additive behaviour in the gasification of charcoal, Brazilian coal blend, where the blend reaction rate was lower [66]. Although the work by Mathieson et al. did not test different blending ratios, it was found that by blending different biomass char just 12% by weight with PCI coal that burnout could be increased or decreased by as much as 7% [58].

2.2.1.5 Lab-scale experiments for PCI coal combustion

It has also been possible to evaluate PCI fuels without the use of specifically designed PCI rigs by instead using a laboratory scale drop tube furnace (DTF) or thermogravimetric analysis (TGA). Du et al. investigated the effect of "fuel ratio" on the burnout behaviour of a number of coal in a DTF operated at 1200 °C [76]. Fuel ratio was defined as the ratio of fixed carbon to volatile matter. It was found that burnout was increased with decreasing fuel ratio. Increasing blast temperature and reducing particle size were also revealed to increase burnout. The effect of blending two different coal types was and it was established that the burnout of a blend can be predicted based on a weighted average of the individual coals. Similarly, Hongyu et al. compared the performance of coals for PCI combustion on both a PCI rig and in a DTF [59], also finding that burnout linearly increased with increasing volatile matter. It was also determined that a DTF can provide a reasonable indication of coal combustion performance compared to a PCI rig. Another study examined the effect of the added catalysts (MnO_2, CaO and Fe_2O_3) on the burnout rate of bituminous and anthracite coals in a similar electrically heated DTF operated at 900 and 1100 °C [77]. All three catalysts, blended with the coal at a ratio of 1:99 were found to increase the burnout of bituminous coal with CaO being the most active followed by Fe_2O_3 then MnO_2. Analysis of the unburnt chars from catalytic combustion by TGA showed that these possessed higher reactivity than pure unburnt char due to their lower activation energy. While the previously mentioned study showed a linear relationship between burnout and blending ratio, it was shown in a different study that blending just 10% of a low-rank coal with high-rank coals can greatly improve combustion performance, even providing better burnout than that of the low-rank coal alone when studied in a DTF and by TGA [78]. It was thought that by blending, the volatile matter amount and heating value of the fuel could be optimised.

2.2.1.6 Modelling of PCI coal combustion

Numerical modelling methods have become increasingly popular for studying pulverised coal injection phenomena due to the advancements in computing power that is needed to run 3-D simulations. Compared to an experiment the advantages of a simulation will be more economical and can be completed in a shorter time. The results will be completely repeatable and all information is available at any time and location point. Modifications to designs and operating parameters with ease. On the contrary, simulations require accurate input data and

validation of results. Simulations will rely on simplifications of real world phenomena so it must be verified that the appropriate model is chosen.

As early as 1975, computational methods were used in the prediction of laboratory scale coal combustion reactions with reasonable similarity to their real world counterparts [79]. Over the past 30 years much progress has been made in terms of computational power available allowing for three-dimensional industrial scale pulverised coal fired furnace simulations in 1988 [80] and more comprehensive validation [81]. Coal combustion can be quite difficult and computationally intense to model as it combines two- phase fluid dynamics, turbulent mixing, fuel evaporation, radiative and convective heat transfer, and chemical kinetics [82].

Some various turbulence and radiation models are summarised below. Table 2.4 summarises the usage of CFD models in various studies on PCI combustion.

2.2.1.6.1 Turbulence

Tian et al. conducted a study on brown coal combustion compared the widely-used k-ε turbulence model and the more advanced Shear Stress Transport (SST) turbulence model [83]. These are both two-transport-equation Eddie viscosity models. The k-ε model is highly robust, commonly utilised and computationally cheap. However, it is only valid where fully turbulent flow is present so may not be as accurate where low Reynolds number flow occurs such as boundary layer flows unlike the k-omega model which allows for more accurate near wall treatment. The SST model combines the best of both worlds, utilising the k-omega model where flow is near to walls and the k-epsilon model where flow is away from walls using a blending function. The study found that both the k-epsilon and SST models were in good agreement with experimental data.

2.2.1.6.2 Thermal Radiation

Radiation in combustion is commonly modelled using either the P1, Monte Carol, Discrete ordinates (DO) or the Discrete Transfer radiation model (DTRM) which have all been used in a wide range of combustion applications. The Monte Carlo model provides the best accuracy for modelling radiation but the large computational time makes it less appealing for industrial scale combustion simulations [84]. Xu et al. found good agreement with plant data using the discrete transfer model [85], while Vuthaluru and Vuthaluru found that simulation results were

close to experimental observations when using the P1 model [86]. A recent study on brown coal combustion found the discrete transfer model had good prediction of radiation profiles, while the P1 model considerably under predicted the wall incident radiation flux [87]. Selçuk compared the DTRM and DO model in a furnace and found that the DO model provided better accuracy while requiring CPU time three orders of magnitude lower that of the DTRM [88].

2.2.1.6.3 Radiation absorption

Nitrogen and oxygen make up most the gasses during air-fired combustion and are transparent to thermal radiation. However, carbon dioxide and water vapour which are found more extensively during oxygen enrichment or oxy-fuel combustion are capable of absorbing and emitting heat radiation [89]. Therefore, high CO_2/H_2O conditions promote radiative heat transfer. The most widely used method of implementing this behaviour is the weighted sum of grey gases model (WSGGM) [90]. Yin et al. developed a new set of WSGGM coefficients that are valid under a range of different air-firing conditions [91]. The new model showed a significantly better prediction of gas temperature in a 609 MW utility boiler simulation.

2.2.1.6.4 Gas phase chemistry

From experiments with methane combustion, it has been determined that the large concentration of CO_2 will have a remarkable effect on the combustion mechanism [92]. Reactions of CO_2 with free radicals such as atomic hydrogen and other hydrocarbon radicals will lead to formation of greater amounts of CO. This will locally increase CO in the reaction area but should not affect CO emissions. In reaction mechanisms commonly used in CFD, to enhance solution robustness and speed, a simplification is used. A common method used in combustion simulations is the 2-step Westbrook Dryer (WD) mechanism to describe the combustion of CH_4 and CO [93]. For coal combustion, the volatile oxidation is treated like CH_4. Yin et al. found that this prediction was not sufficient in high CO_2 concentration environments [94]. Instead a modified WD mechanism [95], which adds a reverse reaction where CO_2 forms CO and O_2 can provide a better prediction of high CO levels and flame temperature in high CO_2/H_2O environments. The same study also found that the Jones & Lindstedt (JL) 4-step mechanism [96] also provided a good prediction CO and flame temperatures with the added addition of H_2. Likewise, Andersen et al. found a better agreement using the modified WD model, and also a modified JL model [97].

Table 2.4 CFD models of PCI coal combustion

Source	Study	Scope of computational grid	Volatile matter model	Coal conversion model	Turbulence model	Gaseous reactions	Radiation
Shen et al. (2011) [98]	Provide a reliable mode for coal/coke combustion.	Lance-blowpipe-tuyere-raceway-coke bed	Two competing rates model	Gibb model (3 reactions)	Standard k-ε	Eddy dissipation model	n.s.
Li et al. (2014)[99]	Optimise parameters for increasing burnout.	Raceway-coke bed	Two competing rates model	Multiple surface reaction model (3 reactions)	Standard k-ε	Eddy break-up model	P-1 model
Zhou et al. (2017)[100]	Combustion behaviour under different O_2 enrichment levels.	Lance–blowpipe–tuyere-raceway	Two competing rates model	Multiple surface reaction model (3 reactions)	Standard k-ε	Eddy break-up model	n.s.
Gu et al. (2010)[101]	Simulate combustion for coals of different VM content.	Tuyere-raceway	Two competing rates model	Multiple surface reaction model (3 reactions)	Standard k-ε	Eddy break-up model	Discrete-ordinates model
Du et al. (2007)[102]	Effect of injection pattern, O_2 content, and inlet temperature.	Blowpipe–tuyere	Two competing rates model	n.s.	RNG k-ε model	n.s.	n.s.
Guo et al. (2005)[103]	Effect of volatile matter content in coal on burnout	Tuyere-raceway	Two competing rates model	Gibb oxidation	RNG k-ε model	Eddy break-up model	Discrete-transfer method
Chen et al. (2017)[104]	Effect of O_2 enrichment and particle size	Raceway-coke bed	Two competing rates model	Kinetic/diffusion oxidation	Standard k-ε	Eddy break-up model	P-1 model

n.s. – not stated

2.3 Literature review summary and gas in research

This chapter has given an in-depth literature review of the current state of knowledge regarding the upgrading of low-rank coals and their application in PCI combustion. Based on this literature review, several gaps in the knowledge base have been identified.

- Firstly, it is of interest to understand the pyrolysis behaviour of Victorian brown coal in greater detail. Previous studies have particularly focused on pyrolysis of small particles which are assumed to be isothermal, rather than a briquette. Pyrolysis research has primarily focused on pyrolysis that occurs immediately prior to combustion rather than as a standalone process.
- The integration of intra-particle heat transfer with pyrolysis modelling has become well understood for biomass pyrolysis, whereas lignite has not been considered as a fuel to be upgraded. With its abundant reserves and low cost, this has attracted much industry attention in recent years, however more knowledge is needed.
- To date, the application of low-rank brown coal char as a PCI fuel for a blast furnace has yet to be tested. Instead, the use of woody charcoal as a PCI substitute fuel for CO_2 emission reduction has been examined. Brown coal char has potential to be used in this field due to its low ash content, however due it is not known if brown coal char will meet many of the other requirements and if the combustion performance will be acceptable.
- Blending combustion is also a worthwhile undertaking for replacement of a portion of the original PCI fuel to progressively adjust to the low-rank coal derived char while minimizing impacts on current operations. It is not always easily foreseeable how the created blend will behave because of possible non-additive/synergistic interactions between different coals or chars.
- The combustion environment with a high CO_2/H_2O level will induce increased radiative heat transfer, increased heat capacity of the gas, lower gaseous diffusion and large presence of CO_2 and steam in the boiler. It has been hypothesised that the altered combustion environment may have greater impacts on the combustion behaviour of low-rank coal due to its high reactivity with CO_2 and steam.

References

1. Quyn, D. M.; Wu, H.; Li, C.-Z., Volatilisation and catalytic effects of alkali and alkaline earth metallic species during the pyrolysis and gasification of Victorian brown coal. Part I. Volatilisation of Na and Cl from a set of NaCl-loaded samples. *Fuel* **2002,** 81, (2), 143-149.
2. Li, C.-Z., Some recent advances in the understanding of the pyrolysis and gasification behaviour of Victorian brown coal. *Fuel* **2007,** 86, (12), 1664-1683.
3. Fei, Y.; Aziz, A. A.; Nasir, S.; Jackson, W. R.; Marshall, M.; Hulston, J.; Chaffee, A. L., The spontaneous combustion behavior of some low rank coals and a range of dried products. *Fuel* **2009,** 88, (9), 1650-1655.
4. Durie, R. A., *The Science of Victorian brown coal : structure, properties, and consequences for utilization*. Butterworth-Heinemann: Oxford, 1991; p xvi, 750 p.
5. Department of Industry Innovation and Science, Resources and Energy Quarterly. In Australian Government,: December 2016.
6. Sujanti, W. Laboratory Studies of Spontaneous Combustion of a Victorian Brown Coal. The University of Adelaide, 1998.
7. Li, C. Z., *Advances in the Science of Victorian Brown Coal*. Elsevier Science: 2004.
8. Kolstad, C.; Young, D., Cost analysis of carbon capture and storage for the Latrobe valley. *Bren School of Environmental Science and Management, University of California, Santa Barbara, California, 35pp* **2010**.
9. Hurley, J. P.; Schobert, H. H., Ash formation during pulverized subbituminous coal combustion. 1. Characterization of coals, and inorganic transformations during early stages of burnout. *Energy & Fuels* **1992,** 6, (1), 47-58.
10. Platts *Coal Methodology & Specifications Guide*; 2017.
11. Mathieson, J. G.; Rogers, H.; Somerville, M.; Ridgeway, P.; Jahanshahi, S., Use of biomass in the iron and steel industry–an Australian perspective. *EECR-METEC InSteelCon* **2011**.
12. Hayashi, J.; Li, C.-Z., Structure and properties of Victorian brown coal. *Advances in the science of Victorian brown coal* **2004**, 11-84.
13. Phillip, R. G.; Bennet, A., Advantages of Low Volatile Coals for PCI. *Report–Department of Mines and Energy–Q Therm Project, Brisbane QLD* **1997**.
14. Reed, T.; Das, A., *Handbook of biomass downdraft gasifier engine systems*. Biomass Energy Foundation: 1988.
15. Dong, N. S., Utilisation of low rank coals. *IEA Report, CCC* **2011,** 182.
16. Wilson, D. Dryer, drying method and drying plant. 2011.
17. Akgün, F.; Arisoy, A., Effect of particle size on the spontaneous heating of a coal stockpile. *Combustion and Flame* **1994,** 99, (1), 137-146.
18. Küçük, A.; Kadıoğlu, Y.; Gülaboğlu, M. Ş., A study of spontaneous combustion characteristics of a turkish lignite: particle size, moisture of coal, humidity of air. *Combustion and Flame* **2003,** 133, (3), 255-261.
19. Hurd, C. D., *The pyrolysis of carbon compounds*. The Chemical Catalog Company: New York, 1929.
20. Solomon, P.; Fletcher, T.; Pugmire, R., Progress in coal pyrolysis. *Fuel* **1993,** 72, (5), 587-597.
21. Tchapda, A.; Pisupati, S., A Review of Thermal Co-Conversion of Coal and Biomass/Waste. *Energies* **2014,** 7, (3), 1098.
22. Jones, J. L.; PHILLIPS, R. C.; TAKAOKA, S.; LEWIS, F. M. In *Pyrolysis, Thermal Gasification, and Liquefaction of Solid Wastes and Residues*, Proceedings of... National Waste Processing Conference, 1978; American Society of Mechanical Engineers: 1978; p 387.

23. Victorian Government, Advanced Lignite Demonstration Program. In Department of Primary Industries, Ed. 2014.
24. Chu, M.; Zhu, S.; Yi, Y.; Deng, Y., Characteristics of Pyrolysis Products of Bori Lignite Briquette. *Energy Procedia* **2012,** 16, 307-313.
25. Radović, L. a. R.; Walker Jr, P. L.; Jenkins, R. G., Effect of lignite pyrolysis conditions on calcium oxide dispersion and subsequent char reactivity. *Fuel* **1983,** 62, (2), 209-212.
26. Quyn, D. M.; Wu, H.; Hayashi, J.-i.; Li, C.-Z., Volatilisation and catalytic effects of alkali and alkaline earth metallic species during the pyrolysis and gasification of Victorian brown coal. Part IV. Catalytic effects of NaCl and ion-exchangeable Na in coal on char reactivity☆. *Fuel* **2003,** 82, (5), 587-593.
27. Suuberg, E. M.; Peters, W. A.; Howard, J. B., Product Composition and Kinetics of Lignite Pyrolysis. *Industrial & Engineering Chemistry Process Design and Development* **1978,** 17, (1), 37-46.
28. Channiwala, S. A.; Parikh, P. P., A unified correlation for estimating HHV of solid, liquid and gaseous fuels. *Fuel* **2002,** 81, (8), 1051-1063.
29. Ranta, J., Production of charcoal: Handbook. *Pieksämäki, Finland* **1994**.
30. Wiklund, C.-M.; Pettersson, F.; Saxén, H., Optimal resource allocation in integrated steelmaking with biomass as auxiliary reductant in the blast furnace. *ISIJ international* **2012,** 52, (1), 35-44.
31. Badzioch, S.; Hawksley, P. G., Kinetics of thermal decomposition of pulverized coal particles. *Industrial & Engineering Chemistry Process Design and Development* **1970,** 9, (4), 521-530.
32. Zhang, J.; Prationo, W.; Zhang, L.; Zhang, Z., Computational Fluid Dynamics Modeling on the Air-Firing and Oxy-fuel Combustion of Dried Victorian Brown Coal. *Energy & Fuels* **2013,** 27, (8), 4258-4269.
33. Howard, J. B.; Fong, W. S.; Peters, W. A., Kinetics of Devolatilization. In *Fundamentals of the Physical-Chemistry of Pulverized Coal Combustion*, Lahaye, J.; Prado, G., Eds. Springer Netherlands: Dordrecht, 1987; pp 77-103.
34. Miura, K., A new and simple method to estimate f (E) and k0 (E) in the distributed activation energy model from three sets of experimental data. *Energy & Fuels* **1995,** 9, (2), 302-307.
35. Bryden, K. M.; Ragland, K. W.; Rutland, C. J., Modeling thermally thick pyrolysis of wood. *Biomass and Bioenergy* **2002,** 22, (1), 41-53.
36. Anthony, D. B.; Howard, J. B.; Hottel, H. C.; Meissner, H. P., Rapid devolatilization of pulverized coal. *Symposium (International) on Combustion* **1975,** 15, (1), 1303-1317.
37. Koufopanos, C. A.; Lucchesi, A.; Maschio, G., Kinetic modelling of the pyrolysis of biomass and biomass components. *The Canadian Journal of Chemical Engineering* **1989,** 67, (1), 75-84.
38. Miller, R.; Bellan, J., A generalized biomass pyrolysis model based on superimposed cellulose, hemicelluloseand liqnin kinetics. *Combustion science and technology* **1997,** 126, (1-6), 97-137.
39. Fletcher, T. H.; Kerstein, A. R.; Pugmire, R. J.; Solum, M. S.; Grant, D. M., Chemical percolation model for devolatilization. 3. Direct use of carbon-13 NMR data to predict effects of coal type. *Energy & Fuels* **1992,** 6, (4), 414-431.
40. Solomon, P. R.; Hamblen, D. G.; Carangelo, R.; Serio, M.; Deshpande, G., General model of coal devolatilization. *Energy & Fuels* **1988,** 2, (4), 405-422.
41. Niksa, S.; Kerstein, A. R., FLASHCHAIN theory for rapid coal devolatilization kinetics. 1. Formulation. *Energy & Fuels* **1991,** 5, (5), 647-665.
42. ANSYS Inc., *ANSYS 15.0 Documentation*. 2014.

43. Grant, D. M.; Pugmire, R. J.; Fletcher, T. H.; Kerstein, A. R., Chemical model of coal devolatilization using percolation lattice statistics. *Energy & Fuels* **1989,** 3, (2), 175-186.
44. Genetti, D.; Fletcher, T. H.; Pugmire, R. J., Development and Application of a Correlation of 13C NMR Chemical Structural Analyses of Coal Based on Elemental Composition and Volatile Matter Content. *Energy & Fuels* **1999,** 13, (1), 60-68.
45. Yan, B.; Cheng, Y.; Xu, P.; Cao, C.; Cheng, Y., Generalized model of heat transfer and volatiles evolution inside particles for coal devolatilization. *AIChE Journal* **2014,** 60, (8), 2893-2906.
46. Lewis, A. D.; Fletcher, T. H., Prediction of Sawdust Pyrolysis Yields from a Flat-Flame Burner Using the CPD Model. *Energy & Fuels* **2013,** 27, (2), 942-953.
47. Fletcher, T. H.; Pond, H. R.; Webster, J.; Wooters, J.; Baxter, L. L., Prediction of Tar and Light Gas during Pyrolysis of Black Liquor and Biomass. *Energy & Fuels* **2012,** 26, (6), 3381-3387.
48. Fletcher, T. H.; Barfuss, D.; Pugmire, R. J., Modeling Light Gas and Tar Yields from Pyrolysis of Green River Oil Shale Demineralized Kerogen Using the Chemical Percolation Devolatilization Model. *Energy & Fuels* **2015,** 29, (8), 4921-4926.
49. Department of Natural Resources and Mines, Queensland high energy coals for the PCI market: Advantages of Low Volatile Coals for PCI. In Queensland Government, Ed. 2003.
50. Ishii, K., *Advanced Pulverized Coal Injection Technology and Blast Furnace Operation*. Elsevier Science Ltd.: Oxford, UK, 2000.
51. Chinese Standards, Specifications of coal used in pulverized coal injection (PCI). In 2008; Vol. GB/T 18512-2008.
52. Carpenter, A. M., *Use of PCI in blast furnaces*. IEA Clean Coal Centre: 2006.
53. Brouwer, R.; Toxopeus, H., Massive coal injection at Hoogovens Ijmauiden blast-furnaces. *Revue de metallugie-cashiers d'informations techniques* **1991,** 88, (4), 323-334.
54. Hutny, W.; Price, J.; Gransden, J. In *Evaluation of coals for blast furnace injection using a computer model*, Ironmaking Conference Proceedings., 1990; 1990; pp 323-330.
55. Lectard, E.; Hess, E.; Lin, R., Behaviour of chlorine and alkalis in the blast furnace and effect on sinter properties during reduction. *Revue de Métallurgie* **2004,** 101, (1), 31-38.
56. GoldsWorthy, P.; Eyre, D. J.; On, E., 17 - Value-in-use (VIU) assessment for thermal and metallurgical coal A2 - Osborne, Dave. In *The Coal Handbook: Towards Cleaner Production*, Woodhead Publishing: 2013; Vol. 2, pp 455-496.
57. Parikh, J.; Channiwala, S. A.; Ghosal, G. K., A correlation for calculating HHV from proximate analysis of solid fuels. *Fuel* **2005,** 84, (5), 487-494.
58. Mathieson, J. G.; Rogers, H.; Somerville, M. A.; Jahanshahi, S., Reducing net CO 2 emissions using charcoal as a blast furnace tuyere injectant. *ISIJ international* **2012,** 52, (8), 1489-1496.
59. Li, H.; Elliott, L.; Rogers, H.; Wall, T., Comparative Study on the Combustion Performance of Coals on a Pilot-Scale Test Rig Simulating Blast Furnace Pulverized Coal Injection and a Lab-Scale Drop-Tube Furnace. *Energy & Fuels* **2014,** 28, (1), 363-368.
60. Lee, J.-M.; Kim, D.-W.; Kim, J.-S., Reactivity study of combustion for coals and their chars in relation to volatile content. *Korean Journal of Chemical Engineering* **2009,** 26, (2), 506-512.
61. Qin, K.; Lin, W.; Fæster, S.; Jensen, P. A.; Wu, H.; Jensen, A. D., Characterization of Residual Particulates from Biomass Entrained Flow Gasification. *Energy & Fuels* **2013,** 27, (1), 262-270.
62. Ichida, M.; Orimoto, T.; Tanaka, T.; Koizumi, F., Behavior of Pulverized Coal Ash and Physical Property of Dripping Slag under High Pulverized Coal Injection Operation. *ISIJ International* **2001,** 41, (4), 325-332.

63. Lu, L.; Sahajwalla, V.; Kong, C.; Mclean, A., Chemical structure of chars prepared under conditions prevailing in the blast furnace PCI operation. *ISIJ international* **2002,** 42, (8), 816-825.
64. Borrego, A. G.; Osório, E.; Casal, M. D.; Vilela, A. C. F., Coal char combustion under a CO2-rich atmosphere: Implications for pulverized coal injection in a blast furnace. *Fuel Processing Technology* **2008,** 89, (11), 1017-1024.
65. Wang, C.; Larsson, M.; Lövgren, J.; Nilsson, L.; Mellin, P.; Yang, W.; Salman, H.; Hultgren, A., Injection of solid biomass products into the blast furnace and its potential effects on an integrated steel plant. *Energy Procedia* **2014,** 61, 2184-2187.
66. Machado, J. G. M. S.; Osório, E.; Vilela, A. C. F.; Babich, A.; Senk, D.; Gudenau, H. W., Reactivity and Conversion Behaviour of Brazilian and Imported Coals, Charcoal and Blends in view of their Injection into Blast Furnaces. *steel research international* **2010,** 81, (1), 9-16.
67. McKendry, P., Energy production from biomass (part 1): overview of biomass. *Bioresource Technology* **2002,** 83, (1), 37-46.
68. Shuji, Y.; Tanaka, S., *Biochar and Compostization: Maximization of Carbon Sequestration with Minigating GHG Emission in Farmlands*. Food and Fertilizer Technology Center: 2013.
69. Yamato, M.; Okimori, Y.; Wibowo, I. F.; Anshori, S.; Ogawa, M., Effects of the application of charred bark of Acacia mangium on the yield of maize, cowpea and peanut, and soil chemical properties in South Sumatra, Indonesia. *Soil Science and Plant Nutrition* **2006,** 52, (4), 489-495.
70. Stucley, C.; Schuck, S.; Sims, R.; Larsen, P.; Turvey, N.; Marino, B., Biomass energy production in Australia. *Revised Edition. Rural Industries Research and Development Corporation, Canberra* **2004**.
71. Chironis, N. P., *Coal age operating handbook of coal surface mining and reclamation*. Coal Age Mining Informational Services: 1978; Vol. 2.
72. Pan, W.-P.; Gan, Y.; Serageldin, M. A., A study of thermal analytical values for coal blends burned in an air atmosphere. *Thermochimica acta* **1991,** 180, 203-217.
73. Riley, J.; Gilleland, S.; Forsythe, R.; Graham Jr, H.; Hayes, F. In *Non-additive analytical values for coal*, Proceedings of the seventh international conference on coal testing, Charleston, WV, USA, 1989; 1989; p 23.
74. Haas, J.; Tamura, M.; Weber, R., Characterisation of coal blends for pulverised fuel combustion. *Fuel* **2001,** 80, (9), 1317-1323.
75. Zhang, J.; Wang, Q.; Wei, Y.; Zhang, L., Numerical Modeling and Experimental Investigation on the Use of Brown Coal and Its Beneficiated Semicoke for Coal Blending Combustion in a 600 MWe Utility Furnace. *Energy & Fuels* **2015,** 29, (2), 1196-1209.
76. Du, S.-W.; Chen, W.-H.; Lucas, J. A., Pulverized coal burnout in blast furnace simulated by a drop tube furnace. *Energy* **2010,** 35, (2), 576-581.
77. Zou, C.; Wen, L.; Zhang, S.; Bai, C.; Yin, G., Evaluation of catalytic combustion of pulverized coal for use in pulverized coal injection (PCI) and its influence on properties of unburnt chars. *Fuel Processing Technology* **2014,** 119, 136-145.
78. Sahu, S. G.; Mukherjee, A.; Kumar, M.; Adak, A. K.; Sarkar, P.; Biswas, S.; Tiwari, H. P.; Das, A.; Banerjee, P. K., Evaluation of combustion behaviour of coal blends for use in pulverized coal injection (PCI). *Applied Thermal Engineering* **2014,** 73, (1), 1014-1021.
79. Lowe, A.; Wall, T. F.; Stewart, I. M., A zoned heat transfer model of a large tangentially fired pulverized coal boiler. *Symposium (International) on Combustion* **1975,** 15, (1), 1261-1270.

80. Boyd, R. K.; Kent, J. H., Three-dimensional furnace computer modelling. *Symposium (International) on Combustion* **1988,** 21, (1), 265-274.
81. Boyd, R. K.; Kent, J. H., Comparison of large scale boiler data with combustion model predictions. *Energy & Fuels* **1994,** 8, (1), 124-130.
82. Viskanta, R.; Mengüç, M. P., Radiation heat transfer in combustion systems. *Progress in Energy and Combustion Science* **1987,** 13, (2), 97-160.
83. Tian, Z. F.; Witt, P. J.; Schwarz, M. P.; Yang, W., Comparison of two-equation turbulence models in simulation of a non-swirl coal flame in a pilot-scale furnace. *Combustion Science and Technology* **2009,** 181, (7), 954-983.
84. U.S. Department of Energy Office of Industrial Technologies and Sandia National Laboratory, Improving Industrial Burner Design with Computational Fluid Dynamics Tools: Progress, Needs, and R&D Priorities. In 2002.
85. Xu, M.; Azevedo, J. L. T.; Carvalho, M. G., Modelling of the combustion process and NOx emission in a utility boiler. *Fuel* **2000,** 79, (13), 1611-1619.
86. Vuthaluru, R.; Vuthaluru, H. B., Modelling of a wall fired furnace for different operating conditions using FLUENT. *Fuel Processing Technology* **2006,** 87, (7), 633-639.
87. Tian, Z. F.; Witt, P. J.; Schwarz, M. P.; Yang, W., Modeling issues in CFD simulation of brown coal combustion in a utility furnace. *The Journal of Computational Multiphase Flows* **2010,** 2, (2), 73-88.
88. Selçuk, N.; Kayakol, N., Evaluation of discrete ordinates method for radiative transfer in rectangular furnaces. *International Journal of Heat and Mass Transfer* **1997,** 40, (2), 213-222.
89. Karwa, R., Heat Transfer in Absorbing and Emitting Media (Gaseous Radiation). In *Heat and Mass Transfer*, Springer: 2017; pp 809-835.
90. Hottel, H.; Sarofim, A., *Radiative Transfer*. 1967; p 20-24.
91. Yin, C.; Johansen, L. C. R.; Rosendahl, L. A.; Kær, S. K., New Weighted Sum of Gray Gases Model Applicable to Computational Fluid Dynamics (CFD) Modeling of Oxy−Fuel Combustion: Derivation, Validation, and Implementation. *Energy & Fuels* **2010,** 24, (12), 6275-6282.
92. Glarborg, P.; Bentzen, L. L. B., Chemical Effects of a High CO2 Concentration in Oxy-Fuel Combustion of Methane. *Energy & Fuels* **2008,** 22, (1), 291-296.
93. Dryer, F. L.; Glassman, I., High-temperature oxidation of CO and CH4. *Symposium (International) on Combustion* **1973,** 14, (1), 987-1003.
94. Yin, C.; Rosendahl, L. A.; Kær, S. K., Chemistry and radiation in oxy-fuel combustion: A computational fluid dynamics modeling study. *Fuel* **2011,** 90, (7), 2519-2529.
95. Westbrook, C. K.; Dryer, F. L., Simplified Reaction Mechanisms for the Oxidation of Hydrocarbon Fuels in Flames. *Combustion Science and Technology* **1981,** 27, (1-2), 31-43.
96. Jones, W. P.; Lindstedt, R. P., Global reaction schemes for hydrocarbon combustion. *Combustion and Flame* **1988,** 73, (3), 233-249.
97. Andersen, J.; Rasmussen, C. L.; Giselsson, T.; Glarborg, P., Global Combustion Mechanisms for Use in CFD Modeling under Oxy-Fuel Conditions. *Energy & Fuels* **2009,** 23, (3), 1379-1389.
98. Shen, Y.; Yu, A.; Zulli, P., CFD Modelling and Analysis of Pulverized Coal Injection in Blast Furnace: An Overview. *steel research international* **2011,** 82, (5), 532-542.
99. Li, Y.; Zhang, X.; Zhang, J.; Zhou, J.; Yan, H., Numerical simulation and optimization of pulverized coal injection with enriched oxygen into blast furnace. *Applied Thermal Engineering* **2014,** 67, (1–2), 72-79.

100. Zhou, Z.; Huo, H.; Wang, G.; Xue, Q.; She, X.; Wang, J., Effect of Oxygen-Coal Lance Configurations on Coal Combustion Behavior. *steel research international* **2017,** 88, (1), 1600197-n/a.
101. Gu, M.; Chen, G.; Zhang, M.; Huang, D.; Chaubal, P.; Zhou, C. Q., Three-dimensional simulation of the pulverized coal combustion inside blast furnace tuyere. *Applied Mathematical Modelling* **2010,** 34, (11), 3536-3546.
102. Du, S.-W.; Chen, W.-H.; Lucas, J., Performances of pulverized coal injection in blowpipe and tuyere at various operational conditions. *Energy Conversion and Management* **2007,** 48, (7), 2069-2076.
103. Guo, B.; Zulli, P.; Rogers, H.; Mathieson, J. G.; Yu, A., Three-dimensional Simulation of Flow and Combustion for Pulverised Coal Injection. *ISIJ International* **2005,** 45, (9), 1272-1281.
104. Chen, T.; Cheng, S.; Xu, W., Model Analysis of the Phenomena of Pulverized Coal Injection in Blast Furnace. In *8th International Symposium on High-Temperature Metallurgical Processing*, Hwang, J.-Y.; Jiang, T.; Kennedy, M. W.; Yücel, O.; Pistorius, P. C.; Seshadri, V.; Zhao, B.; Gregurek, D.; Keskinkilic, E., Eds. Springer International Publishing: Cham, 2017; pp 603-614.

This page is intentionally left blank

This page is intentionally left blank

Chapter 3 – Experimental and Analytical Methods

This page is intentionally left blank

The section outlines the experimental and analytical methods used in this thesis. They can be summarised into three groups, experimental facilities which consists of three lab-scale heating devices, modelling part including computation fluid dynamics (CFD) and one dimensional modelling and lastly the analytical methods used in sample characterisation.

3.1 Experimental facilities

3.1.1 Vertical shaft furnace

Pyrolysis was conducted in a vertical fixed-bed shaft furnace as shown in Figure 3.1. The shaft furnace can reach temperatures up to 1000 °C. The furnace itself can heat at 10 °C/min, however loading the quartz reactor directly into the furnace facilitates a higher heating rate. A quartz reactor of 1 *m* length and 55 *mm* inner diameter was used. Argon at a flow rate of 2 L/min is used to purge the reactor for 20 *min* prior to heating and during the pyrolysis process to sweep both the light gasses and condensable tar gasses to the collection system. The collection system is made up of three impingers surrounded by an acetone-dry ice cooling bath and kaowool was also placed close to the outlet of the impingers to trap liquid entrained in the gas flow. Water in the crude tar collected in impingers was quantified using the Karl-Fischer titration method. The remaining fraction was identified as tar. Gasses exiting the impinger system enter a gas detector which can measure O_2, CH_4, CO, CO_2, H_2S, and SO_2 real-time.

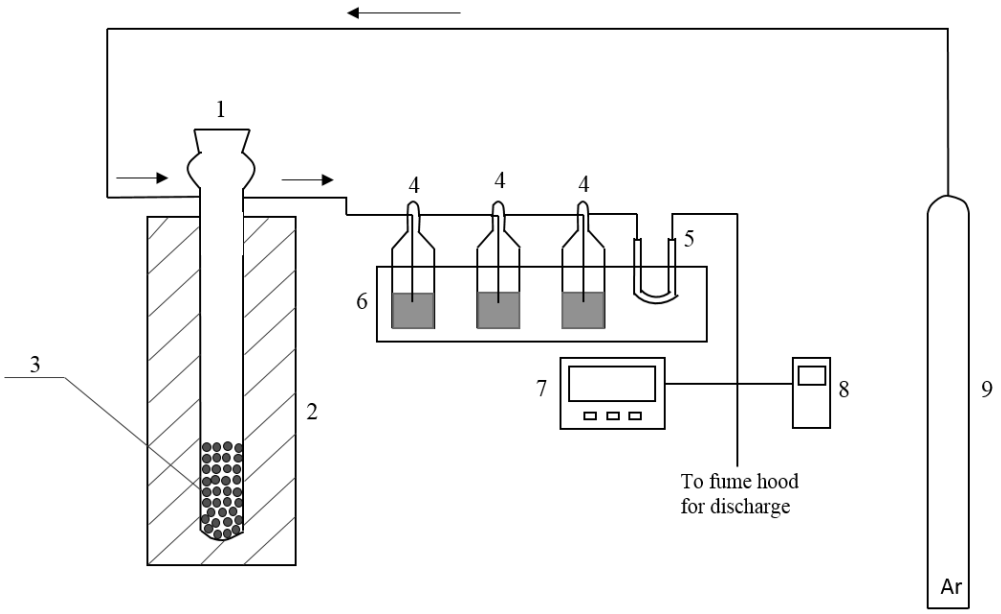

Figure 3.1 Shaft furnace schematic (1. Quartz reactor; 2. Heating furnace; 3. Sample; 4-6. Acetone –containing impinge trains for the tar collection; 7-8: Gas detectors; 9. Argon gas)

3.1.2 Drop tube furnace (DTF)

The DTF is a 2.0 *m* high quartz reactor (Figure 3.2). The heating area consists of 6 electrically heated zones that can be controlled individually up to a maximum temperature of 1000 °C. The quartz reactor contains an inner chamber of 5 cm diameter. An outer annulus of thickness 1.5 cm surrounds this inner chamber, making the reactor diameter 8 *cm* total. The outer annulus is designed to allow gasses to be preheated.

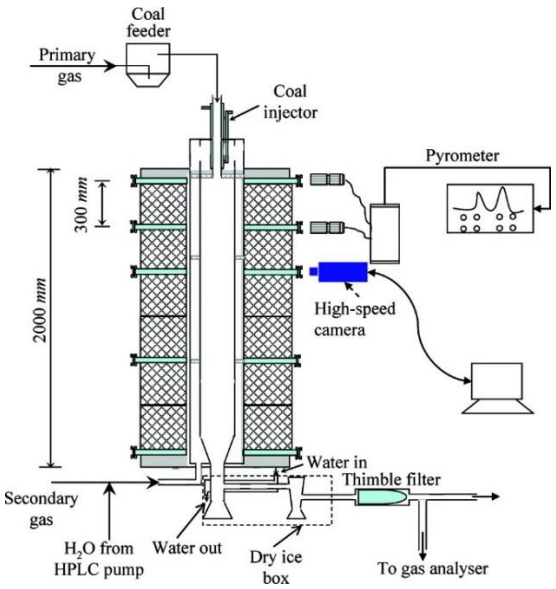

Figure 3.2 Schematic drawing of the DTF reactor facility [1]

The gas controls allow the addition of three different gasses simultaneously. Gasses can be either diverted to primary or secondary gas streams. The primary gas flows through the sample chamber and enters the reactor with the sample. The secondary gas enters the bottom of the reactor and then flows through the outer annulus where it is preheated. It then mixes with the primary gas and sample close to the injector tip. In addition, water can be added via an HPLC pump and enter with the secondary gas. This inlet is close to the reactor so will allow the water to be instantly vaporised due to the high temperature. The typical primary and secondary gas flow rates are 1 L/min and 9 L/min respectively.

The solid sample is stored in a piezo-electric feeder. The feeding rate can be adjusted and is typically set at 0.5 g/min. An air tight chamber surrounds the feeder with only one inlet and one outlet. The inlet allows the primary gas to surround the sample. The sample is fed into the outlet and will become entrained in the gas that also enters this chamber. The outlet contents descend to the reactor via a silicon tube which is connected to a water-cooled injector. The water-cooled injector allows the sample and primary gas to remain below 100 °C until it enters

the inner chamber of the reactor, whereby they will be rapidly heated and mixed with the secondary gas. Three different lengths of injector are available to vary the particle residence time in the reactor. These injector lengths are summarised in Table 3.1.

Table 3.1 Summary of DTF injectors

Injector protrusion into reactor (*m*)	Reaction zone length (*m*)	Approximate particle residence time (s)
1.2	0.6	0.7
0.6	1.2	1.4
0.0	1.8	2.1

At the bottom of the reactor the gaseous products and solid material (unburned char or ash) can be collected. Firstly, they enter a collection tube. Course particles will fall straight down into a collection flask while fine particles will be entrained in the gas flow. A Whatman silica microfiber thimble filter traps the particles while the gasses can pass through. The microfiber filter and flask are cooled with dry-ice to prevent further reactions. Gas that passes through the filter are then sent to an infrared gas detector capable of measuring CO_2, CO, SO_2, NO and O_2.

3.1.3 Flat flame burner (FFB)

For ignition delay testing and flame structure analysis, a flat flame burner (FFB) was used. This has previously been used in another study [2] and is shown in Figure 3.3. Specifically, the type of FFB used is the McKenna burner. The liquid fuel (C_2H_4/H_2) and oxidiser are premixed and evenly distributed through a matrix prior to ignition. The flame provided can be assumed to be one-dimensional and a standard for comparing samples. At the base of the burner the temperature is approximately 1000 °C while the quartz walls are lower temperature, at 500 °C due to heat loss.

Coal is fed from a hopper via a piezo-electric feeder and a carrier gas. The entrained coal particles enter from the base of the burner and pass through the flame and into the heated furnace area and a longer vertical flame will be visible. Flame images are taken using a Nikon P7000 CCD camera. In each image, the distance between the burner base and beginning of the flame can be measured.

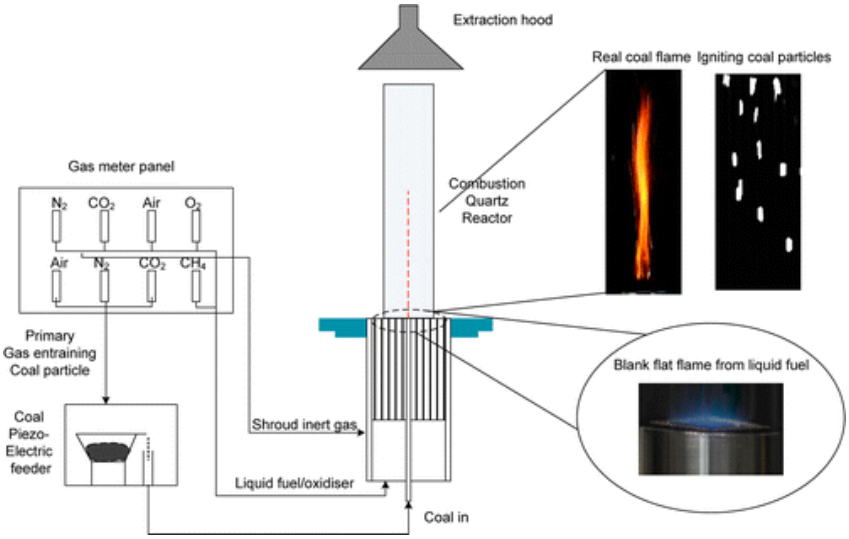

Figure 3.3 Schematics of the flat-flame burner reactor [2].

3.2 Modelling

3.2.1 Computational fluid dynamics (CFD) modelling

CFD modelling is the use of numerical analysis to solve fluid flow problems using the Navier-Stokes equations. The purpose of using CFD software was to perform a comprehensive analysis on flows that occur during combustion in such a detail that is not possible in a laboratory DTF. It was also used for the speed and ease of parameter adjustment.

The software used in CFD modelling is Ansys Fluent 15.0. The computational grid is a representation of the DTF from section 3.1.2. This mesh was created for a previous study by Jian et al. [3]. The grid consists of 231 000 cells and encompasses all features of the drop tube furnace including the primary gas inlet, secondary gas inlet with outer annulus gas preheating, and the water-cooled injector. In the previous study, it was validated through gas and particle temperature measurements and a grid independence test was performed. A visual representation of the mesh is shown in Figure 3.4.

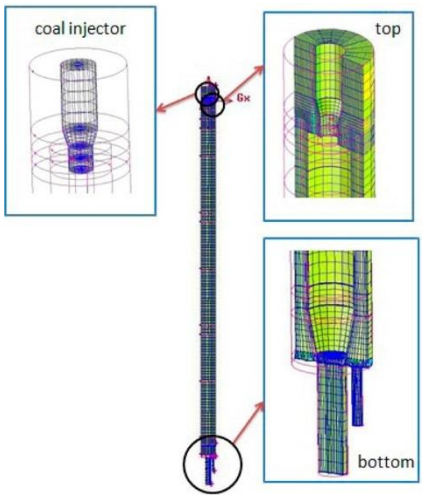

Figure 3.4 Modelling geometry and local expansion diagrams for the DTF. [3]

The following models were used: turbulence – standard *k-ε* model; radiation – discrete ordinates (DO) model; radiation absorption – modified WSGGM for air-fired [4] and oxy-fuel combustion [5]; particle tracking - Lagrangian discrete phase model (DPM); gas phase chemistry – Westbrook-Dryer and modified Westbrook-Dryer model for oxy-fuel combustion; particle reactions – Multiple surface reaction model (char-O_2, char-CO_2, char- H_2O).

Although this model is based on previous work by Zhang et al. [3], some of the changes to this model are detailed as followed. As previously shown (Table 3.1), the drop tube furnace allows different particle residence times by insertion of different water-cooled injectors. Previously the mesh only allowed for the longest residence time, however now it has been modified to simulate all three residence times. For combustion in an O_2/N_2 environment, a modified WSGGM for radiation absorption was implemented based on the work by Yin [4], rather than the default Fluent WSGGM. Temperature and composition dependent gas heat capacity and thermal conductivity were added. Major species ($O_2/N_2/CO_2/CO/H_2$) have their heat capacity and thermal conductivity defined by a polynomial function, while minor species use the kinetic theory model for this. Finally, a method for addition of a second coal stream for coal blending was added. Since the in-built coal calculator function is only compatible with one injection, the coal particle, carbon species and volatile species are duplicated, and the properties are copied from another case, including volatile oxidation reactions, volatile release kinetics, char reactions, and dry basis volatile and char fractions in the particle. A second injection is then created at the site of the first injection (Primary air inlet) and the different volatile species, coal

particle, carbon species, and liquid volume fraction are specified. Blending ratio is controlled by adjusting the mass flow rate of each particle injection.

3.2.2 1-D numerical modelling

The software used for numerical calculations is MATLAB. MATLAB is a computing environment that uses its own programming language which contains many built-in maths functions, graphing tools and solving methods including error minimisation and solving of simultaneous partial and ordinary differential equations.

One of the primary functions used in MATLAB for this work is "pdepe". pdepe is useful for solving systems of parabolic and elliptic PDEs that have one space dimension and one time dimension as well as combining ODEs with one time dimension. The PDE must fit into the following form:

$$c\left(x,t,u,\frac{\partial u}{\partial x}\right)\frac{\partial u}{\partial t}=x^{-m}\frac{\partial}{\partial x}\left(x^{m}f\left(x,t,u,\frac{\partial u}{\partial x}\right)\right)+s(x,t,u,\frac{\partial u}{\partial x})$$

Where *x* is the space variable, t is the time variable, *u* is the variable to be solved and m is the geometry of the problem which can be set to 0, 1, or 2 corresponding to a slab, cylinder or sphere respectively.

3.3 Samples analysis

3.3.1 Proximate and ultimate analysis

The proximate analysis is used to determine the composition of the coal or char sample in terms of moisture, volatile matter, fixed carbon and ash. While the ultimate analysis determines the composition in terms of carbon, hydrogen, nitrogen and sulphur (CHNS) and oxygen. These elements can be assumed to be contained within the volatile matter and fixed carbon. It is important to understand the different bases that are used to report these results and how to convert between them. Under different circumstances, a certain basis may be more useful for comparing samples. For example, dry basis could be used to determine the samples composition after drying.

The following terms are commonly used in this thesis:
Air-dried or ad: This basis assumes the sample has been dried although some moisture is remaining. In terms for the proximate analysis, the moisture, volatile matter, ash content and fixed carbon will sum to 100%. And for the ultimate analysis, the CHNS + oxygen + ash + moisture will sum to 100%.

Dry basis or db: This basis reports the components that would be remaining once moisture is removed. Therefore, for the proximate analysis the volatile matter, ash content and fixed carbon will sum to 100%, while the CHNS + oxygen + ash will sum to 100%.

Dry ash free or daf: This basis excludes both moisture and ash. Therefore, it will indicate on a basis of all the combustible matter in the sample. For the proximate analysis, only volatile matter and fixed carbon are reported and these sum to 100%. For the ultimate analysis, CHNS + oxygen will sum to 100%.

The table below can be used to convert between these bases where A is ash and M is moisture.

Table 3.2 Conversion between air dry, dry basis and dray ash free

To obtain:	Air dry (ad)	Dry basis (db)	Dry ash free (daf)
Multiply			
ad by	-	$100/(100-M_{ad})$	$100/(100-M_{ad}-A_{ad})$
db by	$(100-M_{ad})/100$	-	$100/(100-A_{db})$
daf by	$(100-M_{ad}-A_{ad})/100$	$(100-A_{db})/100$	-

The proximate analysis procedure was carried out per ASTM Standard D3172-13 [6]. Firstly, the sample needs to be ground so that it passes through a 250 μm sieve. The sample should have already been air dried. A muffle furnace, capable of temperatures up to 950 °C is needed, a desiccator for cooling samples and ceramic crucibles with lids to hold the samples. The moisture in the sample is determined per ASTM Standard D3173 – 11 [7]. The sample is placed in a 105 °C oven and held for 1 *h*. Just prior to its removal, a cap is placed on top to prevent moisture being reabsorbed while cooling. Once the sample reaches room temperature, it is weighed and the difference in mass before and after heating, divided by the initial weight, will give the moisture fraction. For the ash content, ASTM Standard D3174 – 12 [8] is used. Either

air dried, or dried coal can be used for this test as well as the following volatile matter test, and the result will be reported on that basis (e.g. ad or db). The sample is placed in the muffle furnace at room temperature. The furnace will then be heated so that 500 °C is reached at the end of 1 *h* and 750 °C by the end of the second hour. It is then held for an additional 2 *h*. The sample can then be removed, cooled down and weighed. The fraction of ash is taken as the remaining mass divided by the initial mass. Following this, the volatile matter is determined per ASTM Standard ASTM D3175 – 11 [9]. The furnace is preheated to 950 °C. The sample is placed inside the crucible with its lid on and placed inside the 950 °C furnace. The lid will prevent air from entering the container and oxidising the sample. Oxygen should theoretically be consumed first by flammable volatile vapours being released. At the end of 7 min, the sample is removed from the furnace and allowed to cool. The difference in initial and final mass, divided by the initial mass, is the fraction of volatile matter. From here, the fixed carbon can be determined as the remaining fraction besides moisture, ash and volatile matter on an air-dried basis. Or the remaining fraction after accounting for ash and volatile matter on a dry basis.

The ultimate analysis was outsourced to an analytical services company. The analysis was performed using a CHNS elemental analyser, which oxidises the sample and analyses the compounds generated by thermal conductivity. CHNS composition is determined directly, and oxygen is assumed to be the remainder of the sample after CHNS, ash and moisture are measured.

3.3.2 Thermogravimetric analysis (TGA)

TGA was carried out in a Shimadzu DTG-60H. It allows for simultaneous measurement of temperature, mass and differential thermal analysis (DTA). The temperature can be increased up to 1500 °C and the heating rate can be set between 1 and 50 °C/min. Mass is measured to a precision of 0.001 *mg*. DTA measures the difference in temperature between a reference and the sample and quantifies this as electric potential difference (voltage). This reading will indicate the extent to which the sample absorbs or releases heat, i.e. whether the reaction is endothermic or exothermic. The entering the TGA may be inert (nitrogen or argon) or reactive (air or carbon dioxide). Three main analysis types were conducted in the TGA listed (ignition temperature analysis, kinetic analysis and burnout determination) and these are detailed below.

For all experiments, the samples do not require drying since this process can be carried out by the instrument. Flow rate of the inert or reactive gas was set to 100 ml/min. For the ignition test and kinetic analysis, the particle size was fixed at 63-105 μm and the amount of sample was varied between 1.5-5 mg. It is important that the heating rate remains linear; using too much sample in an oxidative environment will cause the sample to heat faster than intended. However, enough sample should be provided so that a high resolution can be obtained for the measurement of the mass loss derivative or the DTA signal compared to the noise or baseline drift. Generally, samples with a higher calorific value and low volatile matter will require less sample to be used. Also, samples with a higher activation energy will react in a well-defined temperature region, therefore less sample is needed as the peak will be strong.

3.3.2.1 Ignition temperature analysis

Although the TGA has a relatively slow heating rate compared to combustion in a boiler, there have been several methods created for estimating the ignition temperature. This can be useful for comparing different samples. Two of these methods have been used in this thesis.

The first method was devised by Chao et al. [10], illustrated in Figure 3.5. The heating rate was fixed at 10 °C/min and the sample was heated to a point where all the combustible would be consumed, leaving only ash. The mass curve is differentiated with respect to time, and the point of the maximum reaction rate is found. The corresponding point at this time on the mass curve was determined as point A. From point A, a tangent line was drawn. Another horizontal line is drawn at point C on the mass curve, at a region after the sample has dried (above 110 °C) and has not yet begun decreasing further in mass. The intersection of the horizontal line with the tangent line was determined and this is point B. The corresponding point in time on the temperature curve will be the ignition temperature.

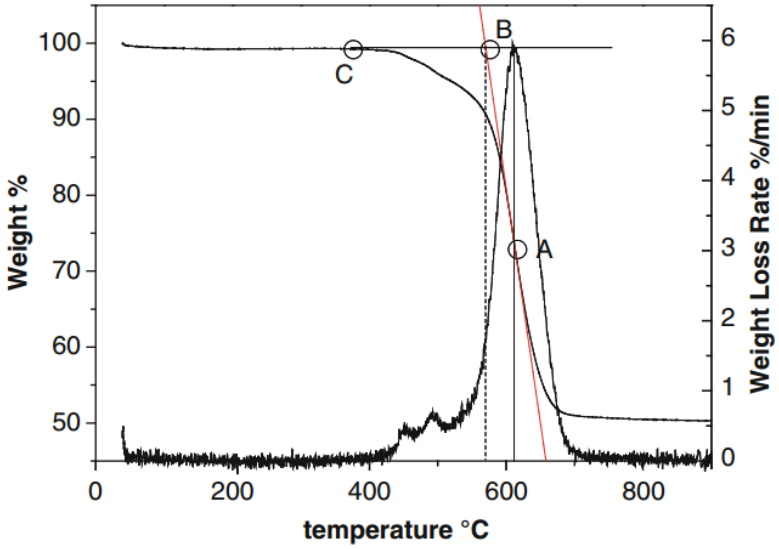

Figure 3.5 Determination of ignition temperature with the Chao et al. method [10]

The drawback of this method is that it is not always simple to choose a maximum reaction rate if there is more than one peak visible. This is especially the case when coals are blended. An alternative method was substituted when coals were blended, devised by Wang et al. [11]. Using the same curve as the previous method, the ignition temperature was defined as the rate at which the weight loss rate measured in %/min reaches 1%. As can be seen in Figure 3.5, this occurs at a similar temperature to the previous ignition point measurement method.

3.3.2.2 Kinetics analysis

The Kissinger method has been used to determine the kinetic parameters, pre-exponential constant and activation energy for solid-gas reactions assuming a first-order reaction with respect to the solid. Equation 3.1 and Equation 3.2 are used to describe the conversion rate of the solid assuming a constant gas concentration and first-order kinetics.

$$\frac{d\alpha}{dt} = k(1-\alpha) \qquad \text{Equation 3.1}$$

$$k = Ae^{-\frac{E_a}{RT}} \qquad \text{Equation 3.2}$$

The Kissinger method adapts the equation for TGA studies with a non-isothermal, linear heating rate in Equation 3.3.

$$\ln\left(\frac{\beta}{T_p^2}\right) = \ln\left(\frac{AR}{E_a}\right) - \frac{E_a}{RT_p} \qquad \text{Equation 3.3}$$

Where β is the heating rate. By plotting $\ln\left(\frac{\beta}{T_p^2}\right)$ against $\frac{1}{T_p}$ the pre-exponential constant and activation energy can be determined from the slope and intercept.

3.3.3 X-ray fluorescence (XRF) spectroscopy

XRF (Spectro iQ II) is a non-destructive technique that is used to determine the elemental composition of a sample. It operating principle is the measurement of secondary radiation emitted by a sample that has been irradiated by high energy X-rays. The X-ray will dislodge an electron from one of the inner orbitals and subsequently the vacancy will be filled by one of the higher energy orbitals. The energy difference between these states is emitted and is characteristic of the element. It is calibrated with three fly ash standard material: SAM 1633a, SARM 163c and SARM 2690.

3.3.4 X-ray diffraction (XRD) spectroscopy

XRD (Rigaku MiniFlex) was used in determining the aromaticity of char samples using the technique of Yen et al. [12]. The low sin(θ/2) region contains both the γ and (002) bands which are representative of aliphatic and aromatic groups respectively. By assuming the peaks are symmetrical and integrating the area underneath them the aromaticity can be determined with Equation 3.4.

$$Aromaticity, fa = \frac{A_{002}}{A_{002} + A_{\gamma}} \qquad \text{Equation 3.4}$$

3.3.5 Mercury intrusion

Mercury intrusion was used in this thesis for the purposes of measuring particle density and permeability. This was accomplished using a Micromeritics' AutoPore IV. A sample mass of approximately 1 g was used and pressure was increased up to a maximum of 60,000 psi_a (4,100 bar). A graph like Figure 3.6 is produced. At point A, the mercury has surrounded the mass of particles and when the pressure is further increased there will be an abrupt change in mercury intrusion volume indicating that mercury is filling the spaces between particles until it reaches point B where mercury has enveloped every particle. Each particle contains micron sized pores. Further increasing the pressure will cause mercury to fill these pores causing another increase in the intrusion volume until point C where these pores have been filled.

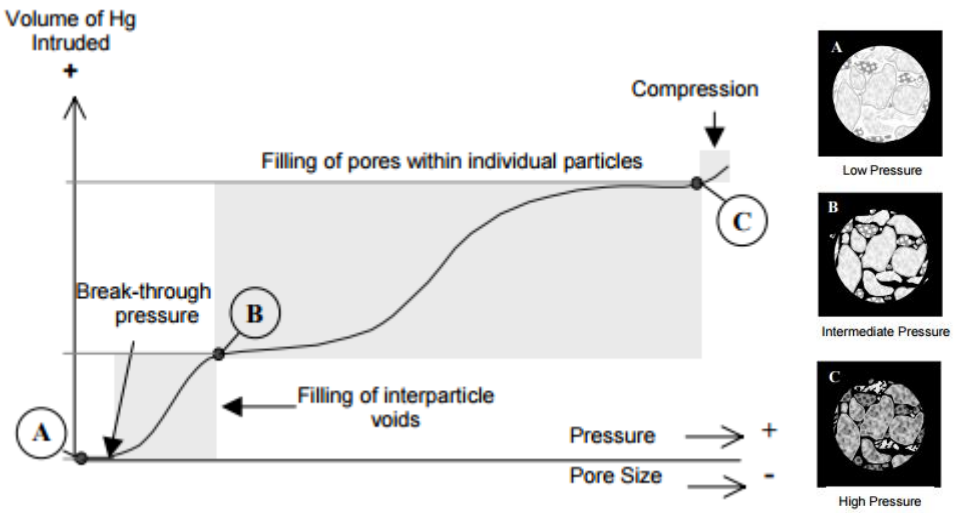

Figure 3.6 Cumulative intrusion plot compared to pressure. At point A the mercury has surrounded the particles, then at B the mercury has filled the gaps in between the particles. Following this the mercury will fill the pores of particles up to point C. [13]

To calculate the envelope density (sometimes referred to as particle density), the total intrusion volume at point B must be known, as well as the empty volume of the vessel. From there the remainder will be the envelope volume which includes the solid, pores, both opened and closed, and possibly also external voids created by the roughness of the surface. Density is then calculated by the measured mass of the powder divided by the envelope volume.

Permeability was also determined using the same mercury intrusion experiment. To calculate permeability, the characteristic length must first be determined. The pressure must be determined where the mercury first spans the sample, known as the threshold pressure. The Washburn equation gives relationship between the applied pressure and pore size that the mercury can be force into. The corresponding pore size for the threshold pressure is the characteristic length. A micrometrics white paper gives further details about this calculation [14].

3.3.6 Electron spin resonance (ESR) spectroscopy

Free radicals in solid char are measured using electron spin resonance (ESR) spectroscopy using a previously established method [15]. The ESR spectrometer (EMXplus-10/12 from Bruker) was operated at 9.85 *GHz* and 0.1 *mW*. The central magnetic field was 348 *mT*, the modulation amplitude was 1.0 *G*, the sweep width was 5 *mT*, the sweep time was 50 *s*, and the time constant was 0.01 *s*. The char or coal samples was loaded into the ESR sample tube and

directly measured at room temperature. By calibrating the area of the ESR signal with 2-diphenyl-1-picrylhydrazyl (DPPH) of known radical concentration, the concentration of unpaired electrons can be determined, expressed in *spins/g*.

3.3.7 Helium pycnometry

Helium pycnometry is used in the calculation of true density. This is with a similar principle to envelope density (0), however the fluid medium is helium instead of mercury which will readily fill pore volume. A Micrometrics AccuPyc 1330 is used for this purpose. The instrument consists of two chambers, one that holds the sample and another of known internal volume [16]. A pressure is applied to the reference chamber and is then vented to the sample chamber. Firstly, this is done for a calibration sample of known volume. Following this the sample volume can be calculated using the Boyle's Law temperature – volume relationship.

References

1. Low, F.; De Girolamo, A.; Dai, B.-Q.; Zhang, L., Emission of Organically Bound Elements during the Pyrolysis and Char Oxidation of Lignites in Air and Oxyfuel Combustion Mode. *Energy & Fuels* **2014,** 28, (6), 4167-4176.
2. Prationo, W.; Zhang, J.; Abbas, H. A. A.; Wu, X.; Chen, X.; Zhang, L., Influence of External Clay and Inherent Minerals on Lignite Optical Ignition and Volatile Flame Propagation in Air-Firing and Oxy-Firing. *Industrial & Engineering Chemistry Research* **2014,** 53, (7), 2594-2604.
3. Zhang, J.; Prationo, W.; Zhang, L.; Zhang, Z., Computational Fluid Dynamics Modeling on the Air-Firing and Oxy-fuel Combustion of Dried Victorian Brown Coal. *Energy & Fuels* **2013,** 27, (8), 4258-4269.
4. Yin, C., Refined Weighted Sum of Gray Gases Model for Air-Fuel Combustion and Its Impacts. *Energy & Fuels* **2013,** 27, (10), 6287-6294.
5. Yin, C.; Johansen, L. C. R.; Rosendahl, L. A.; Kær, S. K., New Weighted Sum of Gray Gases Model Applicable to Computational Fluid Dynamics (CFD) Modeling of Oxy−Fuel Combustion: Derivation, Validation, and Implementation. *Energy & Fuels* **2010,** 24, (12), 6275-6282.
6. ASTM D3172-02, Standard Practice for Proximate Analysis of Coal and Coke. *ASTM International* **2002**.
7. ASTM D3173-11, Standard Test Method for Moisture in the Analysis Sample of Coal and Coke. *ASTM International* **2011**.
8. ASTM D3174-02, Standard Test Method for Ash in the Analysis Sample of Coal and Coke from Coal. *ASTM International.* **2002**.
9. ASTM D3175-11, Standard Test Method for Volatile Matter in the Analysis Sample of Coal and Coke. *ASTM International* **2011**.
10. Chao, J.; Yang, H.; Chen, Y.; Luv, J.; Zhang, H.; Liu, Q., The Investigation of the Coal Ignition Temperature in Oxygen-Enriched Atmosphere by TGA. In *Cleaner Combustion and Sustainable World*, Qi, H.; Zhao, B., Eds. Springer Berlin Heidelberg: Berlin, Heidelberg, 2013; pp 589-593.
11. Wang, C. a.; Liu, Y.; Zhang, X.; Che, D., A study on coal properties and combustion characteristics of blended coals in Northwestern China. *Energy & Fuels* **2011,** 25, (8), 3634-3645.
12. Yen, T. F.; Erdman, J. G.; Pollack, S. S., Investigation of the structure of petroleum asphaltenes by X-ray diffraction. *Analytical Chemistry* **1961,** 33, (11), 1587-1594.
13. Webb, P. A., Volume and density determinations for particle technologists. *Micromeritics Instrument Corp* **2001,** 2, (16), 01.
14. Webb, P. A., An introduction to the physical characterization of materials by mercury intrusion porosimetry with emphasis on reduction and presentation of experimental data. *Micromeritics Instrument Corp, Norcross, Georgia* **2001**.
15. Liu, M.; Yang, J.; Liu, Z.; He, W.; Liu, Q.; Li, Y.; Yang, Y., Cleavage of Covalent Bonds in the Pyrolysis of Lignin, Cellulose, and Hemicellulose. *Energy & Fuels* **2015,** 29, (9), 5773-5780.
16. Lowell, S.; Shields, J. E.; Thomas, M. A.; Thommes, M., Density Measurement. In *Characterization of Porous Solids and Powders: Surface Area, Pore Size and Density*, Springer Netherlands: Dordrecht, 2004; pp 326-338.

This page is intentionally left blank

Chapter 4 – Pyrolysis of Lignite Briquette – Experimental Investigation and 1-Dimensional Modelling Approach

The literature review in Chapter 2 has shown that pyrolysis can generate a char product with a higher heating value that could potentially be used as a substitute for PCI coal. Additionally, briquetting of coal was shown to be an effective method of densifying coal and improving the stability during transport. The first point of interest, is to consider the modelling of this pyrolysis process for a large briquette and understand the mechanisms behind pyrolysis in terms of heat transfer and char structure. This chapter has been reformatted from a manuscript submitted to the Fuel journal.

Abstract

A laboratory-scale shaft furnace was used for the pyrolysis of the lignite briquette together with thermogravimetric analysis to study the intrinsic pyrolysis kinetics under two different heating rates, 10 °C/min and 100 °C/min. Apart from coal conversion rate, the tar yield, quality and radical concentration in char were also measured to explore the difference between lignite briquette and the respective pulverised powder. Additionally, a 1-D model coupled with the chemical percolation devolatilisation (CPD) code was developed to quantitatively understand heat transfer using temperature dependent parameters; product distribution and yields, and the pyrolysis mechanism. It was discovered that heat transfer was the limiting factor for pyrolysis of the lignite briquette, which subsequently lowered the heating rate and led to increased cross-linking and decreased tar production compared to a coal particle. Simultaneously, the primary tar also underwent internal cracking and even deoxygenation to decompose into light aromatics and gases inside the briquette char matrix. Providing a hot gas environment was found to facilitate the cracking of tar species compared to a slow heating rate where tar is released at a lower temperature. The changes in radical concentration in the solid material were linked to the structural changes predicted by the CPD model including bridge-breaking, tar release and cross-linking phenomena.

Keywords

Lignite Briquette Pyrolysis, 1 - D Modelling Coupled with CPD Code, Heating Rate, Radicals

4.1 Introduction

Being the single largest source in Victoria, Australia, Victorian brown coal is a resource with large reserves and can be extracted at a low cost [1]. Upgrading it to higher value products through pyrolysis is one of the promising ways in the carbon-constrained future. The resultant solid char can be used in a number of applications such as the use as a low-volatile pulverized coal injection (PCI) coal replacement in the metallurgy industry, which has a market price of USD $100-150/t in 2015 [2].

The pyrolysis process induces both physical and chemical changes during the conversion to char, liquid tar and gas [3]. To date, plenty of knowledge has been achieved for the pyrolysis of VBC and other lignites, as documented in the two major monographs [1, 4]. However, past research on the pyrolysis has focused on the behaviour of pulverised particles that are generally smaller than 200 μm. From the practical perspective, increasing the transportability (e.g. mechanical strength and particle size) of the pyrolysis char is crucial in the Australian context, since the produced char will be primarily exported overseas to feed the international energy and metallurgy markets. For such a purpose, a prior pelletization of coal fine particles is essential. While the previous studies have provided understanding on the reactions within a small particle [5], little is known about the complicated inter-influences between pyrolysis reactions and physical processes (heat and mass transfer) within a coal briquette. Some research has also been carried out on the pyrolysis of Collie coal briquette in Western Australia, with a focus on the production of metallurgical reductant requiring a mechanical strength of 6.9–30 MPa and a reactivity index of 2.6 - 28% towards CO_2 [6, 7]. However, the results are not directly applicable to Victorian brown coal which has a much higher volatile yield and lower strength. Research has also been conducted on the pyrolysis of low-rank coal – biomass/municipal solid waste plastic (MSW) blends and the briquettes (using commercial humates and molasses as the binders) [8, 9]. However, efforts have yet to be made to examine the pyrolysis behaviour of the briquetted brown coal.

In this paper, we will report the pyrolysis of a Victorian brown coal briquette under the varying conditions in a fixed-bed reactor, including two particle heating rates (10°C/min and 100 °C/min), five terminal temperatures (600 - 1000 °C) and hold-time (10 - 60 min) at 800 °C. The slow heating regime (10 °C/min) is expected to occur in a rotary kiln pyrolyser or the middle zone of an industry - scale fixed - bed, under which the briquette temperature is

expected to be even in the radial direction, whereas for the fast heating (100 °C/min), which is expected to occur close to the furnace wall in an industry-scale pyrolyser, the pyrolysis extent could be limited by the internal heat transfer within the coarse particles or briquette. Apart from the briquette, the parent raw coal was screened to four different sizes and each size was examined for comparison. To quantify the temperature distribution and reaction controlled rates for the solid char production, a 1-D model was further established and coupled with the existing CPD model [10] to integrate structural, temperature and pressure variations within the cylindrical coal briquette. To the best knowledge of the authors, such an effect has yet to be made in the past research where the CPD model has only been applied to smaller particles which are generally assumed isothermal and isobaric. Additionally, the resultant char was characterised for the concentration of radicals within it, which are expected to be related to the extent of the cleavage of the covalent bonds within the briquette matrix [11], as well as tar yield and quality from the briquette pyrolysis. The radical concentration has proven to be one of the effective parameters to correlate the properties of char and tar and the pyrolysis conditions [12, 13].

4.2 Experimental methods

4.2.1 Properties of coal particles and briquette

The feedstock materials for pyrolysis are coal particles of varying size and a coal briquette sampled from the Latrobe Valley, Australia. The coal particles were grouped into four size bands, <2 *mm*, 2-4 *mm*, 4-8 *mm* and > 8 *mm* with the average size in each group approximately 400 μm, 2.9 *mm*, 6.1 *mm* and 11.2 *mm*, respectively. The upper limit of the >8 *mm* size bin is ~16 *mm* and the <2 *mm* size bin contains particles as small as 40 μm. The respective briquette possesses a dimension of 4.0 *cm* in height and 4.8 *cm* in diameter. The manufacturing of coal briquette is the same as that has been detailed previously [1]. In brief, the coal fine particles with a moisture content of around 10 *wt%* were roller pressed at a pressure larger than 100 MPa. The proximate and ultimate analysis for these samples is shown in Table 4.1. The different sizes of the raw coal show slight variation, in particular on the content of ash. The property of coal briquette is however very similar with the four coal sizes, expect for ash and sulphur that are slightly higher in the briquette. This could be due to the preferential use of coal fine particles that are slightly rich in ash-forming elements for coal briquetting, as evident in the size of <2

mm. The coal briquette also contains a lower moisture content than the air-dried pulverised coal, possibly due to the release of the physically trapped moisture upon roll pressing.

Table 4.1 Proximate and ultimate analysis for feed materials

	Air-dried pulverised coal particles				Briquette
Size range	< 2 *mm*	2-4 *mm*	4-8 *mm*	>8 *mm*	
Proximate analysis, *wt%*					
Moisture (ar)	13.67	14.20	14.85	12.37	9.68
Volatile (db)	54.56	55.51	52.43	56.57	55.83
Fixed carbon (db)	42.88	42.76	45.74	41.83	40.56
Ash (db)	2.55	1.72	1.83	1.60	3.61
Ultimate analysis (db), *wt%*					
C	62.22	62.12	61.69	62.43	62.44
H	4.51	4.69	4.81	4.68	4.87
O (by difference)	29.97	30.67	30.91	30.61	28.24
N	0.58	0.62	0.60	0.55	0.61
S	0.16	0.17	0.16	0.14	0.23

4.2.2 Pyrolysis Conditions

Pyrolysis was conducted in a fixed-bed shaft furnace as shown in Figure 4.1. A quartz reactor of 1 *m* length and 55 *mm* inner diameter was used. Argon at a flow rate of 2 L/min is used to purge the reactor for 20 min prior to heating and during the pyrolysis process to sweep both the light gasses and condensable tar gasses to the collection system. The collection system is made up of three impingers surrounded by an acetone-dry ice cooling bath and kaowool was

also placed close to the outlet of the impingers to trap liquid entrained in the gas flow. Note that, the tar deposited on the reactor wall was also weighted and collected by acetone. It was then mixed with the tar collected from the impinge trains and the mixture was analysed hereafter. Water in the crude tar collected in impingers was quantified using the Karl-Fischer titration method. The remaining fraction was identified as tar. Gasses exiting the impinger system enter a gas detector which can measure O_2, CH_4, CO, CO_2, H_2S, and SO_2 real-time.

Coal particles and briquette were pyrolyzed in two different processes which are defined as slow heating and fast heating hereafter. For slow heating, coal particles or briquette were heated with the reactor together at 10 °C/min up to a terminal temperature from 600 to 1000 °C, with increments of 100 °C. For fast heating conditions, the furnace was heated up to 800 °C first, and subsequently, the particle/briquette-laden quartz reactor was inserted into the furnace and held for a time that is varied between 10 and 60 *min*, with increments of 10 *min*. The fast heating rate was measured to be an average of approximately 100 °C/min for the environment surrounding the coal particle/briquette and the terminal 800 °C was reached within approximately 8 min once the coal - laden reactor was injected inside the furnace. After both the heating modes, the quartz tube was removed from the heating furnace and the sample was rapidly cooled in approximately 10 min.

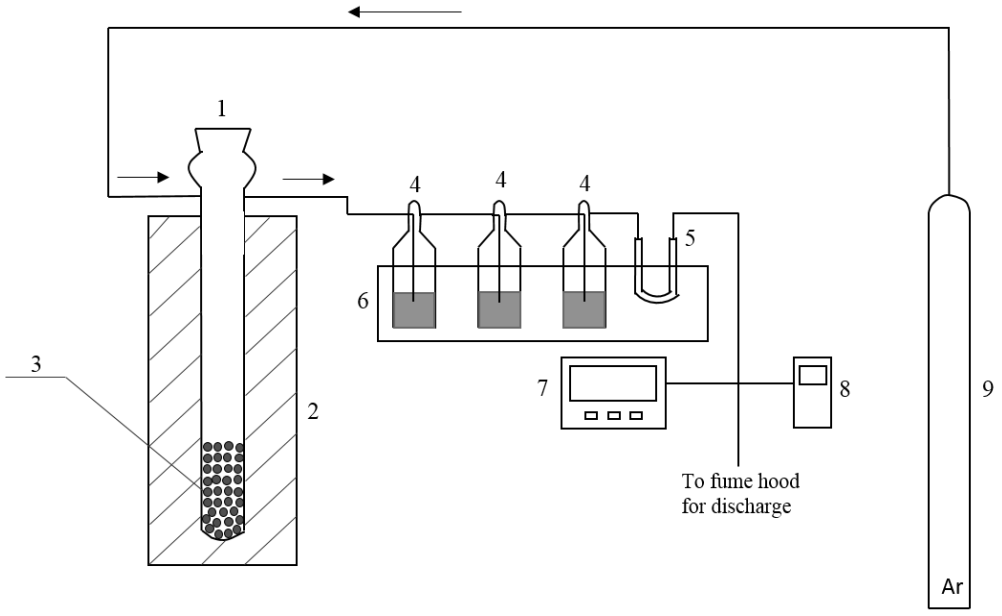

Figure 4.1 Shaft furnace schematic (1. Quartz reactor; 2. Heating furnace; 3. Sample; 4-6. Acetone –containing impinge trains for the tar collection; 7-8: Gas detectors; 9. Argon gas)

4.2.3 Char property analysis and TGA pyrolysis conditions

Particle density (also known as envelope density) was measured using an Autoscan 60 mercury intrusion instrument up to a pressure that will fill inter-particle space but not enter pores. In order to find true density to be used in the calculation of porosity, a helium pycnometer (Micrometrics AccuPyc 1330) was used. Porosity φ was further determined with the following Equation 4.1:

$$\varepsilon = \frac{V_{voids}}{V_{particle}} = 1 - \frac{V_{solid}}{V_{particle}} = 1 - \frac{m_{particle}/\rho_{true}}{m_{particle}/\rho_{particle}} = 1 - \frac{\rho_{particle}}{\rho_{true}} \qquad \text{Equation 4.1}$$

Permeability was determined using a Micrometrics Autopore IV. A white paper by Micrometrics provides the principles used in the calculation of permeability [14].

TGA experiments conducted in a Shimadzu DTG-60H thermogravimetric analyser were first used to validate the intrinsic mass loss rate without any secondary reactions of coal predicted by the model (to be detailed later) at different heating rates. The heating rate was varied from 20 °C/min to 50 °C/min in 10 °C/min increments and the surrounding environment is argon gas supplied at 100 ml/min. To determine the pyrolysis behaviour of lignite briquette, it was first ground to less than 100 μm.

Free radicals in solid char were measured using electron spin resonance (ESR) spectroscopy using a previously established method [12]. The ESR spectrometer (EMXplus-10/12 from Bruker) was operated at 9.85 *GHz* and 0.1 *mW*. The central magnetic field was 348 *mT*, the modulation amplitude was 1.0 *G*, the sweep width was 5 *mT*, the sweep time was 50 *s*, and the time constant was 0.01 *s*. The char or coal samples were loaded into the ESR sample tube and directly measured at room temperature. By calibrating the area of the ESR signal with 2-diphenyl-1-picrylhydrazyl (DPPH) of known radical concentration, the concentration of unpaired electrons can be determined, expressed in *spins/g*.

4.2.4 1-D model formulation

There have been many efforts in the literature to model the pyrolysis process which considers a non-isothermal solid. Devolatilisation is commonly modelled in either a volumetric model

(VM) [15, 16], or shrinking core model (SCM) [17, 18]. For a decomposition process, such as pyrolysis, while SCM can describe the process whereby volatile matter can only escape the particle through the more porous char on the exterior of the pyrolysis front. The intact coal core is still porous, and hence, a volumetric model may be more appropriate. In light of this, a transient 1-D model based on the volumetric model was developed hereafter to describe the volatile release and temperature profile of coal particles/briquette. Thermal conductivity and heat capacity were derived from literature sources and are dependent on temperature and moisture [4, 19].

The rate of coal pyrolysis must also be determined. One of the simplest methods for this is a first-order devolatilisation model which is dependent on the amount of volatiles remaining in the particle (based on a fixed volatile content determined by proximate analysis or experimentally) and the kinetic rate which is temperature dependent and described by an Arrhenius type pre-exponential factor and an activation energy. This method has proven adequate in combustion simulations [20]. However, such a model would be unfeasible for simulating a variety of heating rates during the pyrolysis stage, since for complex materials, the modelled value of the pre-exponential factor and activation energy are generally dependent on the heating rate used to determine them [21]. An extension of the first-order model that aims to encompass this characteristic is the distributed activation energy model (DAEM) which incorporates a large number of parallel first - order reactions [22]. This method is not computationally expensive and can accurately simulate the pyrolysis process at multiple linear heating rates. However, these models do not consider the temperature history of the particle undergoing pyrolysis so may not be valid for non-linear heating rates that usually occur for coarse sizes and briquette. Moreover, these models limit the extent of pyrolysis to one value, neglecting the impact of heating rate on the char yield. If a SCM model was chosen, this type of model would be the only option whereby the pre-exponential factor could be modified from *1/s* to *m/s* [17].

The reactions that occur during pyrolysis are more accurately simulated by a variety of other models which would better fit experimental data at different heating rates and provide useful information on char, tar and gas production. A more complex approach was established by Miller & Bellan for biomass which describes the pyrolysis process with four first - order processes [23]. An active material is initially formed from the raw sample. Subsequently, this

active material converts into either tar (which is then vaporised in a separate equation) or the simultaneous production of char and gas. A more advanced set of methods known as network models are based on the chemical transitions in coal structure which is included in the FG-DVC [24], FLASHCHAIN [25], and CPD models [26].

The CPD code developed by Fletcher & Kerstein [10, 26] is advantageous because its source code is freely available and can therefore be customised, and independently verified with ease. It will therefore be used to describe the pyrolysis rate in this study. It has also been implemented into the commercial CFD software, Ansys Fluent. The CPD model treats coal as aromatic clusters whose labile bonds can be cleaved forming two sets of fragments, including one set with relatively low molecular weight to evolve into a light gas, and another with a higher molecular weight and consists of tar precursors to remain in the coal for a longer time. The latter set can be vaporised through a vapour - liquid equilibrium system based on Raoult's Law or reattach to the coal lattice with a cross - linking mechanism.

The heat balance in the cylindrical briquette is described by the partial differential equation (PDE) in Equation 4.2 below.

$$\rho C_p \frac{\partial \mathrm{T}}{\partial \mathrm{t}} = \frac{1}{r}\frac{\partial}{\partial r}\left(k * \frac{\partial \mathrm{T}}{\partial \mathrm{r}}\right) - \rho(\Delta H_{p,vol}\frac{\partial \alpha}{\partial \mathrm{t}} + \Delta H_{vap,H_2O}\frac{\partial x}{\partial \mathrm{t}}) \qquad \text{Equation 4.2}$$

Where α is the fraction of volatiles remaining at the time *t*, and *x* is the fraction of moisture. Moisture evaporation is described by a first - order equation with the kinetic rate described by the Arrhenius equation once T > 95 °C, similar to Bryden et al. [27], although the pre-exponential factor is modified from 5.13×10^6 to 9.52×10^8 s^{-1} which had a better fit with the experimental data, while the activation energy was kept at 88 *kJ/mol*.

The heat capacity and thermal conductivity of coal/char are taken from a previous study that had analysed lignite properties in the range of 25 – 1000 °C by using a laser flash system for the measurement [19]. It is noticeable that these properties have a large variation with temperature. The measurements were converted to a second or third degree polynomial so that the R^2 fitting coefficient was at least 0.99. Heat capacity and thermal conductivity can be calculated from a weighted average of the water and dry coal/char constituents [4]. For density of the coal containing moisture, it is assumed that the moisture will fill pores in the coal,

increasing its density. Moreover, the combined result of particle shrinkage and mass loss will affect the char density during the pyrolysis process. In this study, coal shrinking during pyrolysis was modelled based on an empirical equation derived from experimental results. This was done by measuring the particle diameter as a function of pyrolysis yield. After almost complete devolatilisation, the particle diameter has been reduced by 25%. During later stages, the shrinkage increases more rapidly compared to the volatile release. Table 4.2 summarises the calculation of the aforementioned properties.

Table 4.2 Calculation of density, specific heat capacity and thermal conductivity as a function of temperature (T [°C]), moisture fraction and volatile fraction remaining (V/V*).

Property	Condition	Equation	Range	Source
Density, ρ (kg/m^3)	Wet coal	ρ_{dry} × (1 + Moisture fraction)	-	-
	Dry coal	1083.9	25 - 100 °C	This study
Shrinkage factor (m/m)	Dry coal	-0.214 × (V/V*)^3 + 0.181× (V/V*)^2 – 0.217 × (V/V*) + 1.0	0-1	This study
Specific heat capacity, C_p (J/kg.K) – Weighted average	Moisture	8.58E-03 × T^2 - 5.83E-01 × T + 4.19E+03	25- 100 °C	[28]
	Coal	-1.58E-06 × T^3 + 2.78E-03 × T^2 - 7.12E-01 × T + 1.36E+03	25 - 1000 °C	[19]
Thermal conductivity, k (W/m.K) – Weighted average	Moisture	-9.37E-06 × T^2 + 2.12E-03 × T + 5.60E-01	25- 100 °C	[29]
	Coal	2.12E-06 × T^2- 4.54E-04 × T+ 9.33E-02	25- 1000 °C	[19]

Heat can be transferred to the briquette via free convection and radiation, according to Equation 4.3 below.

$$-k\frac{\mathrm{dT}}{\mathrm{dr}} = h(T_\infty - T_s) + \varepsilon\sigma({T_\infty}^4 - {T_s}^4) \qquad \text{Equation 4.3}$$

Where k is the thermal conductivity of the coal particle/briquette, h is the heat transfer coefficient, ε is the emissivity of the particle/briquette, and σ is the Stefan–Boltzmann constant, 5.670 $W\ m^{-2}\ K^{-4}$. T_∞ and T_s are the reactor temperature and particle surface temperature respectively. While the experiments were carried out with a large number of particles, a limitation of the 1-D model is that it assumes a single particle is being heated rather than a group. Thus, effects such as inter-particle heat transfer and variations in radiation intensity based on position are neglected. In addition, the electric furnace used here is big enough to be deemed as the single heating source for the reactor and all the reactants. The radiation is also negligible since the temperatures used are quite low. A common method of estimating emissivity is by using a conversion dependent model between unburned coal/char (1.0) and ash (0.6) [30, 31]. Considering that the char conversion is extremely trivial and negligible under the mild pyrolysis conditions tested here, the emissivity of char is assumed at 1.0.

The heat transfer coefficient, h, can by calculated by obtaining the Nusselts number from Equation 4.4which is valid for external natural flow around vertical cylinders [32], and then solving for h in Equation 5

$$Nu = 0.59(Gr.Pr)^{0.25} \qquad \text{Equation 4.4}$$

$$Nu = \frac{hD}{k} \qquad \text{Equation 4.5}$$

Where Pr is the Prandtl number,$\frac{C_p\mu}{k}$ and Gr is the Grashof number calculated in Equation 4.6. Gas properties are assumed to be temperature dependent and equivalent to that of the argon carrier gas.

$$Gr = \frac{g\beta(T_\infty - T_s)D^3}{\nu^2} \qquad \text{Equation 4.6}$$

Where g is the acceleration due to gravity, β is the coefficient of thermal expansion (assumed to be $1/T$ as an ideal gas), and ν is the kinematic viscosity.

The calculation of internal pressure was taken from the work of Hagge and Bryden [15]. It is expected that internal pressure will build up in larger particles, especially when the heating rate

is fast. Equation 4.7 below shows the partial differential equation used in the calculation of pressure, which is modified from the original equation to suit a cylinder instead of a slab.

$$\frac{\partial}{\partial t}\left(\frac{\varepsilon f P}{T}\right)+\frac{f}{r}\frac{\partial}{\partial r}\left(r\frac{P}{T}\frac{\varphi}{\mu}\frac{\partial P}{\partial r}\right)=R\left(\frac{\omega_V}{W_V}+\frac{\omega_L}{W_L}+\frac{\omega_T}{W_T}\right) \qquad \text{Equation 4.7}$$

Where P is pressure, ε is porosity, f is shrinkage factor, φ is permeability, μ is the dynamic viscosity, R is gas constant, W is the molecular weight of the gas and ω is the mass release rate of the gas per unit volume. The subscripts V, L and T are water vapour, light gasses, and tar respectively. The molecular weight of light gasses and tar is calculated by the CPD model. On average the molecular weight is 29.5 *g/mol* and 253 *g/mol* for light gasses and tar respectively. Boundary conditions are set with symmetry at the centre of the cylinder and ambient (1 *atm*) pressure at the outside surface.

4.2.5 Calculation procedure for 1-D model

A flowchart is shown in Figure 4.2 for the overall calculation process. The model allows the user to vary the wall temperature as a function of time and also the diameter and shape of the coal. Other parameters could also be varied such as moisture fraction or ultimate analysis compositions. The temperature and pressure PDEs were solved concurrently with the ordinary differential equation (ODE) for moisture evaporation and the ODEs for the CPD model including the labile bridge fraction, $\pounds$, the side chain fraction, δ, the char bridge fraction, c, and the fraction of light gasses, g_1 and g_2. Since the other variables including porosity, permeability, heat of pyrolysis and shrinkage require the conversion, an initial guess on the coal conversion was made for the first calculation stage assuming that the products are split between char and gas. Next, the flash distillation procedure and cross-linking mechanism calculate the proportion of char, tar and gas. This was compared to the guess used by the previous stage. If the maximum absolute error in the conversion calculation is below 1E-5, the procedure continued to the next step, otherwise the char, tar and gas fractions would be applied to the original PDE/ODE system. The properties will be known in terms of time and distance from the centre. To determine the overall properties, each part of the cylinder or sphere was assigned a calculation weight based on its distance from the centre, r. For a cylinder this is proportional to $2\pi r$ (circumference) and for a sphere it is $4\pi r^2$ (surface area). A weighted average can then be determined at each time point.

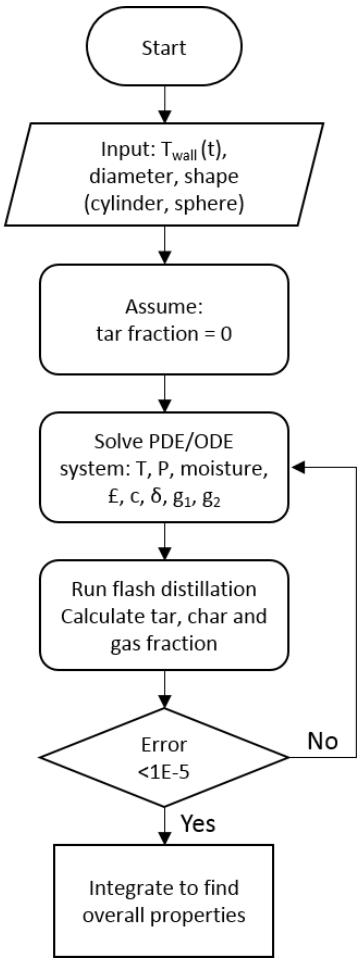

Figure 4.2 Calculation process for the 1-D system coupled with the CPD model

4.3 Results and discussion

4.3.1 Determination of the lignite briquette coal pyrolysis kinetics in TGA

The intrinsic rate of coal devolatilisation without any secondary reactions in a TGA was first tested by using the CPD model. Firstly, the chemical structure parameters must be determined. This is intended to be achieved using ^{13}C NMR spectroscopy, however, these parameters can also be estimated through correlations with the contents of carbon, hydrogen, oxygen and volatile matter in the coal [33, 34]. The approach used by Gnetti et al. was used to determine these parameters [34], with the modification that the calculation of $\sigma + 1$ was re-established using the same fitting equation and the data set of parameters of 30 coals determined by ^{13}C NMR but without omitting outliers such as a lignite which may provide useful information. Despite the extra samples, the r^2 value was increased from 0.24 to 0.36. This modification improved the prediction of mass release and tar yield compared to that experimentally obtained by Tomita et

al. [35]. The prediction of mass release and tar yield were 50.1% and 18.2%, respectively, compared to 51.0% and 21.4% in experiments. The estimated structure parameter values of the lignite based on the modified model are summarised in Table 4.3.

Table 4.3 Estimated chemical structure parameters for use in the CPD model for the lignite tested in this study

Chemical structure parameter	Estimated value for lignite briquette
M_δ	50
M_{cl}	340
p_0	0.68
$\sigma + 1$	3.85
c_0	0.15

Despite the agreement of the model with the experimentally obtained mass release and tar yield reported in the literature [35], there was a poor fit with the mass loss data from TGA obtained here. For the CPD model, the dry-ash-free mass loss is defined as the fraction of light gas and tar produced, assuming that tar will be swept away and will not recombine with the char. Figure 4.3a shows that the CPD model significantly under-predicts the mass loss at lower temperatures, while still accurately predicting the final mass loss. This is attributed to the varying Arrhenius parameters controlling the bridge breaking and gas release reactions, as has been revealed for a Chinese black coal [36], biomass and black liquor [37], and oil shale [38]. Therefore, by finding the best fit using MATLAB software, a new set of kinetic parameters has been obtained, as shown in Table 4.4. Compared to the original data, the activation energy of the bridge-breaking and gas release reactions has been reduced considerably. The activation energy of the cross-linking reaction is also reduced, which is in line with the lower temperature cross-linking behaviour of low-rank coal [39]. Accordingly, the fitted data shows a much improved and satisfactory correlation with mass loss measured in TGA in Figure 4.3b.

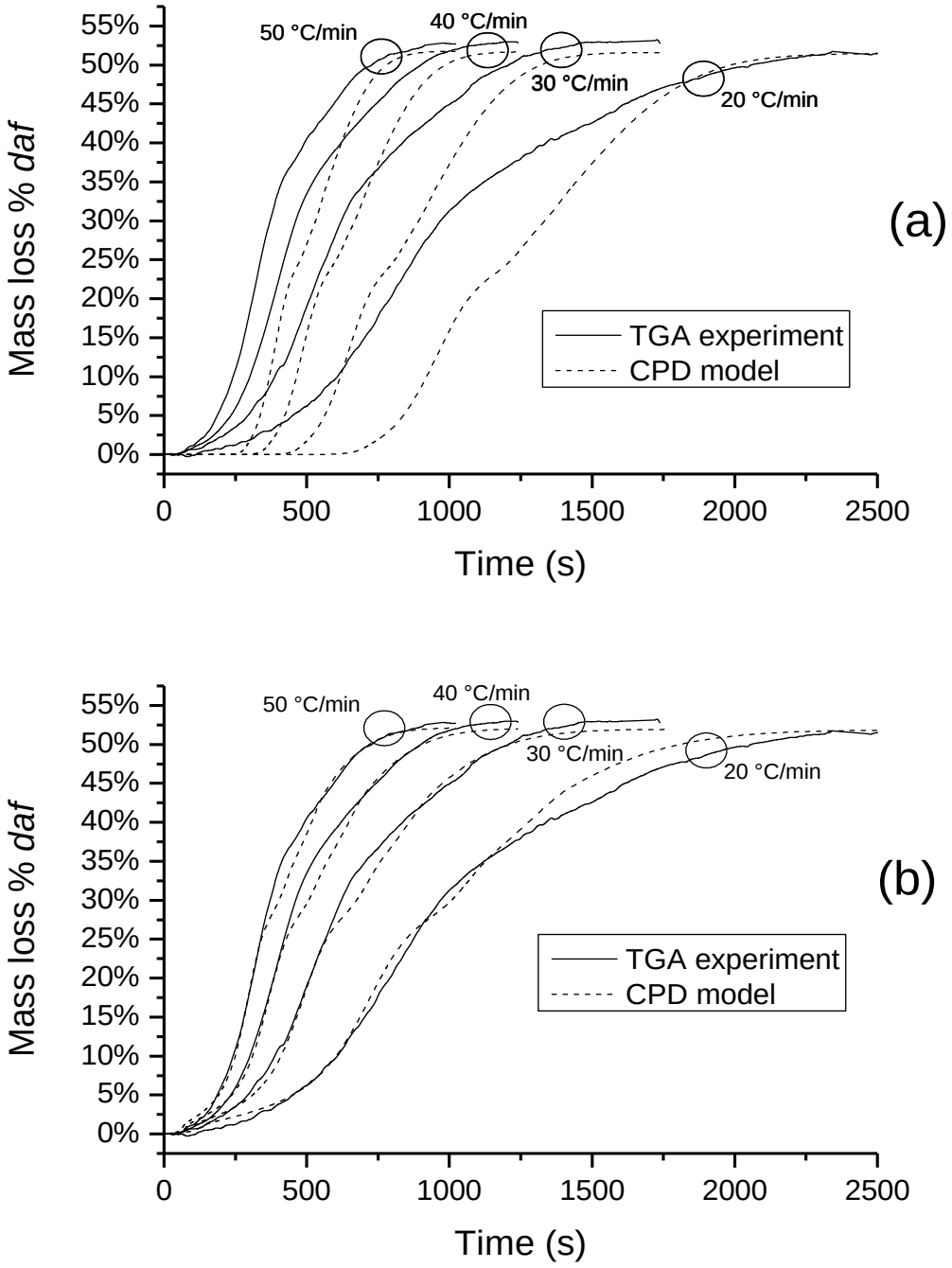

Figure 4.3 Mass loss for coal briquette as a function of time for four heating rates compared to the CPD model result for the (a) original kinetic parameters and (b) refined kinetic parameters.

Table 4.4 Fitted kinetic parameters for use in the CPD model

Parameter	Original CPD model values [10, 26]	Fitted Value
E_b	55400	53000
A_b	2.602×10^{15}	5.4×10^{15}
σ_b	1800	1700
E_g	69000	45000
A_g	3.0×10^{15}	5.0×10^{10}
σ_g	8100	8050
E_{cross}	65000	55000
A_{cross}	3.0×10^{15}	3.55×10^{12}

4.3.2 Density, porosity and permeability changes during pyrolysis

The combined effects of shrinkage and mass loss affect the density of the resultant char during the pyrolysis process. This modelled density can then be compared to experimental values to further validate the modified CPD model. Figure 4.4 shows that the modelling has a good agreement with experimental values and accurately reflects the turning point during the pyrolysis process. Initially, the char density falls due to the release of volatiles and the formation of a porous structure. The continuous release of volatiles leads to a rather linear decrease on the char density. However, from the point for the release of around 70 % of the total volatiles, the density of the remaining char increases. This is a clear indication of a faster shrinkage of the char structure than the release of the remaining volatiles. The shrinkage should be attributed to the collapse and fragmentation of the porous char structure.

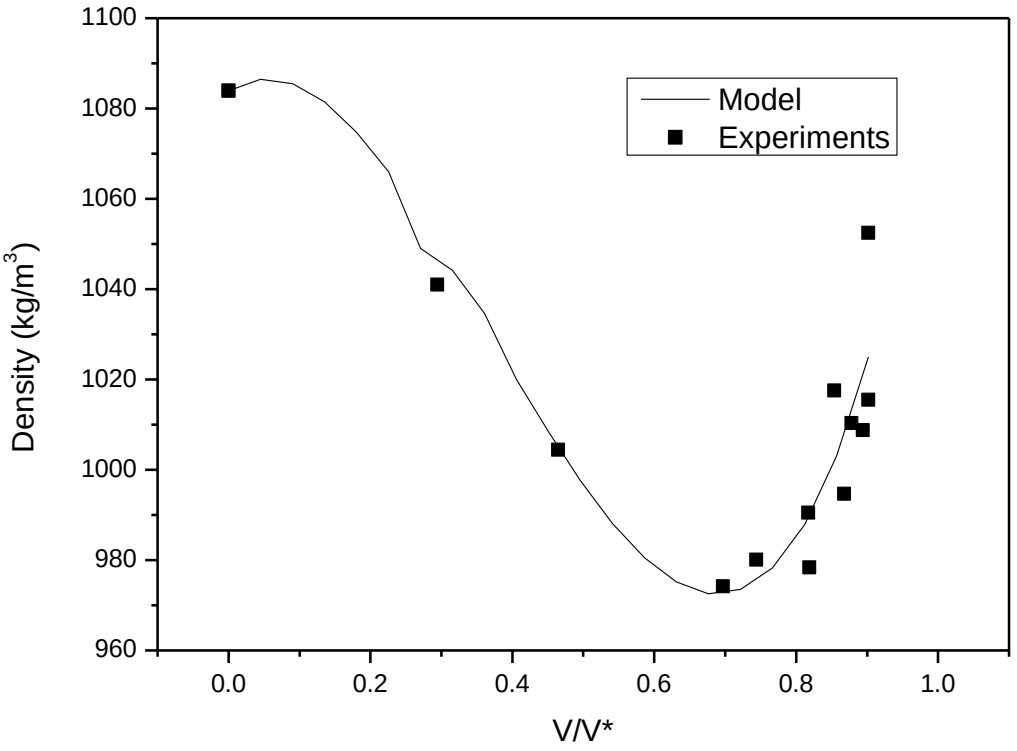

Figure 4.4 Density of the dry coal briquette compared with the expected density based on the modelling of shrinkage and mass loss.

Permeability and porosity are required in the calculation of internal pressure in Equation 4.7. As gasses are generated, including condensable tarry hydrocarbons, light gasses and water vapour, pressure will build up as they diffuse to atmosphere or to lower pressure areas inside the coarse coal particle/briquette. As permeability and porosity increase, gas transport is less obstructed and therefore gasses can escape the particle with less difficulty. In past studies, the permeability of wood was assumed to be 10 mD, while the permeability of wood char was deemed 100 times higher, 1000 mD [40]. For coal, there is a very large range in permeability, for example, Linqard et al found a variation of permeability from 0.1 to 100 mD [41], a span of four orders of magnitude. In this work, the permeability and porosity of char were measured experimentally and the results are shown in Table 4.5. The briquette char has a greater permeability and porosity than the parent briquette. Although the particle densities are similar, the solid density (true density) of the char is higher, due to a larger volume of voids. The pulverised coal and char particles followed the same trend. However, both the permeability and porosity are higher than their respective particle samples, since they were not compressed. In

the model developed hereafter, the permeability is assumed to vary linearly as a function of mass loss relative to the proximate volatile yield.

Table 4.5 Permeability and porosity of lignite and char in particle and briquette forms

	Lignite briquette		Pulverised lignite particles	
	Permeability (mDarcy, mD)	Porosity (%)	Permeability (mDarcy, mD)	Porosity (%)
Dried coal	29	23%	93	39%
Char	86	40%	293	52%

4.3.3 Mass loss during pyrolysis process in the fixed-bed and validation of the model

Figure 4.5a shows the percentage loss of volatiles for the briquette in the fixed-bed reactor, upon slow heating at 10 °C/min to 1000 °C. The majority of the volatiles are released before 600 °C. This is the same as that has been observed upon a similar heating rate in the TG-DTA in Figure 4.3. Up to 700 °C the release of volatiles is relatively fast, however, the rate subsequently diminishes as volatiles are depleted. After 800 °C, only 10% of the volatile matter remains and decreases slowly up to 1000 °C. In the fast heating mode shown in Figure 4.5b, volatile loss increases rapidly up to 91% in 20 min, which is further increased to 96% in 30 min. The remaining volatiles are released slowly up to 60 min. For both heating rates, the modified transient 1-D model coupled with CPD code shows a good agreement.

For the pulverised coal samples in Figure 4.5c, the mass loss decreases slightly as particle size increases from < 2 *mm* to 4-8 *mm*, irrespective of the heating rate. However, increasing the particle size to >8 *mm* lowers the mass loss considerably from 56 to 53%, which is also comparable to the coal briquette that has a mass loss of around 52%. For each size, the mass loss yields are also rather consistent between the two heating rates. The results achieved here are intriguing and indicative of two hypothetical phenomena that could occur at the high-temperature pyrolysis process. First of all, upon a very slow heating, 10 °C/min employed here, both the pulverised coal particles and briquette are expected to experience an identical heat-up profile, the same temperature as the furnace, as well as an even temperature profile on both radial and axial directions for the briquette. Therefore, the mass loss rate is expected to be size - independent, Apparently, this is not the case, hinting that a considerable temperature lag might

still occur for the coarse particle and in particular the briquette. Such a lag may cause a number of consequences other than mass loss. Secondly, for a fast heating rate 100 °C/min employed here, the intra-particle conductive heat transfer is obviously critical for the coarse sizes from >8 *mm* and coal briquette. Although the surface reaches the furnace temperature instantaneously, the centre of the coarse particle and briquette is expected to be heated up slowly, thereby leading to a delay on the release of volatiles from inside the particle/briquette. The released volatiles may also undergo secondary reactions such as coking on the hot edge when it experiences a large temperature gradient as well as encounters the diffusional resistance from the particle tortuosity in the radial direction.

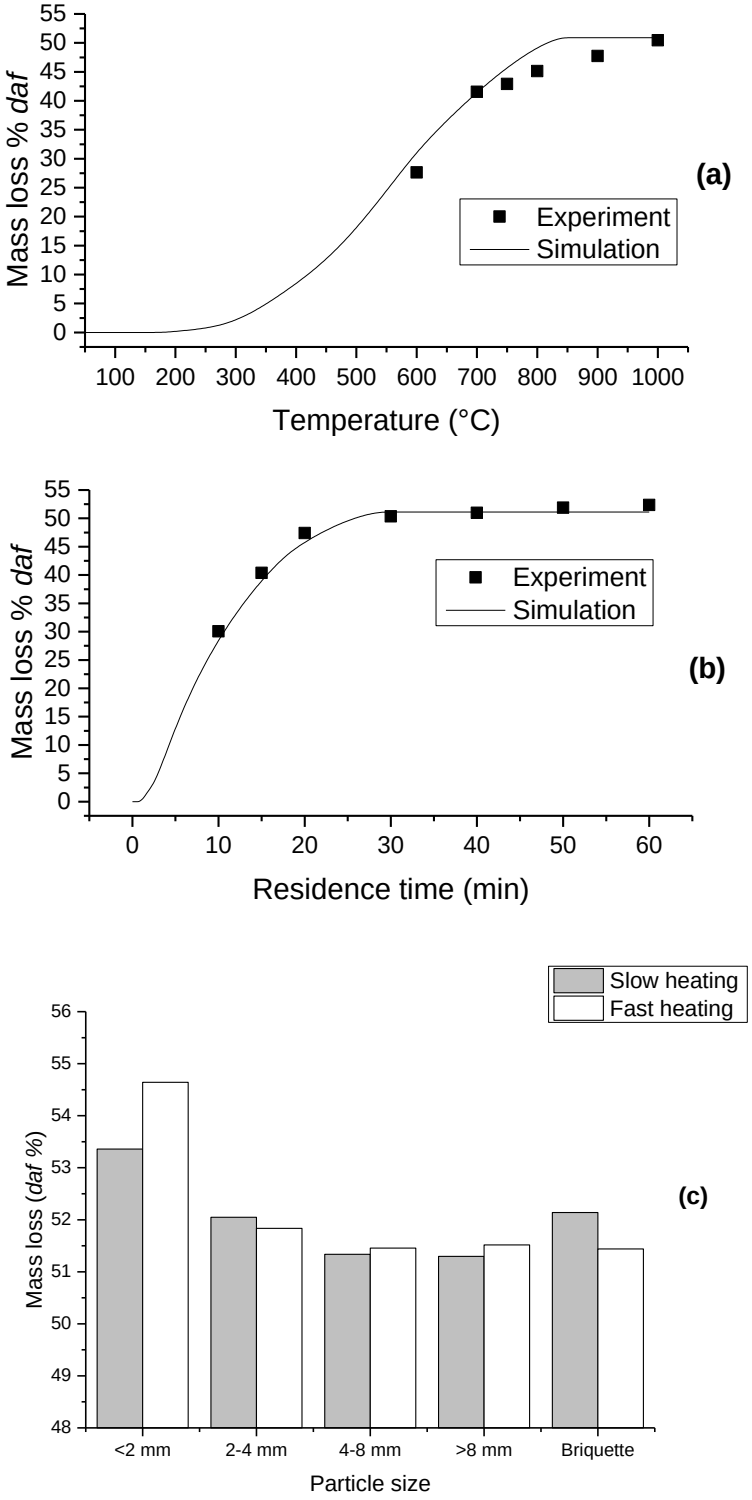

Figure 4.5 Mass loss (daf) for (a) slow heating briquettes, (b) fast heating briquettes, and (c) coal particles at 800 °C.

To prove the afore-mentioned hypothesis, measurement of the temperature at the centre of the coal briquette, upon fast heating, was conducted and also compared with the modelling result. This measurement was achieved by drilling a hole into the centre of coal briquette, then inserting a K-type thermocouple inside the hole. Any gaps between the thermocouple and coal briquette were filled by fine coal particles derived from the same coal briquette. Efforts were not made to measure the coarse size > 8 *mm* because it is not easy to mount the thermocouple into it. As shown in Figure 4.6, both experimental measurement and the modelling prediction suggest an extremely slow heating rate for the centreline of the coal briquette. Compared to the briquette surface that only requires 4.5 min to reach 600 °C where the pyrolysis rate will increase significantly, the centreline requires around 26 min to reach 600 °C, and 30 min to reach the furnace temperature. This obviously delayed the release of volatiles.

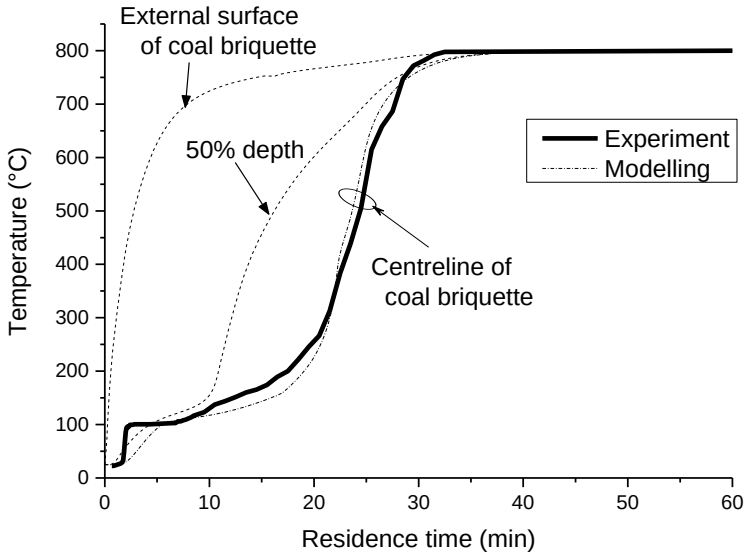

Figure 4.6 Comparison of internal temperature as measured by the model and by experiment

According to the temperature profile for the briquette in Figure 4.6, in just 5 min, a thin layer on the outer surface of the coal briquette reaches about 600 °C and thus begins to pyrolyse, while the inner section plateaus at 100 °C for the continuous evaporation of the inherent moisture. After 15 min, the inherent moisture is completely eliminated and the temperature of the central briquette rises rapidly. However, at this stage the outer surface has turned to around 750 °C that is only 50 °C less than the furnace temperature. Therefore, volatiles are released intensively on the outer surface, but its extent decreases along the radial direction towards the centre of the briquette. After 20 min, only a small portion in the centre remains unreacted. The

process is essentially complete by 25 min when the centreline reaches 600 °C whereas the surface is already 800 °C. The heat transfer limited model developed to some extent resembles a release pattern that would be seen with an unreacted shrinking core model, however, it predicts well for the transition between coal and char. Through further validation of the model, it is possible to model the pyrolysis process, including internal temperature measurements of large particles which are assumed to be spherical. Using average sizes of particles from the 4 size bins, Figure 4.7 depicts that, in the first 3 min upon a fast heating, there can be as much as 500 °C temperature difference between 400 μm sized particles and those of 11 *mm* in diameter (as shown in panel a), although the extra time taken to heat up those coarse particles is relatively short. For all the pulverised sizes <8 *mm*, the release of volatiles appears to be independent on the particle size, as evident in panel b. In other words, the intra-particle heat transfer rate is sufficiently high. Beyond the particle size of 8 *mm*, the coal conversion rate is slightly delayed for around 1 min upon the intra-particle heat transfer resistance. Moreover, the briquette requires a much longer time to reach the reactor temperature and thus conversion is considerably slowed.

For the slow heating at 10 °C/min, all the coal particles except the largest size > 8 *mm* show a very close temperature to the furnace temperature, as shown in Figure 4.8a. In contrast, the coal briquette can have a temperature difference as high as 400 °C between the centre and the furnace. Prior to the furnace reaching 600 °C, the centre of coal briquette remains at 100 °C for a continuous release of the inherent moisture. Once the furnace temperature reaches 600 °C, the centre of the briquette rapidly heats up. This means that part of the briquette will have a heating rate higher than that of the pulverised particles, although the centre zone only represents a small portion of the overall mass for the whole briquette. Due to the delayed heating of the overall briquette, it takes 30 min more for the devolatilisation reaches complete for the coal briquette, as evident in Figure 4.8b.

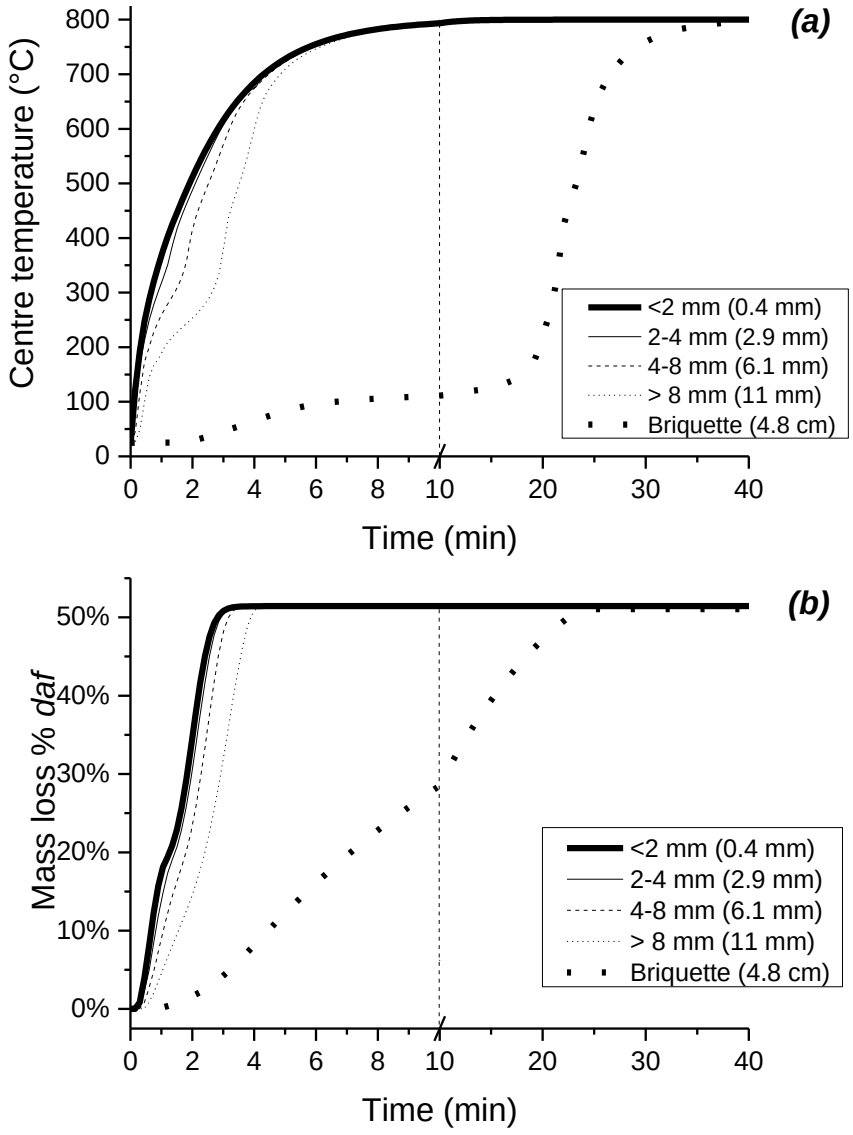

Figure 4.7 (a) Centre temperature and (b) pyrolysis conversion for pulverised lignite particles and briquette under the fast heating (100 °C/min) regime up to 800 °C

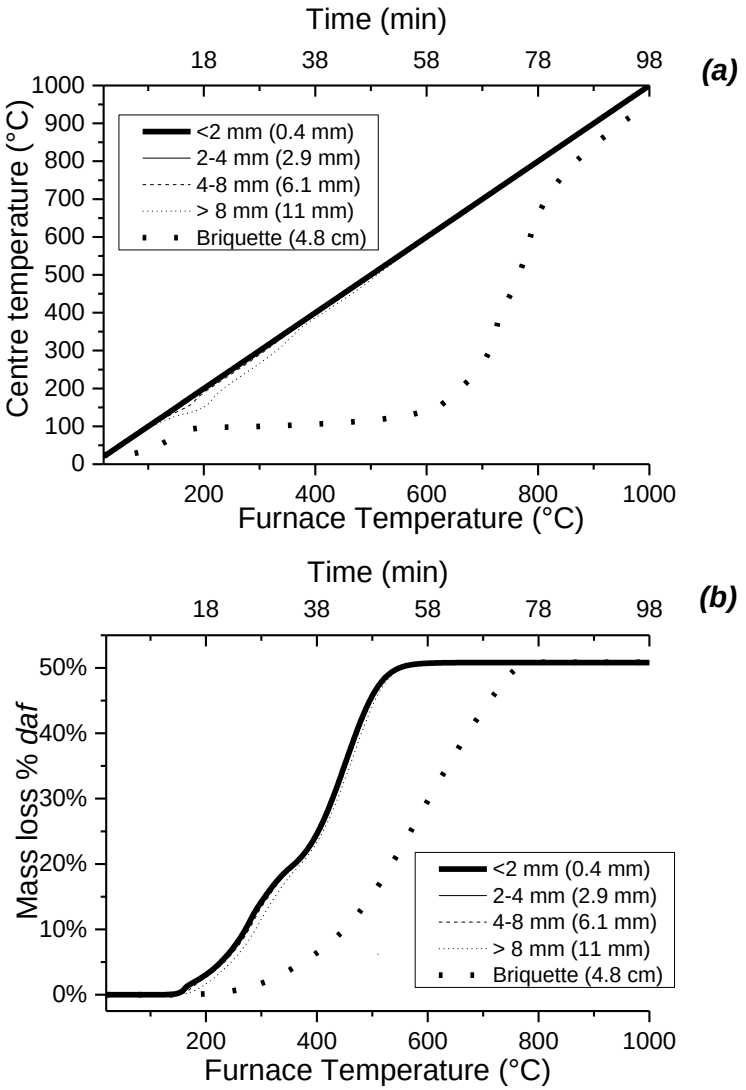

Figure 4.8(a) Centre temperature and (b) pyrolysis conversion for pulverised lignite particles and briquette under the slow heating (10 °C/min) regime up to 800 °C

4.3.4 Tar release and radical changes during the pyrolysis process

Due to the remarkable considerable difference of temperature and volatile release yield between pulverised coal and briquette, the yield and quality of liquid tar as well as the concentration of radicals in solid char are expected to vary considerably [13]. Both the yield and composition of the pyrolysis tar are affected by the extent of its secondary reactions within the char matrix, and even between different char particles [42]. On the other hand, the radical concentration is highly dependent on the temperature of char particles. In light of this, both these two properties have been measured. The tar yield was also predicted by the 1-D model coupled with the CPD model in which the secondary reactions of tar within the solid char

matrix have been considered. The results are depicted in Figure 4.9. Clearly, the model prediction results are reasonably consistent with the experimental values, given that the secondary reactions of tar are very complex in nature. Even so, the discrepancy between the model and the experiment is still noteworthy, which could be attributed to the secondary reactions such as the thermal cracking of tar occurring in the gas phases. This is especially the case for the fast heating scenario where the gas would be much hotter during tar release. Unfortunately, the secondary reactions for tar in the gas phase were not considered here. Irrespective of the heating rate, the briquette shows the lowest tar yield, supporting the expectation that the secondary reactions for the primary tar were enhanced inside the coal briquette. In contrast, the extent of these side reactions is insignificant for all the pulverised coal sizes, suggesting that the inter-particle diffusion of the primary tar is not influential in promoting the secondary reactions. Additionally, since the overall mass loss for a briquette is rather similar with the coarse pulverised coal particles in Figure 4.5, it is inferred that the primary tar mainly underwent the decomposition to convert into light hydrocarbons or gases. The lignite char has proven to be catalytic on the steam/CO_2 reforming of primary tar [43].

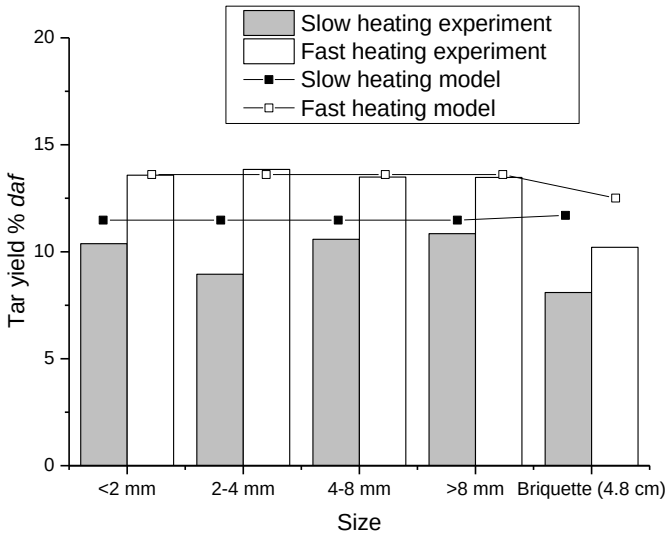

Figure 4.9 Tar yield predicted by the CPD model and from the experiment

The tar samples were further analysed by GC-MS and the chromatographs are shown in Figure 4.10. Table 4.6 summarises the area – based percentages of the major peaks found on the GC-MS chromatograph, as well as the ratios between different groups. Note that, since a portion of heavy hydrocarbons are not able to elute out of the GC-MS column, the results in Figure

4.10 and Table 4.6 are interpreted from a semi-quantitative or even qualitative perspective. Firstly, the heating rate is influential. It is obvious that the proportions of longer chain groups (over 40 min) including alkane >C18 and alkene >C11 are generally high in the slow heating scenario, irrespective of coal size; while under the fast heating there is a greater proportion of light liquids including benzene, cresol and phenol. Assuming the elution of alkane and alkene is complete in the GC-MS analysis, the area ratio of these two groups in Table 4.6 further strength the abundance of light hydrocarbons formed under the fast heating scenario. One the one hand, difference of the previously discussed temperature-profile between the two different heating rates can partly explain this difference. At slow heating rates, the temperature of the tar released is very close to and even identical with the furnace, thereby taking little opportunity to undergo any secondary reactions such as thermal cracking for the heavy hydrocarbons that are released at the later stage of the pyrolysis. The opposite phenomena shall be inferred for the fast heating scenario, the great temperature difference between particle (thus tar out of it) and wall induced the intense secondary reactions of the primary tar such as thermal cracking, thereby resulting in the formation of abundant light fragments and gases.

There is little variation in tar composition for different pulverised coal sizes. Instead, the difference between pulverised coal and briquette is obvious in both the heating scenarios. In the slow heating mode, less heavy hydrocarbons including alkane and alkene are formed from the briquette. Instead, the formation of light benzene, phenol and cresol are favoured from the briquette. Such a difference is in line with the above-mentioned difference between the two heating rates. That is, the fast heating encountered within coal briquette even during the slow heating mode, as shown in Figure 4.8 intensified the secondary reactions for the primary tar released from coal briquette. Apart from the fragmentation into lighter hydrocarbons, a portion of the primary tar from coal briquette shall also decompose into gases, as evident by the decrease on the overall tar yield for briquette in Figure 4.9. The intra-particle diffusion resistance within coal briquette shall also be in favour of promoting the secondary reactions for the primary tar. The abundant alkali and alkaline earth metals, and even iron within lignite have proven to be catalyst for tar reforming [43]. These secondary reactions even include the deoxygenation reaction resulting in the formation of less oxygen-bearing species in the tar, in particular under the fast heating scenario shown in Table 4.6.

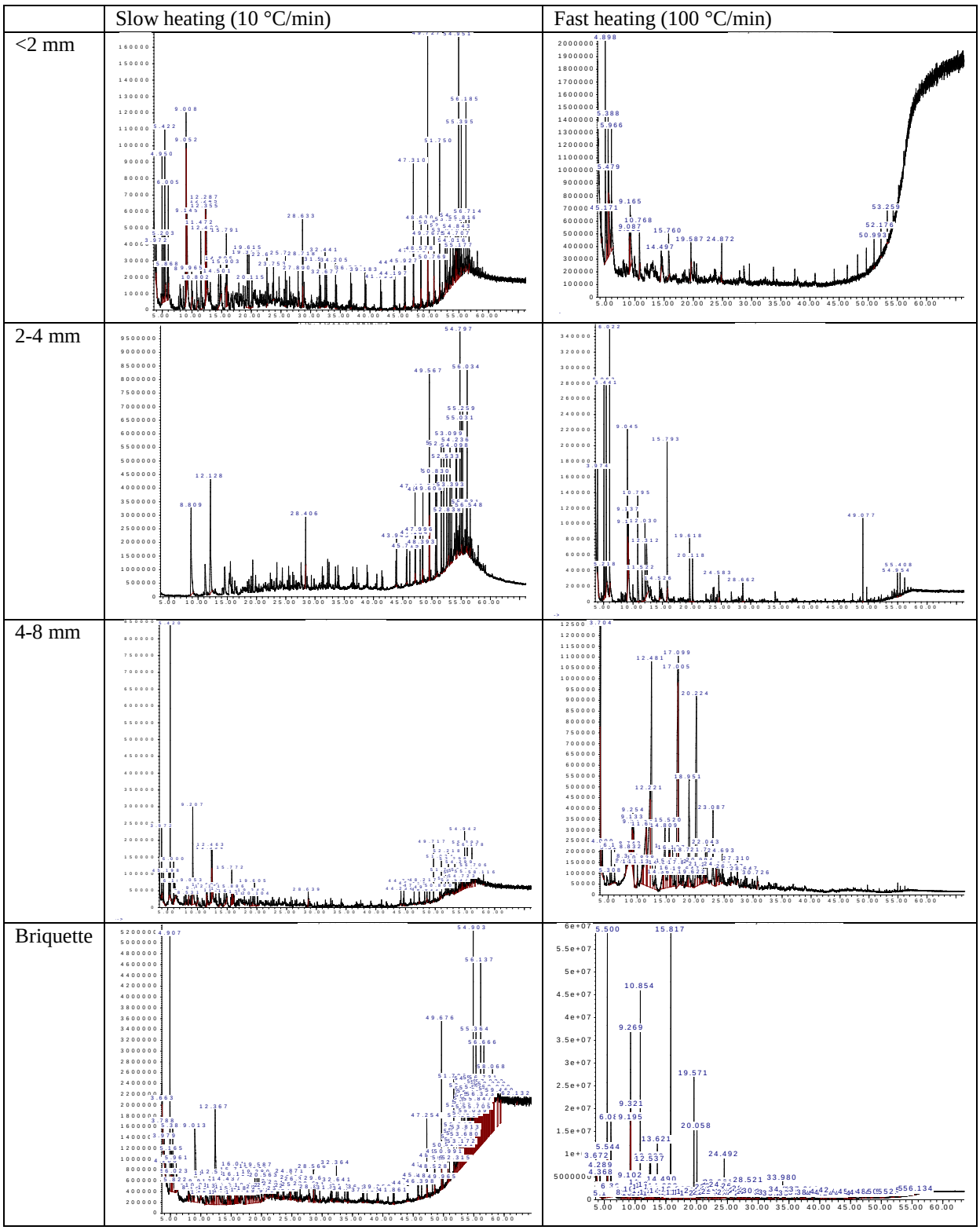

Figure 4.10 GC-MS chromatographs for tar created under slow heating (10 °C/min) and fast heating (100 °C/min) for coal particles and briquette.

Table 4.6 Component relative area % from GC-MS result

Name	Carbon No.	Slow heating (10 °C/min)				Fast heating (100 °C/min)			
		<2	2-4	4-8	Briquette	<2	2-4	4-8	Briquette
Benzene, >C_3	>C_6H_4, C_3	2.32		2.01	5.61	23.86	17.76	1.82	14.14
Naphthalene	$C_{10}H_8$	5.94	5.75	8.06	5.29	5.06	17.72	0.29	26.92
Phenol	C_6H_5OH	10.61	8.55	11.21	9.18	-	17.07	6.13	8.57
Cresol	C_6H_4OH, C_1	13.30	13.06	8.84	14.05	-	11.33	29.94	3.52
Phenol, >C_1	C_6H_4OH, >C_2	6.27	8.37	4	7.56	12.31	-	12.89	2.34
Benzenediol	$C_6H_6O_2$	-	-	-	11.75	-	-	24.67	0.34
Ketone	$C_6H_{12}O_2$	2.16	0.79	16.35	11.59	20.2	10.81	1.42	16.6
Alkane	>C_{18}	-	56.86	34.89	21.01	15.9	-	-	7.74
Alkene,yne	>C_{11}	44.25	-	-	1.21	-	5.93	-	-
Xylene	C_6H_5, C_2	6.97	-	2.82	-	10.28	9.7	2.52	-
Acetic acid	$C_2H_4O_2$	-	-	-	-	5.25		2.9	-
Unknown compounds		8.20	6.62	11.82	12.73	7.13	9.67	17.42	19.84
Ratio of (Benzene+Naphthalene +phenol+cresol)/(alkane + alkene)		0.87	0.63	0.98	1.88	2.59	10.8	NaN	7.17

Efforts were also made to characterise the free radical content remaining in the briquette char matrix, which is another evidence reflecting the extent of secondary reactions in an overall pyrolysis process. The radicals in a solid char are formed by thermal cracking of covalent bonds. At higher temperatures, these radicals may assist in the pyrolysis process which will diminish their concentration, as they form volatile (tar and gas) and non-volatile products (char) [44]. Figure 4.11 shows the change in concentration of radicals with pyrolysis temperature and holding time. For the slow heating samples, radical concentration increases with temperature up until 800 °C which shows the highest radical concentration. Upon a further increase on the temperature, the participation of radicals in cross-linking reactions should dominate. In the fast heating mode, radical concentration increases up to a holding time of 15 min then subsequently decreases. Back to the temperature profile for briquette in Figure 4.6, such a time should respond to the halfway for the whole briquette to reach the furnace temperature. At this point tar production is visibly beginning to increase, which is also rich in radical species [13]. Figure 4.12 compares the radical concentration to the volatile yield (relative to the proximate analysis volatile content) achieved from both two heating modes. Initially, the radical concentration rises rapidly from 4×10^{17} spins/g to ~8×10^{18} spins/g at 28% volatile release. From 25% to 80% the radical concentration is fairly stable, peaking at ~2×10^{19} at 75% volatile release. Further

release of volatiles requires harsher conditions, causing the concentration of radicals to fall to as low as 1×10^{18} due to the increase in polymerisation and release of volatiles at the temperatures required to achieve these conversions. The turning point found here is also the same as that found for the shrinkage of char density in Figure 4.4 Density of the dry coal briquette compared with the expected density based on the modelling of shrinkage and mass loss.. Additionally, the correlation found here was compared to a similar analysis by Qiu, et al. [45] in a study that compared the radical concentration to mass loss for a sub-bituminous coal found in Weihuliang, Xinjiang, China. Mass loss was converted to relative volatile release using a proximate analysis result of 36.3% volatiles (db) in a separate paper that used Weihuliang coal [46]. The change in radical content followed a similar to trend to that of the briquette studied here. However, the radical concentrations in the briquette char samples studied here are generically larger than in the Chinese sub-bituminous coal. This is another indication of the high reactivity for the lignite studied here, as it has been shown before that radical concentration may be linked to oxidation reactivity [47].

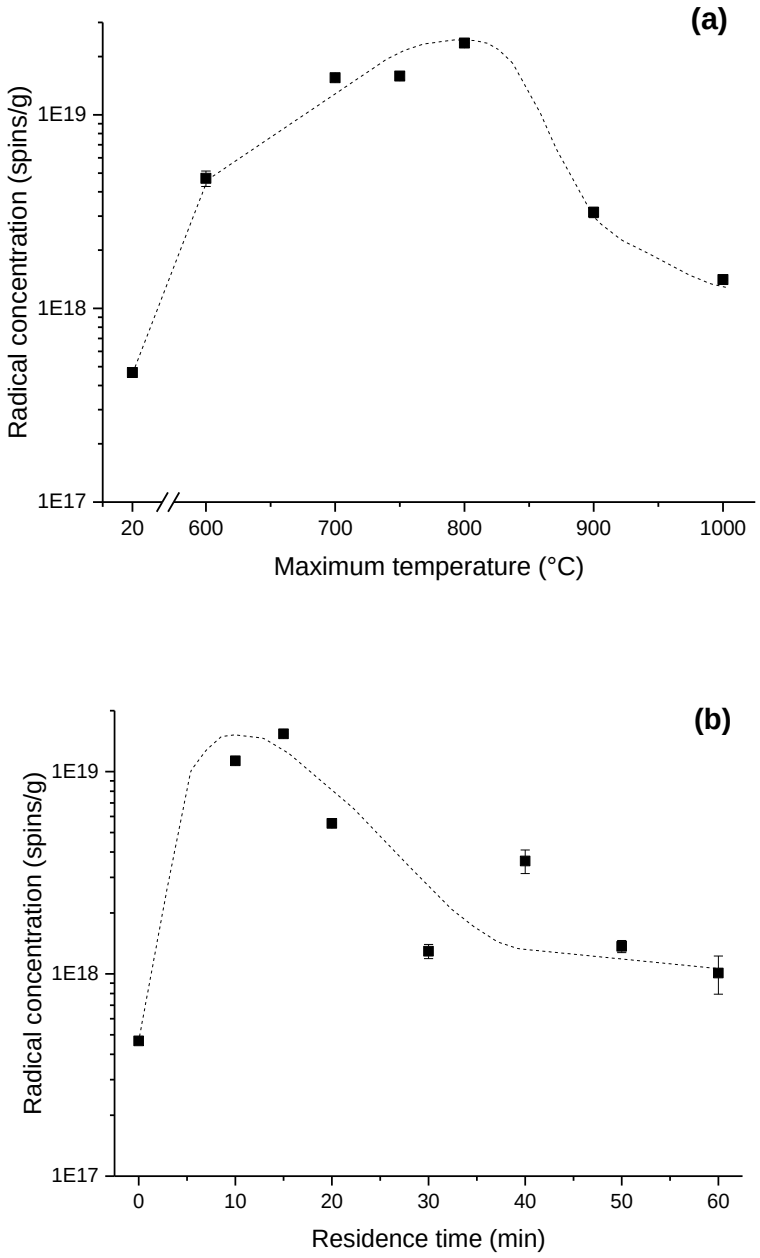

Figure 4.11 Radical concentration (db) for briquette char pyrolyzed under slow (a) and fast (b) heating regimes. Note, the final temperature for fast heating is 800ºC.

The concentrations of radicals for the char samples derived from respective pulverised lignite is also included in Figure 4.12. These concentrations were presumed to follow the same trend as found for the lignite briquette. This is obviously not the case when a fast heating is employed for the pyrolysis. For the pulverised coal particles, the concentrations of radicals in the fast

heating chars are generally larger than in the slow heating char samples, due to the enhanced cross-linking reactions for the radicals upon a long residence inside the reactor [48], same as that has been confirmed for the intensified secondary reaction for the tarry species in above sub-section. Concentrations of radicals in the fast heating (100 °C/min) samples are also higher than the char sample derived from the respective briquette, although the coal briquette experienced a much larger temperature rise than its pulverised counterparts in Figure 4.7a. Clearly, under the typical time scheme encountered upon fast heating, the negative effect of internal diffusion within briquette char matrix is superior, which intensified the secondary reactions for the primary radicals. For the results for the slow heating char samples derived from the pulverised lignite quite, they follow the trend that can be extrapolated from briquette char. This means the diffusion resistance within briquette char turns insignificant upon a slow heating scenario under which the residence time of char is longer enough to cancel off any other negative factors.

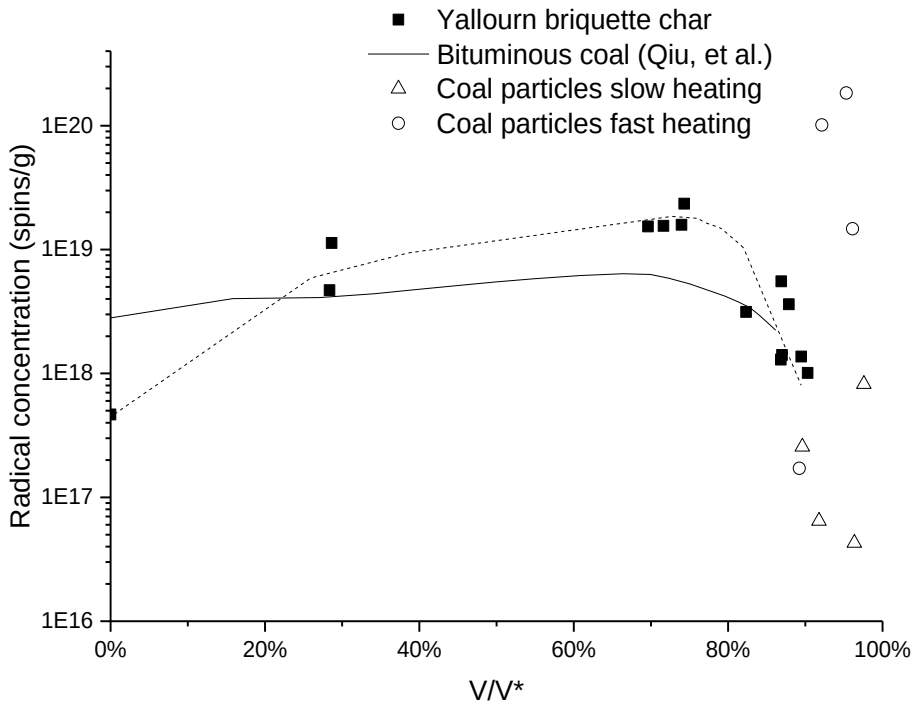

Figure 4.12 Radical concentration compared to relative pyrolysis yield for lignite briquette pyrolysis and Weihuliang bituminous coal [45].

The radical concentration results are also well correlated with the coal structure change that can be predicted by the developed model. Figure 4.13 shows the changes in coal structure as a

function of temperature and residence time for coal briquette and pulverised particles, based on the CPD model prediction. During the initial stages, the bonds between bridges are cleaved, resulting in the formation of detached side chains, gas and tar precursor fragments. This occurs at around 300 °C for the slow heating sample (*panel a*) while takes place almost instantaneously under the fast heating rate (*panel b*). This rupturing of bonds in the initial stages of pyrolysis has been hypothesized as a cause of the formation of radicals [42, 49]. This correlates to the increase in radicals in both Figure 4.11 and Figure 4.12, where the radicals increase during the time spans when bridges are broken, up to 600 °C for slow heating (in *panel a*) and up to 15 min for fast heating (in *panel b*). Beyond 300 °C, tar will begin to be generated and later cross-linking will occur, which appears to be linked with the subsequent downturn in radical concentration in Figure 4.11b and Figure 4.12. Radical fragments can be coupled together to form cross-links during the repolymerisation process, forming irreversible bonds unlike the labile bonds in coal [50]. Since the cross-linking process relies on free radicals, it is reliant on the radical formation process so therefore takes place at higher temperatures. Additionally, Figure 4.13b explains the cross-linking occurs at a delayed time and its extent is also greater in coal briquette than in pulverised particles, more so during fast heating. This corresponds to the reduced release of tar (see Figure 4.9) and fewer radicals in the briquette char (see Figure 4.12). With regarding the slow heating rate results in Figure 4.13a, 800 °C is clearly the threshold temperature beyond which the yield of tar and cross-linking reaction extent should be identical between pulverised coal and the briquette. This is in line with the results in Figure 4.9 and Figure 4.12.

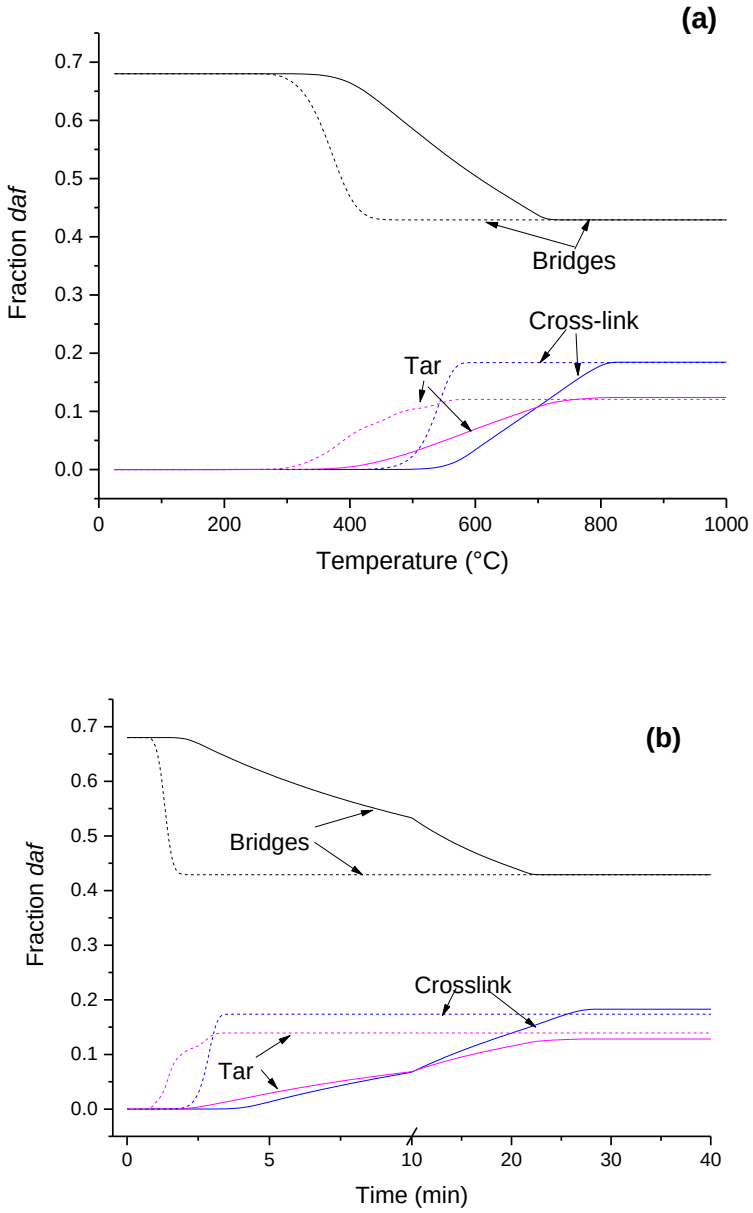

Figure 4.13 Structural changes in the char and tar generation predicted by the CPD model for (a) slow and (b) fast heating to 800 °C for coal briquette (–––) and 3 *mm* diameter pulverised coal particles (---).

4.4 Conclusions

Lignite pyrolysis process has been conducted experimentally and modelled for pulverised particle and briquette sizes that are large enough for a homogenous entity to be a gross oversimplification. A fixed-bed, batch-scale reactor and two typical different heating rates have been tested. Apart from conversion, the tar yield, composition and radical concentration in char

were also measured to explore the difference between lignite briquette and the respective pulverised powder. Additionally, a 1-D model coupled with classic CPD code was developed to reveal the temperature profile within the single briquette particle and its structure change upon pyrolysis.

The following major conclusions have been achieved:

1. The coupling of 1-D modelling and modified CPD code is able to satisfactorily predict the lignite briquette mass loss rate, temperature profile, tar yield and the time-resolved change on coal structure. All the predictions from the model have been fully validated.
2. The non-uniform temperature profile in coal briquette is the largest factor making the pyrolysis of briquette different from the pulverised particles. Even under a slow heating of only 10 °C/min, the middle of coal briquette remains at 100 °C due to the continuous evaporation of the inherent moisture. Upon the completion of moisture evaporation, the coal briquette undergoes a rapid temperature rise, and simultaneously abrupt release of volatiles. The temperature lag is more obvious under the fast heating mode, requiring a longer residence of 20-30 min at the final temperature to ensure the complete release of volatile matter, relative to only a few minutes required for the pulverised parent coal with a maximum size up to 8 *mm*.
3. The temperature gradient competes with the internal diffusion on the yield and compositions of tar. Upon a slow heating, the great temperature variation within coal briquette is superior in promoting the secondary reactions for the volatiles (precursor of the primary tar). However, for a fast heating that the residence time is much shorter, the internal diffusion is more influential in decomposing the primary heavy species.
4. The pyrolysis stage where around 80% volatiles is released is the optimum condition for maximising the radical concentration (and thus reactivity) of the char of coal briquette. This occurs at a final temperature of 800^{o}C upon slow heating, or in 15 min upon a fast heating to 800^{o}C. The use of harsher conditions intensifies the cross-linking and polymerisation of the radical fragments, although the density of the char is improved considerably.

References

1. Li, C. Z., *Advances in the Science of Victorian Brown Coal*. Elsevier Science: 2004.
2. Department of Industry Innovation and Science, Resources and Energy Quarterly. In Australian Government,: December 2016.
3. Tillman, D., *The Combustion of Solid Fuels and Wastes*. Elsevier Science: 2012.
4. Durie, R. A., *The Science of Victorian brown coal : structure, properties, and consequences for utilization*. Butterworth-Heinemann: Oxford, 1991; p xvi, 750 p.
5. Li, C.-Z., Some recent advances in the understanding of the pyrolysis and gasification behaviour of Victorian brown coal. *Fuel* **2007,** 86, (12), 1664-1683.
6. Yip, K.; Wu, H.; Zhang, D.-k., Pyrolysis of Collie Coal Briquettes To Produce Char as a Metallurgical Reductant. *Energy & Fuels* **2007,** 21, (2), 419-425.
7. Yip, K.; Wu, H.; Zhang, D.-k., Mathematical modelling of Collie coal pyrolysis considering the effect of steam produced in situ from coal inherent moisture and pyrolytic water. *Proceedings of the Combustion Institute* **2009,** 32, (2), 2675-2683.
8. Massaro, M. M.; Son, S. F.; Groven, L. J., Mechanical, pyrolysis, and combustion characterization of briquetted coal fines with municipal solid waste plastic (MSW) binders. *Fuel* **2014,** 115, 62-69.
9. Blesa, M. J.; Miranda, J. L.; Moliner, R.; Izquierdo, M. T.; Palacios, J. M., Low-temperature co-pyrolysis of a low-rank coal and biomass to prepare smokeless fuel briquettes. *Journal of Analytical and Applied Pyrolysis* **2003,** 70, (2), 665-677.
10. Fletcher, T. H.; Kerstein, A. R.; Pugmire, R. J.; Solum, M. S.; Grant, D. M., Chemical percolation model for devolatilization. 3. Direct use of carbon-13 NMR data to predict effects of coal type. *Energy & Fuels* **1992,** 6, (4), 414-431.
11. Pullen, J. R., Solvent Extraction of Coal. In *Coal Science*, Larsen, J. W.; Wender, I., Eds. Academic Press: 1983; Vol. 2, pp 173-288.
12. Liu, M.; Yang, J.; Liu, Z.; He, W.; Liu, Q.; Li, Y.; Yang, Y., Cleavage of Covalent Bonds in the Pyrolysis of Lignin, Cellulose, and Hemicellulose. *Energy & Fuels* **2015,** 29, (9), 5773-5780.
13. He, W.; Liu, Z.; Liu, Q.; Liu, M.; Guo, X.; Shi, L.; Wu, J.; Guo, X.; Ci, D., Analysis of tars produced in pyrolysis of four coals under various conditions in a viewpoint of radicals. *Energy & Fuels* **2015,** 29, (6), 3658-3663.
14. Webb, P. A., An introduction to the physical characterization of materials by mercury intrusion porosimetry with emphasis on reduction and presentation of experimental data. *Micromeritics Instrument Corp, Norcross, Georgia* **2001**.
15. Hagge, M. J.; Bryden, K. M., Modeling the impact of shrinkage on the pyrolysis of dry biomass. *Chemical Engineering Science* **2002,** 57, (14), 2811-2823.
16. Grønli, M. G.; Melaaen, M. C., Mathematical Model for Wood PyrolysisComparison of Experimental Measurements with Model Predictions. *Energy & Fuels* **2000,** 14, (4), 791-800.
17. Galgano, A.; Blasi, C. D., Modeling wood degradation by the unreacted-core-shrinking approximation. *Industrial & engineering chemistry research* **2003,** 42, (10), 2101-2111.
18. Moghtaderi, B.; Novozhilov, V.; Fletcher, D.; Kent, J., An integral model for the transient pyrolysis of solid materials. *Fire and Materials* **1997,** 21, (1), 7-16.
19. Kosowska-Golachowska, M.; Gajewski, W.; Musiał, T., Determination of the effective thermal conductivity of solid fuels by the laser flash method. *Archives of Thermodynamics* **2014,** 35, (3), 3-16.

20. Zhang, J.; Prationo, W.; Zhang, L.; Zhang, Z., Computational Fluid Dynamics Modeling on the Air-Firing and Oxy-fuel Combustion of Dried Victorian Brown Coal. *Energy & Fuels* **2013,** 27, (8), 4258-4269.
21. Brown, M. E.; Maciejewski, M.; Vyazovkin, S.; Nomen, R.; Sempere, J.; Burnham, A.; Opfermann, J.; Strey, R.; Anderson, H. L.; Kemmler, A.; Keuleers, R.; Janssens, J.; Desseyn, H. O.; Li, C.-R.; Tang, T. B.; Roduit, B.; Malek, J.; Mitsuhashi, T., Computational aspects of kinetic analysis: Part A: The ICTAC kinetics project-data, methods and results. *Thermochimica Acta* **2000,** 355, (1–2), 125-143.
22. Miura, K., A new and simple method to estimate f (E) and k0 (E) in the distributed activation energy model from three sets of experimental data. *Energy & Fuels* **1995,** 9, (2), 302-307.
23. Miller, R.; Bellan, J., A generalized biomass pyrolysis model based on superimposed cellulose, hemicelluloseand liqnin kinetics. *Combustion science and technology* **1997,** 126, (1-6), 97-137.
24. Solomon, P. R.; Hamblen, D. G.; Carangelo, R.; Serio, M.; Deshpande, G., General model of coal devolatilization. *Energy & Fuels* **1988,** 2, (4), 405-422.
25. Niksa, S.; Kerstein, A. R., FLASHCHAIN theory for rapid coal devolatilization kinetics. 1. Formulation. *Energy & Fuels* **1991,** 5, (5), 647-665.
26. Grant, D. M.; Pugmire, R. J.; Fletcher, T. H.; Kerstein, A. R., Chemical model of coal devolatilization using percolation lattice statistics. *Energy & Fuels* **1989,** 3, (2), 175-186.
27. Bryden, K. M.; Ragland, K. W.; Rutland, C. J., Modeling thermally thick pyrolysis of wood. *Biomass and Bioenergy* **2002,** 22, (1), 41-53.
28. Herington, E., *Recommended Reference Materials for Realization of Physicochemical Properties: Pressure–Volume–Temperature Relationships*. Elsevier: 2013.
29. Sengers, J.; Watson, J. T. R., *Improved international formulations for the viscosity and thermal conductivity of water substance*. 1986.
30. Lockwood, F.; Rizvi, S.; Shah, N., Comparative predictive experience of coal firing. *Proceedings of the Institution of Mechanical Engineers, Part C: Journal of Mechanical Engineering Science* **1986,** 200, (2), 79-87.
31. Chui, E.; HUGHES, P. M.; Raithby, G., Implementation of the finite volume method for calculating radiative transfer in a pulverized fuel flame. *Combustion Science and Technology* **1993,** 92, (4-6), 225-242.
32. McAdams, W. H., Heat transmission, 3rd. *New York* **1954**.
33. Genetti, D.; Fletcher, T.; Pugmire, R. In *Predicting^ 1^ 3C NMR Measurements of Chemical Structure of Coal Based on Elemental Composition and Volatile Matter Content*, PREPRINTS OF SYMPOSIA-DIVISION OF FUEL CHEMISTRY AMERICAN CHEMICAL SOCIETY, 1997; 1997; pp 194-198.
34. Genetti, D.; Fletcher, T. H.; Pugmire, R. J., Development and Application of a Correlation of 13C NMR Chemical Structural Analyses of Coal Based on Elemental Composition and Volatile Matter Content. *Energy & Fuels* **1999,** 13, (1), 60-68.
35. Xu, W.-C.; Tomita, A., Effect of coal type on the flash pyrolysis of various coals. *Fuel* **1987,** 66, (5), 627-631.
36. Yan, B.; Cheng, Y.; Xu, P.; Cao, C.; Cheng, Y., Generalized model of heat transfer and volatiles evolution inside particles for coal devolatilization. *AIChE Journal* **2014,** 60, (8), 2893-2906.
37. Fletcher, T. H.; Pond, H. R.; Webster, J.; Wooters, J.; Baxter, L. L., Prediction of Tar and Light Gas during Pyrolysis of Black Liquor and Biomass. *Energy & Fuels* **2012,** 26, (6), 3381-3387.

38. Fletcher, T. H.; Barfuss, D.; Pugmire, R. J., Modeling Light Gas and Tar Yields from Pyrolysis of Green River Oil Shale Demineralized Kerogen Using the Chemical Percolation Devolatilization Model. *Energy & Fuels* **2015,** 29, (8), 4921-4926.
39. Solomon, P.; Fletcher, T.; Pugmire, R., Progress in coal pyrolysis. *Fuel* **1993,** 72, (5), 587-597.
40. Hagge, M. J., A numerical model for biomass pyrolysis. **2005**.
41. Lingard, P.; Phillips, H.; Doig, I., The permeability of some Australian coals. *Seam gas drainage with particular reference to the working seam,(Ed.: Hargraves, AJ), University of Wollongong, Wollongong, Australia* **1982**, 70-80.
42. Liu, Z.; Liu, Q.; He, W.; Guo, X.; Shi, L. In *Analysis of Coal Pyrolysis Technologies from a Radical Reaction Point of View*, APEC Symposium on Energy Efficiency of Low Rank Coal, Beijing, China, 2012; Beijing, China, 2012.
43. Min, Z.; Yimsiri, P.; Asadullah, M.; Zhang, S.; Li, C.-Z., Catalytic reforming of tar during gasification. Part II. Char as a catalyst or as a catalyst support for tar reforming. *Fuel* **2011,** 90, (7), 2545-2552.
44. Liu, Z.; Guo, X.; Shi, L.; He, W.; Wu, J.; Liu, Q.; Liu, J., Reaction of volatiles – A crucial step in pyrolysis of coals. *Fuel* **2015,** 154, 361-369.
45. Qiu, N.; Li, H.; Jin, Z.; Zhu, Y., Temperature and time effect on the concentrations of free radicals in coal: Evidence from laboratory pyrolysis experiments. *International Journal of Coal Geology* **2007,** 69, (3), 220-228.
46. Li, J.; Zhuang, X.; Querol, X.; Font, O.; Moreno, N.; Zhou, J., Environmental geochemistry of the feed coals and their combustion by-products from two coal-fired power plants in Xinjiang Province, Northwest China. *Fuel* **2012,** 95, 446-456.
47. Ünal, S.; Wood, D. G.; Harris, I. J., Effects of drying methods on the low temperature reactivity of Victorian brown coal to oxygen. *Fuel* **1992,** 71, (2), 183-192.
48. Solomon, P. R.; Serio, M. A.; Despande, G. V.; Kroo, E., Cross-linking reactions during coal conversion. *Energy & Fuels* **1990,** 4, (1), 42-54.
49. Hong, C.; Wang, Z.; Xing, Y.; Li, Y.; Yang, Q.; Jia, M.; Feng, L., Investigation of free radicals and carbon structures in chars generated from pyrolysis of antibiotic fermentation residue. *RSC Advances* **2016,** 6, (112), 111226-111232.
50. Stein, S. E., Free Radicals in Coal Conversion. In *Chemistry of Coal Conversion*, Schlosberg, R. H., Ed. Springer US: Boston, MA, 1985; pp 13-44.

This page is intentionally left blank

Chapter 5 – Pyrolysis of Lignite Briquette – Sensitivity of the Properties of Char upon the Variation in Pyrolysis Condition

Chapter 4 provided a greater understanding of the pyrolysis mechanism and also an appropriate method of modelling the pyrolysis process. From the viewpoint of utilising the char, it is now necessary to evaluate the products that were create during the previous chapter's task for their suitability to the PCI process. From the previously varied parameters (maximum temperature, holding time, heating rate), the char properties under these conditions including density, proximate and ultimate analysis, heating value and reactivity will be evaluated and compared.

Abstract

Lignite briquette pyrolysis products were characterised for a set of experiments where the heating rate, residence time and final temperature were varied. The residence time ranged between 10-60 min while the final temperature was altered between 600-1000 °C. Two heating rates were used, 10 °C/min and 100 °C/min. Under a slow heating (10 °C/min) scenario, a temperature of 900 °C is required to release most of the volatile matter including the oxygen and hydrogen present. At this temperature, the oxidation reactivity is significantly decreased compared to the raw briquette coal. Similarly, a fast heating rate (100 °C/min) up to a fixed temperature of 800 °C with a holding time of 20 min is necessary for the elimination of the majority of the volatile matter. This is also correlated with a decrease in char oxidation reactivity. Accordingly, the decrease in char reactivity was correlated with this change in volatile/fixed carbon ratio. Additionally, the radical concentration was correlated with the reactivity while the true density is negatively correlated with reactivity. These changes had a negative effect on the combustion performance although the char still maintained higher reactivity and faster ignition than the commercial PCI coal that it was compared with.

Keywords

Pyrolysis, Victorian brown coal, pyrolysis products, pulverised coal injection

5.1 Introduction

Pyrolysis is an effective method for increasing the value of the brown coal by increasing its heating value and transportability. However, eliminating part of the volatile matter and heat treatment of the coal is expected to lower combustion performance by decreasing oxidation reactivity [1]. Victorian brown coal has many unique properties compared to other fuels, such as a high oxygen content and presence of alkali and alkaline earth metallic (AAEM) species which will influence its pyrolysis behaviour [2]. AAEM species impeded the release of large aromatic ring systems and assisted in bond forming and bond breaking reactions with the coal matrix [3]. AAEM species could later assist in catalysing char combustion or gasification reactions [4]. Sodium and calcium retention decreases with pyrolysis temperature especially at temperatures greater than 800 °C [4].

The subject of coal pyrolysis conditions has already been explored by a large number of studies. Table 5.1. The effect of changing temperature appears to be dependent on the range studied. Two studies which focused on lower temperatures found increases in reactivity with temperature [5, 6], while reactivity generally fell with temperature increases at higher temperatures [7-9]. Heating rate is also a factor in char reactivity. Several studies found an increase in reactivity with increasing heating rate [8, 10], while another found a decrease in reactivity [7]. A high heating rate could lead to an increase in surface area in the char through the rapid release of volatiles [10], however if mass release is higher under a higher heating rate, than this could lead to increased carbon aromatization and consequently lower reactivity [7]. Compared to other methods that rely on analysis of functional groups such as Raman or FTIR spectroscopy [11, 12], analysis of free radical concentration by ESR spectroscopy could provide a rapid method of producing an easily quantifiable correlation of the chemical structure with char reactivity. Free radicals specified by this measurement indicate the presence of a molecular entity possessing an unpaired electron [13], which will be highly chemically reactive. Several studies have explored the effect of pyrolysis conditions on free radical concentration in the char product [14-16]. The studies found a peak in radical concentration at a specific pyrolysis temperature. Generally radical concentration fell with increased residence time. There is a noticeable gap in the literature concerning the effect of particle size on the pyrolysis process and the pyrolysis of large briquettes.

Table 5.1 Selected works concerning pyrolysis condition investigation

Fuel type	Aim	Findings	Ref.
Woody biomass	CO_2 gasification reactivity	Increased gasification rate with increased heating rate (15–600 °C/min) Decreased gasification rate with increased pressure (0.1–3.0 MPa)	Okumura et al. [17]
Several biomass species (50 and 2000 μm)	CO_2 gasification reactivity	Increased gasification rate and surface area with increased heating rate (40 °C/min-10^5 °C /s) Decreased gasification rate and slight decrease in surface area with increased pressure (1-20 bar)	Cetin et al. [10]
Shanxi bituminous coal	Gasification reactivity	Chars prepared with pyrolysis gas had lower reactivity than with N_2. At temperature range 450-600 °C, char reactivity and surface area increased with temperature.	Wang et al. [5]
Coals ranging from subbituminous to semi-anthracite (106−150 μm)	Oxidation reactivity	Char reactivity decreased with increases in peak pyrolysis temperature (700-1500 °C) and increased with heating rate (4-5E3 K/s).	Cai et al. [8]
Biomass (<150 μm)	Oxidization reactivity	With increasing pyrolysis temperature (300-500 °C), reactivity increased and burnout time decreased.	Park et al. [6]
Loy Yang brown coal (105−150 μm)	Weight loss and Na volatilisation	Maximum weight loss rate ~400 °C and plateaus at ~800° C. Much greater Na volatilisation under fast heating mode.	Quyn et al. [18]
Two bituminous coals and one lignite (63−75 μm)	Intrinsic char oxidation rate	Decreases in reactivity with increasing temperature (~680-1350 °C), heating rate (1E4-2E5 K/s) and holding time (135−1000 ms).	Gale et al. [7]
Demineralised lignite (~170 μm)	Oxidation reactivity	Decrease in reactivity with increased temperature (700-1200 °C) and holding time (0.3 s-1 h). This was correlated with a decrease in surface area.	Radović et al. [9]
Two Australian brown coals (<150 μm)	Radical concentration	Decreased radical concentration with increased heating rate (5-80 K/min). Radical concentration peaks at ~550 °C.	Yokono et al. [14]
Bituminous and subbituminous coals	Radical concentration	Increase in free radical concentration after 400 °C up to highest temperature of 550 °C.	Petrakis et al. [15]
Bituminous Chinese coal (<105 μm)	Radical concentration	Radical concentration peaked at a temperature of 450 °C and decreased with retention time at temperatures >450 °C. Radicals were found to be dependent on mass loss, peaking at 25% loss.	Qiu et al. [16]

The focus of this study is to investigate the effect of altering heating rate, residence time and temperature during pyrolysis of Victorian brown coal in a lab scale vertical furnace in both briquette form and different sizes of loose coal. By varying pyrolysis conditions, a char can be created that has a sufficient calorific value for the intended application, a large and comparable density to that of bituminous coal so that they can blend easily, as well as a large size and strength for long-distance transportation, while also maintaining a high oxidation and gasification reactivity. Physical changes to the pore structure may also be dependent on heating rate, since the ejection rate of volatile matter can alter pore structure and the specific surface area. A variety of analysis techniques are used to measure the resultant char properties including ESR spectroscopy for radical analysis and char-O_2 and char-CO_2 reactivity analysis by TGA. Combustion performance is tested using CFD modelling.

5.2 Materials and methods

The materials and methods for the pyrolysis is the same as the previous chapter, and will be summarised briefly here. Yallourn brown coal briquettes measuring are pyrolysed in two separate schemes in a vertical electrically heated quartz furnace. In the first heating mode, samples are heated at 10 °C/min to various temperatures ranging from 600 to 1000 °C. In the second heating mode, samples are placed in the furnace that is already preheated to 800 °C and held for times varying from 10 min to 60 min. In this scheme the heating rate is approximately 100 °C/min.

Oxidation and gasification reactivity is measured using the thermogravimetric analysis (Shimadzu DTG-60H). Heating rate is varied from 2 °C/min to 10 °C/min. Using the temperature at the maximum rate, the pre-exponential constant and activation energy can be calculated using the Kissinger method [19].

True density is measured using a helium pycnometer (Micrometrics AccuPyc 1330). Apparent density is measured using Autoscan 60 mercury intrusion instrument up to a pressure that will fill inter-particle space but not enter pores.

CFD modelling is performed using Ansys Fluent 15.0. The mesh for this model is representative of the lab scale drop tube furnace used in previous work [20]. The standard k-ε

model is used for turbulence, discrete ordinates for radiation, Westbrook-dryer mechanism for gas phase reactions and multiple surface reaction model for char reactions. The char reactions (char-O_2 and char-CO_2) utilise kinetic data calculated from TGA experiments, while also considering bulk diffusion of the reacting gas to the sample.

Free radicals are measured using electron spin resonance (ESR) spectroscopy using a previously established method [21]. By comparing the area of the ESR signal with a standard of known radical concentration, the concentration of unpaired electrons can be determined, expressed in spins/g.

5.3 Results and discussion

5.3.1 Density and porosity changes during pyrolysis

Figure 5.1 shows the effect of pyrolysis conditions on the true and apparent density as well as the calculated porosity of the char. With increasing temperature, the briquette is observed to shrink as well as lose mass during the pyrolysis process. This led to an initial drop in apparent density, up to 800 °C, followed by an increase in apparent density up to 1000 °C as the rate of mass loss slowed compared to the shrinkage. True density rose with the increasing temperature, particularly for temperatures above 800 °C. For briquettes under the fast heating conditions, apparent density was seen to fall up until 20 min, and remains stable up until the final time of 60 min. This corresponds to a lack of significant shrinkage and mass loss after 20 min was reached. On the other hand, true density steadily increased with pyrolysis time, increasing from the initial density of 1404 kg/m^3 for the raw coal to 1634 kg/m^3 at 20 min then finally 1822 kg/m^3 at 60 min. For loose coal particles (Figure 5.1c), apparent density rose with increasing particle size while true density fell, this is expected based on the mass loss results. The briquette samples shows a much larger apparent density, and this is for the reason that the briquette was densified prior to pyrolysis, rather than a consequence of the pyrolysis process. Compared to a commercial PCI coal which has an apparent density of 1264 kg/m^3, the briquette samples show a closer match which could be beneficial to the blending process and increases the compatibility with existing coal feeders to the furnace.

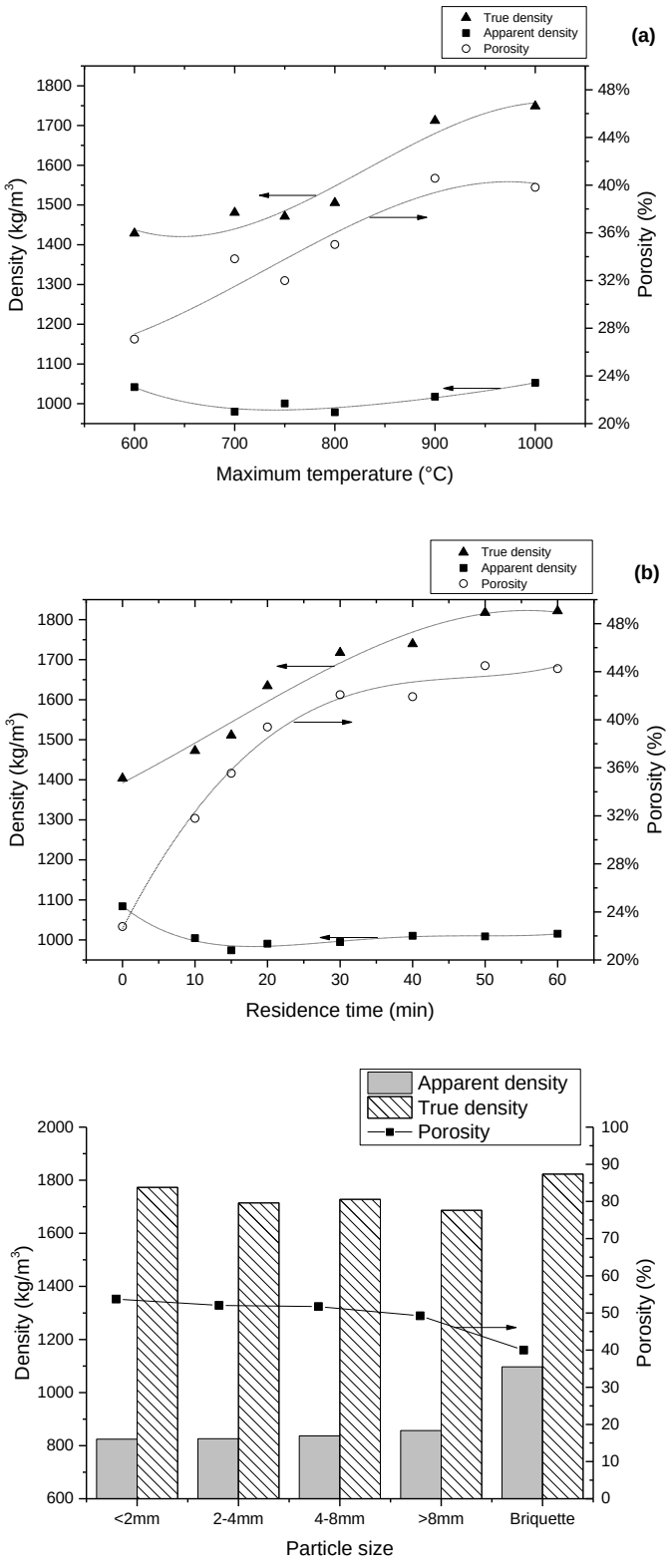

Figure 5.1 True density, apparent density and calculated porosity for Yallourn briquette char under (a) slow, (b) fast heating regimes and (c) slow heating particles.

5.3.2 Effect of pyrolysis conditions on proximate and ultimate properties

As expected, the pyrolysis process resulted in the reduction of volatile matter, and an increase in fixed carbon, ash and higher heating value as the time or temperature increases (Figure 5.2). In the slow heating procedure, up to 800 °C, the most significant reductions changes occur in the char properties, while only small changes are observed above this. For the fast heating at 800 °C, changes to the char properties occur rapidly up until 20 min then properties remain fairly stable as time increases to 60 min. For the slow heating coal particles in Figure 5.2c, it is interesting that ash decreased with increasing particle size while fixed carbon and heating value increased, despite the lower mass loss compared to the smaller particle sizes. The commercial PCI coal sample has a heating value of 31.9 MJ/m^3 on a dry basis, so in order to have a similar value to this property, slow heating briquette samples must reach 800 °C and fast heating samples must be pyrolyzed for 20 min. The heating regimes undertaken by the coal was sufficient to meet this goal in all cases.

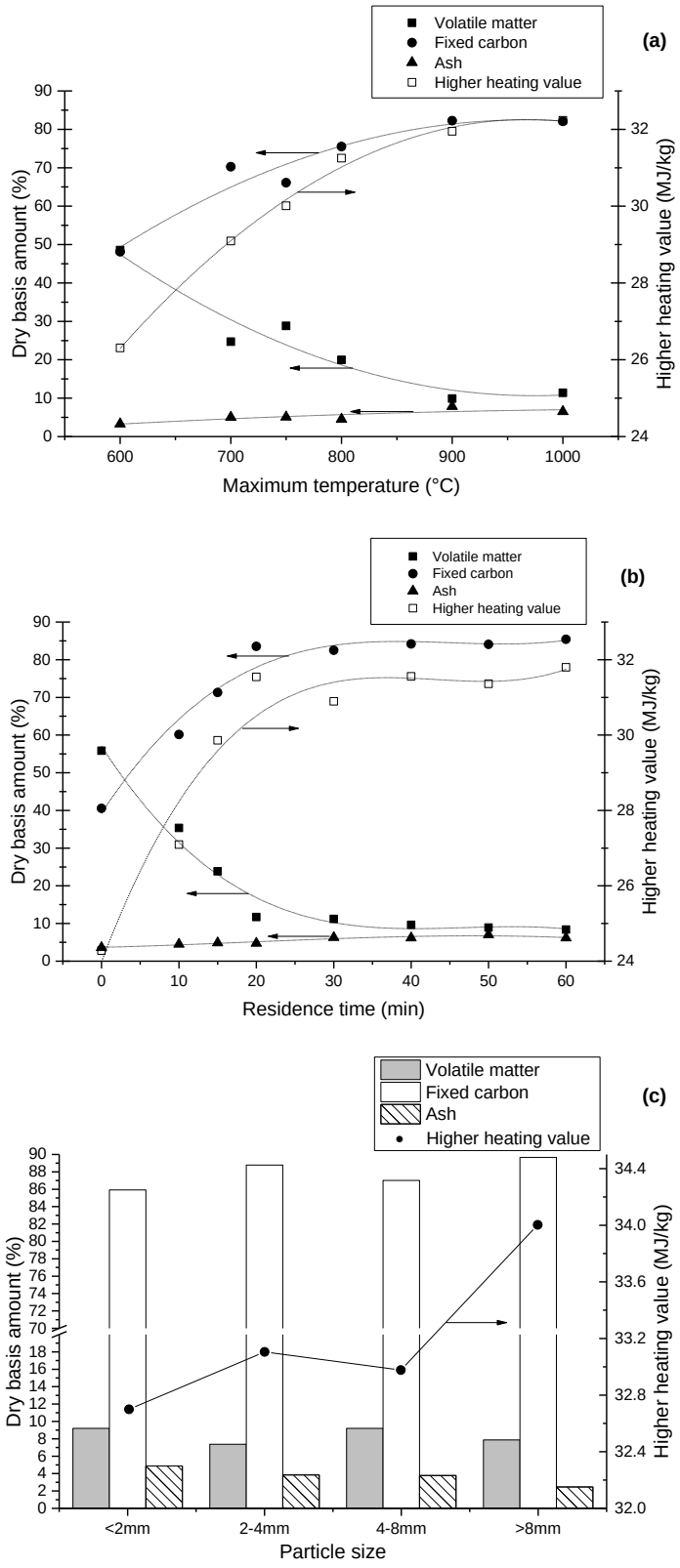

Figure 5.2 Proximate properties and higher heating value (db) for Yallourn briquette pyrolysis under slow (a) and fast (b) heating regimes, and (c) slow heating coal.

Figure 5.3 shows the increase in particle residence time or temperature is correlated the increase in carbon and decrease in both oxygen and hydrogen. Under the slow heating scenario (Figure 5.3b), a temperature of 900 °C is attained before the almost complete release of oxygen is achieved. Below 600 °C, there was little change in the elemental composition, however after this temperature is reached the hydrogen and oxygen fell linearly with increased temperature. Fixed carbon gradually rises to 90.4% at 1000 °C. During fast heating (100 °C/min to 800 °C), oxygen and hydrogen are rapidly lost from the briquette, up to a time of 20 min when their concentrations are 4.6% and 1.7% respectively. Beyond this there is a gradual release of the remaining oxygen and hydrogen. The carbon content increases from 62.4% to 87.6% at 20 min, and beyond this only increases to 90% once 60 min is reached.

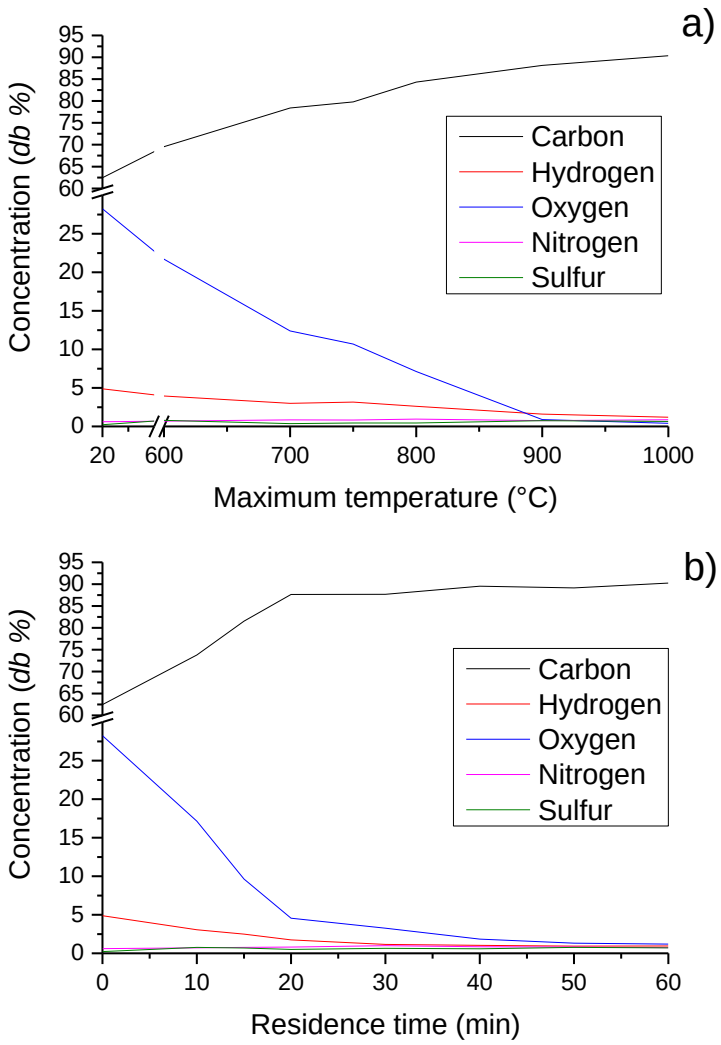

Figure 5.3 Changes in ultimate analysis for a) slow (10 °C/min) and b) fast (100 °C/min) heating

5.3.3 Effect of pyrolysis conditions on reactivity

The oxidation reaction rate is shown in Figure 5.4

Figure 5.4 Oxidation reaction rate for Yallourn char for briquettes for (a) slow and (b) fast heating

shows the calculated intrinsic oxidation rate as measured in air. For slow heating char, there is a significant difference in reaction rate between samples that reached a maximum of 800 °C and below, and samples heated above 800 °C which had significantly lower reactivity. Similarly, for fast heating samples, the raw coal and samples up to 15 min show very high reactivity. This significantly drops once 20 min is reached and rises a small amount after this. Samples in these pyrolysis conditions showed much higher char-O_2 reactivity than the PCI coal. The high reactivity of the Yallourn char will be useful for increasing the PCI feeding rate in the blast furnace without accumulation of unburned char.

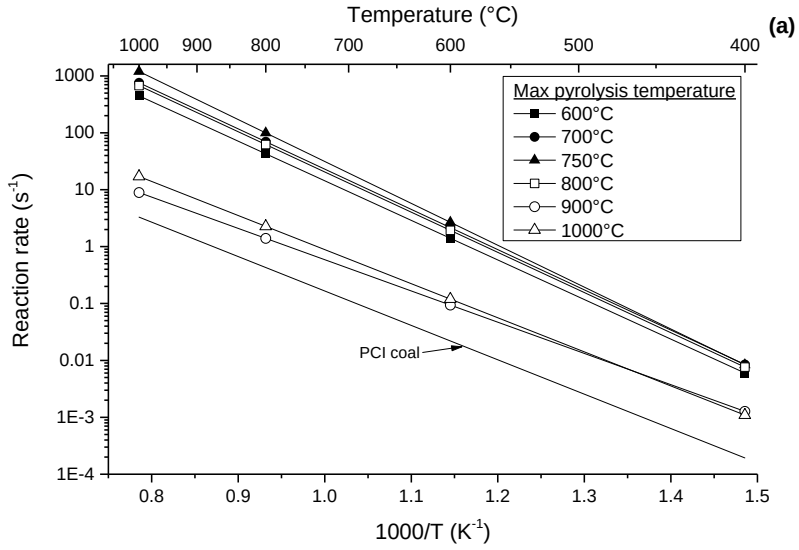

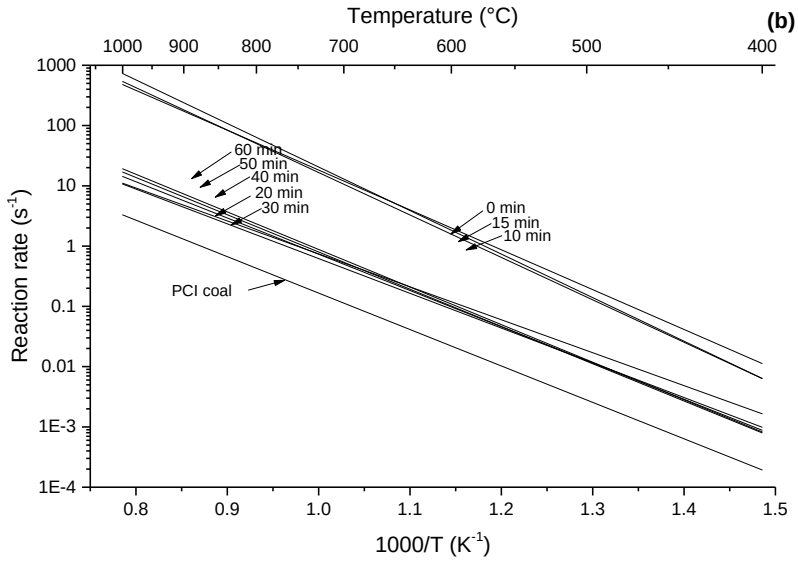

Figure 5.4 Oxidation reaction rate for Yallourn char for briquettes for (a) slow and (b) fast heating

Coal samples all showed very similar reactivity for both slow and fast heating samples. Figure 5.5 shows that fast heating samples all showed a lower activation energy than their slow heating counterparts for every particle size. Since mass loss was very similar between the slow and fast heating coal pyrolysis, this result implies that the heating rate as affected the physical structure by the high rate of volatile matter ejection or chemical structure of the coal by way of the pyrolysis route. This gives a higher oxidation reaction rate for slow heating samples above a combustion temperature of ~700 °C and higher for fast heating samples below this temperature. Compared to the PCI coal, the pyrolyzed loose coal samples showed very similar reactivity.

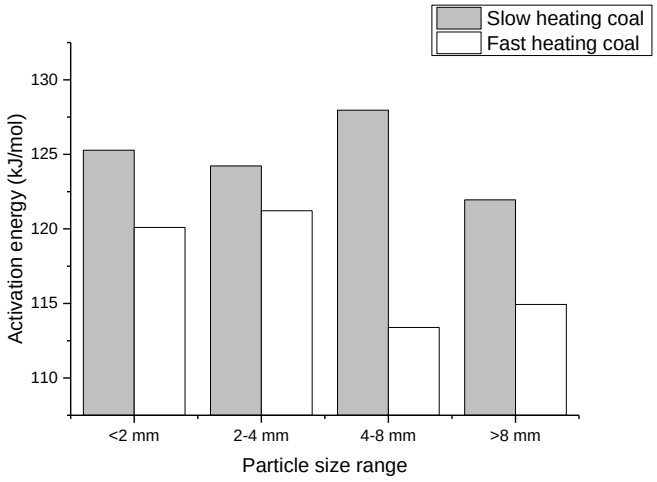

Figure 5.5 Activation energy for coal particles heated to 800 °C with slow and fast heating modes.

Compared to oxidation rate, there is less variation in the gasification rate between samples (Figure 5.6), however similarly to the oxidation rate, the 900 °C and 1000 °C slow heating samples show a lower reactivity. For fast heating samples, most samples show similar gasification reactivity, while the unpyrolyzed briquette has a slightly higher rate and the 60 min sample has slightly lower reactivity.

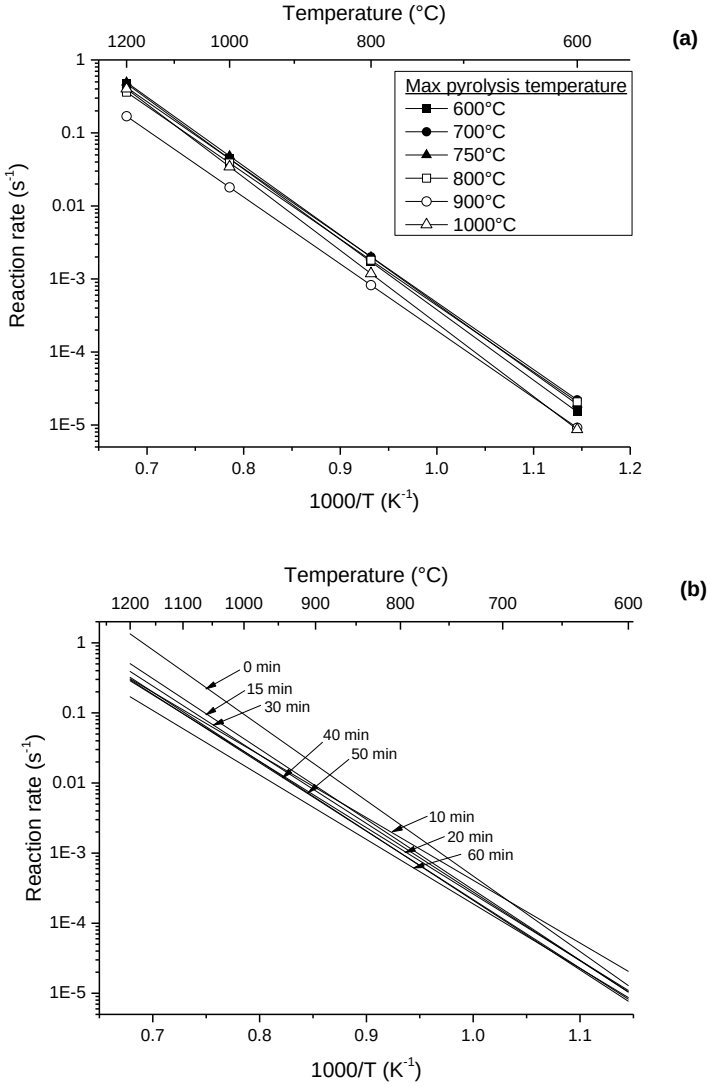

Figure 5.6 Char-CO_2 gasification reaction rate for Yallourn char for (a) slow and (b) fast heating.

5.3.4 Correlation of measured properties with reactivity

Figure 5.7 shows the dependence of the free radical concentration on intrinsic reactivity, true density and volatile/fixed carbon ratio for a variety of samples. Included in this analysis are Yallourn char samples produced in a used in a previous study that were created in an industrial pyrolyser [20]. As expected, the general trend is that reactivity increases with radical concentration, although the trend does not follow for each sample type. Increasing true density which will lead to increased carbon densification and carbon aromaticity [22], which appears to negatively influence the reaction rate. Volatile/fixed carbon ratio also displays a correlation with intrinsic oxidation reactivity. For Yallourn char, decreasing the volatile/fixed carbon ratio below 0.2 will significantly lower the oxidation reaction rate. This will also be strongly correlated with factors such as O/C ratio in the fuel. The results from these analysis techniques may suggest that oxidation rate is dependent on these factors or that they can simply be used as a predictor of oxidation reactivity thus for optimisation of the pyrolysis condition.

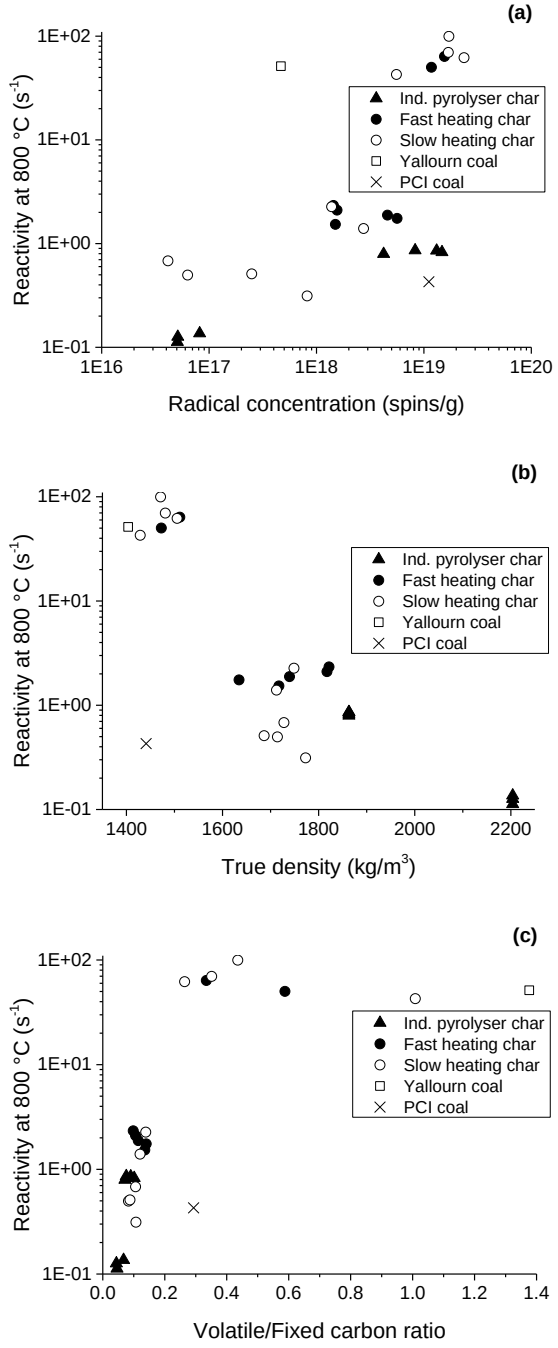

Figure 5.7 Dependency of kinetic reaction rate in air at 800 °C on (a) radical concentration, (b) true density and (c) volatile/fixed carbon ratio

5.3.5 CFD modelling section

5.3.5.1 CFD modelling of combustion performance of produced chars

CFD modelling is useful for efficiently characterising the combustion performance of the char that has been produced. Figure 5.8 compares the changes in particle ignition time and time to

50% burnout for slow and fast heating char samples. Particle ignition time is measured as the maximum of the second derivative of the temperature/time plot, i.e. the moment of the maximum change in temperature gradient, characterised by an upward inflection in the plot. For slow heating char, ignition time is similar for chars created at 800 °C and below. Although volatile content varies widely between these samples between 49% and 20%, the high char reactivity will allow the particles to ignite heterogeneously Beyond 800 °C the lower char-O_2 reactivity will lead to a delay in the ignition point. 50% burnout time, as measured by the conversion of combustible matter in the char (volatiles + fixed carbon), is relatively fast for the 600 °C sample due to the high volatile content. At temperatures above this, 50% burnout time rises slightly until 900 °C is reached whereby there is a substantial increase in the burnout time. For char generated in the fast heating environment, ignition temperature and 50% burnout time is relatively low for 10 and 15 min samples, however once 20 min is reached, the combustion performance remains fairly constant. Compared to the commercial PCI coal, all of the briquette char generated under the slow and fast heating regimes showed better combustion performance.

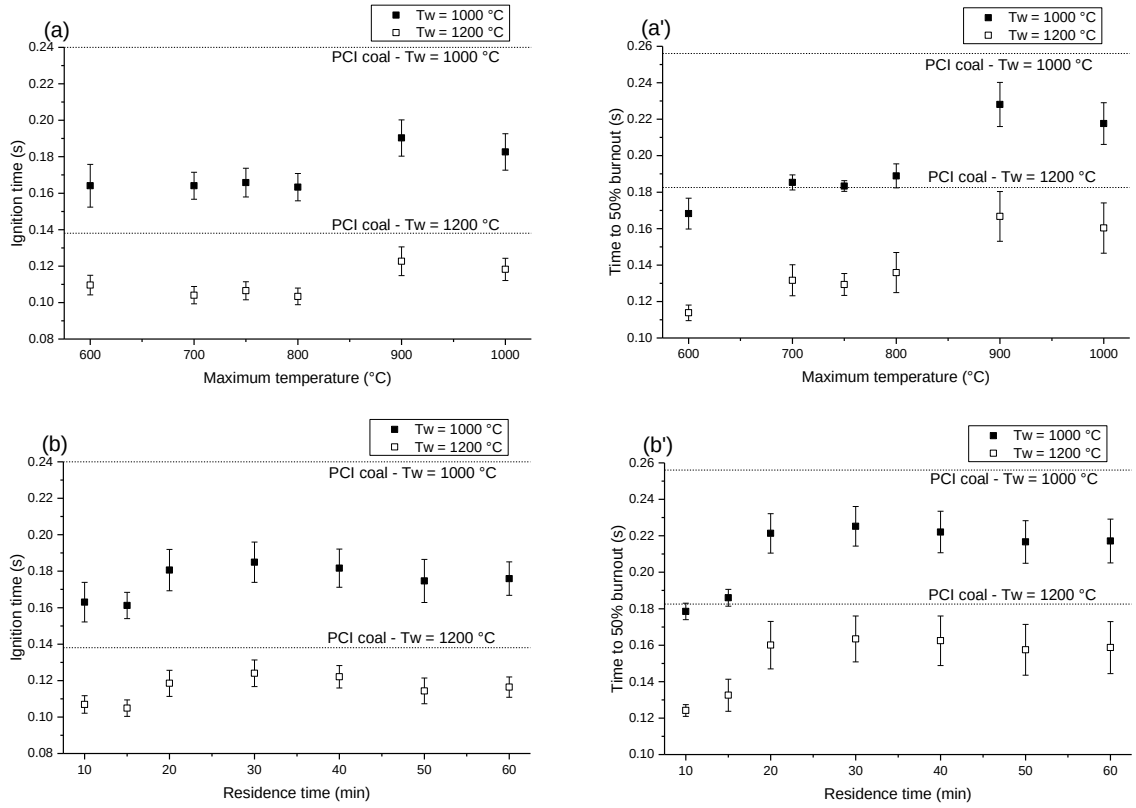

Figure 5.8 Ignition time (a, b) and time to 50% burnout (a',b') of slow (a) and fast (b) heating Yallourn briquette char compared with a commercial PCI coal under two wall temperatures, 1000°C and 1200°C

5.3.5.2 Sensitivity of char properties on combustion performance

Figure 5.9 describes the effect of a number of coal properties on the combustion performance. Similarly to the oxidation reactivity in Figure 5.7b, increasing true density true density had a negative effect on the combustion performance, increasing both ignition time and 50% burnout time. There was not a large variation in apparent density between samples as they were derived from the same coal and subsequently there was little correlation with combustion performance. Porosity had a negative correlation with combustion performance. Since apparent density wasn't greatly changed between samples, the increased true density resulted in greater porosity. Although this could allow greater penetration of reactive gasses into the particle, the reduced reactivity of the denser char due to the increased aromaticity was the dominant factor. Increasing oxidation reactivity, radical concentration and also the volatile/fixed carbon ratio all

had positive effects of both the ignition time and time to 50% burnout. Since there is a large dependence between these three characteristics on each other, e.g. oxidation reactivity on the volatile to fixed carbon ratio, it is difficult to directly attribute them to the reduction in ignition time although these variables will be separated individually in the next section.

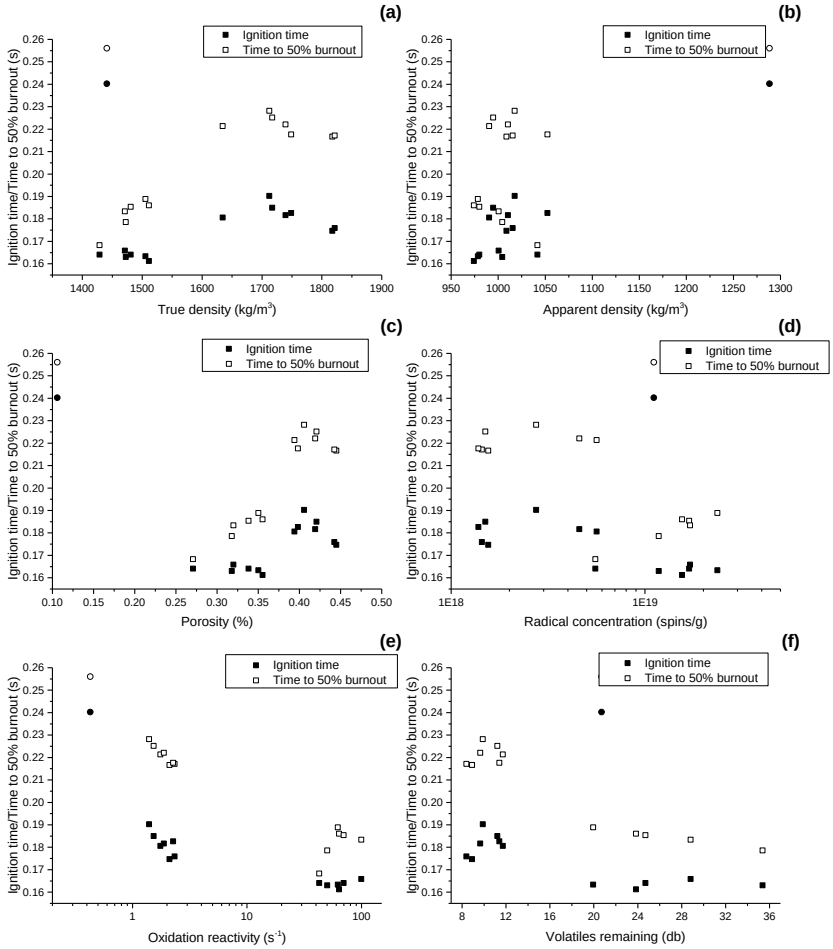

Figure 5.9 Sensitivity of combustion performance on properties (a) true density, (b) apparent density, (c) porosity, (d) radical concentration, (e) oxidation reactivity and (f) volatile/fixed carbon ratio for ■ Yallourn char and ● PCI coal for comparison

Using the 800 °C slow heating case as a basis, individual char properties are modified within the range of values found within the produced char. For ignition time, the oxidation rate is most influential parameter due to the heterogeneous nature of brown coal combustion. A decrease in density has a positive effect on the ignition time. This is since a low density solid fuel will contain a greater number of particles and thus a greater surface area for the same mass. The drawback of this is that energy density measured in MJ/m^3 will be lower and this is an important

consideration in the transport. Increasing pyrolysis yield may only marginally improve the burnout when char reactivity is already high. While volatile combustion will generate heat to assist the char-O_2 reaction, oxygen will be depleted in the local area surrounding the char particles. The effect of the gasification rate and moisture on ignition time is very low. For 50% burnout time, pyrolysis yield is the most significant factor since volatile release is included in the calculation of burnout. Similarly to ignition time, decreasing density and increasing oxidation rate will improve the 50% burnout time. Gasification reactivity will also improve this time due to the consumption of char through the char-CO_2 gasification reaction which will be useful at high temperature zones due to the high activation energy and also in areas of the furnace where oxygen is low or depleted.

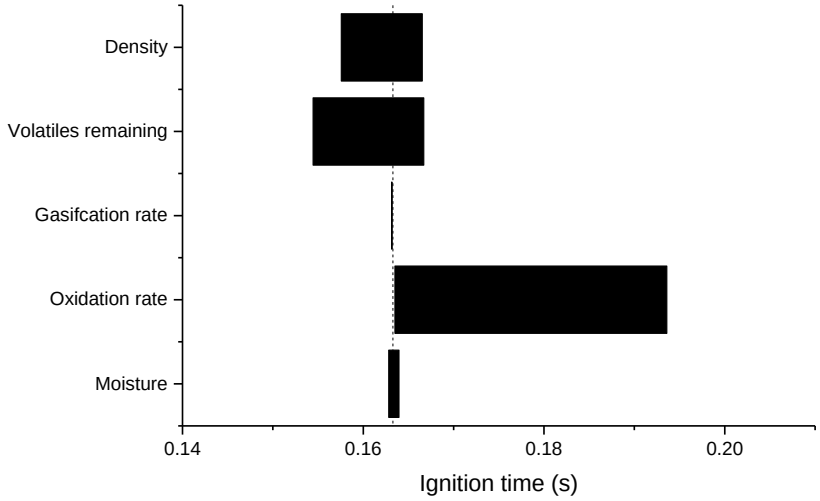

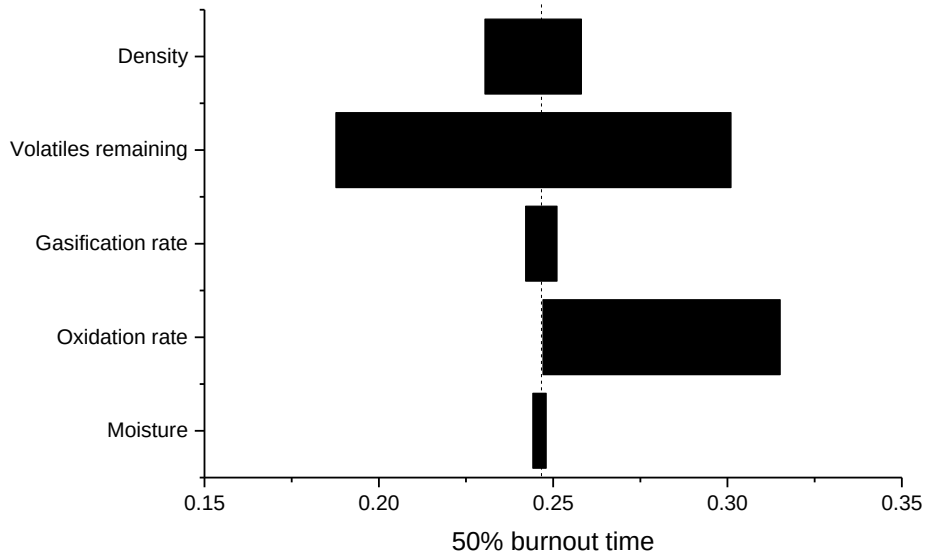

Figure 5.10 Sensitivity of individual CFD input parameters on combustion performance

5.4 Conclusions

The major conclusions from this study are shown as follows:

1. A maximum pyrolysis temperature of 900 °C with a slow heating rate or holding time of 20 min at 800 °C is vital for the elimination of volatile matter from the coal briquette and generation of a char that has an adequate heating value for use in the PCI process. Using differently sized coal, it was seen how the release of volatile matter decreased with increasing particle size and decreased even further once the briquette was used.
2. Once the majority of volatile matter was eliminated from coal, there were minimal changes to the coal mass and proximate properties however it was seen through further analysis that both free radical concentration and coal reactivity drastically decreased beyond a temperature of 800 °C. True density also continued to increase as the pyrolysis process progressed.
3. Combustion performance, as evaluated using CFD modelling, showed a positive performance of all chars generated from the Yallourn briquette compared to PCI coal. It is important that oxidation reactivity is maintained in order to benefit both ignition time and 50% burnout time.

References

1. Chan, M. L.; Jones, J. M.; Pourkashanian, M.; Williams, A., The oxidative reactivity of coal chars in relation to their structure. *Fuel* **1999,** 78, (13), 1539-1552.
2. Li, C.-Z., Some recent advances in the understanding of the pyrolysis and gasification behaviour of Victorian brown coal. *Fuel* **2007,** 86, (12), 1664-1683.
3. Li, C. Z.; Sathe, C.; Kershaw, J. R.; Pang, Y., Fates and roles of alkali and alkaline earth metals during the pyrolysis of a Victorian brown coal. *Fuel* **2000,** 79, (3–4), 427-438.
4. Quyn, D. M.; Wu, H.; Hayashi, J.-i.; Li, C.-Z., Volatilisation and catalytic effects of alkali and alkaline earth metallic species during the pyrolysis and gasification of Victorian brown coal. Part IV. Catalytic effects of NaCl and ion-exchangeable Na in coal on char reactivity☆. *Fuel* **2003,** 82, (5), 587-593.
5. Wang, Q.; Zhang, R.; Luo, Z.; Fang, M.; Cen, K., Effects of Pyrolysis Atmosphere and Temperature on Coal Char Characteristics and Gasification Reactivity. *Energy Technology* **2016,** 4, (4), 543-550.
6. Park, S.-W.; Jang, C.-H., Effects of pyrolysis temperature on changes in fuel characteristics of biomass char. *Energy* **2012,** 39, (1), 187-195.
7. Gale, T. K.; Bartholomew, C. H.; Fletcher, T. H., Effects of Pyrolysis Heating Rate on Intrinsic Reactivities of Coal Chars. *Energy & Fuels* **1996,** 10, (3), 766-775.
8. Cai, H. Y.; Güell, A. J.; Chatzakis, I. N.; Lim, J. Y.; Dugwell, D. R.; Kandiyoti, R., Combustion reactivity and morphological change in coal chars: Effect of pyrolysis temperature, heating rate and pressure. *Fuel* **1996,** 75, (1), 15-24.
9. Radović, L. R.; Walker, P. L.; Jenkins, R. G., Importance of carbon active sites in the gasification of coal chars. *Fuel* **1983,** 62, (7), 849-856.
10. Cetin, E.; Moghtaderi, B.; Gupta, R.; Wall, T. F., Influence of pyrolysis conditions on the structure and gasification reactivity of biomass chars. *Fuel* **2004,** 83, (16), 2139-2150.
11. Li, X.; Hayashi, J.-i.; Li, C.-Z., Volatilisation and catalytic effects of alkali and alkaline earth metallic species during the pyrolysis and gasification of Victorian brown coal. Part VII. Raman spectroscopic study on the changes in char structure during the catalytic gasification in air. *Fuel* **2006,** 85, (10–11), 1509-1517.
12. Solomon, P.; Serio, M.; Carangelo, R.; Bassilakis, R.; Gravel, D.; Baillargeon, M.; Baudais, F.; Vail, G., Analysis of the Argonne premium coal samples by thermogravimetric Fourier transform infrared spectroscopy. *Energy & Fuels* **1990,** 4, (3), 319-333.
13. IUPAC, *Compendium of Chemical Terminology, 2nd ed.* Blackwell Scientific Publications: Oxford 1997.
14. Yokono, T.; Murakami, K.; Sanada, Y., The effect of heating rate on radical concentration during coal pyrolysis. *Fuel Processing Technology* **1987,** 17, (1), 7-11.
15. Petrakis, L.; Grandy, D. W., Free radicals in coals and coal conversion. 3. Investigation of the free radicals of selected macerals upon pyrolysis. *Fuel* **1981,** 60, (2), 115-119.
16. Qiu, N.; Li, H.; Jin, Z.; Zhu, Y., Temperature and time effect on the concentrations of free radicals in coal: Evidence from laboratory pyrolysis experiments. *International Journal of Coal Geology* **2007,** 69, (3), 220-228.
17. Okumura, Y.; Hanaoka, T.; Sakanishi, K., Effect of pyrolysis conditions on gasification reactivity of woody biomass-derived char. *Proceedings of the Combustion Institute* **2009,** 32, (2), 2013-2020.
18. Quyn, D. M.; Wu, H.; Li, C.-Z., Volatilisation and catalytic effects of alkali and alkaline earth metallic species during the pyrolysis and gasification of Victorian brown coal. Part I. Volatilisation of Na and Cl from a set of NaCl-loaded samples. *Fuel* **2002,** 81, (2), 143-149.

19. Kissinger, H. E., Reaction Kinetics in Differential Thermal Analysis. *Analytical Chemistry* **1957,** 29, (11), 1702-1706.
20. De Girolamo, A.; Grufas, A.; Lyamin, I.; Nishio, I.; Ninomiya, Y.; Zhang, L., Ignitability and combustibility of Yallourn pyrolysis char blended with PCI coal under simulated blast furnace conditions. *Energy & Fuels* **2015,** 30, (3), 1858-1868.
21. Liu, M.; Yang, J.; Liu, Z.; He, W.; Liu, Q.; Li, Y.; Yang, Y., Cleavage of Covalent Bonds in the Pyrolysis of Lignin, Cellulose, and Hemicellulose. *Energy & Fuels* **2015,** 29, (9), 5773-5780.
22. Gale, T. K.; Fletcher, T. H.; Bartholomew, C. H., Effects of Pyrolysis Conditions on Internal Surface Areas and Densities of Coal Chars Prepared at High Heating Rates in Reactive and Nonreactive Atmospheres. *Energy & Fuels* **1995,** 9, (3), 513-524.

Chapter 6 – Ignitability and Combustibility of Yallourn Pyrolysis Char under Simulated Blast Furnace Conditions

It was confirmed in Chapter 5 that Victorian brown coal could be upgraded to a char product that has a similar heating value and reactivity to a commercially used PCI coal. This process was scaled up to a pilot scale shaft furnace and two products were obtained that were generated under two residence times. These products are examined in this chapter and their suitability for the PCI process is discussed. This chapter has been reformatted from the published manuscript: De Girolamo, A., Lameu, N. K., Zhang, L., Ninomiya, Y., Ignitability and combustibility of Yallourn pyrolysis char under simulated blast furnace conditions. *Fuel Processing Technology* **2017,** 156, 113-123. Supplementary data is contained in Appendix A.

Abstract

In this paper we have examined the potential of Yallourn brown coal char (collected from an industry-scale pyrolyser) to be used as a pulverised coal injection (PCI) fuel, its size-dependent properties, ignitibility and combustibility under the simulated conditions of the blowpipe-tuyere section in a blast furnace. The combustion of individual sizes for Yallourn char was tested in a lab-scale drop-tube furnace (DTF) using pre-heated hot gas with a temperature up to 1000 °C, and a particle residence time as short as 0.6 *s*. Computational fluid dynamics (CFD) modelling was further conducted to optimize the char combustion conditions via sensitivity analysis. Irrespective of the pyrolysis condition, Yallourn char is superior over bituminous coal for being used as a top grade PCI fuel, due to its higher calorific value (7500-8110 Kcal/kg), lower ash content (<10 *wt%*), high ash melting temperatures (>1550 °C), and abundance of iron (>40 *wt%* in ash). The performance of Yallourn char is also superior over bituminous coal under the simulated blast furnace conditions, for a rapid ignition and burnout even for a coarse char size of 300 μm under the stoichiometric O_2/C molar ratio and using low blast temperatures of 800 - 1000 °C. All these are beneficial for reducing the energy consumption related to particle pulverization and the amount of oxygen for the combustion. With regard to the Yallourn char ignition and combustion in the hot gas, a minimum 6 *wt%* volatile content is essential for a stable and rapid ignition of the volatiles at a gas temperature of 1000 °C or below, since homogeneous ignition is predominant at low temperatures. However, once the blast temperature rises to 1200 °C, the dependence on volatile content turns insignificant due to the dominance of the heterogeneous ignition, high C-O_2 reactivity for the solid char, as well as the minimized pore diffusion control due to the large porosity (52.0 - 63.1%) of the Yallourn char tested here.

Keywords

Blast furnace, Pulverized coal injection (PCI), Yallourn char, Combustibility

6.1 Introduction

With the depletion of the reserves for coking coal in the world, the demand for the use of PCI coal at a high coke replacement ratio is increasing stably in the international steelmaking industry [1]. PCI technology involves directly injecting coal into the blast furnace, increasing productivity, and replacing a part of coke that is used for the process of making iron [2]. The PCI coal has strict requirements in terms of ash composition and amount, volatile content, moisture content and grindability.

Volatiles present in a PCI coal have a double - edged role in blast furnace performance [3]. The injected coal has to devolatilize and combust at the correct location and time, for operational safety and optimal performance. Due to the very short residence times of coal particles in the raceway (15-20 *ms*), controlling combustion and ignition is critical to avoid incomplete burnout and excess unburnt char formation. While higher volatile content is correlated with higher char reactivity and hastened ignition [4], excessive amounts of volatiles may cause unstable combustion in the blowpipe and the degradation of coke [5]. Additionally, volatile content is inversely correlated with the calorific value of a coal. A low-volatile coal with a high calorific value will be able to replace a greater portion of the coke leading to additional cost savings with low volatile coals.

Reactivity of the PCI coal is another important factor in blast furnace performance [6]. In general, as PCI injection rate increases, unburnt char can increase the amount of fine coke particles in the raceway region, which in turn exerts detrimental effects on gas flow and permeability of the coke. However, a generalized conclusion regarding the impact of char reactivity on the performance of blast furnace has yet to be achieved. Phillip suggests that char reactivity may not be a significant factor in the raceway [7]. At the high temperatures in the raceway of up to 1500 °C, the char oxidation will be mainly diffusion controlled, and hence, its rate will be fast enough that any oxygen present at the particle surface will be consumed quickly [8]. On the other hand, Lu proposes that intrinsic char reactivity is a significant factor in burnout due to the highly turbulent regions in the flame and small particle sizes used in PCI combustion [9]. In addition to the char - O_2 reaction, the char - CO_2 gasification will occur beyond the raceway and this is likely to be intrinsically controlled due to the slower rate of reaction and lower temperatures in the furnace stack.

Low-rank brown coal has large reserves in both Australia and China, and also other parts of the world. However, due to its large moisture content, low-rank coal has been mainly used as the feedstock to supply local power plants which generally have a very low efficiency and a high carbon emission rate compared to black coal [10]. Little of low-rank coal is being used as a value-added product in the market for non-power applications including blast furnace use. Upon beneficiation such as mild pyrolysis, the low-rank coal is expected to be upgraded to a char with a higher calorific value that can be used in a variety of advanced applications including power generation, combustion in blast furnace, precursors for activated carbon, and reductants for the production of precious metals in the metallurgical industry. To date, the application of low-rank brown coal char as a PCI fuel for a blast furnace has yet to be tested. Instead, the use of woody charcoal as a PCI substitute fuel for CO_2 emission reduction has been examined [11]. Compared to woody charcoal, the low-rank coal char possesses distinct properties including different ash content and composition, as well as a different carbonaceous structure and reactivity.

This paper follows on from previous work on coal-char blends [12], and aims to validate the viability and benefit of fully replacing the commercial bituminous coal by brown coal char as the single PCI fuel in a blast furnace, rather than through blending them together. In particular, considering that volatile matter is one of the most critical factors for a single PCI fuel [3-5], the primary goal of this paper is to clarify the minimum volatile content in a lignite char that can ignite stably and rapidly whilst reaching its maximum possible calorific value (thus energy density). Such a goal is also significant for tailoring the parent coal pyrolysis conditions since the char is a prepared material, as well as establishing the bond between pyrolysis and the end-use of the pyrolysed char. To date, most of the studies on char properties and reactivity have failed to specify the end-use of the char, thereby providing little advice to both PCI application in the blast furnace, and the optimisation of pyrolysis conditions to meet the needs required by the PCI application. Additional efforts were further made to reveal the maximum possible size for the lignite char that can burn efficiently, so as to reduce the energy consumption required for its milling prior to being injected into the blast furnace.

To achieve the afore-mentioned research objectives, two Yallourn char samples collected from a pilot-scale shaft furnace with a capacity of 200 kg/h have been characterized and tested in this study. Their size-dependent properties and intrinsic reactivity were firstly examined.

Secondly, an experimental study of char particle ignition and burnout was conducted in a lab-scale thermogravimetric– differential thermal analyser (TG-DTA) and drop tube furnace (DTF) as a function of O_2/C molar ratio, furnace temperature and char size. The DTF used is unique, possessing the capability to provide a hot blast gas up to 1000 °C to mimic the industrial blast furnace. Finally, computational fluid dynamics (CFD) modelling was performed to interpret the DTF results and further explore the optimum properties for lignite char in terms of ignition and burnout under the simulated blast furnace conditions. The parent raw coal is sourced from the Latrobe Valley, Australia. As a reference, a bituminous coal currently used commercially as a PCI coal was analysed and compared.

6.2 Material and Methods

6.2.1 Properties of Yallourn char products

Coal for the production of char is sourced from Yallourn in Victoria, Australia. Yallourn lignite has a very high moisture content (65.2 % ar) but is low in ash (2.61% db) [13]. Two char samples were generated by pyrolysis of raw wet Yallourn lignite in a pilot-scale shaft furnace with a capacity of 200 kg/h at approximately 800 °C. These will be referred to as Yallourn char 1 (YC-1) and Yallourn char 2 (YC-2) and their approximate residence times are 5 and 10 hours, respectively. A longer residence time is expected to generate a low-volatile char that thus has a higher energy density. Other products recovered from the pyrolysis included water, gas and coal tar.

Char particles were size segregated prior to analysis. The char produced ranged in diameter from less than 100 μm to over 8 *mm*. Interestingly, the sizes less than 1 *mm* in diameter are mostly present as powdery, darkish particles that are analogous to high-rank black coal, as evident in Figure 6.1 which shows the size-dependent surface morphologies of YC-1. Instead, the chunk sizes larger than 1 *mm* are more like woody charcoal. This is because the woody fibres are abundant in the original lignite. Clearly, the lignite char studied here is intriguing, as its maceral composition is a combination of both black coal and woody biomass. Such a sample has yet to be probed.

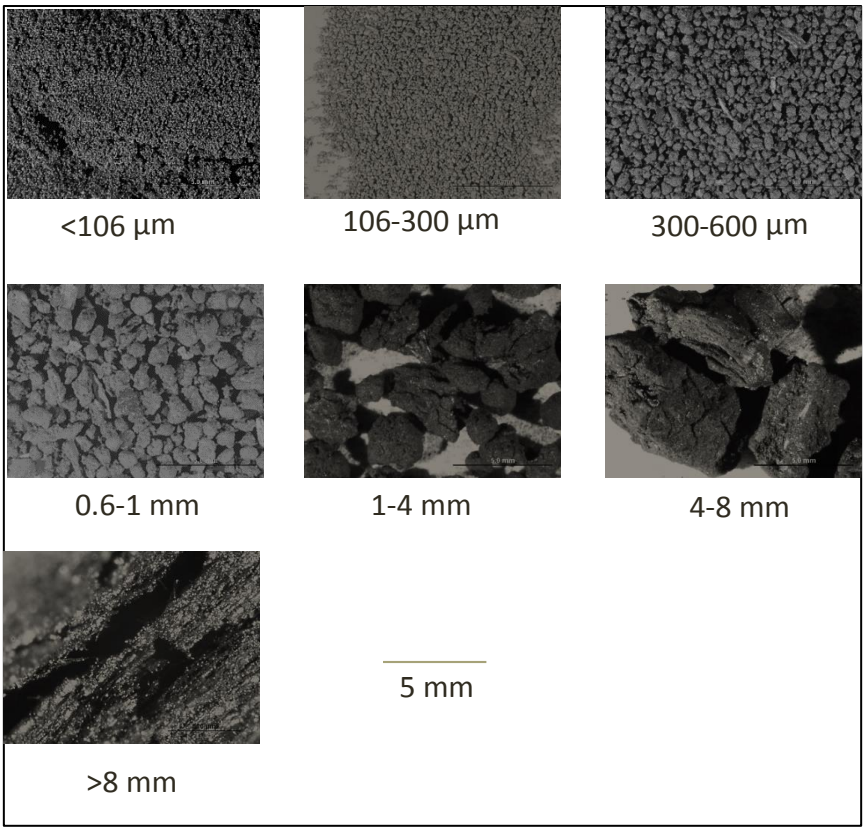

Figure 6.1 Surface morphology of differently sized lignite char, observed by optical microscopy. Scale is relevant to all micrographs.

To determine the crystal structure of char samples, X-ray diffraction (XRD) analysis was conducted in a Rigaku MiniFlex600 instrument. The char samples were demineralized with 1 M HCl washing for 3 hours followed by rinsing with deionised water until the leachate turned neutral prior to the XRD analysis. A scanning speed of 0.1 °/min was selected with a step size of 0.01° for a 2-theta angle from 10^o to 70^o. The maximum capable power of 600 W was used for the XRD characterisation. The samples were ground under the argon protection prior to the analysis.

6.2.2 Ignition temperature, volatile release and char-O_2 reactivity measurement in TG-DTA

Char ignition temperature was measured in TG-DTA (Shimadzu DTG-60H) and was defined as the temperature at the intersection of the tangent of the char mass at the initial point (horizontal line) and the tangent of the char mass curve at the peak of the DTA curve when the

sample is heated at a rate of 10 °C/min. Samples were ground to a size of <106 μm to minimise the diffusion.

Intrinsic char-O_2 reactivity kinetic parameters was calculated using the direct Arrhenius plot method which is based on.

$$\ln\left[\frac{1}{(1-\alpha)}.\frac{d\alpha}{dT}\right] = \ln\left(\frac{A}{\beta}\right) - \frac{Ea}{R}.\frac{1}{T} \qquad \text{Equation 6.1}$$

Where β is the heating rate and α is the conversion. By plotting $\ln\left[\frac{1}{(1-\alpha)}.\frac{d\alpha}{dT}\right]$ against $\frac{1}{T}$, the pre-exponential constant *A*, and activation energy E_a can be calculated. The heating rate was fixed at 50 °C/min and the air flow rate was fixed at 100 ml/min to ensure that the sample will always be supplied with 20.94% O_2. First-order devolatilization kinetics were measured in the same TGA instrument using the non-isothermal Kissinger method [14]. Argon was used at 100 ml/min and heating rates ranged from 10 to 50 °C/min in increments of 10 °C.

6.2.3 DTF experimental setup

A 2-*m* DTF was employed to combust the coal and char sample and a gas analyser recorded the combustion gases exiting the furnace. A schematic of this DTF can be found in previous work [15]. In brief, the sample enters the DTF with a cold primary gas of 1 L/min, while a secondary gas of 9 L/min is preheated through the annulus between the reactor and the furnace, mixing with the coal or char at the injection point. Such a unique pre-heating system for the gas can resemble the blast furnace condition where the hot air is normally heated to ~1000 °C. This is different from the previous study on the test of PCI coal in a lab-scale DTF without extensive preheating of the secondary gas [16]. A water cooled injector was used to inject the sample at a further distance in the reactor so that the particle residence time was approximately 1.4 *s*.

The coal feeding rate was set to approximately 1 g/min. The combustion test was conducted at three furnace temperatures, 800 °C, 900 °C and 1000 °C, and four O_2/C molar ratios ranging from 0.7 to 1.4. For the char and commercial PCI coal, three original sizes of <106 μm, 106-150 μm and 150-300 μm were tested to evaluate the size-dependence of their combustibility.

In addition, the char sizes larger than 1 *mm* were ground to <106 μm and further tested. The experimental conditions are summarized in Table 6.1.

Table 6.1 DTF experimental conditions tested

Sample	Size	Temperature °C	O_2/C ratio
YC-1	<106 μm	800, 900, 1000	0.7-1.4
	106-150 μm		
	150-300 μm		
	1-4 mm ground to <106 μm	1000	0.7
	4-8 mm ground to <106 μm	1000	0.7
YC-2	<106 μm	800, 900, 1000	0.7
	106-150 μm		
	150-300 μm		
	1-4 mm ground to <106 μm	1000	0.7-1.4
	4-8 mm ground to <106 μm	1000	0.7
Commercial PCI coal	<106 μm	800, 900, 1000	0.7-1.4
	106-150 μm		
	150-300 μm		

Coal/char burnout was measured by examining the mass balance of combustible matter before and after each test. The unburnt residue from each run was fully collected via a flask and thimble filter installed at the bottom of the DTF reactor. The ash percentage in the residue, A_r was measured by the TGA instrument by burning it in air upon heat-up to 800 °C at a heating rate of 10 °C/min. By employing the original mass (M_o, dried) of the injectant, its ash content ($A_{original}$, *wt%* on dried basis) and the mass of the residue (M_r), one can calculate the burnout (B) using Equation 6.2 below:

$$B = (1 - \frac{M_r}{M_o}\frac{(100 - A_r)}{(100 - A_o)})\times 100 \quad \text{Equation 6.2}$$

This method is expected superior over the traditional ash-tracer method in which the conservation of ash mass is assumed during the combustion process. The low-rank coal and its derivatives including char give a non-negligible ash loss upon the combustion [15].

6.2.4 CFD modelling methodology

A three-dimensional CFD model of the DTF was established to interpolate and extrapolate the DTF results so as to gain a better understanding of the burnout profile of different fuels. Although the DTF experiments shown are able to show the discrepancy of the burnout between different fuels, an accurate estimation of the influence of a single parameter is difficult. This is due to the limitation of the feeding system that rarely allows for an identical feeding rate for different samples with different density and different O_2/C molar ratios. Such a problem was solved easily by CFD modelling once it is fully validated. For the modelling in this study, the furnace wall temperature was varied from 800 to 1200 °C, as this is closest to the temperature of the hot air stream that the particles are injected inside the blowpipe-tuyere section in a blast furnace [6]; the O_2/C molar ratios was set identical with that which has been tested in the DTF, and all the different sizes of char and PCI coal were tested to conduct a sensitivity analysis of the char burnout as a function of particle size and operating conditions.

The mesh and model for the DTF was taken from a previous study of brown coal combustion in the same rig, which has been fully validated [17]. The mesh is made up of 231,000 cells and encompasses all of the drop tube furnace features, including the primary and secondary gas inlets, secondary gas preheating zone, the water-cooled injector, and mixing of gasses and char at the injector tip. This mesh was validated in a grid independence test as well as with measurements of particle temperature in the previous study. The models used in the simulation are summarized as follows: Turbulence: k-ε model is used which has shown sufficient accuracy in modelling combusting flows [18]; Radiation – the discrete ordinates (DO) method was chosen due to suitability for all optical thicknesses and level of accuracy [19]; Radiation absorption: the weighted-sum-of-grey-gases model (WSGGM) which is commonly used for coal CFD simulations as it is efficient and shows a good agreement with experimental observations [20];

Particle reactions – Multiple surface reaction model; and Gas phase reactions – Westbrook & Dryer mechanism [21].

Particle surface reaction kinetics, as well as devolatilisation rates were taken from the TGA experiments described earlier and diffusion rate constants were found in literature [22]. The mass loss and Kissinger plot can be found in supporting information (SI), Figure S1 and Figure S2, respectively. The devolatilisation rate of Yallourn char samples was assumed to be similar to that of raw Yallourn coal. First-order rate kinetic parameters A and E_a were determined to be 6.88×10^{13} s^{-1} and 205 *kJ/mol*, respectively using the previously described Kissinger method. While the pyrolysis reaction proceeds relatively fast compared to the char conversion reactions, the high activation energy here is indicative of the high temperature dependence of the volatile release. For PCI coal the Arrhenius equation constants were taken from the work of Badziok and Hewksley (A=4.92×10^5 s^{-1}, E_a=74 kJ/mol) [23].

6.3 Results and Discussion

6.3.1 Char property analysis

The proximate property analysis was conducted on each size group and a trend was found linking a decrease in size with a decrease in fixed carbon and an increase in moisture, ash and volatile matter shown in Figure 6.2. This variance in properties was much greater for YC-1 than YC-2 that was produced at a longer residence time. The trend of this variation initially appears counterintuitive, i.e. smaller particles would be expected to lose a greater amount of volatiles due to the lesser heat and mass transfer resistance. Instead, the result here may suggest a secondary condensation of both volatiles and even the ash-forming elements once they were evaporated from their local positions in the coal matrix. For both char samples, the size bin <106 μm showed an ash content above the standard for a Grade 1 PCI fuel (<10 % ash) [24]. However, all the other sizes have an ash content that is much lower. The lengthier pyrolysis time to produce YC-2, compared to YC-1 increased the percentage of fixed carbon in the sample while decreasing volatile matter and moisture. Apart from the continued release out of coal matrix, the volatile residues may also be partially solidified upon a variety of secondary reactions such as formation of soot and coke, and also interaction with the char matrix [13].

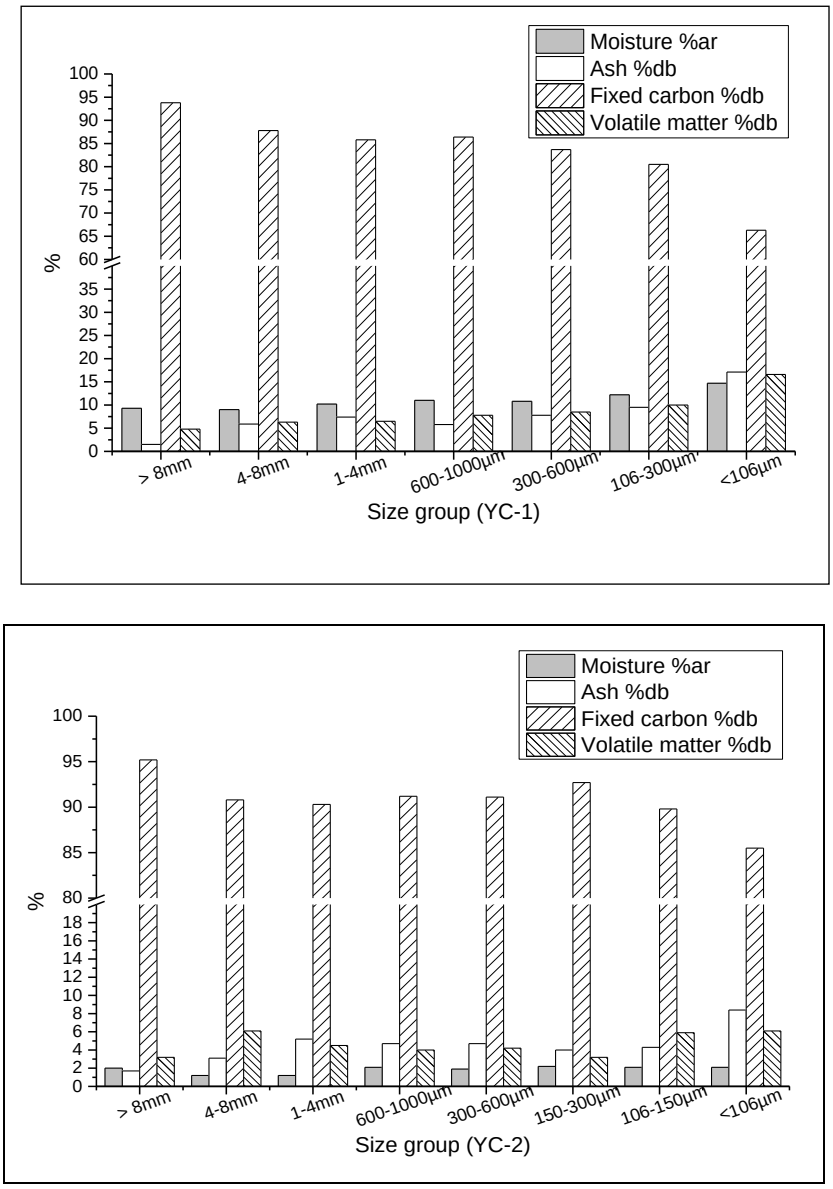

Figure 6.2 Proximate analysis of size segregated YC-1 (top) and YC-2 (bottom).

The true and apparent densities of two char samples were also measured (Table 6.2). For comparison, a commercial PCI bituminous coal was also tested, which is composed of 20.3 *wt%* volatile matter, 8.7 *wt%* ash, 1.9 *wt%* moisture and 70.6 *wt%* fixed carbon on a dry basis. As can be seen, the longer pyrolysis duration of YC-2 resulted in a larger porosity, a lower apparent density and a larger true density than its counterpart char sample YC-1. Its true density is almost as high as a pure graphite crystal (2260 kg/m^3) [25], which is another sign of the strong secondary reactions such increases in carbon aromaticity [26], or coke/soot formation from the primary volatile release. However, the low apparent density for the two char samples implies

probable changes on the aerodynamics of char particles in both the mill and the blowpipe when they are used as a substitute for bituminous coal. Finally, the calorific value (i.e. energy content) of the three fuels is noteworthy. As evident in Table 6.2, YC-2 has the largest energy content, followed by PCI coal and YC-1 in a descending sequence. This is because YC-2 has the least volatile and ash content, as an expense of increasing the particle residence time in the pyrolyser.

Table 6.2 True density, apparent density, calculated porosity, calorific value and surface area of PCI coal, YC-1 and YC-2

	PCI coal (<106 μm)	YC-1 (1-4 mm)	YC-2 (1-4 mm)
True density (kg/m^3)	1441	1863*	2204*
Apparent density (kg/m^3)	1264	894.3*	813.1*
Bulk density (kg/m^3)	644.2	510.7*	417.8*
Porosity, [-]	12.3%	52.0%	63.1%
Calorific value (KCal/kg)	7801	7517	8114
BET surface are (m^2/g)	Not measured	334	56.7

*: The size of <106 μm for each char sample has also been analysed, showing little difference with the size of 1-4 mm

X-ray diffraction (XRD) was also used to examine the differences in carbon structure for the 1-4 *mm* size fractions of both YC-1 and YC-2 char as well as PCI coal (Figure 6.3). It can be seen in this figure that the demineralisation procedure was sufficient to be able to analyse the carbon properties without significant interference from inorganic minerals. The concentration of species in the entire sample, as measured by XRF, can be found in supporting information Table S1. YC-2 char exhibits a sharper (002) graphite peak, at ~24° and a sharper (100) graphite peak at ~43° indicating a greater degree of ordered carbon structures. The (002) peak which is associated with aromatic side chains is expected to also be influenced by the overlapping γ peak which is associated with aliphatic side chains [27]. PCI coal also shows a very sharp peak in this region which is expected since aromaticity increases with coal rank [28]. Increased carbon

aromaticity is linked with increased carbon ordering and true density and will negatively influence the reaction rate [26]. It is possible to split the first peak into symmetrical (002) and γ peaks, and subsequently integrate to calculate the degree of aromaticity, f_a with Equation 6.3.

$$f_a = \frac{A_{(002)}}{A_{(002)} + A_\gamma} * 100\ \% \qquad \text{Equation 6.3}$$

Where A_{002} is the area under the (002) and A_γ is the area under the γ peak.

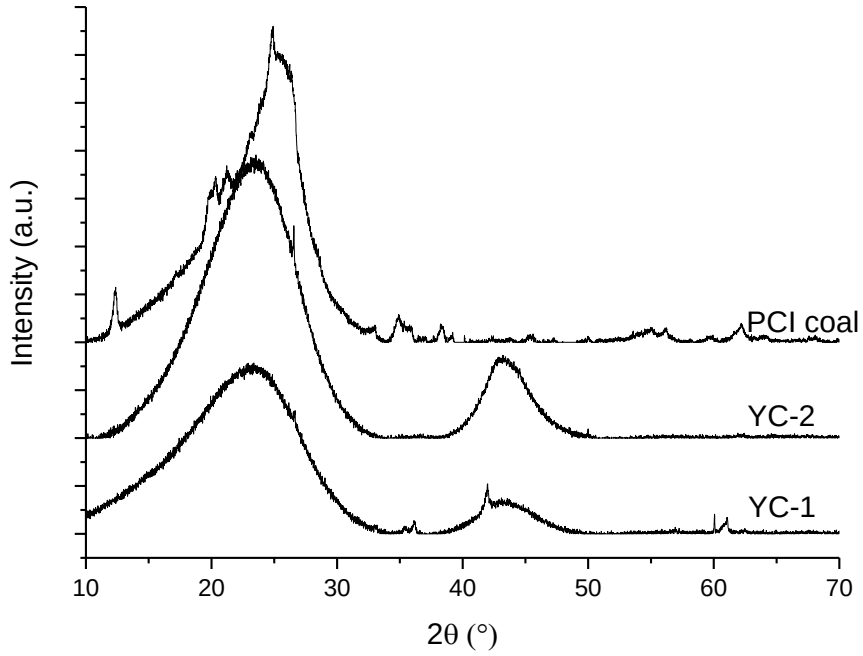

Figure 6.3 XRD spectra for YC-1 and YC-2 char samples as well as PCI coal

The curves used in the calculation of the area can be found in supporting information Figure S3. For both char samples, two symmetrical peaks were able to match the original peak with an adjusted R^2 value above 0.998. The aromaticity of YC-1 and YC-2 chars were determined to be 67.8% and 82.8% respectively, indicating that the char aromaticity is increased in the case of YC-2 char.

Table 6.3 further summarizes the ash compositions (in its most stable oxide form) for the different sizes of YC-1 sample and ash fusion temperature. The most abundant element is Fe, followed by Mg and Ca, whereas the contents of alkali metals (Na and K) are extremely low. This is different from woody charcoal which is rich in alkali metals [11]. Due to the abundance of Fe and Mg, the ash melting temperature is also higher than 1550 °C. All these properties are

superior over the bituminous coal with the abundance of silicon, aluminium, calcium, iron and even sodium in the ash. Due to the co-existence of these five elements, the bituminous coal ash has a larger tendency to melt and cause fouling in the burner vicinity. Such problems would be obviously avoided in the case that the Yallourn char was used as the PCI fuel.

Table 6.3 Size-dependent ash compositions of YC-1 sample and ash fusion temperatures

	Char size, μm							
Element	>8000	4000-8000	1000-4000	600-1000	300-600	106-300	<106	PCI coal
SiO_2	0.6	0.8	1.5	1	1	1.2	1.3	40.5
Al_2O_3	0.8	1.7	1.4	1.4	1.3	1.4	1.3	27.6
Fe_2O_3	20.1	34.7	34.9	36	39	41	48.4	16.0
MgO	28.3	27.6	26.5	26.9	27.6	28.4	28.4	0.02
CaO	23.2	15.7	17.2	16.5	14.6	13.7	11.4	13.1
SO_3	22.2	16.5	15	14	13.6	11.5	6.7	6.6
K_2O	2.2	1.5	1.9	1.6	1.1	0.8	0.5	0.5
Na_2O	0.3	0.2	0.2	0.2	0.2	0.2	0.3	3.7
Ash fusion temperature, °C								
	Reducing atmosphere			Oxidizing atmosphere				
Deformation temperature	>1550			>1550				
Hemispherical temperature	>1550			>1550				
Spherical temperature	>1550			>1550				
Flow temperature	>1550			>1550				

6.3.2 Reactivity and ignition in TGA

The results in Figure 6.4 indicate that the ignition point of YC-1 is close to that of the PCI coal, although the volatile contents of YC-1 are less than that of its counterpart. YC-2 has an ignition point approximately 100 °C above that of YC-1. This should be attributed to a high volatile content for YC-1 char (as evident in Figure 6.2) as well as an increased surface area of YC-1 char as evident in Table 6.2. Increasing particle size shows a marginal increase in the ignition temperature, further supporting the dominance of heterogeneous ignition mechanism for the Yallourn char.

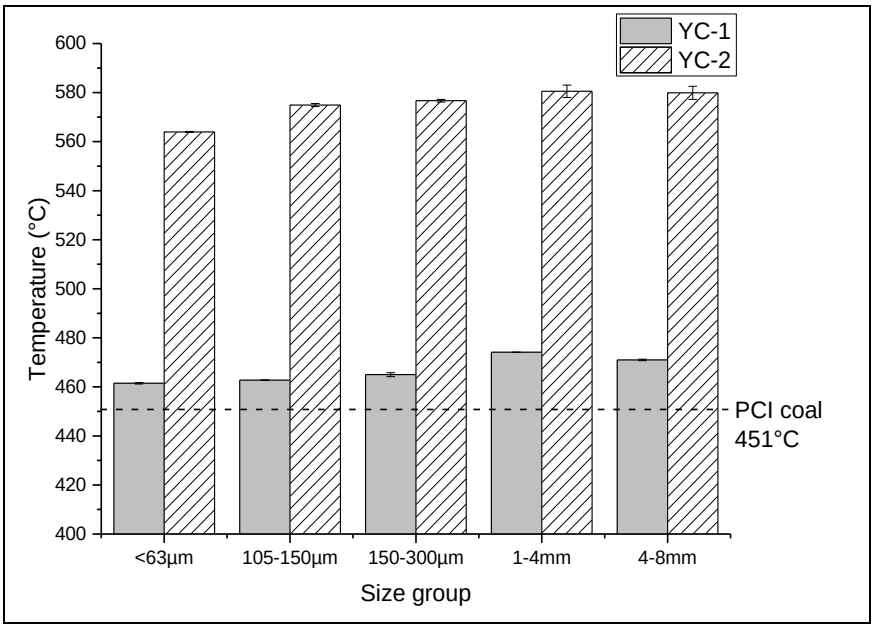

Figure 6.4 Ignition temperatures for lignite char samples and PCI coal

Figure 6.5 was plotted to compare the intrinsic char-O_2 reactivity of different samples. These reaction rates were plotted based on the kinetic parameters found by analysing the char mass loss curves (Figure S4) using the previously described direct Arrhenius plot method (Figure S5). The results show significantly higher reactivity for YC-1 samples, irrespective of its size. PCI coal showed lower reactivity than YC-1 char, while YC-2 char generally had the lowest reactivity below 800 °C. Above 800 °C, YC-2 shows a similar reactivity to PCI coal. This is expected due to the increased pyrolysis time of YC-2, resulting in a lower surface area, higher true density (Table 6.2) and more ordered carbon structure (Figure 6.3). The partially demineralised samples used in the XRD analysis were also analysed for their char-O_2 reactivity to discover whether the higher reactivity of YC-1 can be attributed to the increased presence of ash forming minerals which could catalyse the char conversion reactions. The previously mentioned supporting information Table S1 shows that the demineralised YC-1 char contains less iron and also less total ash then the unwashed YC-2 char. However, the results from the demineralised char samples were almost identical to the unwashed char, proving that differences in char-O_2 reactivity are purely due to the carbon structure rather than the higher ash content of YC-1 compared to YC-2. This comparison plot is shown in Figure S6 in the supporting information. In terms of particle size group, smaller sizes showed increased reactivity, due to the larger specific surface area and the minimal/negligible diffusion control.

Ground samples showed a comparable reactivity to that of samples of a similar size that were not ground. Clearly, the broad variation of the reactivity of char as a function of size should pose an effect on its combustibility. This will be examined by sensitivity analysis via CFD modelling later.

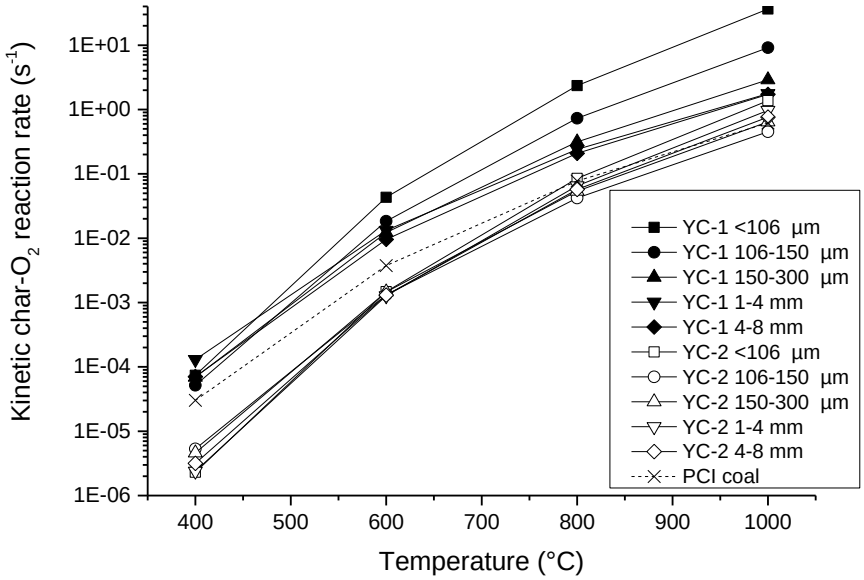

Figure 6.5 Intrinsic char-O_2 reactivity of lignite char samples and PCI coal

6.3.3 Ignition and Burnout in DTF experiments

A CCD camera was used to capture the YC-1 particles ignition sequence after it is injected into the hot blast in the DTF at 1000 °C and an O_2/C ratio of 1.2, as shown in Figure 6.6. Upon an exposure time of 0.25 *s*, the char particles sparkled individually, forming a long trajectory in the field of view (FOV) of the camera. Such an ignition should be mainly assigned to heterogeneous ignition of char surface, since the volatiles in this char are very lean. Otherwise, a large fireball formed upon the homogeneous firing of volatiles should be observed, as has been confirmed for raw lignite coal combustion [29]. The char combustion was continued stably, radiating strong heat in the FOV of the camera in 0.5 *s*. In addition, it is noteworthy that, the heterogeneous sparkling of char particles observed here, due to the shortage of volatiles, is beneficial in providing a low pressure drop and hence a stable operation of the tuyere of the blast furnace [30].

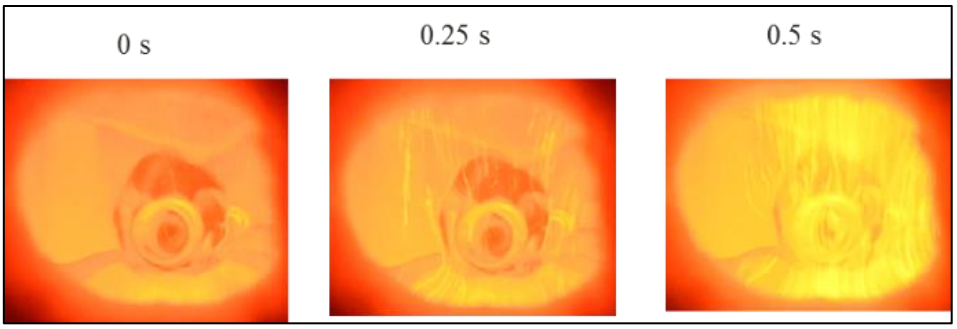

Figure 6.6 Char ignition sequence of YC-1 <106 μm at O_2/C=1.2 and 1000 °C

The effects of char particle size and O_2/C molar ratio were tested for the burnout of YC-1 at three temperatures. Figure 6.7(a) for YC-1 char shows that, irrespective of O_2/C ratio and reaction temperature, the particle size range of 106-150 μm only showed slightly decreased burnout compared to the smallest size <106 μm for the same char, while the large size 150-300 μm show a much decreased burnout particularly at 800 °C and 900 °C. Such a decrease should be attributed to two reasons, one is the enlarged resistance against the internal diffusion of oxygen within char particle, and another one should be the decreased volatile matter content upon the increase of char particle size, as evident in Figure 6.2. However, discrepancy between the three char sizes was narrowed considerably by increasing both the O_2/C molar ratio and furnace temperature. An increase in the O_2/C molar ratio is beneficial in reducing the resistance against the external diffusion of oxygen for larger particle sizes. The similar observation was confirmed for YC-2 with a much lower volatile content in *panel b*.

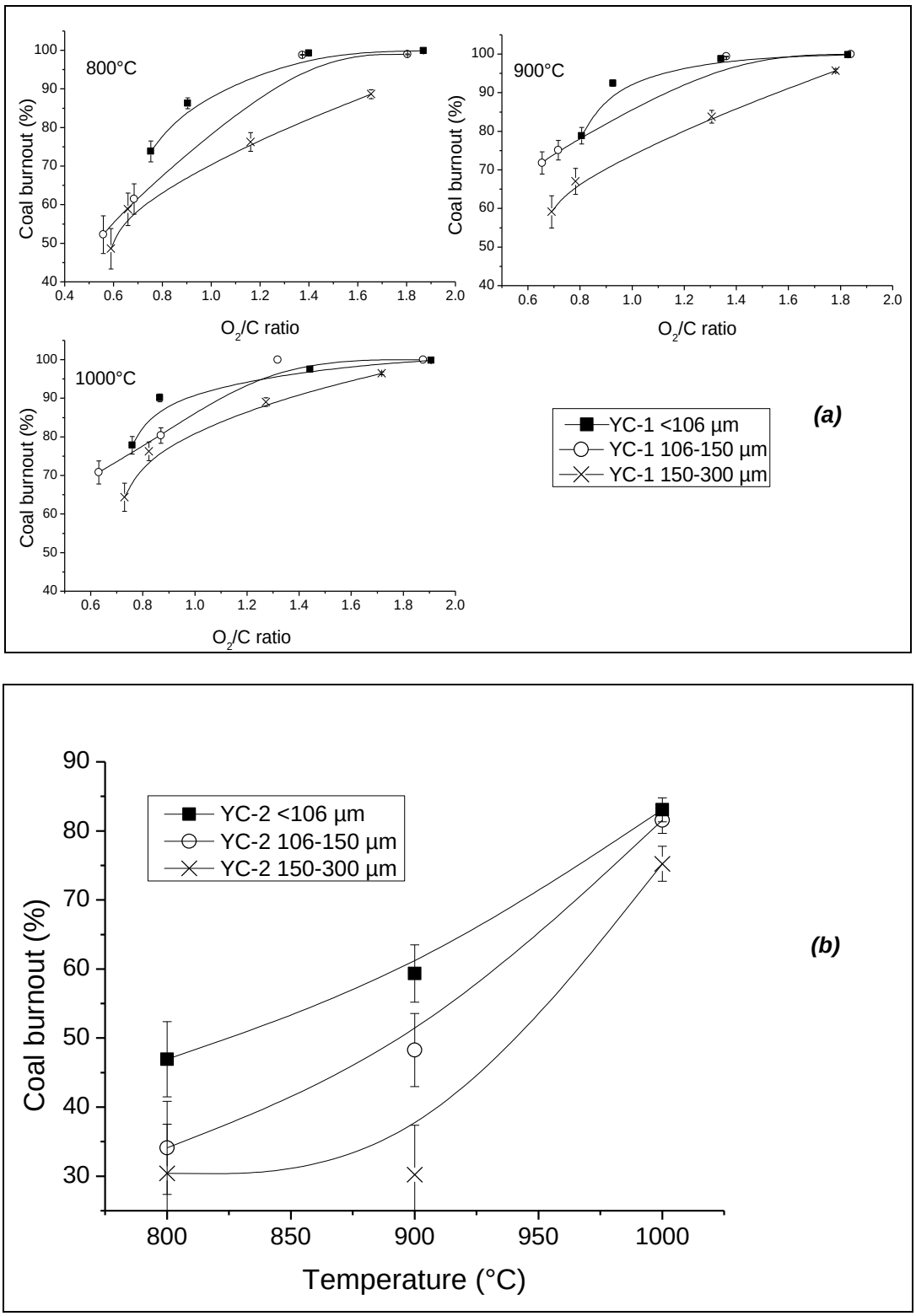

Figure 6.7 Effect of particle size on burnout for (a) YC-1 at three O_2/C ratios and (b) YC-2 at a fixed O_2/C ratio of approximately 0.9

Figure 6.8 further compares the burnout rate as a function of O_2/C molar ratio between two lignite chars and the bituminous coal reference at 1000 °C, which is much closer to the temperature profile in the blowpipe in a real blast furnace. Note that, all the three samples are smaller than 106 μm in size. As can be seen, the commercial bituminous coal requires a minimum O_2/C molar ratio of 1.2 to reach its maximum possible burnout at 92.5 *wt%*. However, under such an excess O_2 condition, YC-1 sample reached a complete burnout, whereas YC-2 achieved around 95 *wt%* burnout, which is still higher than that of the commercial PCI coal. Apart from the high reactivity, the large porosity of Yallourn char is also another important variable affecting the necessary amount of oxygen for combustion. Compared to Yallourn char having a porosity of 52-63.1%, the bituminous coal tested here has a much smaller porosity of 12.3% which thus poses a larger resistance against the internal diffusion, in particular in the later stage of coal combustion where the oxygen in bulk gas is insufficient and its diffusion is thus critical.

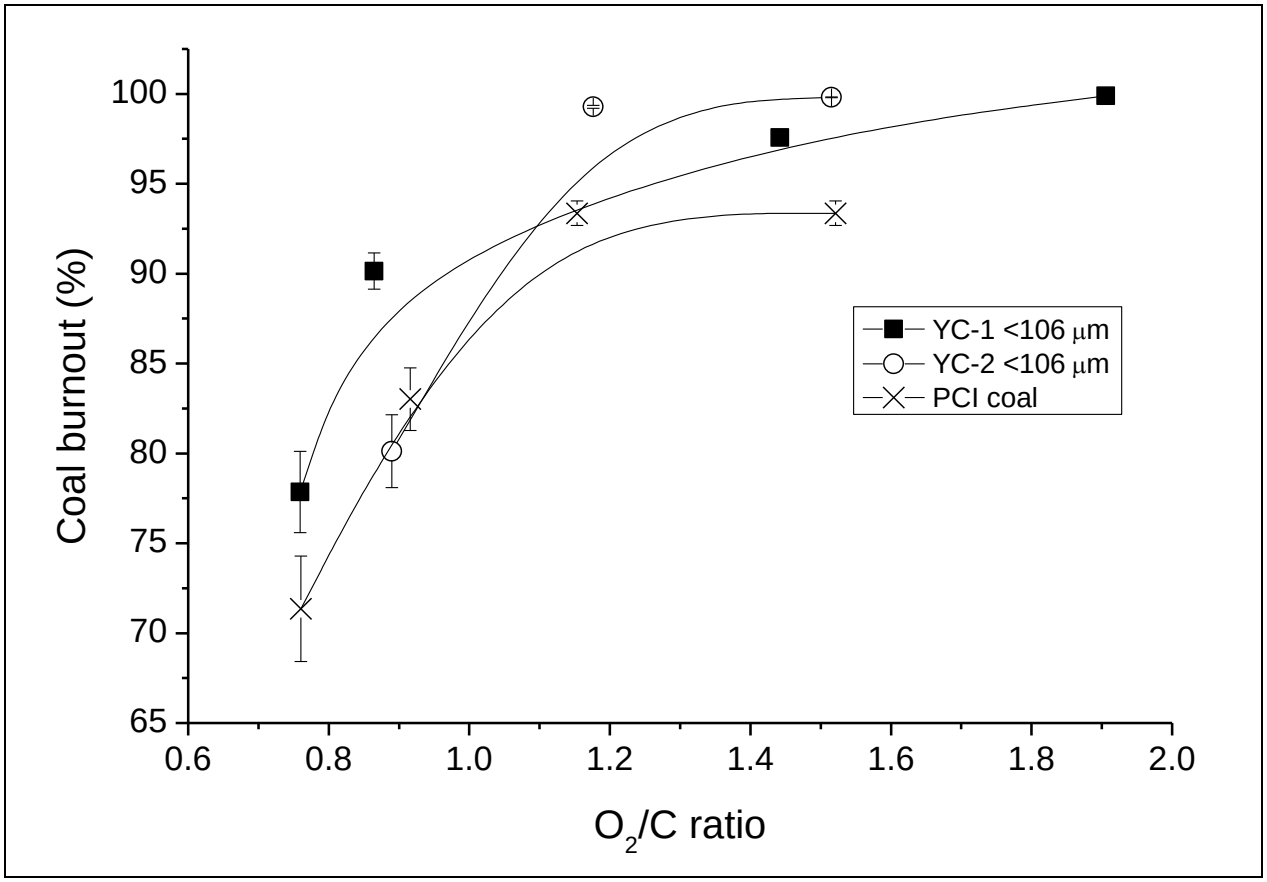

Figure 6.8 Differences in reactivity between the two Yallourn char samples and PCI coal at 1000 °C

Figure 6.9 further substantiates the high burnout of Yallourn char and its distinct combustion mechanism at a fixed O_2/C molar ratio of 0.8-0.9 that is close to the stoichiometric ratio for the combustion. For the YC-1 char sample, increasing its particle size resulted in a reverse exponential decrease on the carbon burnout, substantiating the above hypothesis that the external diffusion of oxygen is the control step for the three blast temperatures tested here. Even so, the burnout for YC-1 is still very high, reaching a value of approximately 70 *wt%-daf* for the largest size that is close to the results for bituminous coal achieved at 1000 °C. With regard to the commercial bituminous coal, it is obvious that the external oxygen diffusion is insignificant at these three blast temperatures, as reflected by a rather comparable burnout between the three coal sizes at each temperature. To reiterate, the slow reaction rate and internal diffusion due to the small porosity are more important for bituminous coal combustion.

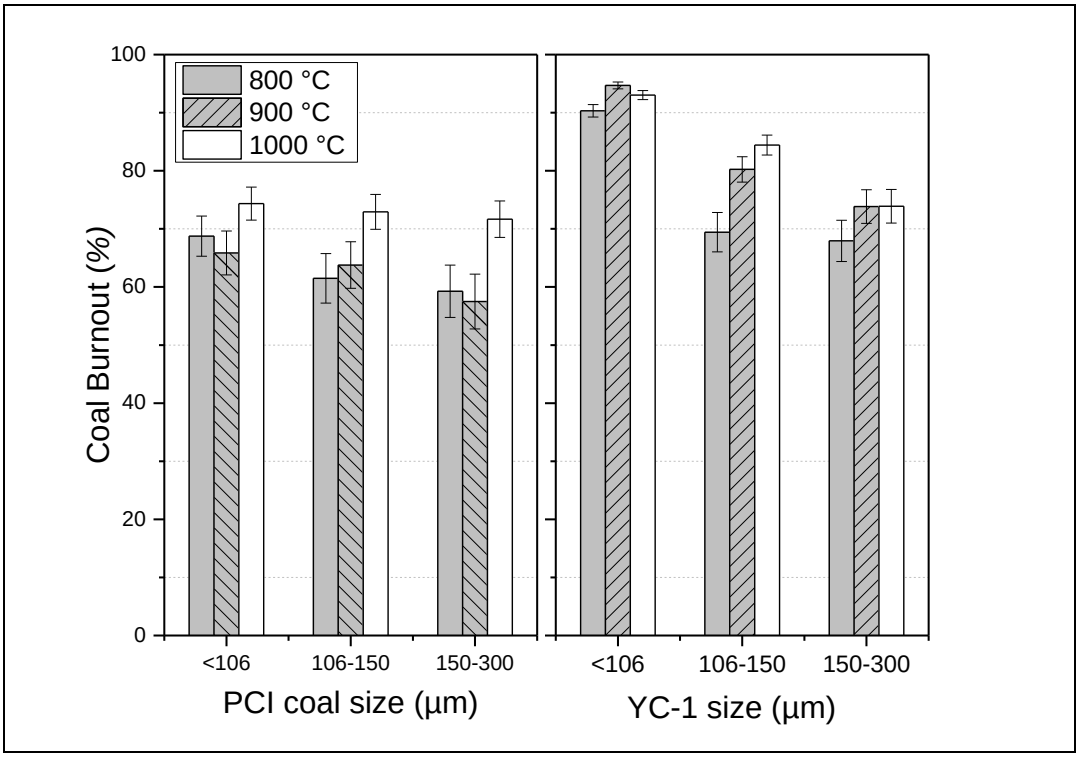

Figure 6.9 Comparison of the burnout of differently sized YC-1 char (right) and commercial PCI coal (left) at an O_2/C molar ratio of 0.8-0.9

Finally, the burnout of lignite char as a function of volatile matter was established in Figure 6.10 at a fixed O_2/C molar ratio of 0.8-0.9 and 1000 °C. This is to assess the dependence of

such a low-volatile char combustion on its volatile matter content, as well as to determine the minimum volatile content in the char to ensure a complete burnout. For the PCI coal application in the blast furnace, the volatile content is deemed as the most influential criteria for the coal selection [16]. Interestingly, a single linear trend line was not observed. Instead, the two char samples show rather different trend lines with different slopes. The YC-1 char has a smaller slope which is estimated to be around 0.68 for a volatile content down to 6 *wt%*. Such a slope was also much smaller than that has been established for commercial PCI coals in the literature [16]. However, for the YC-2 char produced with less volatiles under harsh conditions, a much steeper slope was found for its volatiles ranging from ~ 3 *wt%* to 6 *wt%*. By combining the trend lines for the two chars, it is obvious that ~ 6 *wt%* is the minimum volatile content requested for the prepared lignite char, otherwise its burnout at 1000 °C and below would drop dramatically to a level that is even lower than the commercial PCI coal. Compared to the natural bituminous coal, the char tested here is a prepared material, and thus, change on its volatile content will lead to the change on the other properties including porosity, structure and reactivity of the remaining carbonaceous matrix. Since all these changes will interlay and affect the performance of the char combustion jointly, the results from CFD modelling in the next section will be further interpreted to appropriately address the combustion of Yallourn char under the simulated blast furnace conditions.

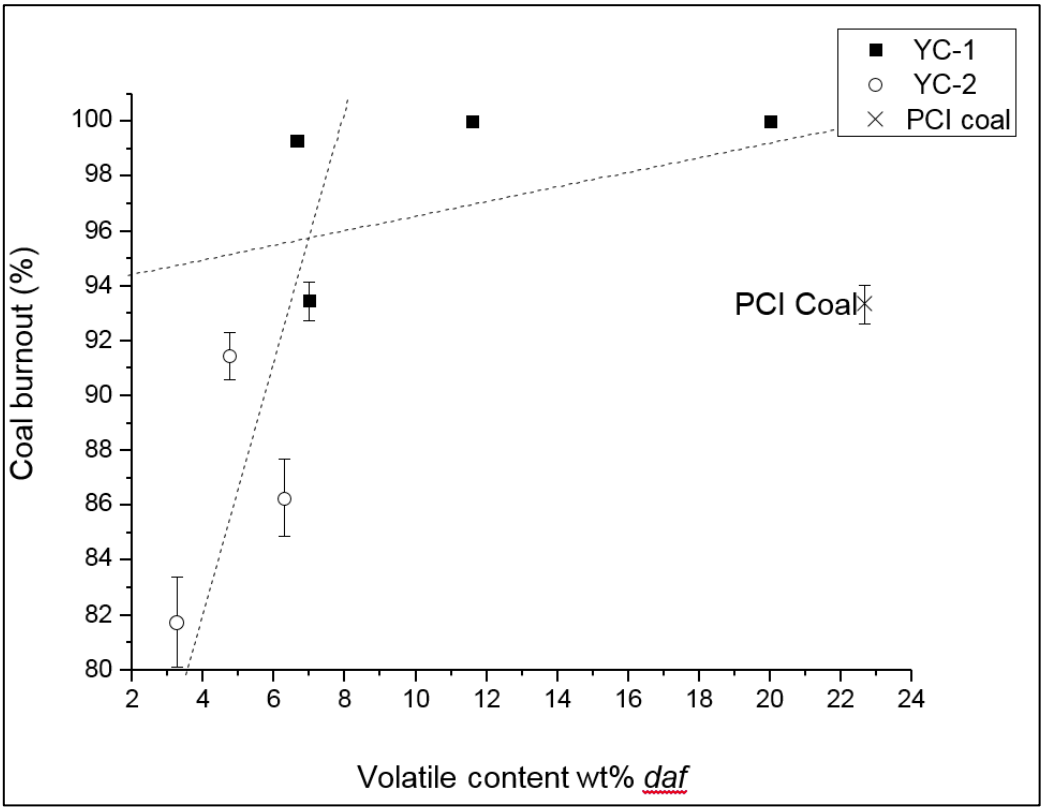

Figure 6.10 Char burnout versus volatile content for two Yallourn chars at a fixed O_2/C ratio of 0.8-0.9 and 1000 °C

6.3.4 CFD modelling

6.3.4.1 Model Validation

Apart from the previously described grid independence test and particle temperature measurements [17], the model for char burnout was further validated here by comparison of char burnout and outlet O_2 concentration in flue gas as obtained from the DTF experiments and as predicted by the CFD model. The comparison plots can be found in Figure 6.11. A reasonable relationship is seen between the experimental and simulated results. Some variation is expected due to the sensitivity of DTF inputs and measurements.

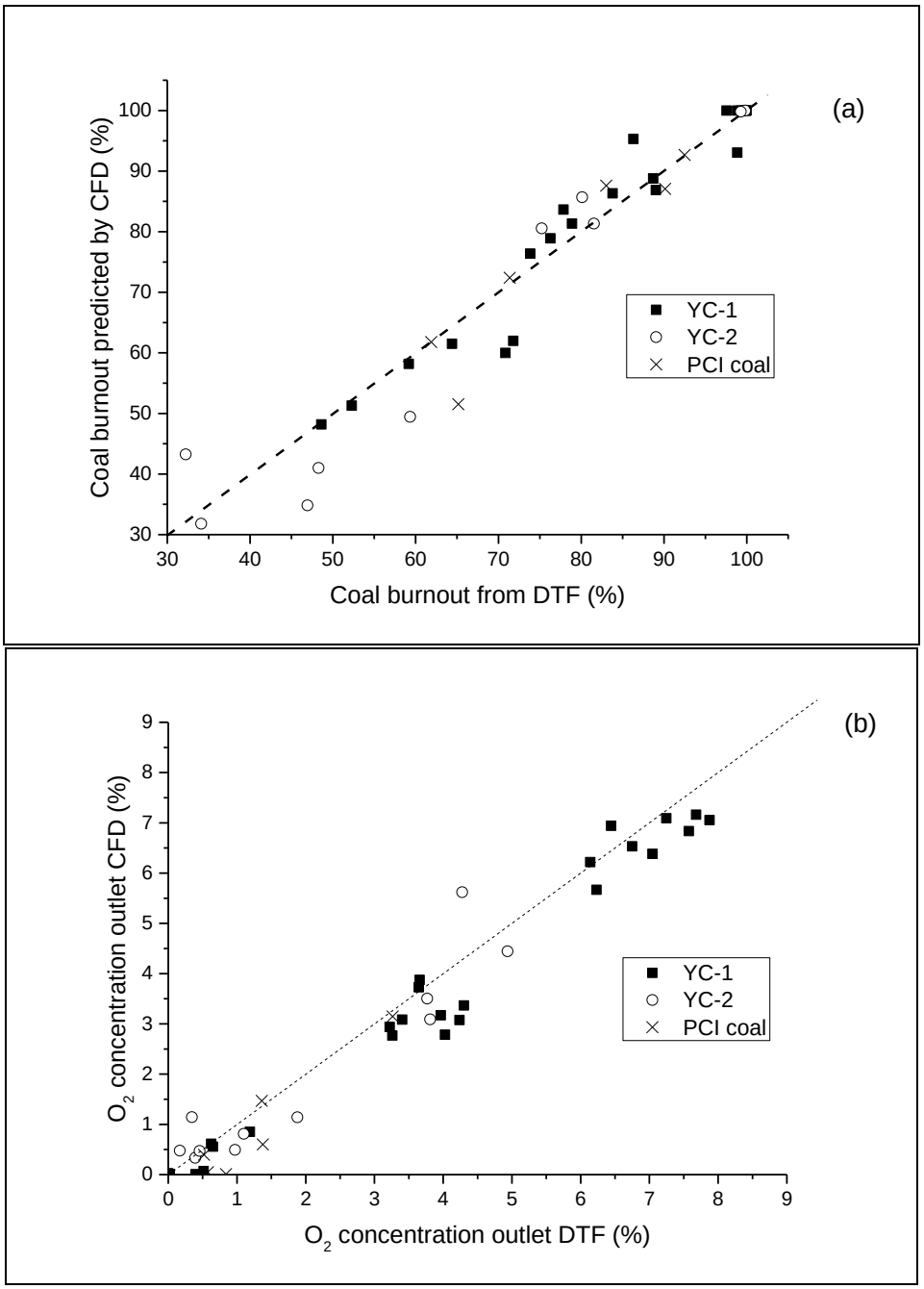

Figure 6.11 Comparison of (a) burnout and (b) O_2 concentration in outlet between DTF and CFD model

6.3.4.2 CFD Results Interpretation

Figure 6.12 first compares and predicts the effect of varying wall temperature, and subsequently the preheated gas temperature for the two Yallourn chars versus the reference coal, at a fixed O_2/C ratio of 1.0 (stoichiometric ratio) with a constant feeding rate and modified O_2 concentration. For the reference bituminous coal, its burnout profile shows a great dependence on the temperature. At 900 °C, it reaches a final burnout of only 60 % at the exit of the whole reactor for a residence time of 1.8 *s*. The burnout profile consists of two steps, with the first step being finished in 0.2 *s* for the release and combustion of the volatiles, whereas the latter one for the heterogeneous oxidation of the char. Upon the rise of reaction temperature to 1100 °C, the two steps overlap considerably. This results in a relatively smooth burnout profile and the completion of the combustion in 1.4 *s*. Increasing the temperature to 1200 °C further enhanced the overlapping between different stages, and shortened the burnout time to about 1.0 *s*.

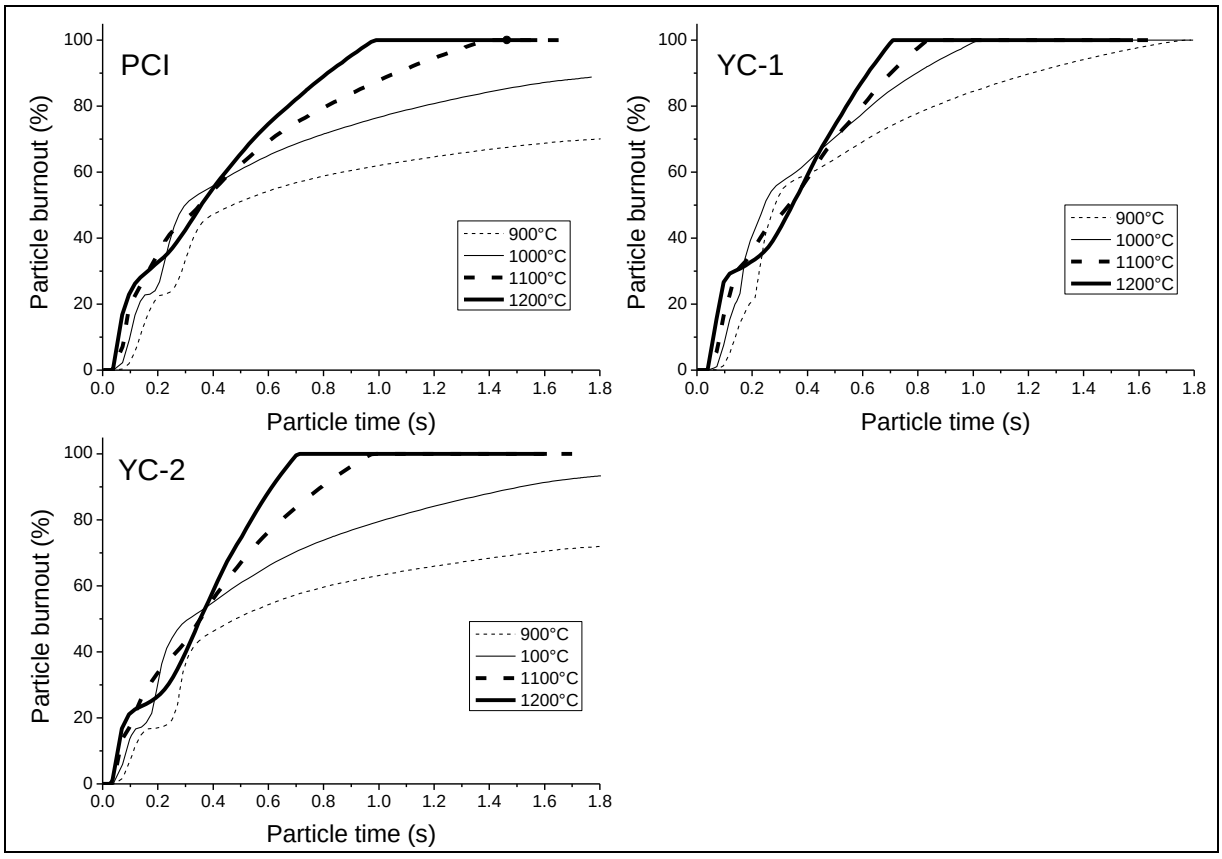

Figure 6.12 Effect of temperature on particle burnout at O_2/C=1.0

The YC-1 char combustion shows a less dependence on the temperature, even accomplishing its burnout in 1.6 *s* at 900 °C. Upon the rise of combustion temperature, the time to complete its burnout was further decreased to 1.0 *s*, 0.8 *s* and 0.7 *s* at 1000 °C, 1100 °C and 1200 °C, respectively. Moreover, the first step for YC-1 combustion, completed at around 0.3 *s* for 900 °C resulted in a loss of around 60 *wt%* of the char. By revisiting the visualized ignition sequence for this char in Figure 6.6, one can clarify that the heterogeneous ignition occurred concurrently with the ignition of volatiles in such a short distance. The heterogeneous ignition even predominated since the volatiles only account for maximum 15 *wt%* (see Figure 6.2) for YC-1 char. More interestingly, it is also referable from Figure 6.12 that the two steps for YC-1 char are rather split at 1200 °C. The overall burnout profile at this temperature is also rather similar with that of the bituminous coal, suggesting the analogy of the combustion performance of these two fuels at the high furnace temperature. In other words, the properties of the original fuel are insignificant at high temperature. This could hold true, considering that the solid combustion generally shifts from reaction control to external diffusion control upon the elevation of the reaction temperature. The similar phenomena was also observed for another Yallourn char, YC-2.

Figure 6.13 demonstrates the time-resolved particle temperature profile for bituminous coal versus YC-1 char at 1000 °C and 1200 °C at the stoichiometric O_2/C molar ratio of 1.0. According to *panels (a)* for bituminous coal, a particle was continuously heated until it reached a peak temperature which was around 1300 °C and 1400 °C at the furnace temperature of 1000 °C and 1200 °C, respectively. This is due to the exothermic nature of the combustion providing heat feedback to the particle self. The respective first-order derivative in *panel (a')* further explored the existence of different combustion stages for bituminous coal. At 1000 °C, the initial peak for ignition was rather weak for bituminous coal, substantiating a slow release and ignition for the volatiles. A much stronger and broader peak at the residence time of 0.2 *s* was observed, reflecting the combustion of both the lagged volatiles and solid char at this stage. Increasing the furnace temperature to 1200 °C accelerated the volatile release rate, as echoed by a remarkable increase on the intensity of the first peak in panel (a'), and the second peak also shifted remarkably to a shorter residence which is around 0.1 *s*. Clearly, the PCI coal char reactivity holds a more sensitive variation than the volatiles upon the variation of the temperature. Since the distance between two stages was shortened at 1200 °C, the burnout

profile in Figure 6.12 is thus relatively smoother for the PCI coal at such a high furnace temperature.

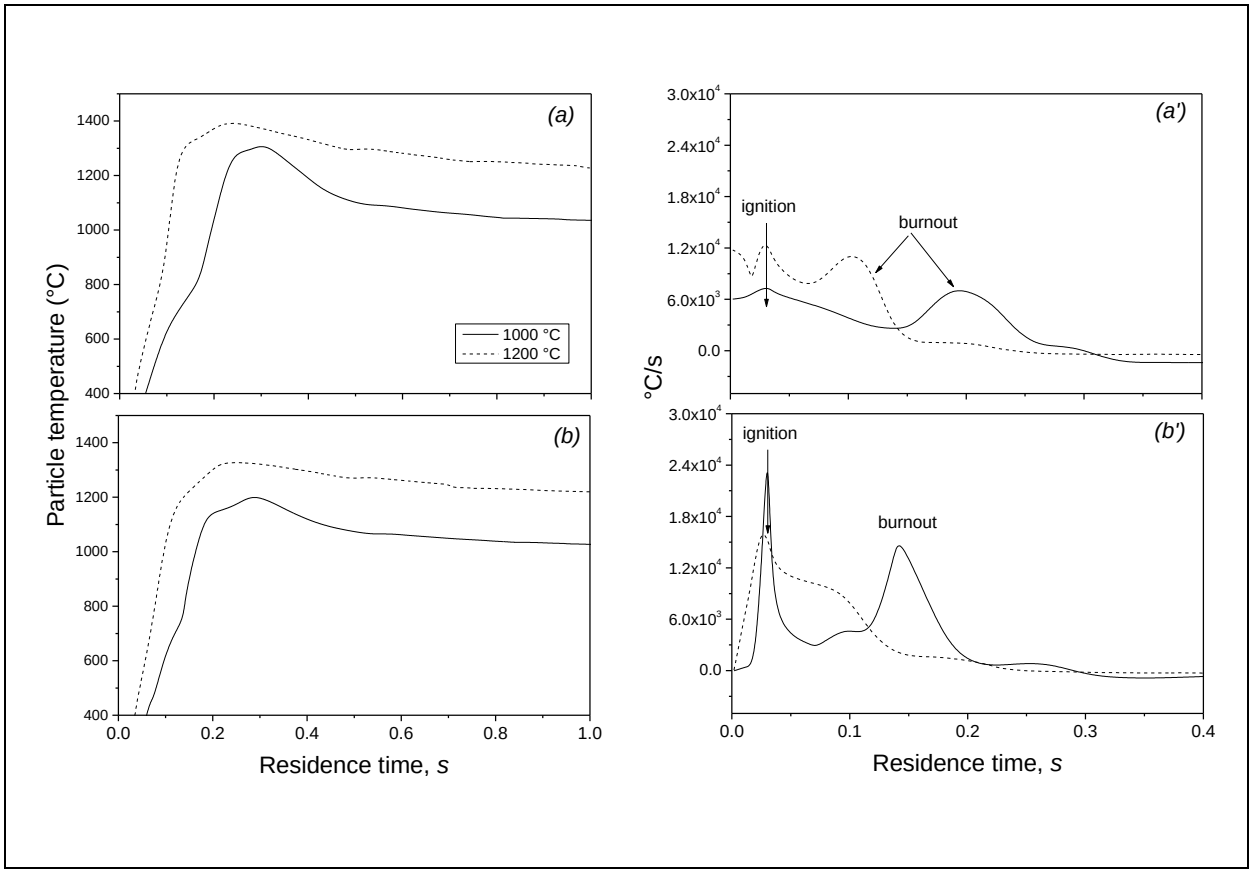

Figure 6.13 Temperature distributions for PCI coal (a) and YC-1 char (b) near the injection zone with wall temperature (a) 1000 °C and (b) 1200 °C at O_2/C=1.0. Panels (a') and (b') are the first-order derivative of panel (a) and (b), respectively.

The results of Figure 6.13(b) for the time-resolved particle temperature of YC-1 are quite similar with the PCI coal in panel (a). However, the respective first-order derivative in panel (b') explored a rather distinct combustion behaviour for the Yallourn char. Even at the low furnace temperature of 1000 °C, the first peak for particle ignition is much stronger than that observed for the bituminous coal. Obviously, this peak should be partially attributed to the heterogeneous ignition of char particle, otherwise, less heat would be provided to heat up the particle rapidly. The amount of char participating in the first stage should also be considerable, thereby releasing sufficient heat feedback to heat up the particle at a peak rate of 2.4 x 10^4 °C/s, which is around four times of the particle heating rate observed for the bituminous coal. Consequently, around 60 *wt%* of the YC-1 was consumed at the first stage, as evident in Figure 6.12. Regarding the temperature rise to 1200 °C, the left shift of the second peak for char

burnout is not surprising, which can be fully assigned to the high reactivity of Yallourn char. However, it is more intriguing to observe a decreased intensity for the first peak when compared to 1000 °C. This explained the reduction on the mass loss at the first stage back to the burnout profile for YC-1 char in Figure 6.12. It may also reveal a different reaction route for YC-1 char at such a high temperature. Since the radiative heat transfer from the furnace wall was enhanced upon the furnace temperature rise, it is very likely that the exothermic reaction such as C-CO_2 gasification has taken place at this stage. Otherwise, the particle would be heated up more quickly. As has been confirmed in a separate study [17], the gasification reaction contribution is remarkable for Victorian brown coal char. This should also be the case for the YC-1 and YC-2 char samples tested here, since they are also collected from the Latrobe valley.

Effort was further made by the CFD modelling to clarify the effect of particle size on the burnout of Yallourn char at 1200 °C for a stoichiometric oxygen to carbon molar ratio. As substantiated in Figure 6.14, as particle size increased to a range of 150-300 μm, the burnout profile of YC-1 char is still comparable to PCI coal. The large specific surface area of woody charcoal was also proven accounting for its higher reactivity than the PCI coal [30]. Beyond that, the burnout for the particle of 300-450 μm dropped sharply due to the decreased surface area available and increased diffusional resistance. Clearly, irrespective of the pyrolysis conditions, the use of large size such as 300 μm for Yallourn char is viable, reaching a comparable burnout rate to the bituminous coal.

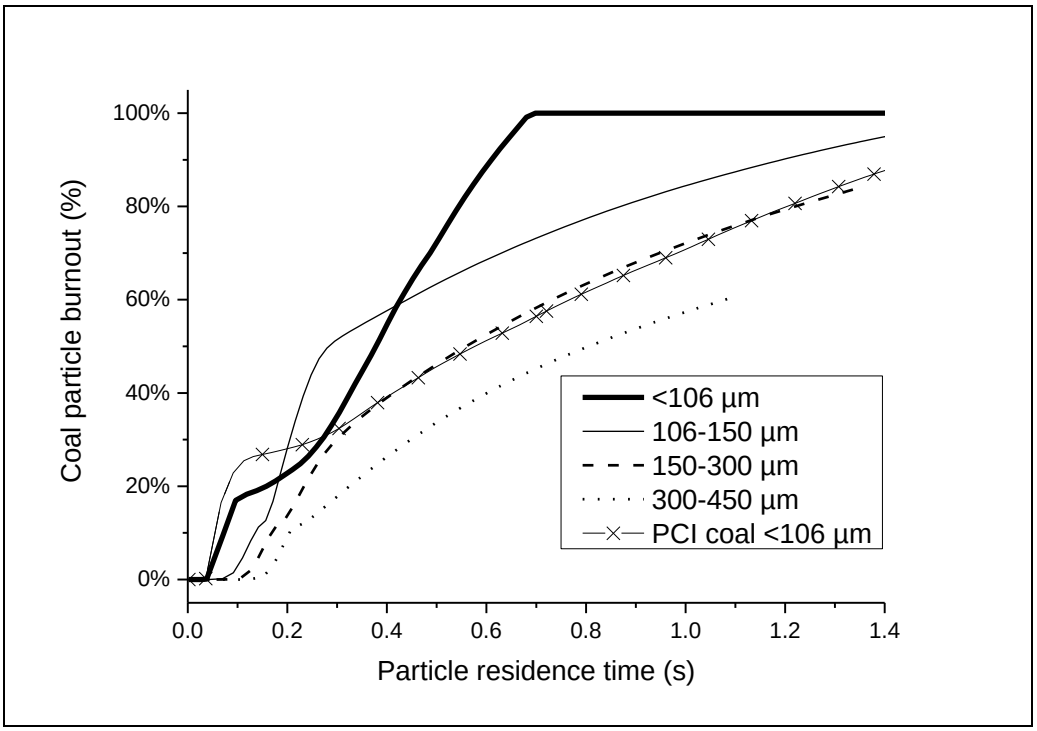

Figure 6.14 Difference in burnout of YC-1 char with respect to particle size at 1200 °C and O_2/C=1.0.

The last thing of interest to us is to further validate the burnout of Yallourn char versus its volatile content, so as to elucidate the minimum volatile content that is a critical criteria for the selection of PCI coal. For this, CFD modelling was further conducted to extend the experimentally established results in Figure 6.10 to three furnace temperatures, 800 °C, 1000 °C and 1200 °C, at a fixed O_2/C molar ratio of 1.0 and a fixed residence time, 0.7 *s* for the first two temperatures and 0.5 *s* for the last one. A residence time of 0.5 *s* rather than 0.7 *s* was chosen for 1200 °C, because both YC-1 and YC-2 char samples completed their burnout in 0.7 *s* at 1200 °C, as evident in Figure 6.12. The different sizes of each char sample were reduced to the same particle size range (<106 μm) while keeping its reactivity unchanged. As illustrated in Figure 6.15, the critical volatile content of 6 *wt%* was confirmed for 800 °C and 1000 °C, which agrees with the experimental observation as shown in Figure 6.10. For YC-1 char with its volatile content varying from 6 *wt%* up to 20 *wt%*, it holds a clear upward trend for its burnout versus the volatile content. However, for the YC-2 char with a maximum 6 *wt%* volatile content, its broad scattering rather suggests that, for the char with extremely low volatile content, the higher heterogeneous combustibility and larger porosity of char could

outweigh the volatile content, enhancing the burnout rate of char via dominantly heterogeneous oxidation. Increasing the blast temperature to 1200 °C alleviates the dependence of lignite char burnout on its volatile content, as evident by a rather flat slope for the trend line and insignificant variation of char burnout versus the volatile content. All the burnouts are also far higher than that of the PCI coal at this temperature, although its volatile content is high. Clearly, in an industrial blast furnace employing a hot blast temperature close to 1200 °C, the use of the lignite char tested here, irrespective of its preparation condition, is beneficial in offering a higher injection rate, thereby improving the coke replacement ratio and the productivity of the blast furnace.

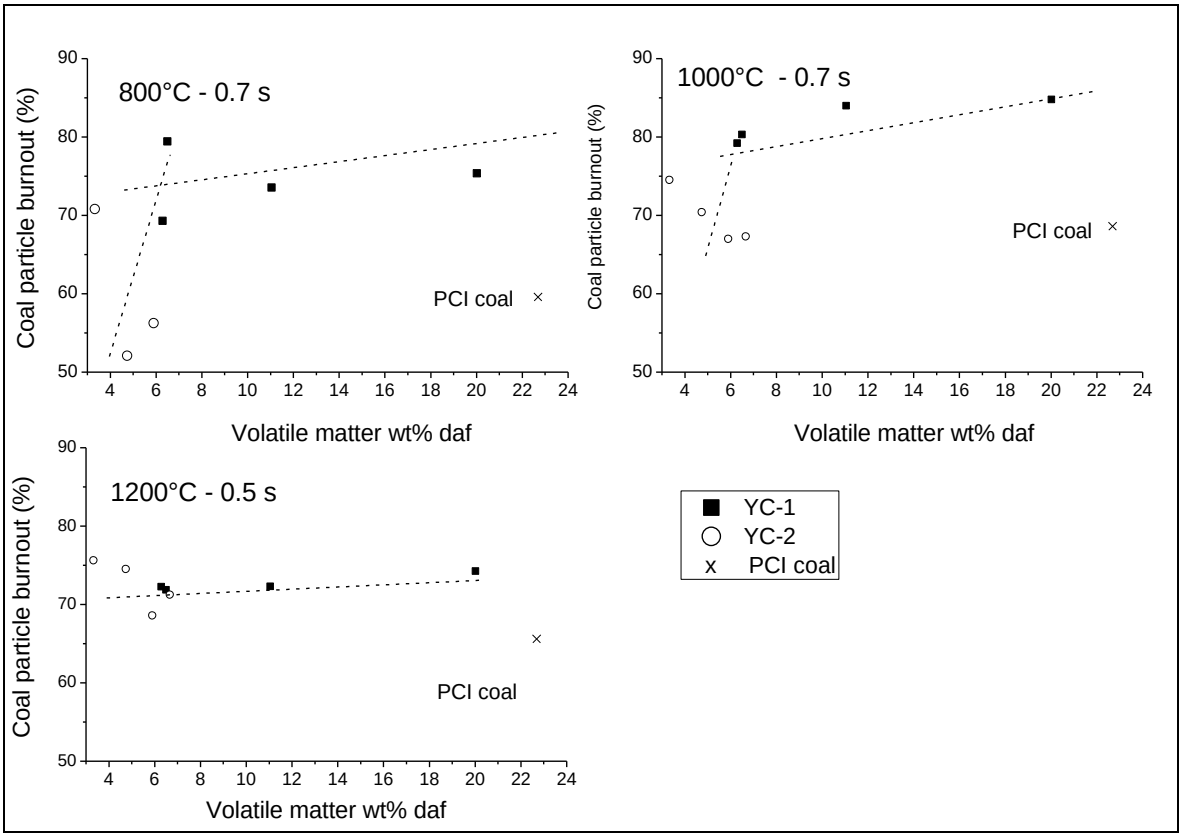

Figure 6.15 Dependence of burnout on volatile matter predicted by CFD at 0.7 *s* (800 °C, 1000 °C) or 0.5 *s* (1200 °C)

6.4 Conclusions

In this paper, we have for the first time tried to establish the linkage between brown coal pyrolysis condition and the end-use of the resultant char as a PCI fuel in the blast furnace. Efforts have been made to quantitatively examine the size - dependent properties of Yallourn

char collected from an industry-scale shaft furnace, its potential and benefits for the replacement of commercial bituminous coal in the blast furnace. The major original findings from this study can be drawn as the follows:

1. Irrespective of the pyrolysis condition, the char derived from Yallourn coal is suitable for the use as the top-grade PCI fuel in blast furnace. Compared to the bituminous coal requiring a very fine size (e.g. <106 μm), excessive oxygen and high temperature (e.g. >1200 °C) for a complete burnout, the Yallourn char tested can achieve the comparable burnout rate under the rather mild conditions, *e.g.* 150-300 μm in size, stoichiometric O_2/C molar ratio of 1 and a furnace temperature as low as 1000 °C.
2. The homogeneous ignition of the remaining volatiles in Yallourn char is predominant at furnace temperatures of 1000 °C and below. Therefore, a minimum volatile content of 6 *wt%* in the prepared char is essential to ensure a stable ignition. The char structure is also influential in controlling the later heterogeneous char burnout. However, an elevation of the hot blast gas temperature to 1200 °C can compensate for the negative effect of volatile contents less than 6 *wt%* and the influence of char structure as well, due to the enhanced heterogeneous ignition and shift of the reaction to the diffusion control zone.
3. The larger porosity and surface area of Yallourn char is helpful for minimising the gas diffusion resistance, therefore, the coarse Yallourn char of 300 μ*m* in size can burn efficiently under the stoichiometric O_2/C molar ratio at a high furnace temperature. Reducing the Yallourn char size is further beneficial in alleviating the external diffusion resistance to achieve a nearly complete burnout at 800 °C.

References

1. Bennett, P.; Fukushima, T. In *Impact of PCI coal quality on blast furnace operations*, Proceedings of the 12th International Conference on Coal Science. Cairns, Australia., 2003; 2003.
2. Carpenter, A. M., *Use of PCI in blast furnaces*. IEA Clean Coal Centre: 2006.
3. Lüngen, H.; Poos, A., Injection of coal into the blast furnace—ECSC synthesis report. *Cokemaking International* **1996,** 8, 14-31.
4. Zhang, S., Theoretical consideration of problems relating to high coal rate injection into blast furnaces. *Ironmaking & steelmaking* **2003,** 30, (6), 467-474.
5. Gomes, M. d. L. I.; Osório, E.; Vilela, A. C. F., Thermal analysis evaluation of the reactivity of coal mixtures for injection in the blast furnace. *Materials Research* **2006,** 9, (1), 91-95.
6. Ishii, K., *Advanced Pulverized Coal Injection Technology and Blast Furnace Operation*. Elsevier Science Ltd.: Oxford, UK, 2000.
7. Phillip, R. G.; Bennet, A., Advantages of Low Volatile Coals for PCI. *Report–Department of Mines and Energy–Q Therm Project, Brisbane QLD* **1997**.
8. Wu, Z.; IEA Coal Research. Clean Coal Centre, *Fundamentals of Pulverised Coal Combustion*. International Energy Agency Coal Research: 2005.
9. Lu, L.; Sahajwalla, V.; Kong, C.; Mclean, A., Chemical structure of chars prepared under conditions prevailing in the blast furnace PCI operation. *ISIJ international* **2002,** 42, (8), 816-825.
10. Traa, Y., Is a renaissance of coal imminent?—challenges for catalysis. *Chemical Communications* **2010,** 46, (13), 2175-2187.
11. Ng, K. W.; Giroux, L.; MacPhee, T.; Todoschuk, T., Combustibility of charcoal for direct injection in blast furnace ironmaking. *Iron and Steel Technology* **2012,** 9, (3), 70.
12. De Girolamo, A.; Grufas, A.; Lyamin, I.; Nishio, I.; Ninomiya, Y.; Zhang, L., Ignitability and combustibility of Yallourn pyrolysis char blended with PCI coal under simulated blast furnace conditions. *Energy & Fuels* **2015,** 30, (3), 1858-1868.
13. Li, C. Z., *Advances in the Science of Victorian Brown Coal*. Elsevier Science: 2004.
14. Kissinger, H. E., Reaction Kinetics in Differential Thermal Analysis. *Analytical Chemistry* **1957,** 29, (11), 1702-1706.
15. Low, F.; De Girolamo, A.; Dai, B.-Q.; Zhang, L., Emission of Organically Bound Elements during the Pyrolysis and Char Oxidation of Lignites in Air and Oxyfuel Combustion Mode. *Energy & Fuels* **2014,** 28, (6), 4167-4176.
16. Li, H.; Elliott, L.; Rogers, H.; Wall, T., Comparative Study on the Combustion Performance of Coals on a Pilot-Scale Test Rig Simulating Blast Furnace Pulverized Coal Injection and a Lab-Scale Drop-Tube Furnace. *Energy & Fuels* **2014,** 28, (1), 363-368.
17. Zhang, J.; Prationo, W.; Zhang, L.; Zhang, Z., Computational Fluid Dynamics Modeling on the Air-Firing and Oxy-fuel Combustion of Dried Victorian Brown Coal. *Energy & Fuels* **2013,** 27, (8), 4258-4269.
18. Al-Abbas, A. H.; Naser, J.; Dodds, D., CFD modelling of air-fired and oxy-fuel combustion of lignite in a 100KW furnace. *Fuel* **2011,** 90, (5), 1778-1795.
19. Ma, L.; Gharebaghi, M.; Porter, R.; Pourkashanian, M.; Jones, J. M.; Williams, A., Modelling methods for co-fired pulverised fuel furnaces. *Fuel* **2009,** 88, (12), 2448-2454.
20. Smith, T. F.; Shen, Z. F.; Friedman, J. N., Evaluation of Coefficients for the Weighted Sum of Gray Gases Model. *Journal of Heat Transfer* **1982,** 104, (4), 602-608.
21. Westbrook, C. K.; Dryer, F. L., Simplified Reaction Mechanisms for the Oxidation of Hydrocarbon Fuels in Flames. *Combustion Science and Technology* **1981,** 27, (1-2), 31-43.

22. Chen, L.; Yong, S. Z.; Ghoniem, A. F., Oxy-fuel combustion of pulverized coal: Characterization, fundamentals, stabilization and CFD modeling. *Progress in Energy and Combustion Science* **2012,** 38, (2), 156-214.
23. Badzioch, S.; Hawksley, P. G., Kinetics of thermal decomposition of pulverized coal particles. *Industrial & Engineering Chemistry Process Design and Development* **1970,** 9, (4), 521-530.
24. Chinese Standards, Specifications of coal used in pulverized coal injection (PCI). In 2008; Vol. GB/T 18512-2008.
25. Han, J.; Cho, K.; Lee, K.-H.; Kim, H., Porous graphite matrix for chemical heat pumps. *Carbon* **1998,** 36, (12), 1801-1810.
26. Gale, T. K.; Fletcher, T. H.; Bartholomew, C. H., Effects of Pyrolysis Conditions on Internal Surface Areas and Densities of Coal Chars Prepared at High Heating Rates in Reactive and Nonreactive Atmospheres. *Energy & Fuels* **1995,** 9, (3), 513-524.
27. Yen, T. F.; Erdman, J. G.; Pollack, S. S., Investigation of the structure of petroleum asphaltenes by X-ray diffraction. *Analytical Chemistry* **1961,** 33, (11), 1587-1594.
28. Odeh, A. O., Comparative Study of the Aromaticity of the Coal Structure during the Char Formation Process under Both Conventional and Advanced Analytical Techniques. *Energy & Fuels* **2015,** 29, (4), 2676-2684.
29. Binner, E.; Zhang, L.; Li, C.-Z.; Bhattacharya, S., < i> In-situ</i> observation of the combustion of air-dried and wet Victorian brown coal. *Proceedings of the Combustion Institute* **2011,** 33, (2), 1739-1746.
30. Mathieson, J. G.; Rogers, H.; Somerville, M. A.; Jahanshahi, S., Reducing net CO 2 emissions using charcoal as a blast furnace tuyere injectant. *ISIJ international* **2012,** 52, (8), 1489-1496.

This page is intentionally left blank

Chapter 7 – Ignitability and combustibility of Yallourn pyrolysis char blended with PCI coal under simulated blast furnace conditions

In Chapter 6 different size-segregated fractions of the pyrolysis char product were evaluated for their performance under PCI combustion conditions. While several fractions were found to be suitable for the PCI process, the low volatile matter content of the most abundant fraction had a negative impact on the combustion performance. In this chapter, both of the previously tested industrially made lignite chars are tested as a blend with a commercially used PCI coal. This chapter has been reformatted from the published manuscript: De Girolamo, A., Grufas, A., Lyamin, I., Nishio, I., Ninomiya, Y., Zhang, L., Ignitability and combustibility of Yallourn pyrolysis char blended with PCI coal under simulated blast furnace conditions. *Energy & Fuels* **2015,** 30, (3), 1858-1868.

Abstract

Pulverized coal injection (PCI) is a widely used blast furnace technology aimed at reducing costs and increasing productivity. The prospect of blending PCI coal with a lower cost char, derived from Yallourn brown coal, is evaluated in this study by means of thermogravimetric analysis (TGA), flat flame burner reactor and drop tube furnace experiments at four different blending ratios as well as CFD modelling. Yallourn char has desirable properties compared to PCI coal including a lower ash content and a higher heating value, although the reactivity is lower and ignition temperature is higher. Since the combustion behaviour of a blend is not always easily predicable based on the performance of the individual parent fuels, two Yallourn char samples (YC-1 and YC-2) are analysed after blending with PCI coal at four ratios. According to particle ignition time, a maximum 40 *wt%* is allowable for YC-1 char which is comparably reactive with the commercial PCI coal. However, a maximum 20 *wt%* is only allowed for YC-2 which is less reactive. The negative heat sink effect of YC-2 char is influential, whereas the heterogeneous ignition of YC-1 overlapped considerably with the ignition of PCI coal which is mainly in the homogeneous gas phase. In addition, it was found that the later char oxidation rate was accelerated greatly for the PCI coal blended with YC-1, irrespective of its blending ratio. In contrast, the heat sink effect is further obvious for the YC-2, the increase on the blending ratio of which greatly decreased the overall burnout rate, especially at low furnace temperatures (800°C and 900°C) and a shorter residence time such as 0.8 *s*. For YC-1 char, its blending ratio is insignificant in the overall burnout. Increasing the furnace temperature to 1000°C and the O_2/C ratio of 1.2 can assist in achieving a nearly complete burnout for all of its blends, even at a short residence time of 0.8 s. In contrast, for YC-2 char, a furnace temperature of 1200°C and O_2/C ratio of 1.2 are essential to complete the burnout of all its blends. The Yallourn pyrolysis conditions for the preparation of its char is critical. A good synergistic interaction between Yallourn char and commercial PCI in terms of reactivity is also essential for a broad blending ratio to be used in the blast furnace.

Keywords

Pulverised coal injection, blending, Yallourn pyrolysis char, blast furnace

7.1 Introduction

Currently, 70% of iron production for steelmaking is attained through smelting iron ore by reduction with a carbon source (coke/coal) in a blast furnace [1]. To reduce the consumption of expensive coke and increase productivity, the pulverised coal injection (PCI) method is used to replace a portion of the coke used in the blast furnace [2]. This has been implemented in nearly all blast furnaces in China, Japan, Korea and Taiwan and over half of those in North America, South America and Europe[3]. As a result of this, the demand for coal suitable for PCI has been increasing steadily [4].

Victorian brown coal (VBC) contains a relatively high amount of moisture and has a low ash yield. It is predominantly used for electricity generation at local power plants where it is inefficient and very carbon intensive [5]. One of the promising applications for VBC is as a substitute for bituminous coals used in PCI in a blast furnace. Unprocessed Brown coal is not suitable for blast furnace applications due to its high moisture content and low calorific value. Through a mild pyrolysis process, VBC could be upgraded to a higher value char which is produced alongside other derivatives, coal gas and coal tar [6]. The VBC char could then be injected via the PCI method as a complete replacement for the commercial PCI coal or as a blend.

A previous study has confirmed the viability of a complete replacement of commercial PCI coal with two chars derived from Yallourn brown coal [7, 8]. The char replacement has both advantages and disadvantages compared to the PCI coal. Yallourn char has a lower cost than the PCI coal and contains a higher calorific value, meaning it can replace a greater portion of coke. It also has lower ash (<4 *wt%*) and moisture contents. On the other hand, the previous study showed that Yallourn char has a higher ignition temperature due to its lower volatile content, which in turn would cause a delay in the ignition and the formation of plenty of unburnt carbon entering the blast furnace.

Char can be blended with the normal PCI coal to balance these char characteristics, however it is not always easily foreseeable how the created blend will behave due to possible non-additive/synergistic interactions between different coals or chars [9]. Some properties of coals are always additive (C,H,O,N,S analysis, moisture content and lower calorific value (LCV)) [10], while others may be additive or non-additive depending on the parent coals. Haas et al. [10]

determined that non-additive effects were greater when parent coals had a larger difference in coal rank. Stability of low volatile coals could be enhanced by blending with a higher volatile coal (with the exception of low-rank coal), while burnout of blends will follow a linear trend [11] with burnout being higher for coals with a larger volatile content [12, 13]. Ignition temperatures of coal blends have been shown to decrease with an increased proportion of volatile matter (VM) in the blend, however several studies have found the actual ignition temperature of blends lower than that predicted by a weighted average of the parent coals, therefore the ignition temperature will approach that of coal with higher VM [9, 14, 15].

Table 7.1 provides a summary of a number of studies that have been completed on blending combustion. Blend analysis by TGA has provided useful information about ignition and interactions between blends although there is no clear consensus on whether a given blend will show non-additive behaviour. DTF and other lab - scale rigs provide heating rates which are much more applicable to those experienced by coal injection into a blast furnace and will allow volatile matter to potentially interact with fixed carbon. For industry scale assessment, CFD modelling has been favoured due to the lower cost and ability to measure key performance parameters and modify input parameters with ease. However, the effect of chemical interaction between blends may not be possible to fully take into account if only parent coal char characteristics are considered. With this current state of research, it can only be assumed that blend behaviour will usually be expected to fall within or close to the constraints given by their parent fuels, therefore analysis of each blending ratio should be examined prior to application in industry.

Table 7.1 Summary of selected works on blending combustion

Purpose	Testing method	Findings	Reference
Investigate combustion characteristics of coal and pine sawdust blends.	TGA	No synergistic effects observed.	Gil et al., 2010 [16]
Investigate the combustion characteristic and kinetic behaviour of microalgae/Yallourn brown coal blends.	TGA	Synergistic effect observed in reactivity and ignition.	Tahmasebi et al., 2013 [17]
Investigate pyrolysis and combustion behaviour of lignite/olive residue blends under air and oxy-fuel conditions.	TGA/FTIR	Experimental ignition temperature increased and burnout temperature is higher compared to a theoretical blend.	Yuzbasi & Selçuk, 2011 [18]
Compare combustion characteristics of biomass/biochar blends.	TGA	Addition of biochar to biomass had similar combustibility up to a 30% blend.	Yi et al., 2013 [19]
Assess whether the combustion behaviour of blends could be predicted from that of the parent coals.	IPFR	Ash yield, proximate VM, LCV, char burnout and true density are additive. VM yield in IPFR and apparent density not additive.	Haas et al., 2001 [10]
Simulate flow and combustion of binary coal blends under BF conditions.	BF CFD model	Synergistic effect on the overall burnout observed.	Shen et al., 2009 [20]
Investigate blending combustion performance of brown coal and char in boiler.	600MW boiler CFD	A 50% blend ratio provided an optimum balance of moisture and combustibles.	Zhang et al., 2015 [21]
Predict efficiency deviations in the combustion of coal blends in power plants.	DTF	Blended coals with large rank differences showed improved burnout compared to weighted average.	Ulloa et al., 2005 [22]
Evaluate the dependencies between the properties of coal blends and parent coals according to their mass contributions.	EFR	Some properties could be predicted (HGI, SO_2 emission) while others were specific for the blend (NO_x emission, burnout).	Moroń & Rybak, 2007 [23]
Test combustion behaviour and flame structure of blends of biomass with coal of different ranks	TGA/Slit burner	10% biomass addition could improve combustion efficiency of low rank coal but had no apparent impact on high rank coal.	Moon et al., 2013 [24]
Study interaction of Ningxia coals of varying FC/VM ratios	TGA	Ignition of blends is closer to that of the higher reactivity coal. Additive behaviour observed for similar ranks.	Zhang et al., 2011 [9]
Blended combustion of high ash and low ash Indian coals	TGA/DTF	Burnout of blends with 50% of high ash coal showed better burnout than individual coals.	Biswas et al., 2006 [25]
Evaluate performance of blending Brazilian sub-bituminous coal with imported PCI coal and wood charcoal	Laboratory injection rig	Blending of Brazilian coal with the imported coal led to substantial increase in conversion. Charcoal in blends increased conversion and reduced ash.	Machado et al., 2010 [26]
Modelling the simultaneous injection of pulverized coal and charcoal into the blast furnace through the tuyeres with oxygen enrichment	BF CFD model	An increase in productivity was observed with the addition of higher reactivity and higher volatile matter charcoal.	de Castro et al., 2013 [27]
To verify combustion performance of biomass charcoal products was comparable with PCI coals	Pilot-scale PCI rig	Charcoal showed superior flame stability and combustion performance. Burnout for blends could was adequately predicted by a weighted-average.	Mathieson et al., 2011 [28]

In this study, the properties, reactivity and interaction of different mixtures of Yallourn char and a commercial PCI coal will be analysed to determine an optimum ratio of blending. This research aims to clarify both ignition and burnout rate for char – coal blends, which are critical for the combustion of PCI in the tuyere/blowpipe of a blast furnace. Techniques used include thermogravimetric analysis, ignition time measured in a flat-flame burner, DTF experiments and CFD modelling. The DTF used is able to pre-heat the gas temperature up to 1000°C which can thus resemble an industrial blast furnace. It is of interest to maximise the replacement of PCI coal and thus have a greater content of Yallourn char in the blend in order to reduce fuel costs and ash burden. Additionally, if a Yallourn char blend is chosen with a higher calorific value than PCI coal, a higher coke replacement ratio would be achieved and thus additional cost savings in coke requirement would ensue. However, since these benefits could come at the cost of reduced reactivity and delayed ignition, it is pivotal to establish a blending ratio that balances the beneficial and detrimental effects. While it was established that both Yallourn char samples had a higher ignition temperature and larger ignition delay than the PCI coal (which was correlated with the higher volatile content of PCI coal), the blends containing Yallourn char with PCI coal will have a volatile matter content higher than that of the individual Yallourn char samples. If the heterogeneous nature of the blend allows PCI coal with higher volatile matter to ignite sooner, then the heat feedback from its volatile matter combustion may in turn assist with the heterogeneous ignition and burnout of Yallourn char. In addition, the blending of char would increase the local O_2/C molar ratio for the PCI volatiles, thus promoting its ignition. However, if the reactivity of the char is very low and does not match the PCI, it could act as an ‘inert’ species causing heat sink near the igniting/burning PCI coal particles. This would in turn postpone the overall burnout. All these hypotheses will be tested in this study, which is expected to ultimately diversify the use of Victorian brown coal by creation of a product that can be exported to the international market.

7.2 Experimental methodologies

7.2.1 Materials

Yallourn char for this study is obtained by pyrolysis of raw wet Yallourn brown coal in a pilot - scale shaft furnace. As in the previous study [7], two types of Yallourn char were produced under different conditions. These will be referred to as Yallourn char 1 (YC-1) and Yallourn char 2 (YC-2). The char is created under relatively mild conditions (around 800°C) and YC-2

was pyrolyzed over a longer time (~10 hours) period than YC-1 (~5 hours). The most common size fraction was taken from each of these (1-4 *mm*), ground to a size of <106 μm and mixed with a commercial PCI coal at four different ratios from 20% to 80% (mass fraction) char with the remaining PCI coal. The proximate and ultimate analysis of both fuels is shown in Table 7.2. Although Yallourn char samples have similar volatile matter and fixed carbon content, their physical properties vary considerably (Table 7.3).

Table 7.2 Proximate and ultimate analysis of fuels

	YC-1	YC-2	PCI coal
Proximate analysis			
Moisture % *ar*	10.2	1.2	1.9
Ash % *db*	7.4	5.2	8.7
Volatile matter % *db*	6.5	4.5	20.7
Fixed carbon % *db*	86.1	90.3	70.6
Ultimate analysis % *db*			
Carbon	87.1	93.22	80.84
Hydrogen	1.2	0.49	3.90
Oxygen*	3.31	0.00	4.89
Nitrogen	0.66	0.76	1.20
Sulfur	0.33	0.38	0.47

*By difference

Table 7.3 True density, apparent density, calculated porosity and lower heating value for fuels

	YC-1	YC-2	PCI coal
True density (kg/m^3)	1863	2204	1441
Apparent density (kg/m^3)	510.7	417.8	644.2
Calculated porosity*, [-]	72.6%	81.0%	55.3%
Lower heating value (MJ/kg)	27.2	32.3	30.5

*Porosity = (True density-Apparent density)/True density x 100%[29]

The kinetic parameter analysis (Table 7.4) showed a large variation in activation energy between YC-1 and YC-2 char (103.0 and 151.6 kJ/mol respectively), although these two chars possess the similar properties in terms of the content of remaining volatiles and ash. The method of determination of kinetic parameters is detailed in section 7.2.2. Likely the pyrolysis condition is critical in affecting the char structure and its reactivity. In terms of the reaction rate at high temperature, YC-1 shows higher reactivity, closer to the reactivity of PCI coal. The level of metal oxides in the ash of each fuel is shown in

Table 7.5.Error! Reference source not found.Table 7.4 Kinetic parameters for Yallourn char and PCI coal

	Pre-exponential constant (s^{-1})	Activation energy (kJ/mol)	Reaction rate at 800°C (s^{-1})	Reaction rate at 1000°C (s^{-1})
YC-1	5.33E+04	103.0	0.52	3.16
YC-2	3.90E+06	151.6	0.16	2.35
PCI coal	8.20E+05	129.0	0.43	4.19

Table 7.5 Composition of ash wt % oxides

Metal oxide	YC-1	YC-2	PCI
SiO_2	1.79	1.58	40.46
Al_2O_3	2.41	3.82	27.61
Fe_2O_3	41.14	20.31	5.99
MgO	30.23	34.43	0.02
CaO	7.39	12.62	13.06
SO_3	8.99	13.16	6.57
K_2O	0.36	0.91	0.46
Na_2O	6.05	11.36	3.73

7.2.2 Thermogravimetric analysis (TGA)

TGA (Shimadzu DTG – 60H) was used to determine the ignition temperature of the coal - char blends, the intrinsic reactivity kinetic parameters for pure fuels (both activation energy and pre-exponential factors) and the ash content of the unburned residues collected after the drop tube furnace experiments.

A Kissinger plot was used to determine the activation energy and pre-exponential factor for the two Yallourn char samples and PCI coal. The Kissinger method considers the effect of heating rate on the variation in the temperature at which the maximum reaction rate occurs [30]. Heating rates were varied between 4°C/min and 10°C/min to ensure that the temperature at the maximum rate was in the chemical kinetic control regime. Ignition temperature is defined as the temperature at which the combustion rate, for a certain heating rate, rises to 1 *wt%/min* of the current mass [31].

7.2.3 Flat flame burner reactor (FFBR) experiments

Ignition tests were also carried out in a FFBR to complement the TGA observation where ignition was measured at a slow heating rate. The FFBR was operated at atmospheric pressure with a measured flame temperature of approximately 1062°C before the feeding of coal/char.

A magnitude of 10^5 °C/s is expected for the heat-up of coal/char particles in the FFBR[32], which is close to the industrial blast furnace heating rate[3]. Oxygen fraction was fixed at 0.21 and the O_2/C molar ratio was fixed at 2.5. The feed rate of coal/char to the burner is approximately 1 g/min with deviations of up to 10% from this in order to maintain the correct O_2/C ratio for each sample. At least 100 images were captured with a Nikon P7000 CCD camera and analysed for each blend to quantify the ignition point of each sample as a distance from the burner base. A high speed camera was used to measure particle velocity and thus calculate the ignition time. Further information about the FFBR can be found in a previous study [32].

7.2.4 DTF experiments

A 2 *m* high drop tube furnace (DTF) was used to combust the coal and char samples and a gas analyzer recorded the combustion gases exiting the furnace. A schematic drawing of the DTF setup can be found in previous work [33]. The sample enters the DTF with a low volume primary gas (1.0 L_{STD}/min), while a secondary gas (9.0 L_{STD}/min) is preheated to the furnace temperature and mixes with the coal or char at the injection point. Such a unique pre-heating system for the gas can resemble the blast furnace condition where coal is injected into a hot air stream. The coal/char feeding rate was approximately 0.7 g/min. Oxygen was added to the secondary gas to achieve the desired O_2/C ratio. Particle residence time was approximately 1.4 s in the furnace. The following parameters were varied in this study: Blending ratio (with respect to Yallourn char content): 0%, 20%, 40%, 60% 80% and 100%; Furnace temperature: 800°C, 900°C and 1000°C; and O_2/C molar ratio: 0.7, 0.85, 1.0 and 1.3.

7.2.5 CFD modelling

A three-dimensional CFD model of the DTF was used to gain a better understanding of the interactions of different blends. The mesh for this was taken from a previous study [34]. The model has been validated using particle temperature measurements and a grid independence test was conducted to optimize the mesh cell number [20]. Blends were added to the model as two coal injections at the same inlet surface. This method may be used to study the interactions caused by differences in volatile content and reactivity. This mesh was validated in a grid independence test as well as with measurements of particle temperature. The models used in the simulation are summarised as follows: Turbulence – k-ε model; Radiation – Discrete Ordinates (DO) model; Radiation absorption: weighted-sum-of-gray-gases model (WSGGM); Particle reactions – Multiple surface reaction model; and Gas reactions – Westbrook & Dryer

mechanism [35]. The 3D double-precision pseudo-transient coupled solver was used with an initial pseudo-time-step of 0.001 s for the first 30 iterations, followed by 0.1 *s* for the remainder of the calculation. Second-order discretization schemes were used for all equations apart from discrete-ordinates which remains as the default setting of first-order. Relaxation factors are kept as the default settings with the exception of the reduction of the species relaxation factor from 0.75 to 0.5 and the discrete particle phase relaxation factor from 0.5 to 0.25. The solver is set to run until all residuals were reduced below 10^{-7} to ensure that all variables monitored concurrently with the solution procedure including temperature, velocity and reaction rate variables were entirely stable and unchanging with further iterations. This overall strategy ensured all cases could be solved with a steady reduction in residuals without divergence.

7.3 Results and Discussion

7.3.1 Ignition analysis

Figure 7.1 shows the TGA measured ignition temperature as a function of the Yallourn char blending ratio at a heating rate of 10°C/min. Ignition temperature generally increases with increasing Yallourn char content. This is due to the lower VM % in the Yallourn char sample. However, the ignition temperature of blends increases non-linearly with reduced volatile matter content in the coals. To some degree this is to be expected and could be predicted based on the burnout of the pure coal or char. If the parent fuels do not interact in the blend, the fuel with the lower ignition temperature will still have the opportunity to ignite independently. Therefore, this can be an advantage specific to heterogeneous fuels. Simulated curves are also shown in Figure 1 for ignition of the blends based on the weighted averaging of the burnout of the pure coal/char. These simulated curves predict the ignition point that would be measured if the blends do not interact in the TGA. Clearly, the experimental results show that for both YC-1 and YC-2 blends the predicted ignition temperature is lower than both the simulated prediction. Therefore, a weighted average of each respective coals ignition temperature is non - additive. A synergistic interaction could be due to the catalytic effect of minerals in Yallourn coal char which is rich in Fe and alkaline earth metals. With respect to the difference between the two chars, it is obvious that the increase extent for the blending of YC-1 with PCI coal is much lower than that of YC-2, although they bear the same volatile content as evident in Table 1. For the use of YC-1 char, the ignition temperature was only increased by around 13°C upon the shift from pure PCI coal to pure YC-1 char. The use of up to 40 *wt%* of YC-1 caused little

change on the ignition time. The physical properties of the two chars are not the affecting factors, because YC-2 char is indeed more porous than its counterpart, as evident in Error! Reference source not found.. It is most likely that YC-1 holds a distinct carbonaceous structure, which is clearly more reactive and prone to ignite heterogeneously. With regard to the use of YC-2 char, Ignition temperature of blends by thermogravimetric analysis suggests that its blending ratio for YC-2 has to be limited to maximum 20 *wt%*, otherwise the ignition for the coal-char blend would be delayed considerably, by a rise of the ignition temperature from 405°C for pure PCI coal to 431°C for 40 *wt%* YC-2 in the blend, and as high as 503°C for pure YC-2.

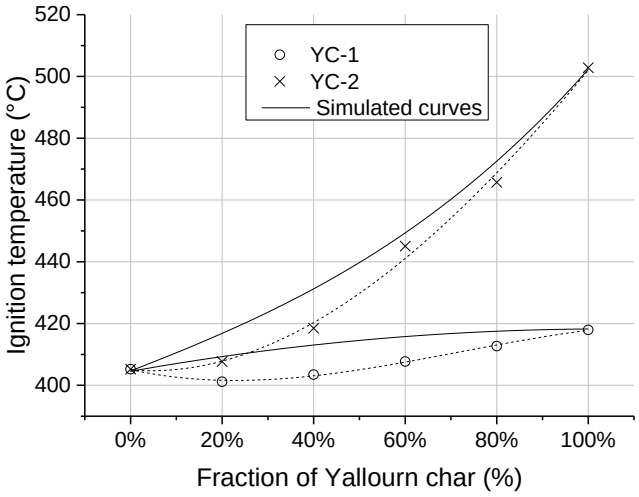

Figure 7.1 Ignition temperature of blends by thermogravimetric analysis

Figure 7.2 further plotted the correlation between the blend ignition temperature and its volatile content, which was calculated by linear combination of the volatile contents in the two pure fuels. It is evident that a non-linear correlation exists between ignition temperature and volatile content. In addition, the trend for YC-1 and YC-2 chars (from different size fraction groups) have their own dependencies of ignition temperature on volatile content. The degree to which ignition temperature will depend on volatile content is greater for YC-1 than YC-2 indicated by the steeper curve. To reiterate, this supports the importance of char structure on its reactivity.

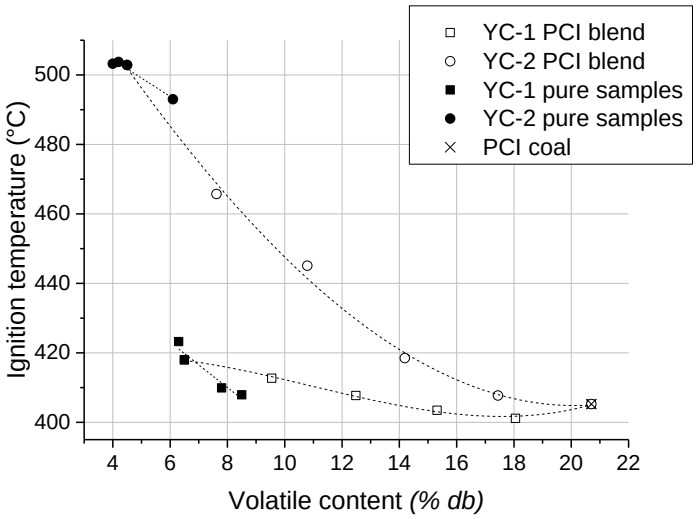

Figure 7.2 Effect of volatile matter on ignition temperature in TGA

The direct observation of coal/char ignition in FFBR employing a very fast heating rate in Figure 7.3 shows an agreement with the ignition behaviour for coal blends observed in TGA. That is, the ignition for char-coal blends was unaffected by blending at low ratios (up to 20%). A clear decrease on the ignition time is obvious upon increasing the char blending ratio. Although the coal/char particles are fed continuously into the FFBR and they are supposed to have little inter-particle interaction. Same as has been observed in TGA employing a very slow heating rate and the use of pre-loaded samples with only a few amount, YC-2 blends shows a larger ignition delay than for YC-1 blends. The flames for the blends using YC-2 char are even discontinuous, indicative of the difficulty for their ignition. For YC-1, blends 60% and below showed similar flame length and ignition points to that of PCI coal. In contrast, increasing the amount of YC-2 will drastically increase the ignition distance/time after 40% and increase the flame length.

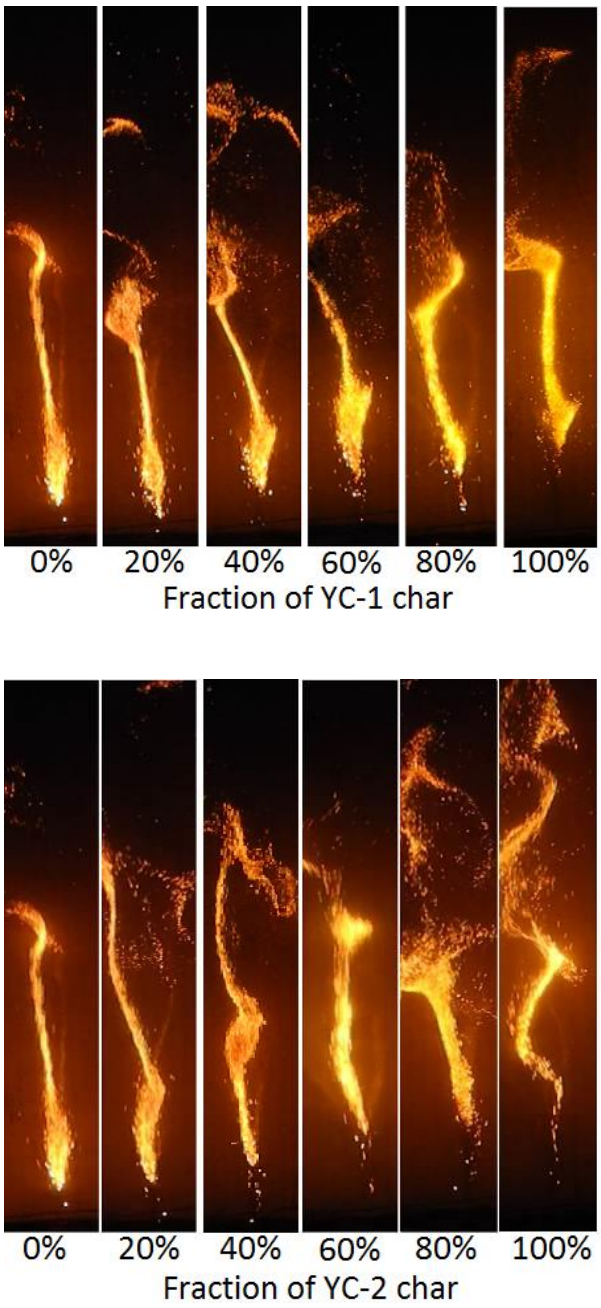

Figure 7.3 Effect of blend ratio on flame structure for YC-1 (top) and YC-2 (bottom).

Figure 7.4 further quantifies the ignition time as a function of Yallourn char blending ratio. Clearly, the ignition delay for blending YC-1 with PCI coal is less obvious. The use of up to 40 *wt%* YC-1 char resulted in the same ignition time with the pure PCI coal. Such an observation is in line with the TGA results (in Figure 7.1) using a very slow heating rate. On the other hand, the use of maximum 20 *wt%* is only allowed for the YC-2 char, otherwise the ignition would be delayed considerably. As was done previously for ignition temperature in

TGA, the relationship between ignition delay and volatile content is illustrated in Figure 7.5. Similarly, ignition delay will decrease with volatile content, although this relationship is not linear for blends. Moreover, by comparing Figure 7.2 and Figure 7.5, one can see that the discrepancy between the curves for the two chars in FFBR is rather narrow and their error bars even overlap one another. This is an indicator of the strong influence of particle heating rate on its ignition. Upon a very fast heating rate in the FFBR, the heterogeneous ignition could occur once the char particles are injected into the hot gas stream. This is evident by the appearance of individual sparkling spots near the burner base in Figure 7.3**.** In other words, the influence of carbonaceous structure on the coal-char blend ignition should be marginal in an industrial blast furnace. At least, its influence is less significant than the particle heating rate. In addition, from Figure 7.5 it can be seen that 14 *wt%* is the minimum volatile content in the char-coal blend, causing little change on the ignition time compared to the pure PCI coal. Such a volatile content corresponds to maximum *~40 wt%* of Yallourn char to be mixed with the PCI coal.

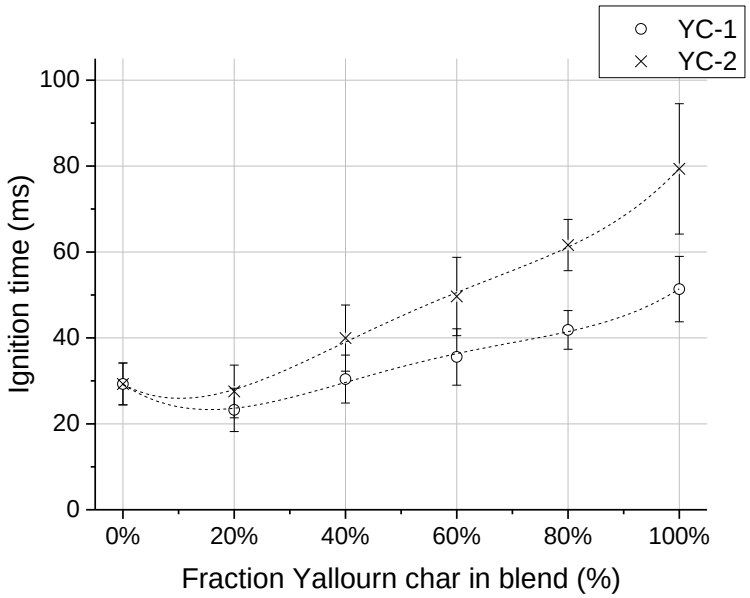

Figure 7.4 Ignition time for char blends as measured in the flat flame burner.

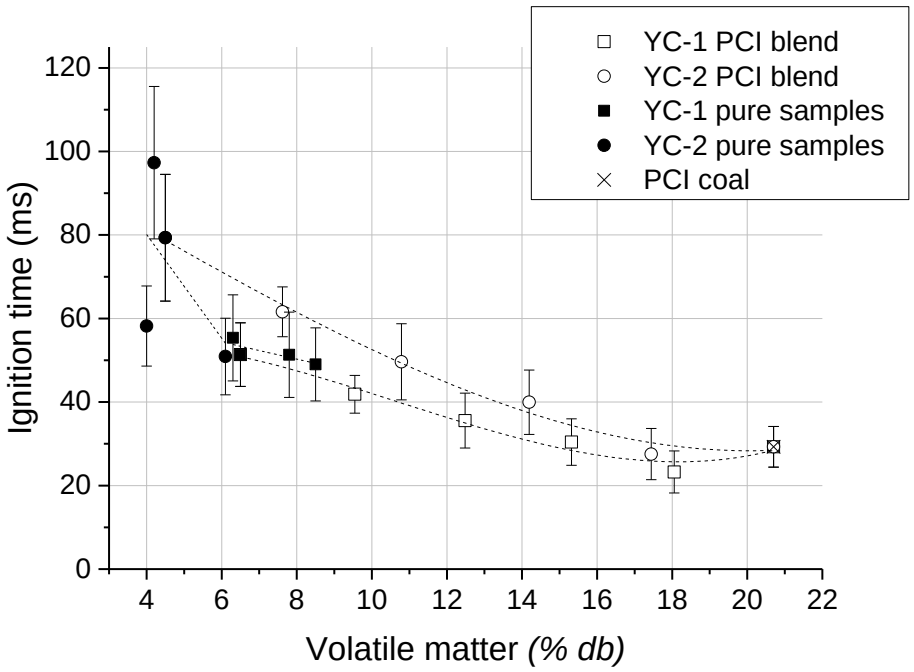

Figure 7.5 Effect of volatile matter content on ignition delay in the flat flame burner.

7.3.2 DTF experiment results

Figure 7.6 shows the burnout results for YC-1 char blended with PCI coal at six ratios, in different O_2/C ratios, 1000°C and a gas residence time of 1.4 *s*. As can be seen, although the blending of 20 *wt%* YC-1 lowered the burnout irrespective of the O_2/C ratio, the blending ratio of 80 *wt%* YC-2 char clearly gave the best burnout at every O_2/C ratio. Such a finding is apparently contradictory to the ignition results discussed above. One probable reason is the large experimental error related to particle feeding in the DTF system. The YC-1 char was found strongly sticky and electrostatic, which largely slowed down its feeding rate.

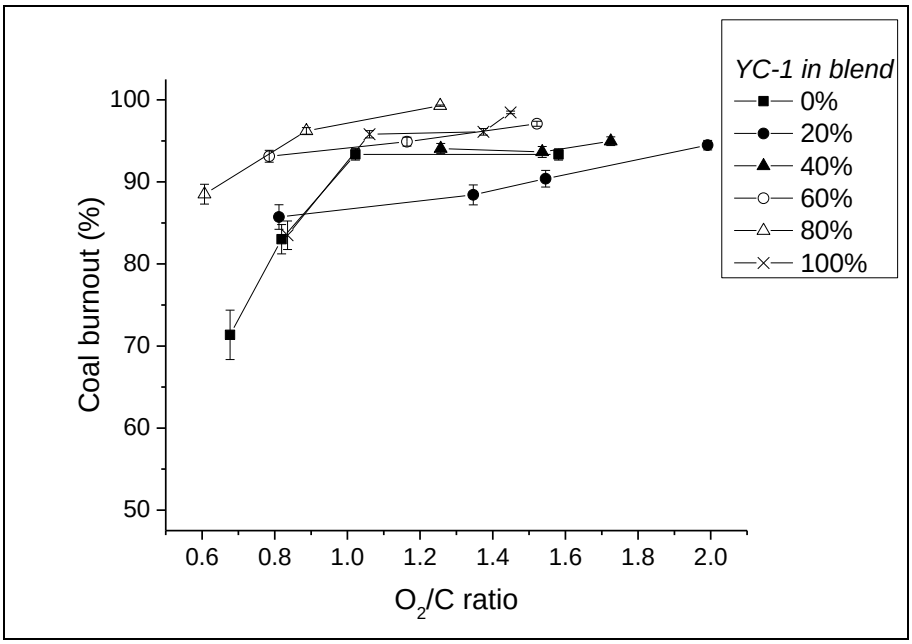

Figure 7.6 Burnout in the drop tube furnace for different blends for YC-1

The results for YC-2 char – coal blends in Figure 7.7 are much more reasonable, showing a clearer trend for the burnout versus O_2/C ratio, furnace temperature and char blending ratio as well. This is because the feeding problem does not exist for the YC-2 char, as observed during the experiments. Except 800°C, the blending ratio of YC-2 char is clearly less significant. At each temperature, The O_2/C ratio-dependence trends for different blends overlap significantly. Back to the previous conclusion for a maximum 40 *wt%* allowable blending ratio for YC-2 char in terms of ignition, it is apparent that the later char oxidation step for the blend combustion, irrespective of the char blending ratio was occurring faster than the single PCI coal char. One reason could still be the inter-particle heat feedback between char and PCI coal particles. The fast ignition of PCI volatiles induced the heat-up and heterogeneous ignition/oxidation of char, which in turn released more heat (due to its larger calorific value) to accelerate the oxidation of PCI char. For these two temperatures, increasing the O_2/C molar ratio above 1.2 is clearly beneficial in promoting the burnout close to completion. Regarding the lowest temperature examined here, 800°C, the combustion rate, irrespective of blending ratio is very low, thereby requiring an O_2/C ratio above 1.6 to achieve a close-to-completion burnout. Interestingly, the 20 *wt*% ratio for YC-2 shows the least burnout even at an O_2/C ratio as high as 1.6, whereas the use of 60 *wt%* YC-2 char was even able to achieve a burnout close to 95 *wt%* at the same O_2/C ratio. This indicates that the ignition delay is insignificant in

affecting the final burnout rate for the coal-char blends. One reason could be due to the relatively long residence time (1.4 *s*) used here.

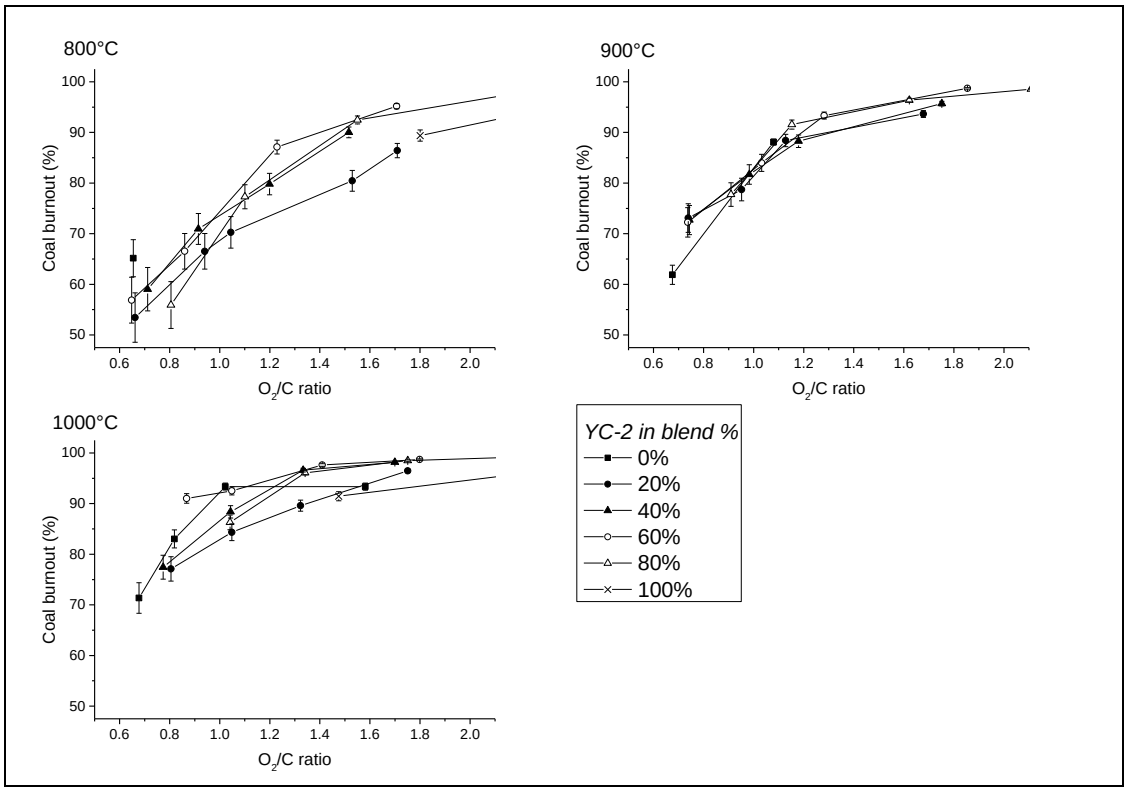

Figure 7.7 Burnout in the drop tube furnace for different blends for YC-2

7.3.3 CFD modelling prediction

7.3.3.1 Influences of O_2/C ratio, blending ratio and furnace temperature

Since the experimental conditions in the DTF are difficult to control, and in most cases, changing only one variable was unavailable for the DTF system. For instance, the calibration curve between coal feeding rate and the voltage for the piezoelectric feeder varies broadly for different blends, and hence, the influence of individual parameters is difficult to be assessed. In this sense, CFD modelling has been conducted to manipulate the experimental conditions so as to assess the influence of individual variables. The use of this model was validated by comparison of burnout and exit O_2% in flue gas with the respective values predicted by the CFD model. Figure 7.8 shows a reasonable agreement between these values given the variable nature of the DTF.

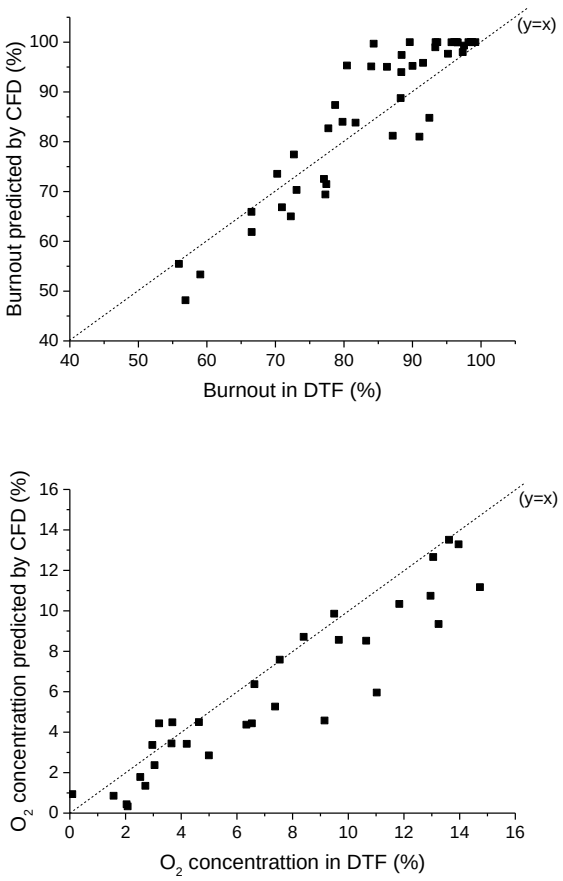

Figure 7.8 Experimental validation by comparing DTF experiment burnout and O_2 outlet concentration with CFD prediction

Figure 7.9 shows the effect of temperature on burnout for both Yallourn char samples at three O_2/C ratios. At a lowest O_2/C ratio of 0.85 in which O_2 is insufficient, YC-1 blends show more comparable burnout for different blending ratios, especially at the temperatures of 900°C and above. At 800°C, the burnout was slightly decreased from the blending ratio of 40 *wt%* for YC-1. In combination with the ignition results, it is evident that the overall burnout was slightly negated by the initial ignition delay. But such a delay is trivial and even negligible, which indicates the comparable/similar reaction rate for YC-1 char with the PCI coal at such a low furnace temperature. Consequently, these two fuels burnt rather concurrently in the furnace. Upon increasing the furnace temperature to 900°C and 1000°C that is identical with the FFBR temperature, the initial ignition delay, as observed in Figures 1-5 was non-influential in the final burnout rate. Again, this should be due to the inter-particle heat feedback that accelerated the YC-1 char ignition and oxidation rate. In other words, the heterogeneous oxidation of char

YC-1 should overlap greatly with the initial ignition stage, rather than in a consecutive mode. In contrast, the results observed for the YC-2 char showed a stronger dependence of burnout on the blending ratio at 800°C and even 900°C. This further supports a lower reactivity for YC-2 char than the PCI coal. Therefore, blending YC-2 char into the PCI coal provided a heat sink effect on the ignition and burnout. A maximum blending ratio of 20 *wt%* was further confirmed for the YC-2 char at 800°C, which is consistent with the ignition results discussed above.

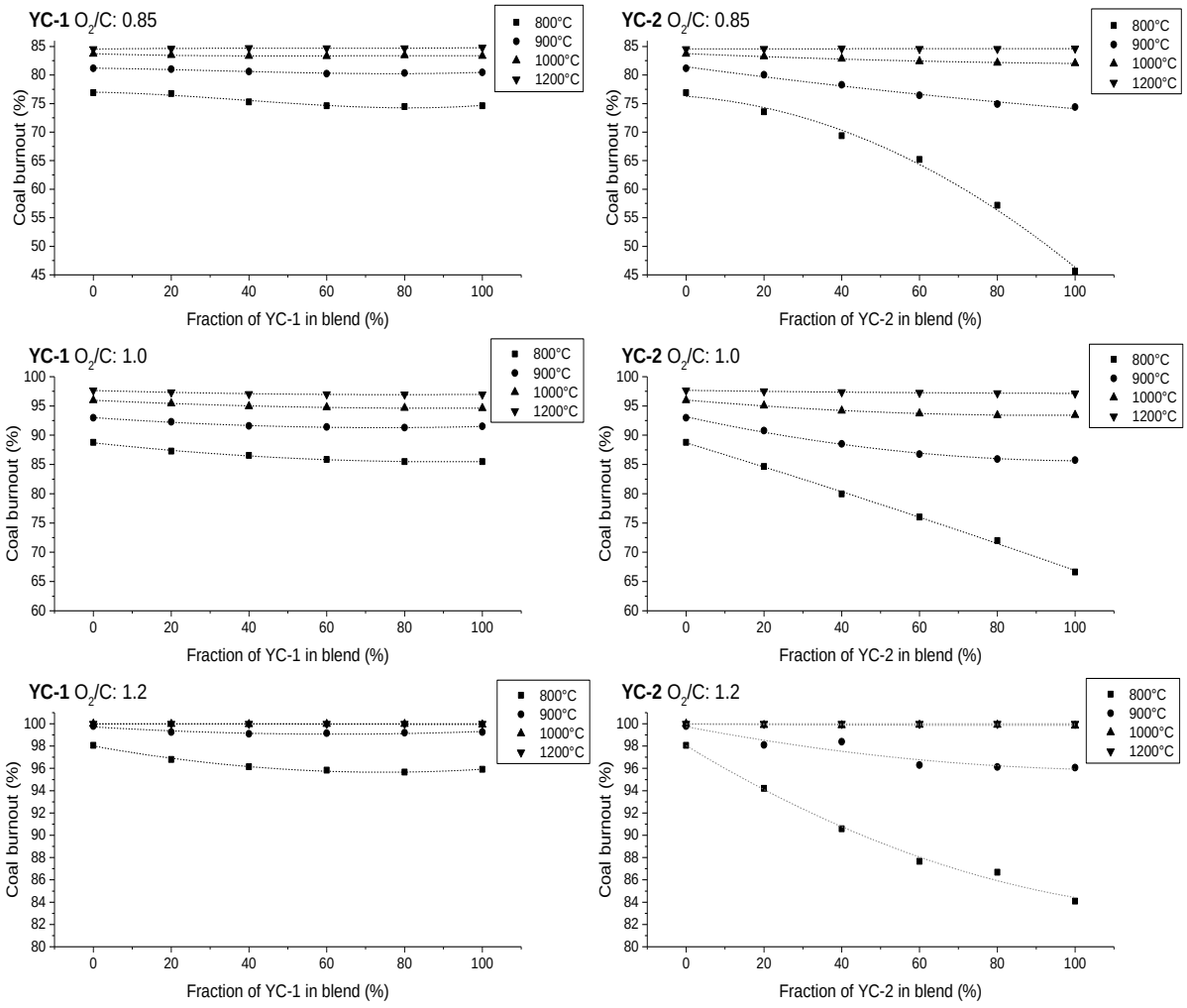

Figure 7.9 Effect of blend ratio and temperature on burnout at three O_2/C ratios for YC-1 (left) and YC-2 (right)

The results observed at a stoichiometric O_2/C molar ratio of 1.0 show a similar trend for both chars with their respective results at the lowest O_2/C molar ratio of 0.85. The effect of blending ratio is much weaker for YC-1 char, even at 800°C. This further substantiates a strong

overlapping between different steps for the combustion of YC-1 char and PCI coal blends, particularly at the temperatures from 900°C onwards. In contrast, the different steps took place rather consecutively at 800°C. This is particularly the case for YC-2 char which has a slower ignition, and also a lower reactivity. Therefore, its heat sink effect is stronger. The 800°C results for YC-2 char blends are rather linear versus the blending ratio.

Increasing the O_2/C ratio to 1.2 closed the discrepancy in the burnout between blends and pure PCI coal from 900°C and above for YC-1 char, and 1000°C and above for YC-2 char. At 800°C, the burnout of the blends still depended on the blending ratio, even for YC-1 char. This is due to the reaction control for the combustion at such a low temperature. The inherent reactivity (or the nature) of the fuel is more important than the O_2 partial pressure in the furnace. Upon the increase in the furnace temperature, the overall burnout gradually moves to the diffusion control regime, therefore, the nature of the blends is insignificant. In other words, using a higher O_2/C ratio for oxygen-enriched combustion and a blast temperature above 1000°C can eliminate the dependence of the overall burnout on the char blending ratio.

7.3.3.2 Influence of gas residence time

Since the residence time in a blast furnace is very short, effort was further made by evaluating the burnout at a shorter residence time in the DTF, 0.8 *s*. The results are shown in Figure 7.10 for three O2/C molar ratios for two chars at varying blending ratios. For comparison, the respective results for the residence time *1.4 s* were also included here. With respect to YC-1 char at the lowest O_2/C ratio 0.85, its results observed at 0.8 s are very similar with the longer residence time 1.4 s, except a clearer decrease on the overall burnout upon increasing the char blending ratio at 1000°C. The decrease on the burnout is more obvious upon the blending of YC-2 at 1000°C and 0.8 *s*. Such a descending trend also reflects the ignition results observed in Figures 1-5, further proving our previously mentioned hypothesis that the ignition delay mainly exerted its effect on the initial stage, whereas the later char oxidation stage was accelerated upon the blending of char and PCI coal. For the YC-2 char, its negative effect on the overall burnout is even discernible at 1200°C in 0.8 *s*. This substantiates the strong heat sink impact of YC-2 char which has a much lower reactivity and thus failed to synchronise with PCI coal in terms of combustion.

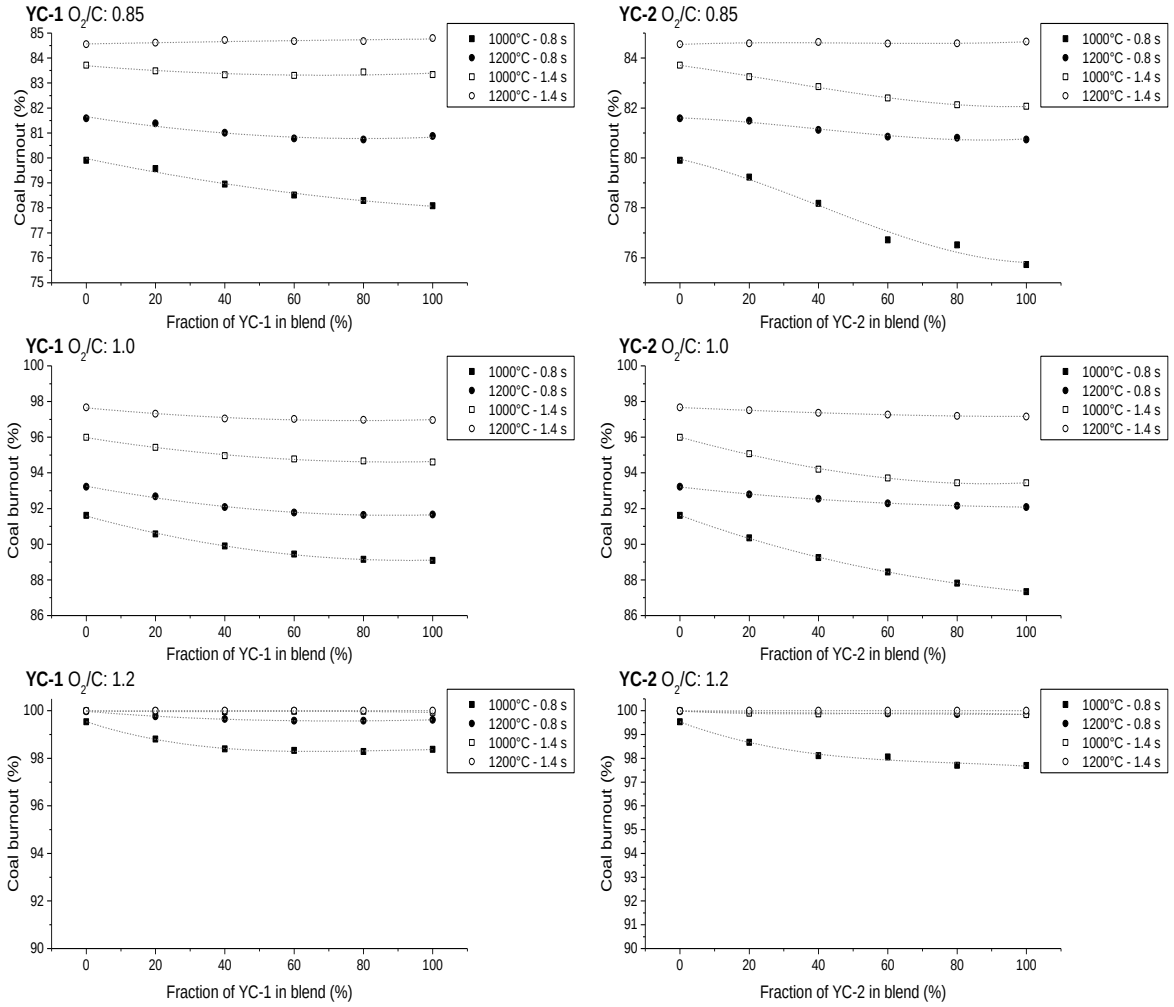

Figure 7.10 Effect of blend ratio and residence time on burnout at three oxygen to carbon ratios for YC-1 (left) and YC-2 (right)

The similar phenomena were observed for the two chars at the stoichiometric O_2/C ratio of 1.0. In particular, the use of a furnace temperature of 1200°C is essential to eliminate the negative heat sink effect of YC-2 char at a short residence time of 0.8 *s*. Such a conclusion is further strengthened at the excessive O_2/C molar ratio of 1.2.

7.3.3.3 Particle temperature profile

The temperature contours in Figure 7.11 show how the temperature shifts along the reactor from the injection point as blend ratio increases for both YC-1 and YC-2 for a fixed condition, furnace temperature of 1000°C and O_2/C 1.0. The heat sink effect of YC-1 char, although it is not very strong, is still influential at the initial particle heat-up and volatile ignition stage. That

is, upon the blending of char, the total volatile concentration will be lower. Consequently, the particles remain hot and glowing, whereas their ignition was delayed. This is supported by the ignition flame in Figure 7.3 and a gradual decrease on the ignition position in the CFD temperature contour in Figure 7.11**.** The similar results were predicted for the YC-2 char. Its dilution effect (for heat sink) is more obvious, leading to a greater decrease on the flame front position and the intensity of flame as well. Also, similar to the ignition results in Figure 7.3, for both char blends the delay in the flame position shifts gradually with increasing char content at low blend ratios, while having a more noticeable delay in ignition above a 60% blend.

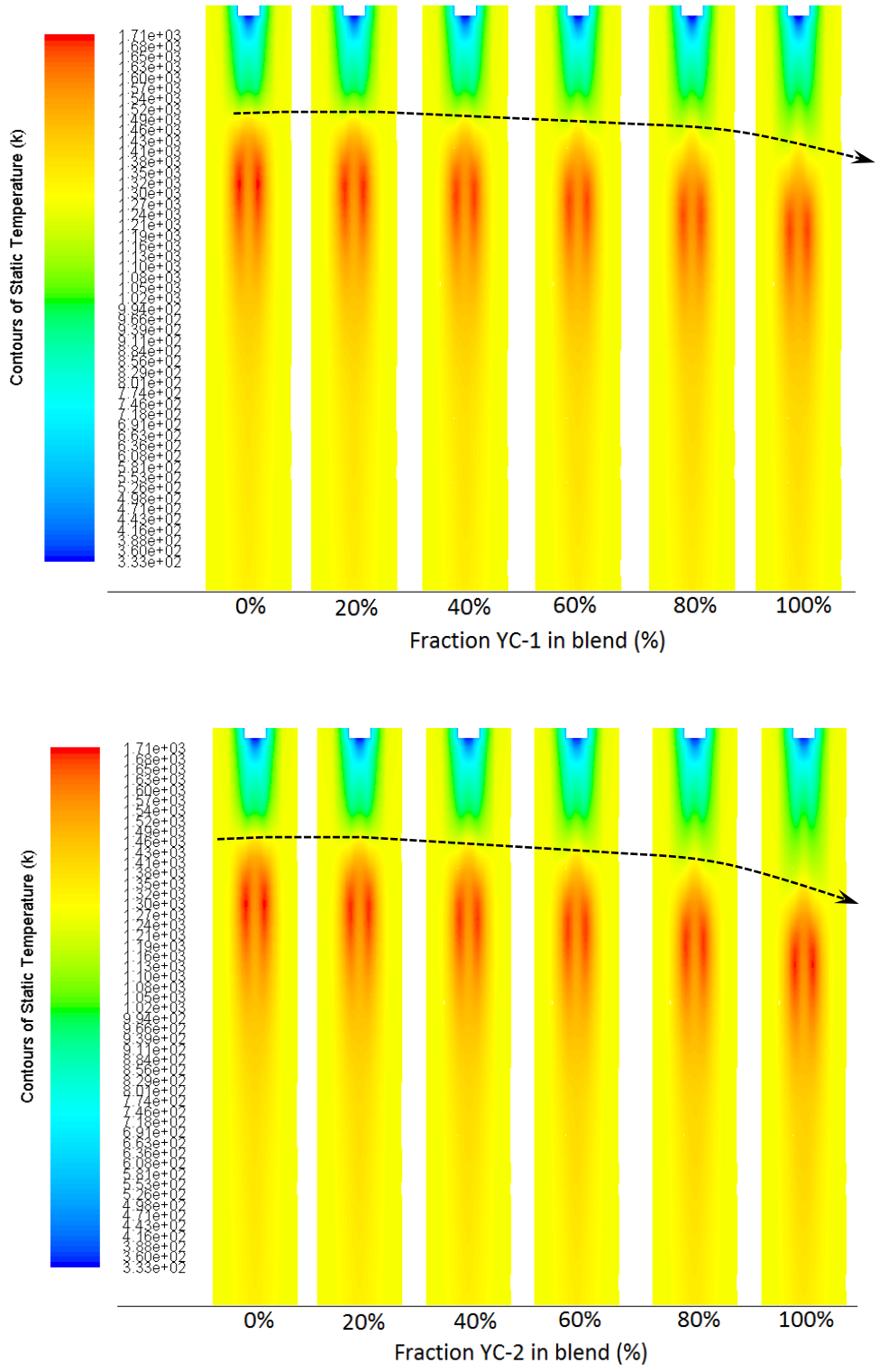

Figure 7.11 Contours of temperature for YC-1 (top) and YC-2 (bottom) blends at 1000°C and O_2/C ratio 1.0

Figure 7.12 further illustrates the average temperature for each distance away from the injector of the reactor for YC-1 and YC-2 char under the same condition. For either YC-1 or YC-2 char, increasing its blending ratio leads to a gradual decrease in the particle temperature before 0.15 m, which refers to the particle heat-up and ignition stage. The peak temperature was decreased considerably at the distance of 0.15-0.2 *m* for the flame propagation regime. All the blends with YC-1 char produced a marginal drop within 20°C, while for YC-2 increasing to only a 60% blending ratio will decrease the temperature by the same amount. Such a temperature gap should be mainly caused by the heat sink effect of YC-2 char which is difficult to ignite and burn. Above an 80% blend for YC-2, a slight increase in peak temperature since the char will combust in the same location further from the injector than for PCI coal. The distance to the peak temperature confirms a rather close relationship for all the YC-1 blends varying only 0.04 *m* between pure PCI coal and pure YC-1 (denoting the heterogeneous char oxidation stage) onwards. This is a strong evidence of the comparable reactivity of PCI char and YC-1 char and their concurrent oxidation. On the contrary, the peak gas temperature varies broadly with the YC-2 blending ratio extending the distance to the peak temperature by 0.06 *m*, further indicating its strong dilution and heat sink effect. This further suggests that optimizing the brown coal pyrolysis conditions is critical in maximizing the blending performance of the resultant char under the blast furnace combustion conditions.

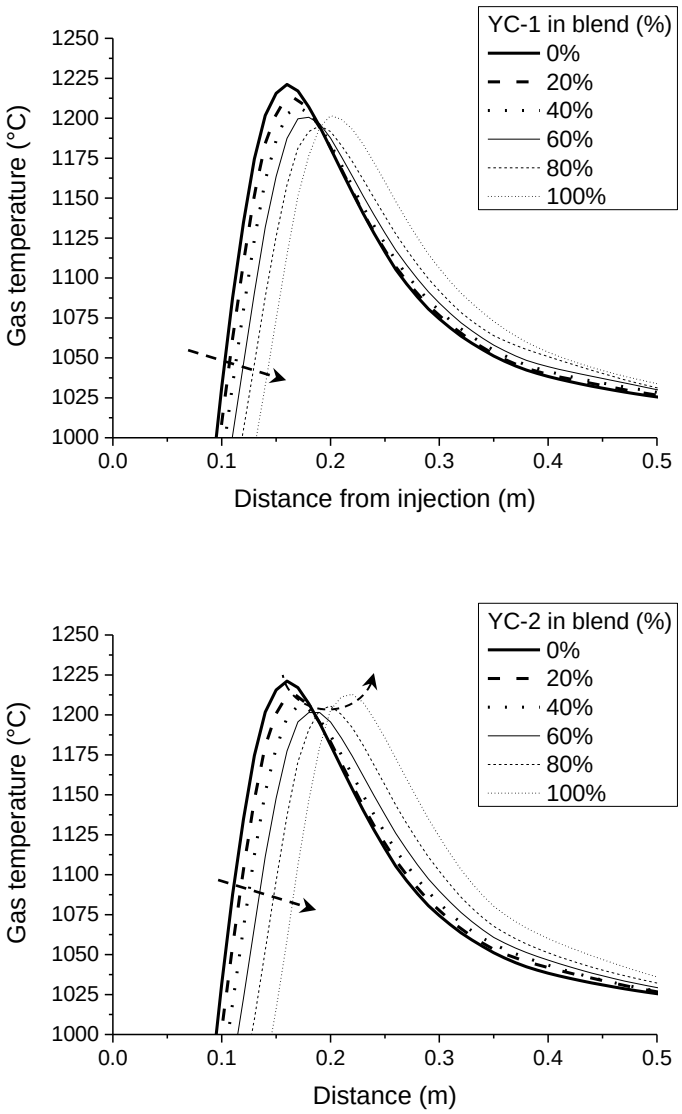

Figure 7.12 Effect of blend ratio on gas temperature profile for YC-1 (top) and YC-2 (bottom) blends at 1000°C and O_2/C ratio 1.0

7.4 Conclusions

Through the joint efforts on experimental investigation and CFD modelling, the combustion performance of two Yallourn char, produced under different pyrolysis conditions have been evaluated by blending it with a commercial PCI under different ratios. The influences of furnace temperature and O_2/C molar ratio were also assessed. The ignition of char – coal blends at both slow and fast heating rates were also diagnosed. The major conclusions can be drawn as follows:

1) According to particle ignition time, a maximum 40 *wt%* is allowable for YC-1 char which is comparably reactive with the commercial PCI coal. However, a maximum 20 *wt%* is only allowed for YC-2 which is less reactive. The negative heat sink effect of YC-2 char is influential, whereas the heterogeneous ignition of YC -1 overlapped considerably with the ignition of PCI coal which is mainly in the homogeneous gas phase.

2) Consistent with the burnout rate observed by DTF experiments and CFD modelling, the later char oxidation rate was accelerated greatly for the PCI coal blended with YC-1, irrespective of its blending ratio. In contrast, the heat sink effect is further obvious for the YC-2, the increase on the blending ratio of which greatly decreased the overall burnout rate, especially at low furnace temperatures (800°C and 900°C) and a shorter residence time such as 0.8 *s*.

3) For YC-1 char, its blending ratio is insignificant in the overall burnout. Increasing the furnace temperature to 1000°C and the O_2/C ratio of 1.2 can assist in achieving a nearly complete burnout for all of its blends, even at a short residence time of 0.8 s. In contrast, for YC-2 char, a furnace temperature of 1200°C and O2/C ratio of 1.2 are essential to complete the burnout of all its blends.

4) The Yallourn pyrolysis conditions for the preparation of its char is critical. A good synergistic interaction between Yallourn char and commercial PCI in terms of reactivity is also essential for a broad blending ratio to be used in the blast furnace.

References

1. World Coal Association *Coal & Steel Statistics*; London, 2014.
2. Ishii, K., *Advanced Pulverized Coal Injection Technology and Blast Furnace Operation*. Elsevier Science Ltd.: Oxford, UK, 2000.
3. Carpenter, A. M., *Use of PCI in blast furnaces*. IEA Clean Coal Centre: 2006.
4. IEA *Coal information 2005 with 2004 data.* ; OECD/IEA: Paris, France, 2005; p 498.
5. Traa, Y., Is a renaissance of coal imminent?—challenges for catalysis. *Chemical Communications* **2010,** 46, (13), 2175-2187.
6. Clarke, M. C. *Low rank coal/lignite upgrading technologies*; M.E.T.T.S. Pty Ltd: 2014.
7. De Girolamo, A.; Lameu, N. K.; Zhang, L.; Ninomiya, Y., Ignitibility and Combustibility of Lignite Pyrolysis Char under Simulated Blast Furnace Conditions. *Submitted to Fuel* **2015**.
8. De Girolamo, A.; Lameu, N. K.; Zhang, L.; Ninomiya, Y., Ignitibility and Combustibility of Lignite Pyrolysis Char under Simulated Blast Furnace Conditions. In *The 8th International Symposium on Coal Combustion* Beijing, China, 2015.
9. Zhang, X.; Liu, Y.; Wang, C. a.; Che, D., Experimental study on interaction and kinetic characteristics during combustion of blended coals. *J Therm Anal Calorim* **2011,** 107, (3), 935-942.
10. Haas, J.; Tamura, M.; Weber, R., Characterisation of coal blends for pulverised fuel combustion. *Fuel* **2001,** 80, (9), 1317-1323.
11. Su, S.; Pohl, J. H.; Holcombe, D.; Hart, J. A., Techniques to determine ignition, flame stability and burnout of blended coals in p.f. power station boilers. *Progress in Energy and Combustion Science* **2001,** 27, (1), 75-98.
12. Zhang, S., Theoretical consideration of problems relating to high coal rate injection into blast furnaces. *Ironmaking & steelmaking* **2003,** 30, (6), 467-474.
13. Ariyama, T., *Combustion behavior of PC particle group*. – Elsevier Science: Oxford, UK, 2000.
14. Gao, Y. H.; Bian, L. T. In *A Evaluation on Pulverized Coal Combustion Properties Using a Thermogravimetric Analyze Method*, Applied Mechanics and Materials, 2013; Trans Tech Publ: 2013; pp 609-613.
15. Qiu, J.; Li, F.; Zeng, H.; Yao, B.; Ma, Y., Determination of optimum blending ratio during coal blends combustion. *Combustion science and technology* **2000,** 157, (1), 167-184.
16. Gil, M. V.; Casal, D.; Pevida, C.; Pis, J. J.; Rubiera, F., Thermal behaviour and kinetics of coal/biomass blends during co-combustion. *Bioresource Technology* **2010,** 101, (14), 5601-5608.
17. Tahmasebi, A.; Kassim, M. A.; Yu, J.; Bhattacharya, S., Thermogravimetric study of the combustion of Tetraselmis suecica microalgae and its blend with a Victorian brown coal in O2/N2 and O2/CO2 atmospheres. *Bioresource Technology* **2013,** 150, 15-27.
18. Yuzbasi, N. S.; Selçuk, N., Air and oxy-fuel combustion characteristics of biomass/lignite blends in TGA-FTIR. *Fuel Processing Technology* **2011,** 92, (5), 1101-1108.
19. Yi, Q.; Qi, F.; Cheng, G.; Zhang, Y.; Xiao, B.; Hu, Z.; Liu, S.; Cai, H.; Xu, S., Thermogravimetric analysis of co-combustion of biomass and biochar. *J Therm Anal Calorim* **2013,** 112, (3), 1475-1479.
20. Shen, Y.; Guo, B.; Yu, A.; Zulli, P., A three-dimensional numerical study of the combustion of coal blends in blast furnace. *Fuel* **2009,** 88, (2), 255-263.
21. Zhang, J.; Wang, Q.; Wei, Y.; Zhang, L., Numerical Modeling and Experimental Investigation on the Use of Brown Coal and Its Beneficiated Semicoke for Coal Blending Combustion in a 600 MWe Utility Furnace. *Energy & Fuels* **2015,** 29, (2), 1196-1209.

22. Ulloa, C.; Borrego, A. G.; Helle, S.; Gordon, A. L.; García, X., Char characterization and DTF assays as tools to predict burnout of coal blends in power plants. *Fuel* **2005,** 84, (2–3), 247-257.
23. Moroń, W.; Rybak, W., Combustion characteristics of blended coals. In *Third European Combustion Meeting*, Crete, Greece, 2007.
24. Moon, C.; Sung, Y.; Ahn, S.; Kim, T.; Choi, G.; Kim, D., Effect of blending ratio on combustion performance in blends of biomass and coals of different ranks. *Experimental Thermal and Fluid Science* **2013,** 47, 232-240.
25. Biswas, S.; Choudhury, N.; Sarkar, P.; Mukherjee, A.; Sahu, S. G.; Boral, P.; Choudhury, A., Studies on the combustion behaviour of blends of Indian coals by TGA and Drop Tube Furnace. *Fuel Processing Technology* **2006,** 87, (3), 191-199.
26. Machado, J. G. M. S.; Osório, E.; Vilela, A. C. F.; Babich, A.; Senk, D.; Gudenau, H. W., Reactivity and Conversion Behaviour of Brazilian and Imported Coals, Charcoal and Blends in view of their Injection into Blast Furnaces. *steel research international* **2010,** 81, (1), 9-16.
27. de Castro, J. A.; Araújo, G. d. M.; da Mota, I. d. O.; Sasaki, Y.; Yagi, J.-i., Analysis of the combined injection of pulverized coal and charcoal into large blast furnaces. *Journal of Materials Research and Technology* **2013,** 2, (4), 308-314.
28. Mathieson, J. G.; Rogers, H.; Somerville, M. A.; Jahanshahi, S.; Ridgeway, P., Potential for the use of biomass in the iron and steel industry. In *Chemeca 2011*, Sydney, Australia, 2011.
29. Xie, K. C., *Structure and Reactivity of Coal: A Survey of Selected Chinese Coals*. Springer Berlin Heidelberg: 2015.
30. Kissinger, H. E., Reaction Kinetics in Differential Thermal Analysis. *Analytical Chemistry* **1957,** 29, (11), 1702-1706.
31. Wang, C. a.; Liu, Y.; Zhang, X.; Che, D., A study on coal properties and combustion characteristics of blended coals in Northwestern China. *Energy & Fuels* **2011,** 25, (8), 3634-3645.
32. Prationo, W.; Zhang, J.; Abbas, H. A. A.; Wu, X.; Chen, X.; Zhang, L., Influence of External Clay and Inherent Minerals on Lignite Optical Ignition and Volatile Flame Propagation in Air-Firing and Oxy-Firing. *Industrial & Engineering Chemistry Research* **2014,** 53, (7), 2594-2604.
33. Low, F.; De Girolamo, A.; Dai, B.-Q.; Zhang, L., Emission of Organically Bound Elements during the Pyrolysis and Char Oxidation of Lignites in Air and Oxyfuel Combustion Mode. *Energy & Fuels* **2014,** 28, (6), 4167-4176.
34. Zhang, J.; Prationo, W.; Zhang, L.; Zhang, Z., Computational Fluid Dynamics Modeling on the Air-Firing and Oxy-fuel Combustion of Dried Victorian Brown Coal. *Energy & Fuels* **2013,** 27, (8), 4258-4269.
35. Westbrook, C. K.; Dryer, F. L., Simplified Reaction Mechanisms for the Oxidation of Hydrocarbon Fuels in Flames. *Combustion Science and Technology* **1981,** 27, (1-2), 31-43.

This page is intentionally left blank

Chapter 8 – Contribution of Char-CO_2 and Char-steam gasification reactions for combustion of Victorian brown coal char

In Chapters 6 and 7, two industrially produced chars were evaluated for their application to PCI combustion. The studies concluded that the blending of brown coal char should be explored as a substitute for PCI coal either is a complete replacement or a blend. Compared to air-fire combustion in a power plant, the gas concentration is markedly different. In this chapter, combustion in these gasses will be investigated and the differences between brown coal char and bituminous coal combustion will be highlighted.

Abstract

This paper aims to clarify the extent to which char gasification reactions contribute in the overall char conversion of low rank coal under the high CO_2 or H_2O conditions. At lower temperatures, many studies on bituminous coal have found gasification reactions to be negligible on the overall char conversion, though for low rank coal a higher gasification rate is expected. While the kinetic rate of reaction may be much smaller for the char-CO_2 reaction compared to char oxidation, the elevated levels of CO_2 in oxy-fuel or oxygen enrichment in PCI combustion and may affect the conversion rate. In wet flue gas recycle, a large amount of steam may accumulate, especially for coals with higher moisture content such as Victorian brown coal. This will convert char in the form of the char-H_2O gasification reaction. The degree of char conversion and rate of char reactions which affect particle temperature as well as the surrounding gas environment. This investigation uses a drop tube furnace with a unique preheating system that preheats a secondary stream of gas to 1000°C. Subsequent CFD modelling, combined with TGA kinetics study was used to evaluate the effect of the gasification reactions in more detail. Oxygen concentration is varied between 5-12%, while the diluent gas is made up of 0-40%H_2O with the remainder N_2 or CO_2. Experimental results indicate that Victorian brown coal has high gasification reactivity which will significantly lower particle temperature by up to 106 K. Overall burnout under oxygen deficient conditions could be increased by up to 5% and burnout rate could be increased by as much as 25%. Overall reaction contribution could be as high as 28.8% for VBC char during complete char burnout.

8.1 Introduction

Brown coal combustion is the most carbon intensive of common resources [1]. Several studies deemed oxy-fuel technology to be the most favourable in terms of CO_2 abatement due to its technological and economic feasibility [2, 3]. In air-fired combustion, N_2 which makes up the majority of the combustion gasses is relatively inert, whereas for oxy-fuel combustion, the rate of char burnout and atmosphere on the particle surface may be affected by the high concentration of CO_2, as well as the presence of steam if the flue gas is recycled before condensing (wet recycle). The nature of pulverised coal injection (PCI) combustion in the blast furnace combustion where the O_2/C ratio is close to 1.0, also promotes a similar environment where the particle will be surrounded by a high CO_2 atmosphere before combustion is complete and relies on the CO_2 gasification to complete its burnout. This is especially true for the case of oxygen enrichment, where up to 40% of the inlet gas is O_2 which will greatly increase the concentration of CO_2 in the furnace.

The effect of the altered gas environment is multifaceted due to the intricate relationships of the many aspects altered from air-fired combustion. These include changes to gas density, heat capacity, radiation absorption, char-gasification reactions and diffusion of reactants to the char particle surface. Due to the complex relationship between these variables, it can be difficult to predict changes to furnace parameters including retrofitting to oxy-firing or how changes to a different coal rank will alter char burnout, local gas environment and particle temperature. For example, gasification reactions will occur more readily in the presence of high concentrations of CO_2 and steam. Due to the high activation energy, these reactions will become more influential at higher temperatures, however because of the endothermic nature of these reactions, particle temperature will be reduced as gasification rate increases. Although these reactions will complement the char consumption by O_2, the reduction in particle temperature could potentially lower the overall char burnout rate.

Carbon content in the parent coal is a large factor in the reactivity of chars in gasification environments. Generally, char reactivity will decrease with parent coal rank [4], however other factors are also important such as the amount of oxygen-containing surface groups and exchangeable cations such as Ca and Na [5]. While these reactions will contribute towards char conversion, they are endothermic so will reduce the char particle temperature. Due to the higher reactivity, this effect is expected to be greater with brown coal.

There have been several studies examining the contribution of gasification reactions for bituminous coal [6-8]. Chen et al. estimated this contribution using a simplified multiple surface reaction model [6]. This model assumes a particle size of 80 μm and considers kinetic reaction rates for char oxidation and gasification reactions as well as diffusion. The study finds an increase in gasification contribution with temperature and an inverse relationship with oxygen concentration. At a particle temperature of 1600 K, gasification reactions contributed 2% or 8%, for oxygen rich and deficient cases respectively and these increased to 3% and 21% at 1800 K. Hecht et al. investigated the contribution under wet and dry recycle conditions at various oxygen concentrations for a 100 μm bituminous char particle using Surface Kinetics in Porous Particles (SKIPPY) code [8]. With 12% oxygen which produced a particle temperature of 1800 K, gasification reactions contributed 19.8% of the char consumption rate. With increasing oxygen concentration, this contribution increased due to the higher particle temperature. Also when steam concentration was increased, the contribution by steam increased while the CO_2 contribution fell producing a slightly higher overall gasification contribution.

Table 8.1 summarises the modelling studies that assess the contribution of gasification reactions during O_2/CO_2 combustion. Despite these studies, the majority of studies have concentrated on higher rank coals with a high oxygen content and high furnace/gas temperatures for raw coals. Models have focused on steady state single particles or steady state gas conditions rather than a time dependent environment. All these differ from this study focusing on mild combustion environment and low-rank coal char with a volatile content down to 6 wt%.

Table 8.1 Summary of completed studies on contribution of gasification reactions during high CO_2/H_2O conditions

Aim of study	Finding	Model	Coal type	Parameters	Ref.
Assess impact of gasification reactions on the oxy-fuel combustion of coal char	10% increase in char consumption rate. Gasification contribution up to 31.8% at T_p = 2300 K	SKIPPY	Sub-bituminous char	3 O_2, 2 % steam Balance gas CO_2, Fixed T_g: 1690 K	Hecht et al. [8]
Assess the contribution of the gasification reactions to the total carbon consumption	Higher gasification contribution when O_2 is deficient.	Multi-surface reaction model	Kinetics from graphite gasification	O_2: rich and deficient Balance gas N_2 /CO_2 T_p: 900-2000 K	Chen et al. [6]
Contribution to Char Burnout from Gasification by H_2O and CO_2	Slight contribution of gasification reactions to burnout	Spherical particle model	Bituminous coal	T_p: 1600 K 6% O_2, 6% H_2O	Stanmore et al. [7]
To validate a CFD model for use with air and oxyfuel combustion	Lower peak particle temperature in oxyfuel combustion caused by gasification reactions	Multi-surface reaction model with CFD	Victorian brown coal	T_w: 1000°C Air, 21% O_2/ CO_2, 27% O_2/CO_2	Zhang et al. [9]
Assess contribution of gasification to char burnout of wet brown coal	Contribution of internal moisture to gasification. O_2 increased gasification contribution.	1-D transient model	Wet and dry Victorian brown coal	T_w: 1100°C 21%/31% O_2, 18% H_2O balance CO_2.	Prationo et al. [10]
Measure the effect of CO_2 gasification on char combustion in oxy-fuel conditions	Burnout improved and particle temperature reduced by gasification	Single film model	Sub-bituminous coal	T_g: 1600 K 5,21,30% O_2 Air/Oxyfuel	Kim et al. [11]

In this study, char derived the pyrolysis of two low rank coals, Victorian brown coal and Xinjiang coal were studied in a drop tube furnace that features a unique gas pre-heating system (up to 1000°C). Computational fluid dynamics (CFD) software was used to assess differences in burnout kinetics, temperatures and gas concentrations utilising kinetic data collected from thermogravimetry-differential thermal analysis (TG-DTA) as parameters for the multiple surface reaction model and incorporating a recently developed weighted-sum of grey gas model (WSGGM) for gaseous radiation absorption. Comparison was also made between char and its parent raw coal on particle temperature and gasification contribution. By these efforts, we aim to clarify the gasification reaction contribution for low-rank coal char burnout under high CO_2/H_2O conditions, and therefore, improve the deployment of this advanced low-emission combustion technology for low-rank coal.

8.2 Experimental

8.2.1 Char properties

The chars used were derived from Victorian brown coal and Xinjiang coal. Victorian brown coal (VBC) is sourced from Loy Yang, Victoria, Australia. Xinjiang coal (XJC) is a sub-bituminous coal from Xinjiang, China. The chars were generated in a drop tube furnace at 1000 °C with a short particle residence time of 0.7 s. VBC char and XJC char have high concentrations of Na, Fe and Mg (Table 8.2). While XJC char also has high amounts very high concentration of Ca, making up 1.74% of the total weight of the char. Metals that promote the gasification reactivity of the char include Ca [12], Fe [13] and Na [14]. The proximate and ultimate analysis is shown in Table 8.3. Although the parent coals are of different ranks; the chars show very similar properties.

Table 8.2 Elemental analysis of metals in VBC char and XJC char

	Concentration (ppm)	
Element	VBC char	XJC char
Al	6506	2105
Ca	805	17361
Fe	1166	2676
K	101	199

Mg	1175	2632
Na	2030	1856

Table 8.3 Proximate and ultimate analysis of VBC char and XJC char

Proximate Analysis (wt %)	VBC char	XJC char
Moisture $_{ar}$	3.2	1.7
Volatile Matter $_{db}$	6.2	6.3
Fixed Carbon $_{db}$	87.8	87.3
Ash $_{db}$	6.0	6.4
Ultimate Analysis	(wt %, db)	
Carbon	88.9	87.7
Hydrogen	1.1	1.0
Oxygen	3.05	3.72
Nitrogen	0.72	0.69
Sulphur	0.23	0.49

8.2.2 Kinetics

For char-O_2 and char-CO_2, kinetic parameters were determined using a simultaneous thermogravimetry/differential thermal analyser (Shimadzu DTG-60) and the method proposed by Kissinger for differential thermal analysis [15], based on the variation of the temperature at which the maximum rate occurs with heating rate. By plotting $\ln\left(\frac{\beta}{T_{\max}^2}\right)$ against $\frac{1}{T_{max}}$, a linear fit can be obtained to determine the pre-exponential factor and activation energy shown in Table 8.4. This method advantages because of the use of multiple heating rates and multiple sampling, so that the overall result is more representative of the entire sample.

Table 8.4 Kinetic parameters for char-O_2 and char-CO_2 reaction as determined by Kissinger method

Reaction	VBC char		XJC char	
	A ($kg/m^2.s.Pa$)	E_a (kJ/mol)	A ($kg/m^2.s.Pa$)	E_a (kJ/mol)
C-O_2	0.0121	97.63	0.00591	92.52
C-CO_2	810.4	287.5	4.492	219.6

For steam gasification a quartz thermogravimetric analyser was used. Due to the nature of quartz the sample can only be heated to 1000°C and to prevent condensation in the reactor, a steam concentration of 5-20% is used. This prevents the gasification reaction from reaching its maximum rate at higher heating rates; therefore, the Kissinger-Akahira-Sunose (KAS) method (described below) will be used instead of the Kissinger method.

Reaction order is determined by analysing the reaction at a single heating rate with steam concentrations of 5, 10, and 20%. For both char samples, the reaction order conforms to a single value as the temperature approaches 1000 °C. Since char is relatively unreactive with steam at low temperatures, the converged value will be used for the reaction order. The reaction orders were determined to be 0.68 and 0.44 for VBC and XJC char respectively. This falls within the range of 0.4 to 0.72 found in various studies examining char-steam gasification reaction order [16-18].

The results are summarised in Table 8.5 and indicate the both VBC and XJC char are both relatively reactive compared to bituminous coal kinetic parameters reported in literature [19], however they are within range of brown coal reactivity values [20].

Table 8.5 Kinetic parameters for steam gasification of VBC char and XJC char.

Char name	Pre-exponential constant (s^{-1})	Pre-exponential constant ($kg/m^2.s.Pa^n$)	Activation energy (kJ/mol)	Rate at 1273 K (s^{-1}) 0.05 atm steam
VBC char	9.129E+04	2.467	172.48	7.63E-03
XJC char	7.367E+04	15.42	165.90	1.15E-02

8.2.3 Drop tube furnace (DTF) experiments

The generation of the char as well as the experiments on char conversion are conducted in a 2 m high drop tube furnace (DTF). More detail about this furnace including a schematic can be found in previous works [21]. The furnace wall temperature is set to 1000 °C, although flame temperatures are expected to exceed this. This set wall temperature is applied to induce the flame temperature that can be expected during brown coal combustion. Compared to bituminous coal combustion the flame temperature may be several hundred degrees lower [20]. One CFD study of an industrial scale boiler reported flame temperatures in the range 910-1430°C [22].

The approximate residence time of a particle in the reactor is approximately 2.1 s. Unburned char particles were collected in a flask and a silica microfiber thimble filter. Oxygen is fixed at 5% v/v of the total gas flow rate to ensure an O_2/C ratio of 0.58 to necessitate only a partial conversion of carbon in order to better compare differences in burnout between gas conditions. 12% O_2 (O_2/C ratio: 1.39) was also used to test the complete burnout of char where the calculated unreacted O_2 should be similar to that of coal fired boiler (3.4% O_2).

8.2.4 CFD model

The geometry and mesh for the drop tube furnace was taken from a previous study of the same reactor [9]. The mesh is made up of 231 000 cells and was validated experimentally and in a grid independence test. Turbulence is modelled using the k-ε model which has shown sufficient accuracy in modelling combusting flows [23]. Radiation in pulverized coal applications is often modelled by either the discrete ordinates (DO) or P1 model [24]. In this case the DO method was

chosen due to suitability for all optical thicknesses and level of accuracy. Gaseous radiative properties are calculated using a refined weighted sum of grey gases model (WSGGM) which was implemented into FLUENT via a user defined function (UDF) from the work of Yin et al. for O_2/N_2 [25] and O_2/CO_2 conditions [26]. For air-fired combustion, the Westbrook and Dryer mechanism is used to describe the oxidation of carbon monoxide [27], while for O_2/CO_2 combustion a refined version of the Westbrook and Dryer mechanism is used which has been refined for O_2/CO_2 conditions [28]. The refined model includes the reverse reaction of the carbon monoxide oxidation and will better predict major species concentrations. Hydrogen oxidation is also included for both O_2/N_2 and O_2/CO_2 conditions. A multiple surface reaction model is utilized to consider char reactions with O_2, CO_2 and H_2O, which uses harmonic weighting averaging between diffusion and kinetic rates. Intrinsic kinetic parameters were taken from experiments described in section 8.2.2. Mass diffusion-limited constant values are taken from literature [6].

8.3 Results and Discussion

8.3.1 Experimental results and validation of CFD model

Drop tube furnace (DTF) experiments were undertaken to analyse the effect of steam concentration, balance gas (N_2 and CO_2) and particle residence time on the overall char conversion, as well as to validate the CFD model. Experimental results in Figure 8.1 show the minimal effect steam has on the overall char conversion. As expected, char conversion increases with residence time. Most of the char is converted within the first 1.4 seconds, following this, char conversion will peak at 2.7 seconds when all the oxygen is consumed.

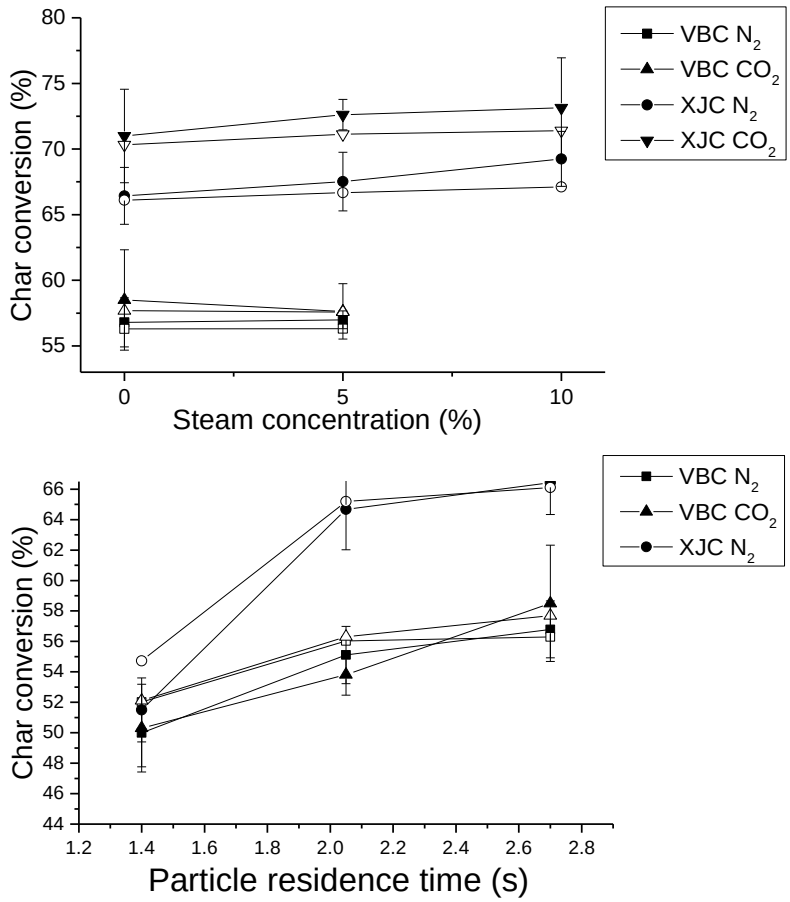

Figure 8.1 Drop tube furnace results showing effect of steam concentration and particle residence time on char conversion with CFD results for comparison (open symbols) for VBC and XJC char with 5% O_2.

Figure 8.2a shows validation of the CFD model using experiments Datong coal combustion where particle temperature was measured using a 2-colour pyrometer described in previous works [29]. Next, the char conversion predicted by the CFD model and compared against the experimental results (Figure 8.2b). Both tests show a reasonable prediction which verifies that the model can be used satisfactorily and extrapolated to different conditions. A grid independence study and particle temperature validation were conducted for a previous study with the same mesh and drop tube furnace [9].

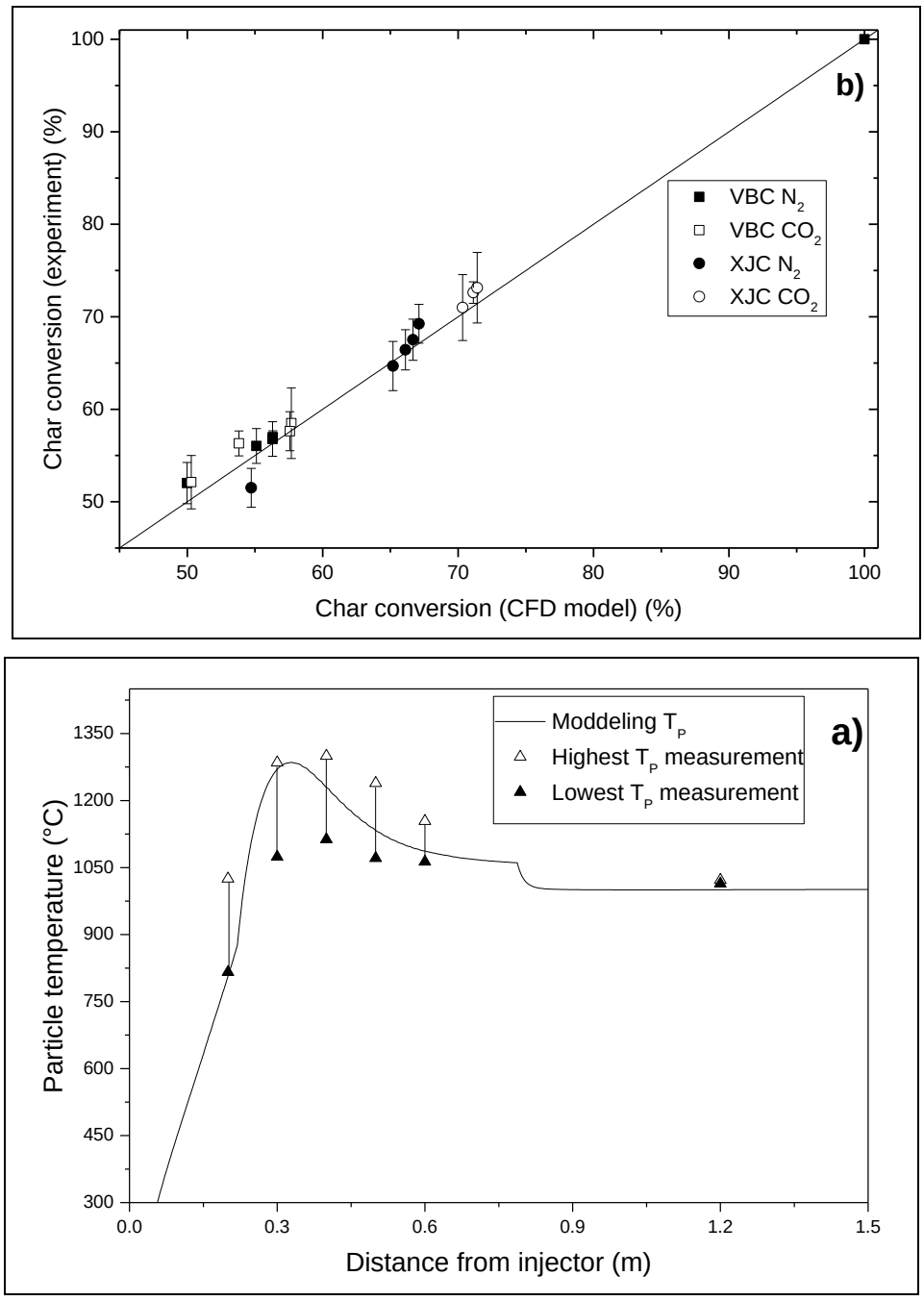

Figure 8.2 Experimental validation of CFD model using a) particle temperature measurements with Datong black coal combustion in air at 1000°C and b) VBC and XJC char conversion with balance gas N_2 and CO_2.

It was also of interest to determine that the char would be completely burnt out in an environment of 12% O_2 for cases with both N_2 and CO_2. This was tested by replicating these conditions in the drop tube furnace, followed by ashing of the remains at 600°C for 3 hours.

The burnout can then be calculated by an ash tracer method. The burnout was determined to be 99.9±0.1% for each case tested with 12% O_2, further validating the CFD model.

8.3.2 Contribution of gasification reactions

Figure 8.3a shows the contribution of the char gasification reactions on the overall char conversion under O_2/N_2 and O_2/CO_2 conditions for VBC char. Gasification reactions are most significant under oxygen deficient conditions, accounting for up to 28.8% of the total char conversion when 40% steam is combined with CO_2 or 23.7% in the absence of CO_2 since oxygen will be deleted quickly by char oxidation and oxidation of gasification products. In comparison, XJC char, shown in Figure 8.3b, is more reactive overall in the presence of CO_2, rising to a 39% contribution, 11% higher than the maximum contribution of VBC char. However, XJC char is more sensitive to the reduction in gasification contribution through addition of O_2, showing a contribution barely above that for VBC char once sufficient O_2 is supplied.

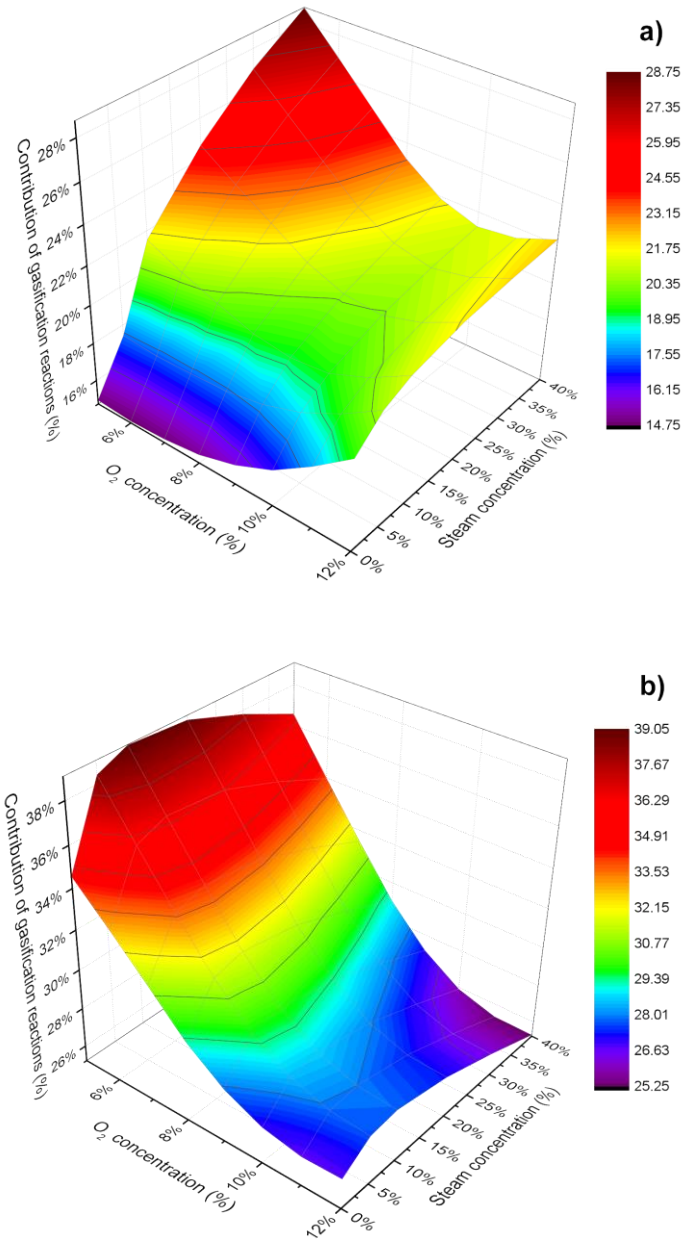

Figure 8.3 Contribution of gasification reactions to char conversion at T_w=1000°C with balance gas CO_2 for a) VBC char and b) XJC char.

Figure 8.4 demonstrates how the gasification reactions will compete with increasing steam concentration. While steam replaces CO_2, the overall contribution will increase since this char is more reactive with steam than CO_2. These contributions are lowered to a maximum of 15% and 22% for balance gasses N_2 and CO_2 respectively when sufficient oxygen is supplied. However, due to the increased particle temperature at high oxygen concentrations and the high activation energy of the gasification reactions, the absolute rate of gasification reactions will

increase with O_2 concentration. In O_2/N_2 conditions, at higher steam concentrations, the contribution of gasification reactions increases when O_2 concentrations are greater than 10%. Compared to a study on gasification reaction contribution to a bituminous coal [6], these results show a much greater gasification reactivity, even at the lower temperature employed here, which is to be expected based on the coal rank.

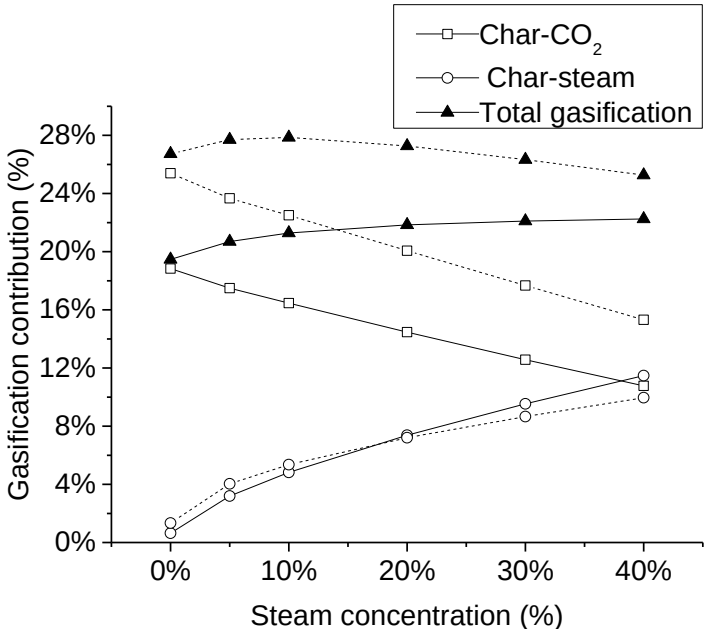

Figure 8.4 Competition of char-CO_2 and char-steam gasification reactions for 12% O_2 (O_2/C ratio: 1.39) for VBC char (–––) and XJC char (---).

The high activation energy of the char-CO_2 and char-H_2O reactions will cause these reactions to become much more significant at higher temperatures as shown in Figure 8.5. In O_2 deficient cases (where O_2 is limited to 5%), this rise in temperature will produce a much greater increase in the contribution of gasification reactions compared to cases where sufficient O_2 is supplied (12% O_2) as in later stages these reactions become more significant. This can be up to 20% higher in cases with N_2 or 35% higher when CO_2 is the balance gas. While adding steam to cases with N_2 will increase the contribution of gasification reactions, this affect is even less significant under CO_2 and will lead to the contribution reaching a plateau or even decreasing slightly.

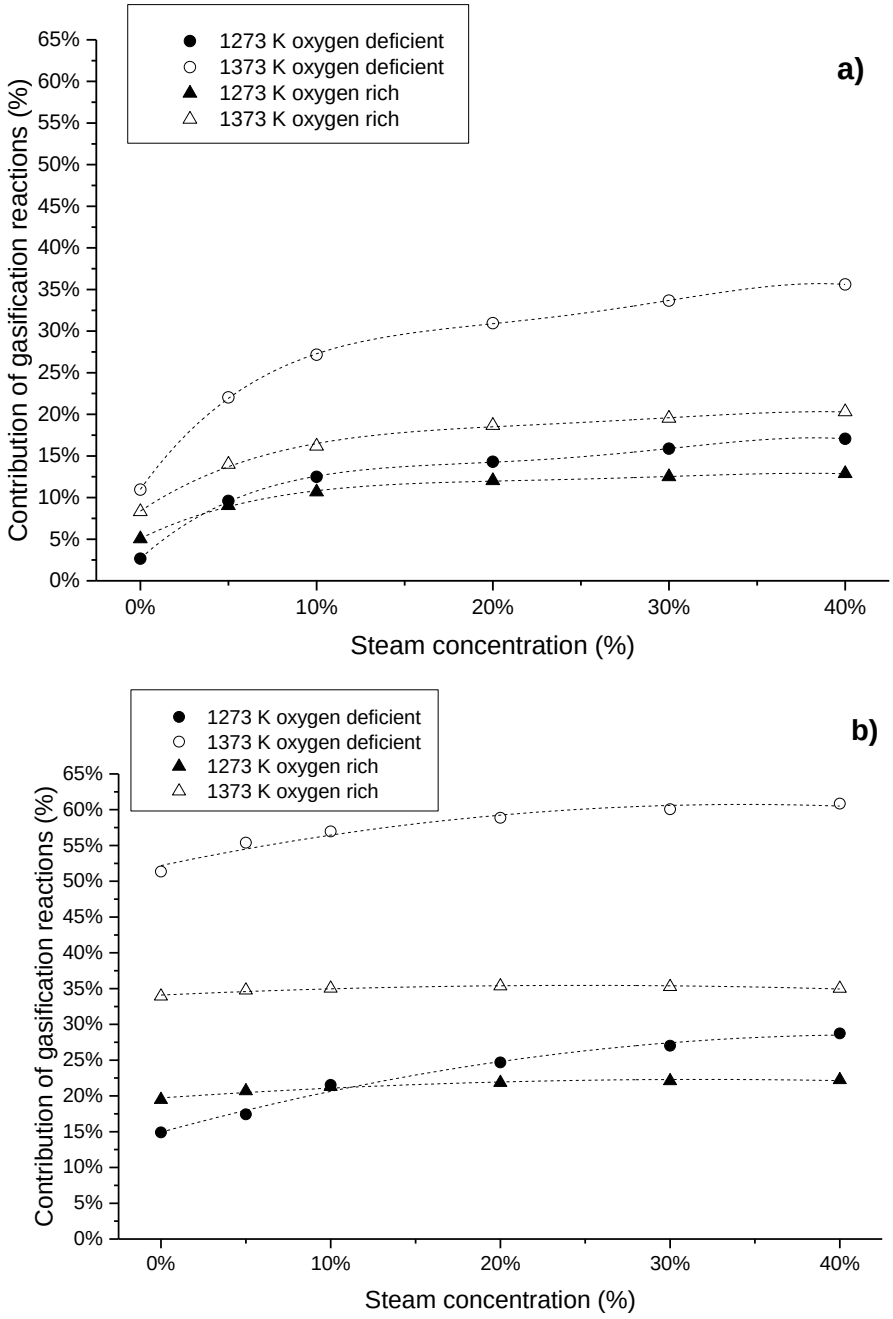

Figure 8.5 Dependence of wall temperature to the contribution of gasification reactions to total char conversion in a) N_2 and b) CO_2 for VBC char.

As a function of distance from the injection point, Figure 8.6 shows that the instantaneous gasification rate along the centreline of the furnace. For 12% O_2 with balance N_2 the gasification rate peaks at 2.7 mol/m^3.s. For this condition the overall gasification contribution for gasification reactions for with balance gas N_2 is only 6.3%, however the contribution of gasification reactions along the centreline of the reactor peaks at 49.8% which occurs when O_2

is mostly depleted in that region, CO_2 product concentration is built up and gas temperature is still high. As expected this peak is delayed compared to those with balance gas CO_2 since CO_2 is already present in high concentrations. The gasification rate will increase to 16.2 mol/m^3.s when N_2 is substituted with CO_2 and further increases to 16.9 mol/m^3.s when 40% H_2O is added. The addition of 40% steam will increase the peak gasification contribution will increase from 46.3% to 51.4% and the position of the peak will be closer to the injector.

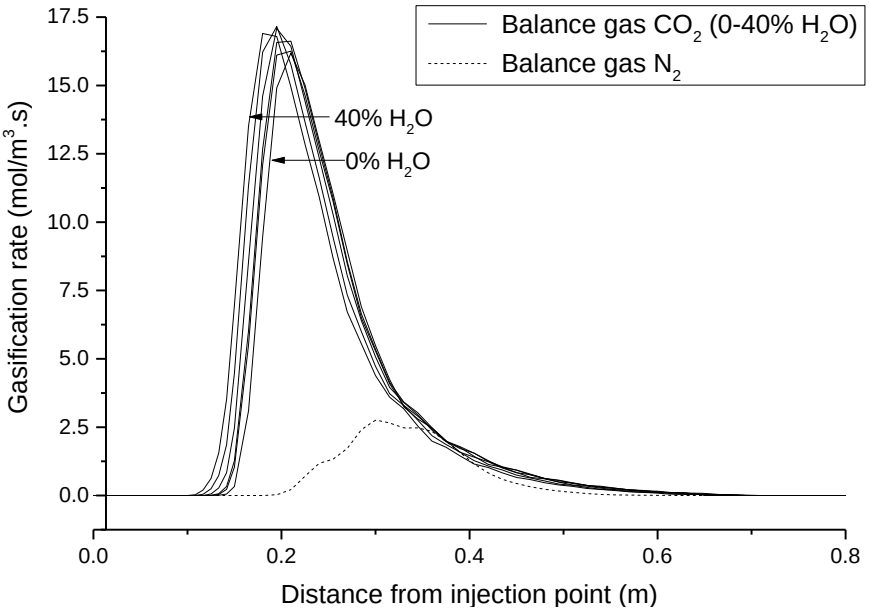

Figure 8.6 Contribution of gasification reactions as a function of distance from injection point at T_w=1000°C and 12% O_2 (O_2/C ratio: 1.39) for VBC char.

A previous study compared the contribution of the gasification reaction for brown coal under O_2/N_2 and O_2/CO_2 conditions [9] which was reproduced in Figure 8.7. Compared to this study peak gasification contributions are higher, although a lower oxygen fraction is used in this study. The lower gasification contribution for raw coal should mainly be due to the shielding effect of volatile clouds that prevent separate solid char particles from getting in touch with bulk gases [30]. The volatile-char interaction has been reported to be major resistance retarding the char gasification rate.

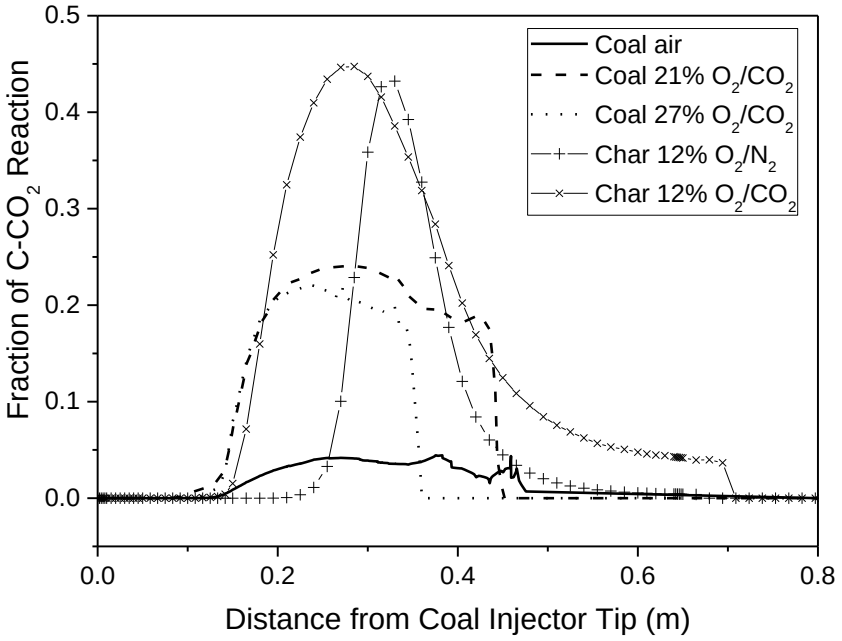

Figure 8.7 Comparison of C-CO_2 gasification contribution for VBC char compared to VBC coal from another study [9].

At a fixed O_2 concentration of 5% it can be compared how CO_2 and steam will affect the overall conversion of char. Figure 8.8 shows that the transition from balance gas N_2 to CO_2, burnout can increase by as much as 1.6% for VBC char or 6.0% for XJC char. For VBC char, increasing steam up to 7.5% will show an insignificant effect on the overall char conversion. Above this, char conversion will firstly rise sharply then increase steadily since char is more reactive in H_2O compared to the CO_2 it is displacing. Increasing steam up to 40% can raise the overall conversion by 4.1%.

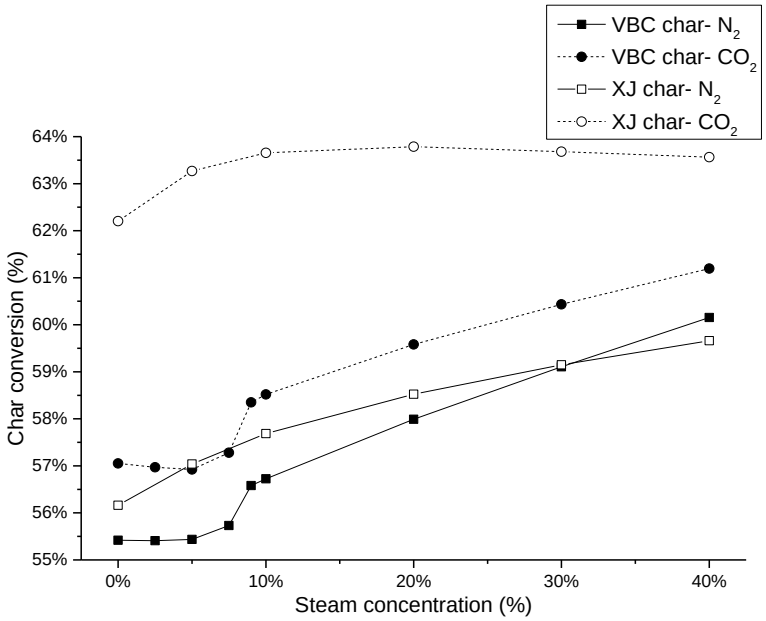

Figure 8.8 Effect of CO_2 environment on overall char conversion for cases with 5% O_2 (O_2/C ratio: 0.58) at T_w=1000°C for a) VBC and b) XJC char.

Figure 8.9 shows how the change from balance gas N_2 to CO_2 will affect the overall burnout rate. For both 5% and 12% O_2, the peak burnout of the char will occur at a shorter distance to the reactor. The height of this peak is larger under the 5% O_2 condition where O_2 is depleted, however for 12% O_2 the peak is the same height of 5.5 mol/m^3.s for all conditions. Addition of steam marginally decreases the delay before the maximum carbon consumption rate is achieved, however peak rate is unaffected.

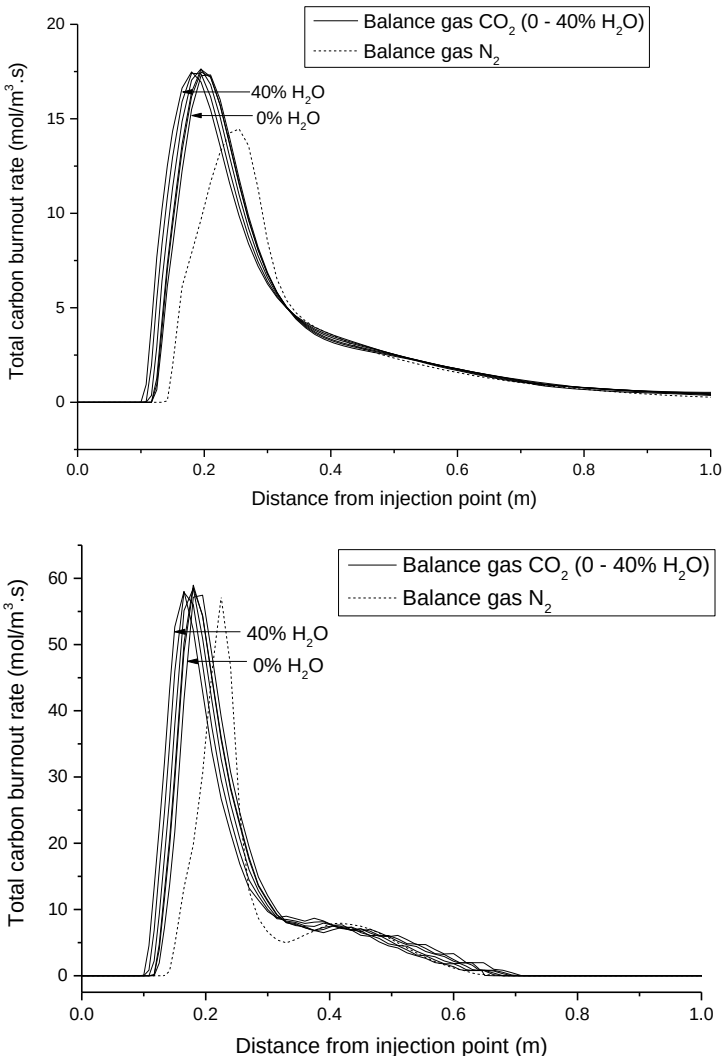

Figure 8.9 Effect of O_2/CO_2 environment on total carbon burnout rate for VBC char at T_w=1000°C for a) 5% O_2 (O_2/C ratio: 0.58) and b) 12% O_2 (O_2/C ratio: 1.39).

8.3.3 Implications

8.3.3.1 CFD prediction of particle temperature

Due to the increased radiative heat transfer, particles will initially be heated faster in CO_2 conditions and reach peak temperature in a faster time as shown in Figure 8.10, while the flame is less intense overall. However the peak particle temperature at 5% O_2 is only 1125 K, lower than 1195 K when N_2 is the balance gas. Again, this is due to the higher heat capacity of CO_2 but also the endothermic nature of the CO_2 gasification reaction. Figure 8.10b shows that at a higher oxygen concentration, steam combined with CO_2 can increase the peak particle temperature compared to that of CO_2 only. This is because the heat of reaction is lower for C-H_2O (131.4 kJ/mol) compared to C-CO_2 gasification (173.0 kJ/mol).

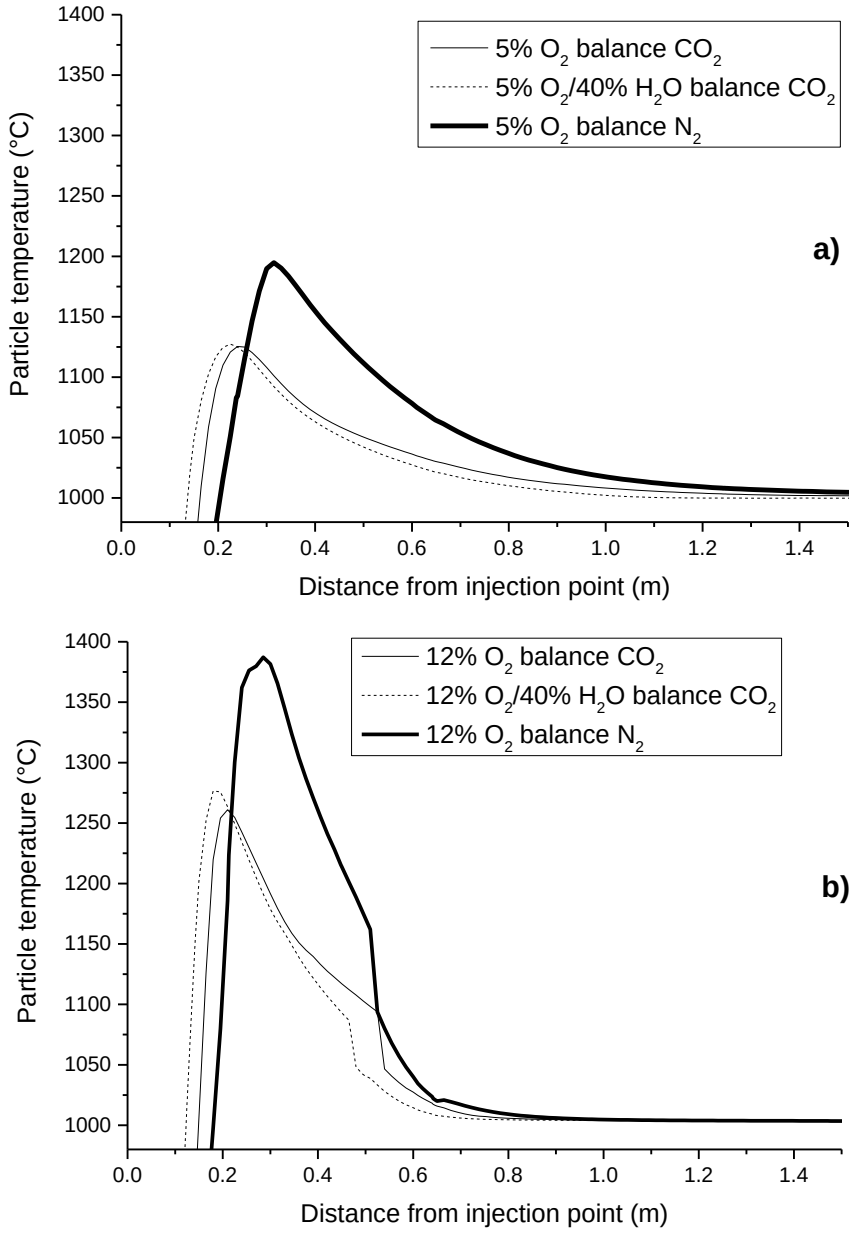

Figure 8.10 Particle temperature for T_w=1000°C for a) 5% O_2 (O_2/C ratio: 0.58) and b) 12% O_2 (O_2/C ratio: 1.39).

Figure 8.11 demonstrates how particle temperature is affected by the increased reactivity VBC char has compared to a higher rank coal. With kinetic parameters substituted with those for a bituminous coal obtained from literature, it was found that a decrease in gasification reactivity will increase particle temperature, from 1483 K to 1560 K. This is due to the endothermic nature of the gasification reactions.

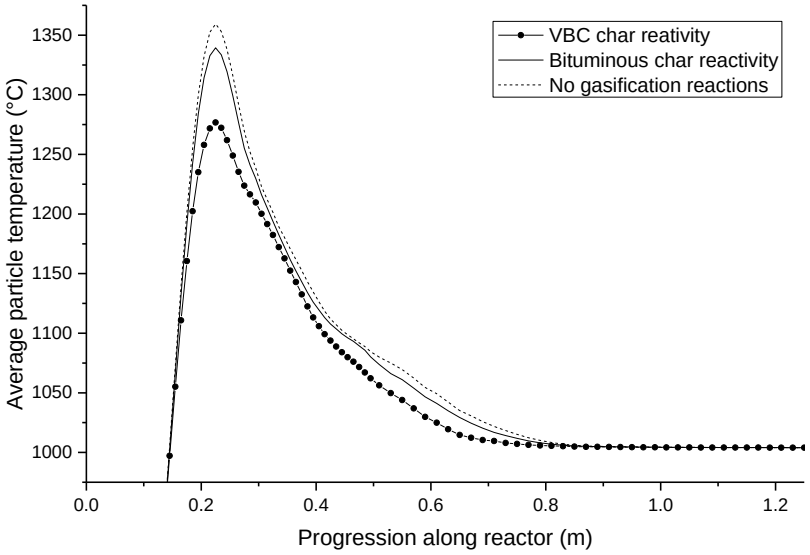

Figure 8.11 Comparison in particle temperature between char with reactivity of VBC char and bituminous coal char at T_w=1000°C and 12% O_2 (O_2/C ratio: 1.39).

8.3.3.2 CFD prediction of surface gas concentration

The Multiple Surface Reaction model in utilises a single-film model to model the combustion process. A single spherical coal particle is surrounded by a boundary layer of the bulk gas. Components of the bulk gas (O_2, CO_2, H_2O) may diffuse across the boundary layer to the particle surface. Using single-film assumption that gas-gas reactions only occur in the bulk gas, concentrations of different gas components may be predicted on the particle surface. These concentrations will be dependent on the rate of consumption and emission of the gasses at the particle surface, as well as diffusion to and from the bulk gas.

Figure 8.12 demonstrates how the ratio of CO/CO_2 on the particle surface may be modified between low-rank VBC-char and a bituminous coal char. CO/CO_2 ratio has been calculated and utilised in several studies to predict vaporisation of metals [31, 32]. On one hand, the bituminous coal char will reach a higher peak particle temperature which will increase the rate of the char reactions, creating a higher amount of CO. In contrast, low-rank coal will be more reactive with H_2O and CO_2, producing CO from these reactions. Initially it can be seen that CO/CO_2 ratio is similar between the chars, however after the majority of oxygen has been consumed by the particle, gasification reactions will become more influential leading to a higher CO/CO_2 ratio with low rank coal char.

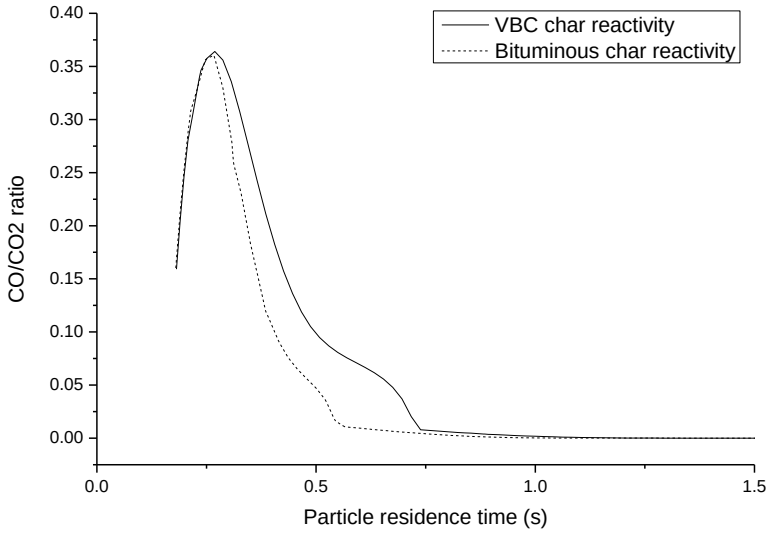

Figure 8.12 CO/CO2 ratio on particle surface in 12% O_2, 40% H_2O environment with balance gas CO_2.

8.4 Conclusions

The following conclusions can be drawn:

- Both low-rank coal chars have high reactivity and a rapid burnout rate even under the low-oxygen O_2/CO_2 combustion environment, suggestive of the suitability of this low-emission technology for low-rank coal.
- Gasification reactions can make a large contribution (up to 29% for VBC char) to the overall char conversion, especially in low oxygen environments and at higher temperatures. They may increase the burnout rate and overall char burnout. Particle reactivity can alter the gaseous environment on the particle surface due to the increased production of CO from gasification reactions.
- Char particles in CO_2 will experience a lower peak particle temperature compared to N_2, however particle temperature will initially be higher due to the higher radiative heat transfer in CO_2.

References

1. Lenzen, M., Life cycle energy and greenhouse gas emissions of nuclear energy: A review. *Energy conversion and management* **2008,** 49, (8), 2178-2199.
2. Buhre, B. J. P.; Elliott, L. K.; Sheng, C. D.; Gupta, R. P.; Wall, T. F., Oxy-fuel combustion technology for coal-fired power generation. *Progress in Energy and Combustion Science* **2005,** 31, (4), 283-307.
3. Singh, D.; Croiset, E.; Douglas, P. L.; Douglas, M. A., Techno-economic study of CO_2 capture from an existing coal-fired power plant: MEA scrubbing vs. O_2 /CO_2 recycle combustion. *Energy Conversion and Management* **2003,** 44, (19), 3073-3091.
4. Kwon, T.-W.; Kim, S. D.; Fung, D. P., Reaction kinetics of char—CO< sub> 2</sub> gasification. *Fuel* **1988,** 67, (4), 530-535.
5. Takarada, T.; Tamai, Y.; Tomita, A., Reactivities of 34 coals under steam gasification. *Fuel* **1985,** 64, (10), 1438-1442.
6. Chen, L.; Yong, S. Z.; Ghoniem, A. F., Oxy-fuel combustion of pulverized coal: Characterization, fundamentals, stabilization and CFD modeling. *Progress in Energy and Combustion Science* **2012,** 38, (2), 156-214.
7. Stanmore, B.; Visona, S., The Contribution to Char Burnout from Gasification by H< sub> 2</sub> O and CO< sub> 2</sub> During Pulverized-Coal Flame Combustion. *Combustion and flame* **1998,** 113, (1), 274-276.
8. Hecht, E. S.; Shaddix, C. R.; Geier, M.; Molina, A.; Haynes, B. S., Effect of CO2 and steam gasification reactions on the oxy-combustion of pulverized coal char. *Combustion and Flame* **2012,** 159, (11), 3437-3447.
9. Zhang, J.; Prationo, W.; Zhang, L.; Zhang, Z., Computational Fluid Dynamics Modeling on the Air-Firing and Oxy-fuel Combustion of Dried Victorian Brown Coal. *Energy & Fuels* **2013,** 27, (8), 4258-4269.
10. Prationo, W.; Zhang, J.; Cui, J.; Wang, Y.; Zhang, L., Influence of inherent moisture on the ignition and combustion of wet Victorian brown coal in air-firing and oxy-fuel modes: Part 1: The volatile ignition and flame propagation. *Fuel Processing Technology*.
11. Kim, D.; Choi, S.; Shaddix, C. R.; Geier, M., Effect of CO2 gasification reaction on char particle combustion in oxy-fuel conditions. *Fuel* **2014,** 120, (0), 130-140.
12. Ohtsuka, Y.; Tomita, A., Calcium catalysed steam gasification of Yallourn brown coal. *Fuel* **1986,** 65, (12), 1653-1657.
13. Ohtsuka, Y.; Tamai, Y.; Tomita, A., Iron-catalyzed gasification of brown coal at low temperatures. *Energy & Fuels* **1987,** 1, (1), 32-36.
14. Walker Jr, P. L.; Matsumoto, S.; Hanzawa, T.; Muira, T.; Ismail, I. M. K., Catalysis of gasification of coal-derived cokes and chars. *Fuel* **1983,** 62, (2), 140-149.
15. Kissinger, H. E., Reaction Kinetics in Differential Thermal Analysis. *Analytical Chemistry* **1957,** 29, (11), 1702-1706.
16. Zhang, L.; Huang, J.; Fang, Y.; Wang, Y., Gasification Reactivity and Kinetics of Typical Chinese Anthracite Chars with Steam and CO2. *Energy & Fuels* **2006,** 20, (3), 1201-1210.
17. Fermoso, J.; Arias, B.; Pevida, C.; Plaza, M. G.; Rubiera, F.; Pis, J. J., Kinetic models comparison for steam gasification of different nature fuel chars. *J Therm Anal Calorim* **2008,** 91, (3), 779-786.
18. Li, C.; Zhao, J.; Fang, Y.; Wang, Y., Effect of pressure on gasification reactivity of three Chinese coals with different ranks. *Front. Chem. Eng. China* **2010,** 4, (4), 385-393.
19. Smoot, L. D.; Pratt, D. T., *Pulverized-coal combustion and gasification: theory and applications for continuous flow processes*. Plenum Press: 1979.

20. Durie, R. A., *The Science of Victorian brown coal : structure, properties, and consequences for utilization*. Butterworth-Heinemann: Oxford, 1991; p xvi, 750 p.
21. Low, F.; De Girolamo, A.; Dai, B.-Q.; Zhang, L., Emission of Organically Bound Elements during the Pyrolysis and Char Oxidation of Lignites in Air and Oxyfuel Combustion Mode. *Energy & Fuels* **2014,** 28, (6), 4167-4176.
22. Tian, Z. F.; Witt, P. J.; Schwarz, M. P.; Yang, W., Numerical Modeling of Victorian Brown Coal Combustion in a Tangentially Fired Furnace. *Energy & Fuels* **2010,** 24, (9), 4971-4979.
23. Al-Abbas, A. H.; Naser, J.; Dodds, D., CFD modelling of air-fired and oxy-fuel combustion of lignite in a 100KW furnace. *Fuel* **2011,** 90, (5), 1778-1795.
24. Ma, L.; Gharebaghi, M.; Porter, R.; Pourkashanian, M.; Jones, J. M.; Williams, A., Modelling methods for co-fired pulverised fuel furnaces. *Fuel* **2009,** 88, (12), 2448-2454.
25. Yin, C., Refined Weighted Sum of Gray Gases Model for Air-Fuel Combustion and Its Impacts. *Energy & Fuels* **2013,** 27, (10), 6287-6294.
26. Yin, C.; Johansen, L. C. R.; Rosendahl, L. A.; Kær, S. K., New Weighted Sum of Gray Gases Model Applicable to Computational Fluid Dynamics (CFD) Modeling of Oxy−Fuel Combustion: Derivation, Validation, and Implementation. *Energy & Fuels* **2010,** 24, (12), 6275-6282.
27. Westbrook, C. K.; Dryer, F. L., Simplified Reaction Mechanisms for the Oxidation of Hydrocarbon Fuels in Flames. *Combustion Science and Technology* **1981,** 27, (1-2), 31-43.
28. Andersen, J.; Rasmussen, C. L.; Giselsson, T.; Glarborg, P., Global Combustion Mechanisms for Use in CFD Modeling under Oxy-Fuel Conditions. *Energy & Fuels* **2009,** 23, (3), 1379-1389.
29. Zhang, L.; Binner, E.; Qiao, Y.; Li, C.-Z., In situ diagnostics of Victorian brown coal combustion in O 2/N 2 and O 2/CO 2 mixtures in drop-tube furnace. *Fuel* **2010,** 89, (10), 2703-2712.
30. Li, C.-Z., Some recent advances in the understanding of the pyrolysis and gasification behaviour of Victorian brown coal. *Fuel* **2007,** 86, (12), 1664-1683.
31. C.L. Senior, T. P., Adel F. Sarofim, Joseph J. Helble, Formation of Ultra-Fine Particulate Matter from Pulverized Coal Combustion. In *American Chemical Society, Division of Fuel Chemistry*, 2000.
32. Krishnamoorthy, G.; Veranth, J. M., Computational modeling of CO/CO2 ratio inside single char particles during pulverized coal combustion. *Energy & fuels* **2003,** 17, (5), 1367-1371.

This page is intentionally left blank

Chapter 9 Conclusions and Recommendations for Future Work

This page is intentionally left blank

9.1 Conclusions and innovation of research

This thesis has for the first time presented a detailed study on the overall process of brown coal upgrading and utilisation with the PCI process. Through pyrolysis, a higher value char product was created that could meet the set requirements for a PCI fuel. This product could be used as substitute for PCI coal as a complete replacement or as a blend.

9.1.1 Investigation on the pyrolysis of a briquette and 1-D modelling

Firstly, it was of interest to explore the impact of pyrolysis conditions on the generation of char that has a large density and large size for long-distance transportation. Modifications were made to the pyrolysis condition such as temperature, duration, heating rate and the raw coal size and form (coal particles and pelletised coal). Efforts were made to clarify the optimum conditions and mechanisms for the pyrolysis of coal pellet, which is expected to enhance the strength and size of the char product. Heat transfer inside the coal pellet is the controlling factor for the release of volatiles under the fast heating rate. Regarding the release of volatiles, it follows a volumetric model limited by heat transfer. The pyrolysis process can be effectively modelled by the CPD model which adequately described the structural changes in the char and generation of char, tar and gas products. The structural changes were correlated with the radical changes in the char.

9.1.2 Sensitivity of the briquette char properties on the pyrolysis condition

A maximum pyrolysis temperature of 800 °C and a holding time of 20 min at 800 °C is vital for the pellet devolatilisation, generating a char that has an adequate heating value for use in the PCI process. Compared to coal particles, the char product from coal pellets has a higher density, which is more comparable to the bituminous coal. This implies a more dense energy storage in the pellet char and better compatibility in terms of blending and feeding to the furnace. Once the majority of volatile matter was eliminated from coal, there were minimal changes to the coal mass and proximate properties. However, it was seen through further analysis that true density continued to increase as the pyrolysis process progressed, and reactivity was lowered. The combustion performance analysis showed a positive performance of all chars generated from the pellet compared to PCI coal. It is important that oxidation reactivity is maintained to benefit both ignition time and 50% burnout time.

9.1.3 Combustibility of lignite char under simulated blast furnace conditions

The potential of using Yallourn brown coal char (collected from an industry-scale pyrolyser) as a PCI fuel was investigated. Combustion performance was tested in the DTF as well as through CFD modelling. A broad variation of properties with size was observed for Yallourn char. A general trend was confirmed for fixed carbon content to increase with particle size while volatile matter, moisture and ash all decreased with increasing char particle size. Irrespective of the pyrolysis condition, Yallourn char is superior over bituminous coal for being used as a top-grade PCI fuel, due to its higher calorific value, lower ash content, high ash melting temperatures, and abundance of iron in the ash. For the Yallourn char produced at a relatively short residence time, its volatile content of 5 – 17 *wt%* was sufficient for a rapid ignition at approximately 460 °C, which is comparable with the commercial PCI coal with a volatile content of 20 *wt%* and igniting at 451 °C. For a complete burnout, the Yallourn char tested can achieve this under rather mild conditions including larger particle sizes (up to 300 μ*m*), 1000 °C furnace temperatures and a stoichiometric O_2/C ratio, compared to the bituminous coal requiring a very fine size (e.g. <106 μ*m*), excessive oxygen and high temperature (e.g. >1200 °C) for a complete burnout.

9.1.4 Combustibility of lignite char blended with PCI coal under simulated blast furnace conditions

Although the Victorian brown coal showed reasonable performance under the simulated blast furnace conditions, the blending of either of the two brown coal char products with a fuel currently used in a commercial PCI process is a more realistic avenue for introduction of brown coal char to this field. Blending of the more volatile bituminous coal with low-volatile char was thus further conducted at four different ratios, 20 - 80% Yallourn char. A synergistic relationship was found for ignition of blends in both TGA and FFB experiments, with ignition points being lower than would be expected based on a weighted average of parent char ignition. The higher volatile PCI coal will assist in ignition of the low volatile char. Flame structure was found to be more stable for the PCI coal due to the heterogeneous ignition as a result of increased volatiles, however blending at 40% Yallourn char and below was found to produce a similar flame length and stability. According to the burnout rate observed by DTF experiments and CFD modelling, the later char oxidation rate was accelerated greatly for the PCI coal blended with the Yallourn char made under a shorter pyrolysis time, irrespective of its blending ratio. In contrast, the heat sink effect is more obvious for the less reactive Yallourn

char pyrolysed with a longer residence time, the increase on the blending ratio greatly decreased the overall burnout rate, especially at low furnace temperatures (800 and 900 °C) and a shorter residence time, such as 0.8 s.

9.1.5 Contribution of Char-CO2 and Char-steam gasification reactions for combustion of Victorian brown coal char

Lastly, the reactivity of Victorian brown coal char under environments with CO_2 and steam presence was studied. It was concluded that there exist relatively large impacts of this environment for low-rank coal relative to bituminous coal or a combustion model that neglects the CO_2 and steam gasification reactions of char. A lowered particle temperature compared to bituminous coal due to the endothermic nature of the gasification reactions. While these reactions lowered particle temperature and thus oxidation reaction rate, the added conversion through the gasification enhanced the overall carbon conversion rate. Increased production of the gasification reaction products, CO and H_2 will lead to a greater reducing environment on the particle surface. Such outcomes would also be beneficial in other applications such as PCI combustion which relies on conversion of carbon to gasification products to assist in the reduction of iron and to prevent blockages in pores caused by unburned particles.

9.2 Recommendations for future work

9.2.1 Further development of 1-D model

The 1-D model could effectively demonstrate the pyrolysis of a spherical particle or cylindrical briquette. However, in an industrial scale furnace, the packing of particles or briquettes is going to introduce three-dimensional effects to the process i.e. pellets or particles may be heated mainly from one side more than the other. It is not known how much heat a pellet in the centre of a fixed bed reactor will receive. Additionally, in a 1-D model, the gas phase reactions such as tar reforming cannot be resolved. This could potentially be achieved by converting the model to a 3-D CFD model. This would allow the model to be scaled up to larger dimensions.

9.2.2 Application of briquette derived char to larger scale PCI tests

Although, lab scale tests showed promising results for the brown coal char and its blends, it needs to be demonstrated that the combustion performance will be as expected in a PCI rig. This could include monitoring of flame structure and burnout.

9.2.3 Costs analysis of char upgrading process

The scope of this study included the upgrading of raw brown coal to the higher value char product and the evaluation of this char product. The hypothesis was that an upgraded char product could replace the more expensive currently used PCI coal in the blast furnace. However, it remains to be adequately proven that the brown coal can be upgraded with a cost not exceeding the current cost of PCI coal. This could be achieved through an economic analysis of the process including capital investment and operational costs using Aspen Plus software.

This page is intentionally left blank

Appendix A – Supplementary data for Chapter 6

This page is intentionally left blank

Table S1 Mineral concentrations in Yallourn char and PCI coal before and after washing

	YC-1		YC-2		PCI coal	
Major species (%)	Before washing	After washing	Before washing	After washing	Before washing	After washing
MgO	2.35	1.60	2.26	0.45	0.20	0.01
Al2O3	0.11	0.07	0.10	0.09	2.25	1.77
SiO2	0.26	0.20	0.28	0.27	3.09	2.51
Fe2O3	3.54	1.64	2.15	0.50	0.82	0.46
Others	2.50	1.80	2.88	1.63	2.79	1.66
Total inorganics (%)	8.76	5.31	7.68	2.94	9.15	6.42

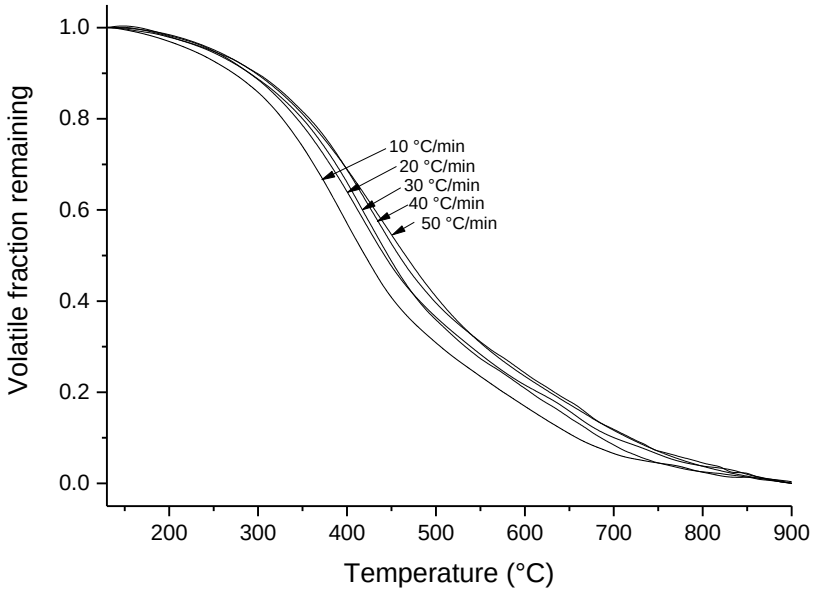

Figure S1 Volatile mass loss curves for Yallourn coal under argon in TGA

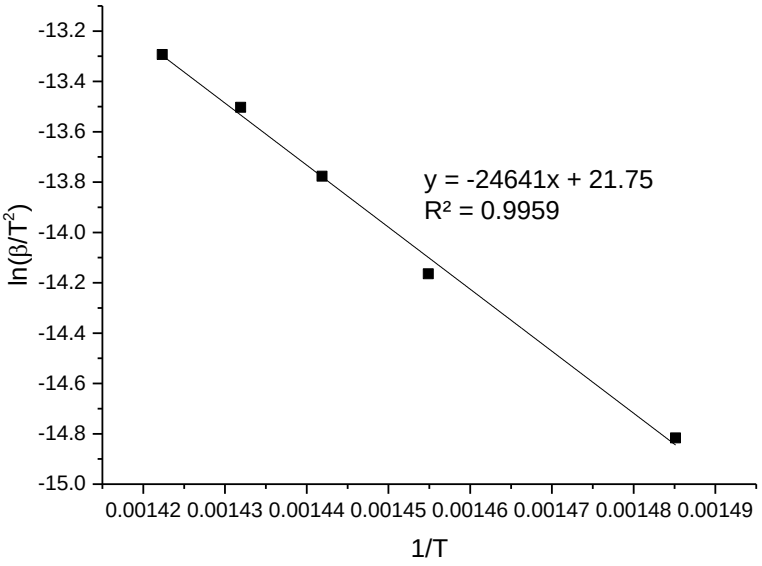

Figure S2 Kissinger plot for determination of pre-exponential constant and activation energy of first-order volatile release

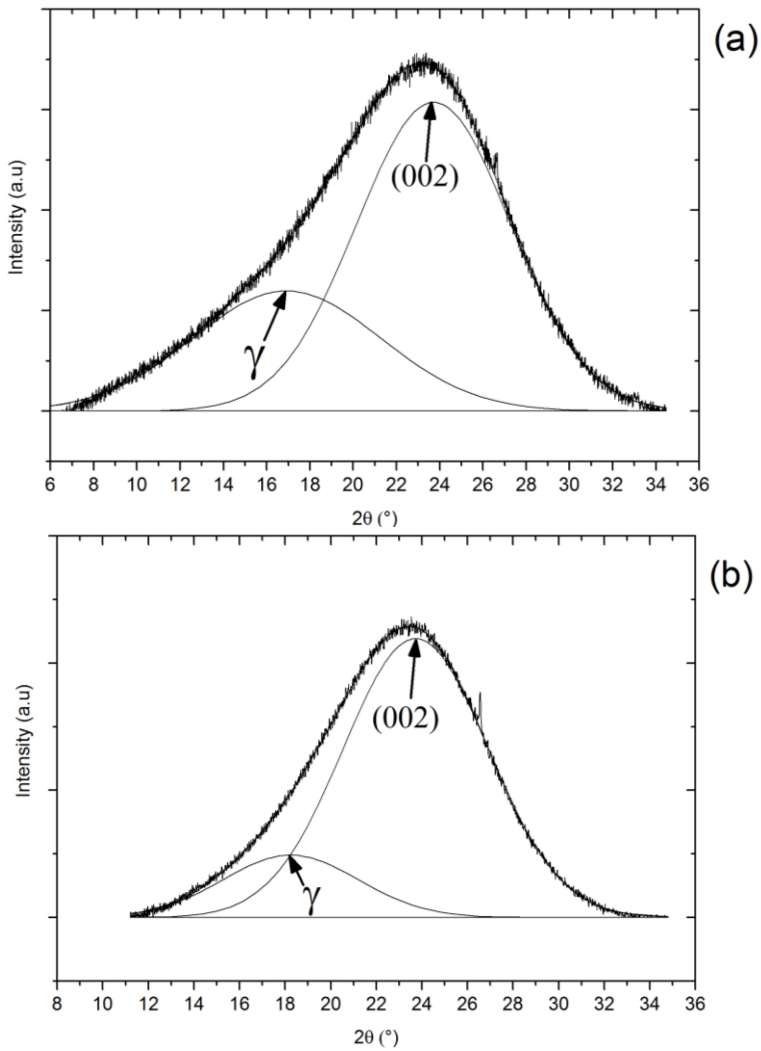

Figure S3 Fitting of γ and (002) peaks in order to find the degree of aromaticity for (a) YC-1 and (b) YC-2 char

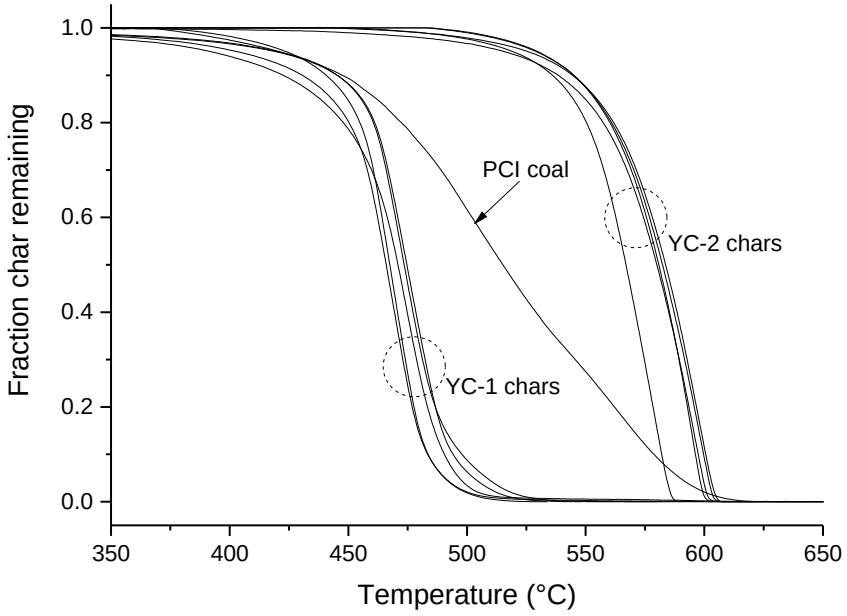

Figure S4 Mass loss curves under an air atmosphere for Yallourn char and PCI coal in TGA

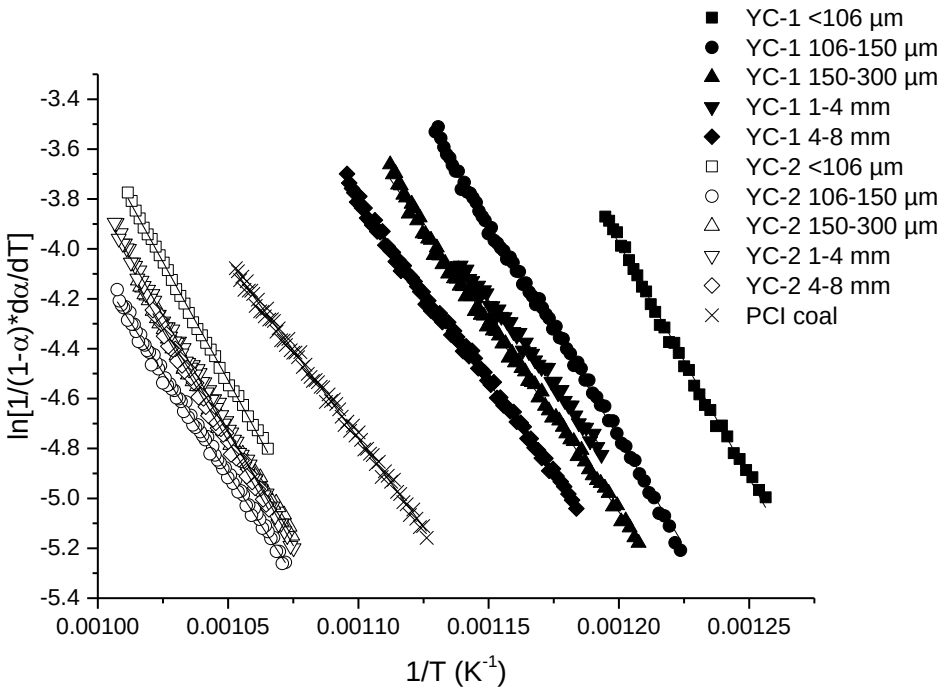

Figure S5 Calculation of kinetic parameters using the direct Arrhenius model

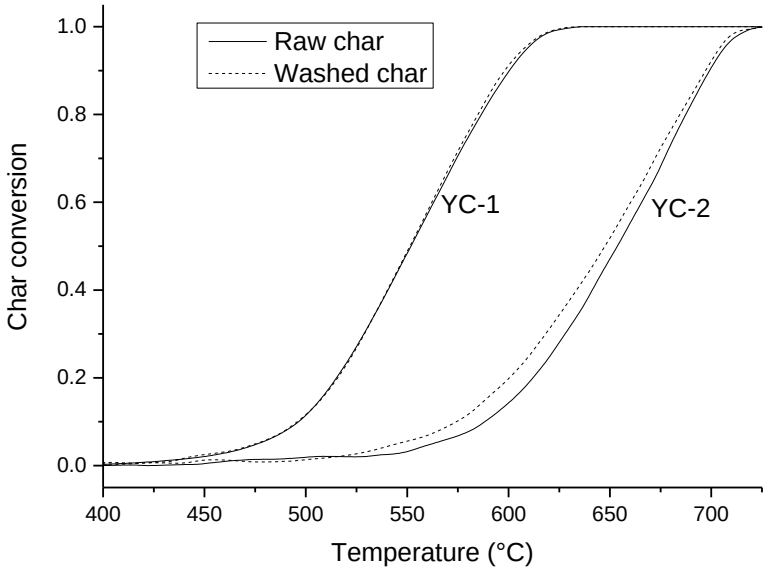

Figure S6 Char conversion for unwashed and washed Yallourn char in air using TGA at 50 °C/min

This page is intentionally left blank

Appendix B – Chapter 6 in publication form

This page is intentionally left blank

Fuel Processing Technology 156 (2017) 113–123

Contents lists available at ScienceDirect

Fuel Processing Technology

journal homepage: www.elsevier.com/locate/fuproc

Research article

Ignitability and combustibility of Yallourn pyrolysis char under simulated blast furnace conditions

Anthony De Girolamo [a], Natalia Kelly Lameu [a], Lian Zhang [a,*], Yoshihiko Ninomiya [b]

[a] Monash University, Wellington Road, Clayton, Victoria 3800, Australia
[b] Department of Applied Chemistry, Chubu University, 1200 Matsumoto-Cho, Kasugai, Aichi 487-8501, Japan

ARTICLE INFO

Article history:
Received 28 June 2016
Received in revised form 23 October 2016
Accepted 26 October 2016
Available online 5 November 2016

Keywords:
Blast furnace
Pulverized coal injection (PCI)
Yallourn char
Combustibility

ABSTRACT

In this paper we have examined the potential of Yallourn brown coal char (collected from an industry-scale pyrolyser) to be used as a pulverized coal injection (PCI) fuel, its size-dependent properties, ignitability and combustibility under the simulated conditions of the blowpipe-tuyere section in a blast furnace. The combustion of individual sizes for Yallourn char was tested in a lab-scale drop-tube furnace (DTF) using pre-heated hot gas with a temperature up to 1000 °C, and a particle residence time as short as 0.6 s. Computational fluid dynamics (CFD) modelling was further conducted to optimize the char combustion conditions via sensitivity analysis. Irrespective of the pyrolysis condition, Yallourn char is superior over bituminous coal for being used as a top grade PCI fuel, due to its higher calorific value (7500–8110 kcal/kg), lower ash content (<10 wt%), high ash melting temperatures (> 1550 °C), and abundance of iron (> 40 wt% in ash). The performance of Yallourn char is also superior over bituminous coal under the simulated blast furnace conditions, for a rapid ignition and burnout even for a coarse char size of 300 μm under the stoichiometric O_2/C molar ratio and using low blast temperatures of 800–1000 °C. All these are beneficial for reducing the energy consumption related to particle pulverization and the amount of oxygen for the combustion. With regard to the Yallourn char ignition and combustion in the hot gas, a minimum 6 wt% volatile content is essential for a stable and rapid ignition of the volatiles at a gas temperature of 1000 °C or below, since homogeneous ignition is predominant at low temperatures. However, once the blast temperature rises to 1200 °C, the dependence on volatile content turns insignificant due to the dominance of the heterogeneous ignition, high C-O_2 reactivity for the solid char, as well as the minimized pore diffusion control due to the large porosity (52.0–63.1%) of the Yallourn char tested here.

1. Introduction

With the depletion of the reserves for coking coal in the world, the demand for the use of PCI coal at a high coke replacement ratio is increasing stably in the international steelmaking industry [1]. PCI technology involves directly injecting coal into the blast furnace, increasing productivity, and replacing a part of coke that is used for the process of making iron [2]. The PCI coal has strict requirements in terms of ash composition and amount, volatile content, moisture content and grindability.

Volatiles present in a PCI coal have a double-edged role in blast furnace performance [3]. The injected coal has to devolatilize and combust at the correct location and time, for operational safety and optimal performance. Due to the very short residence times of coal particles in the raceway (15–20 ms), controlling combustion and ignition is critical to avoid incomplete burnout and excess unburnt char formation. While higher volatile content is correlated with higher char reactivity and hastened ignition [4], excessive amounts of volatiles may cause unstable combustion in the blowpipe and the degradation of coke [5]. Additionally, volatile content is inversely correlated with the calorific value of a coal. A low-volatile coal with a high calorific value will be able to replace a greater portion of the coke leading to additional cost savings with low volatile coals.

Reactivity of the PCI coal is another important factor in blast furnace performance [6]. In general, as PCI injection rate increases, unburnt char can increase the amount of fine coke particles in the raceway region, which in turn exerts detrimental effects on gas flow and permeability of the coke. However, a generalized conclusion regarding the impact of char reactivity on the performance of blast furnace has yet to be achieved. Phillip suggests that char reactivity may not be a significant factor in the raceway [7]. At the high temperatures in the raceway of up to 1500 °C, the char oxidation will be mainly diffusion controlled, and hence, its rate will be fast enough that any oxygen present at the particle surface will be consumed quickly [8]. On the other hand, Lu proposes that intrinsic char reactivity is a significant factor in burnout due to the highly turbulent regions in the flame and small particle sizes used in PCI combustion [9]. In addition to the char - O_2 reaction, the

* Corresponding author.
E-mail address: lian.zhang@monash.edu (L. Zhang).

http://dx.doi.org/10.1016/j.fuproc.2016.10.028
0378-3820/

char - CO_2 gasification will occur beyond the raceway and this is likely to be intrinsically controlled due to the slower rate of reaction and lower temperatures in the furnace stack.

Low-rank brown coal has large reserves in both Australia and China, and also other parts of the world. However, due to its large moisture content, low-rank coal has been mainly used as the feedstock to supply local power plants which generally have a very low efficiency and a high carbon emission rate compared to black coal [10]. Little of low-rank coal is being used as a value-added product in the market for non-power applications including blast furnace use. Upon beneficiation such as mild pyrolysis, the low-rank coal is expected to be upgraded to a char with a higher calorific value that can be used in a variety of advanced applications including power generation, combustion in blast furnace, precursors for activated carbon, and reductants for the production of precious metals in the metallurgical industry. To date, the application of low-rank brown coal char as a PCI fuel for a blast furnace has yet to be tested. Instead, the use of woody charcoal as a PCI substitute fuel for CO_2 emission reduction has been examined [11]. Compared to woody charcoal, the low-rank coal char possesses distinct properties including different ash content and composition, as well as a different carbonaceous structure and reactivity.

This paper follows on from previous work on coal-char blends [12], and aims to validate the viability and benefit of fully replacing the commercial bituminous coal by brown coal char as the single PCI fuel in a blast furnace, rather than through blending them together. In particular, considering that volatile matter is one of the most critical factors for a single PCI fuel [3–5], the primary goal of this paper is to clarify the minimum volatile content in a lignite char that can ignite stably and rapidly while reaching its maximum possible calorific value (thus energy density). Such a goal is also significant for tailoring the parent coal pyrolysis conditions since the char is a prepared material, as well as establishing the bond between pyrolysis and the end-use of the pyrolysed char. To date, most of the studies on char properties and reactivity have failed to specify the end-use of the char, thereby providing little advice to both PCI application in the blast furnace, and to the optimisation of pyrolysis conditions to meet the needs required by the PCI application. Additional efforts were further made to reveal the maximum possible size for the lignite char that can burn efficiently, so as to reduce the energy consumption required for its milling prior to being injected into the blast furnace.

To achieve the afore-mentioned research objectives, two Yallourn char samples collected from a pilot-scale shaft furnace with a capacity of 200 kg/h have been characterized and tested in this study. Their size-dependent properties and intrinsic reactivity were firstly examined. Secondly, an experimental study of char particle ignition and burnout was conducted in a lab-scale thermogravimetric–differential thermal analyser (TG-DTA) and drop tube furnace (DTF) as a function of O_2/C molar ratio, furnace temperature and char size. The DTF used is unique, possessing the capability to provide a hot blast gas up to 1000 °C to mimic the industrial blast furnace. Finally, computational fluid dynamics (CFD) modelling was performed to interpret the DTF results and further explore the optimum properties for lignite char in terms of ignition and burnout under the simulated blast furnace conditions. The parent raw coal is sourced from the Latrobe Valley, Australia. As a reference, a bituminous coal currently used commercially as a PCI coal was analysed and compared.

2. Material and methods

2.1. Properties of Yallourn char products

Coal for the production of char is sourced from Yallourn in Victoria, Australia. Yallourn lignite has a very high moisture content (65.2% ar) but is low in ash (2.61% db) [13]. Two char samples were generated by pyrolysis of raw wet Yallourn lignite in a pilot-scale shaft furnace with a capacity of 200 kg/h at approximately 800 °C. These will be referred to as Yallourn char 1 (YC-1) and Yallourn char 2 (YC-2) and their approximate residence times are 5 and 10 h, respectively. A longer residence time is expected to generate a low-volatile char that thus has a higher energy density. Other products recovered from the pyrolysis included water, gas and coal tar.

Char particles were size segregated prior to analysis. The char produced ranged in diameter from less than 100 μm to over 8 mm. Interestingly, the sizes less than 1 mm in diameter are mostly present as powdery, darkish particles that are analogous to high-rank black coal, as evident in Fig. 1 which shows the size-dependent surface morphologies of YC-1. Instead, the chunk sizes larger than 1 mm are more like woody charcoal. This is because the woody fibres are abundant in the original lignite. Clearly, the lignite char studied here is intriguing, as its maceral composition is a combination of both black coal and woody biomass. Such a sample has yet to be probed.

To determine the crystal structure of char samples, X-ray diffraction (XRD) analysis was conducted in a Rigaku MiniFlex600 instrument. The char samples were demineralized with 1 M HCl washing for 3 h followed by rinsing with deionised water until the leachate turned neutral prior to the XRD analysis. A scanning speed of 0.1°/min was selected with a step size of 0.01° for a 2-theta angle from 10° to 70°. The maximum capable power of 600 W was used for the XRD characterisation. The samples were ground under the argon protection prior to the analysis.

2.2. Ignition temperature, volatile release and char-O_2 reactivity measurement in TG-DTA

Char ignition temperature was measured in TG-DTA (Shimadzu DTG-60H) and was defined as the temperature at the intersection of the tangent of the char mass at the initial point (horizontal line) and the tangent of the char mass curve at the peak of the DTA curve when the sample is heated at a rate of 10 °C/min. Samples were ground to a size of <106 μm to minimise the diffusion.

Intrinsic char-O_2 reactivity kinetic parameters were calculated using the direct Arrhenius plot method which is based on Eq. (1).

$$\ln\left[\frac{1}{(1-\alpha)}\cdot\frac{d\alpha}{dT}\right] = \ln\left(\frac{A}{\beta}\right) - \frac{Ea}{R}\cdot\frac{1}{T} \quad (1)$$

where β is the heating rate and α is the conversion. By plotting $\ln\left[\frac{1}{(1-\alpha)}\right.$

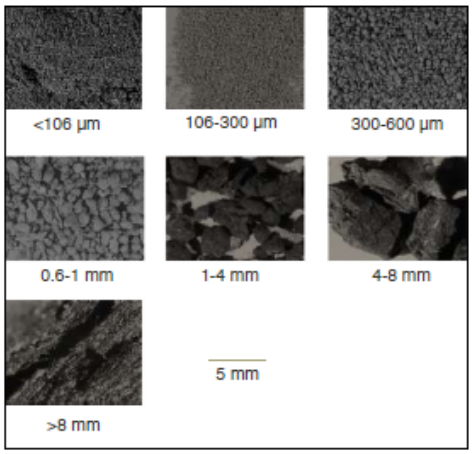

Fig. 1. Surface morphology of differently sized lignite char YC-1, observed by optical microscopy. Scale is relevant to all micrographs.

$\frac{dx}{dt}$ against $\frac{1}{T}$, the pre-exponential constant A, and activation energy E_a can be calculated. The heating rate was fixed at 50 °C/min and the air flow rate was fixed at 100 mL/min to ensure that the sample will always be supplied with 20.94% O_2. First-order devolatilization kinetics were measured in the same TGA instrument using the non-isothermal Kissinger method [14]. Argon was used at 100 mL/min and heating rates ranged from 10 to 50 °C/min in increments of 10 °C.

2.3. DTF experimental setup

A 2-m DTF was employed to combust the coal and char sample and a gas analyser recorded the combustion gases exiting the furnace. A schematic of this DTF can be found in previous work [15]. In brief, the sample enters the DTF with a cold primary gas of 1 L/min, while a secondary gas of 9 L/min is preheated through the annulus between the reactor and the furnace, mixing with the coal or char at the injection point. Such a unique pre-heating system for the gas can resemble the blast furnace condition where the hot air is normally heated to ~1000 °C. This is different from the previous study on the test of PCI coal in a lab-scale DTF without extensive preheating of the secondary gas [16]. A water cooled injector was used to inject the sample at a further distance in the reactor so that the particle residence time was approximately 1.4 s.

The coal feeding rate was set to approximately 1 g/min. The combustion test was conducted at three furnace temperatures, 800 °C, 900 °C and 1000 °C, and four O_2/C molar ratios ranging from 0.7 to 1.4. For the char and commercial PCI coal, three original sizes of < 106 μm, 106–150 μm and 150–300 μm were tested to evaluate the size-dependence of their combustibility. In addition, the char sizes larger than 1 mm were ground to < 106 μm and further tested. The experimental conditions are summarized in Table 1.

Coal/char burnout was measured by examining the mass balance of combustible matter before and after each test. The unburnt residue from each run was fully collected via a flask and thimble filter installed at the bottom of the DTF reactor. The ash percentage in the residue, A_r was measured by the TGA instrument by burning it in air upon heat-up to 800 °C at a heating rate of 10 °C/min. By employing the original mass (M_o, dried) of the injectant, its ash content ($A_{original}$, wt% on dried basis) and the mass of the residue (M_r), one can calculate the burnout (B) using Eq. (2) below:

$$B = \left(1 - \frac{M_r\,(100 - A_r)}{M_o\,(100 - A_o)}\right) \times 100 \tag{2}$$

This method is expected superior over the traditional ash-tracer method in which the conservation of ash mass is assumed during the combustion process. The low-rank coal and its derivatives including char give a non-negligible ash loss upon the combustion [15].

Table 1
DTF experimental conditions tested.

Sample	Size	Temperature °C	O_2/C ratio
YC-1	<106 μm 106–150 μm 150–300 μm	800, 900, 1000	0.7–1.4
	1–4 mm ground to <106 μm	1000	0.7
	4–8 mm ground to <106 μm	1000	0.7
YC-2	<106 μm 106–150 μm 150–300 μm	800, 900, 1000	0.7
	1–4 mm ground to <106 μm	1000	0.7–1.4
	4–8 mm ground to <106 μm	1000	0.7
Commercial PCI coal	<106 μm 106–150 μm 150–300 μm	800, 900, 1000	0.7–1.4

2.4. CFD modelling methodology

A three-dimensional CFD model of the DTF was established to interpolate and extrapolate the DTF results so as to gain a better understanding of the burnout profile of different fuels. Although the DTF experiments shown are able to show the discrepancy of the burnout between different fuels, an accurate estimation of the influence of a single parameter is difficult. This is due to the limitation of the feeding system that rarely allows for an identical feeding rate for different samples with different density and different O_2/C molar ratios. Such a problem was solved easily by CFD modelling once it is fully validated. For the modelling in this study, the furnace wall temperature was varied from 800 to 1200 °C, as this is closest to the temperature of the hot air stream that the particles are injected inside the blowpipe-tuyere section in a blast furnace [6]; the O_2/C molar ratios was set identical with that which has been tested in the DTF, and all the different sizes of char and PCI coal were tested to conduct a sensitivity analysis of the char burnout as a function of particle size and operating conditions.

The mesh and model for the DTF was taken from a previous study of brown coal combustion in the same rig, which has been fully validated [17]. The mesh is made up of 231,000 cells and encompasses all of the drop tube furnace features, including the primary and secondary gas inlets, secondary gas preheating zone, the water-cooled injector, and mixing of gases and char at the injector tip. This mesh was validated in a grid independence test as well as with measurements of particle temperature in the previous study. The models used in the simulation are summarized as follows: Turbulence: k-ε model is used which has shown sufficient accuracy in modelling combusting flows [18]; Radiation – the discrete ordinates (DO) method was chosen due to suitability for all optical thicknesses and level of accuracy [19]; Radiation absorption: the weighted-sum-of-grey-gases model (WSGGM) which is commonly used for coal CFD simulations as it is efficient and shows a good agreement with experimental observations [20]; Particle reactions – Multiple surface reaction model; and Gas phase reactions – Westbrook & Dryer mechanism [21].

Particle surface reaction kinetics, as well as devolatilisation rates were taken from the TGA experiments described earlier and diffusion rate constants were found in literature [22]. The mass loss and Kissinger plot can be found in Supporting information (SI), Figs. S1 and S2, respectively. The devolatilisation rate of Yallourn char samples was assumed to be similar to that of raw Yallourn coal. First-order rate kinetic parameters A and E_a were determined to be $6.88 \times 10^{13}\ s^{-1}$ and 205 kJ/mol, respectively using the previously described Kissinger method. While the pyrolysis reaction proceeds relatively fast compared to the char conversion reactions, the high activation energy here is indicative of the high temperature dependence of the volatile release. For PCI coal the Arrhenius equation constants were taken from the work of Badzioch and Hawksley ($A = 4.92 \times 10^5\ s^{-1}$, $E_a = 74$ kJ/mol) [23].

3. Results and discussion

3.1. Char property analysis

The proximate property analysis was conducted on each size group and a trend was found linking a decrease in size with a decrease in fixed carbon and an increase in moisture, ash and volatile matter shown in Fig. 2. This variance in properties was much greater for YC-1 than YC-2 that was produced at a longer residence time. The trend of this variation initially appears counterintuitive, i.e. smaller particles would be expected to lose a greater amount of volatiles due to the lesser heat and mass transfer resistance. Instead, the result here may suggest a secondary condensation of both volatiles and even the ash-forming elements once they were evaporated from their local positions in the coal matrix. For both char samples, the size bin < 106 μm showed an ash content above the standard for a Grade 1 PCI fuel (<10% ash) [24]. However, all the other sizes have an ash content that is much lower. The lengthier

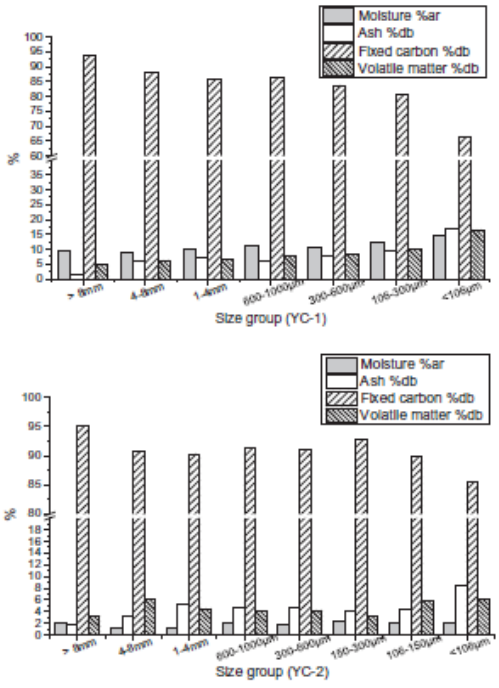

Fig. 2. Proximate analysis of size segregated YC-1 (top) and YC-2 (bottom).

pyrolysis time to produce YC-2, compared to YC-1 increased the percentage of fixed carbon in the sample while decreasing volatile matter and moisture. Apart from the continued release out of coal matrix, the volatile residues may also be partially solidified upon a variety of secondary reactions such as formation of soot and coke, and also interaction with the char matrix [13]. The true and apparent densities of two char samples were also measured (Table 2). For comparison, a commercial PCI bituminous coal was also tested, which is composed of 20.3 wt% volatile matter, 8.7 wt% ash, 1.9 wt% moisture and 70.6 wt% fixed carbon on a dry basis. As can be seen, the longer pyrolysis duration of YC-2 resulted in a larger porosity, a lower apparent density and a larger true density than its counterpart char sample YC-1. Its true density is almost as high as a pure graphite crystal (2260 kg/m^3) [25], which is another sign of the strong secondary reactions which can increase the carbon aromaticity [26], or coke/soot formation from the primary volatile release. However, the low apparent density for the two char samples implies probable changes on the aerodynamics of char particles in both the mill and the blowpipe when they are used as a substitute for bituminous coal. Finally, the calorific value (i.e. energy content) of the three fuels is noteworthy. As evident in Table 2, YC-2 has the largest energy content, followed by PCI coal and YC-1 in a descending sequence. This is because YC-2 has the least volatile and ash content, as an expense of increasing the particle residence time in the pyrolyser.

Table 2
True density, apparent density, calculated porosity, calorific value and surface area of PCI coal, YC-1 and YC-2.

	PCI coal (<106 μm)	YC-1 (1–4 mm)	YC-2 (1–4 mm)
True density (kg/m^3)	1441	1863[a]	2204[a]
Apparent density (kg/m^3)	1264	894.3[a]	813.1[a]
Bulk density (kg/m^3)	644.2	510.7[a]	417.8[a]
Porosity, [–]	12.3%	52.0%	63.1%
Calorific value (kcal/kg)	7801	7517	8114
BET surface are (m^2/g)	Not measured	334	56.7

[a] The size of <106 μm for each char sample has also been analysed, showing little difference with the size of 1–4 mm.

XRD was also used to examine the differences in carbon structure for the 1–4 mm size fractions of both YC-1 and YC-2 char as well as PCI coal (Fig. 3). The concentrations of individual ash-forming elements in the entire sample, as measured by XRF, can be found in Table S1 in SI. The demineralised YC-2 char exhibits a sharper (002) graphite peak, at ~24° and a sharper (100) graphite peak at ~43° indicating a greater degree of ordered carbon structures. The (002) peak which is associated with aromatic side chains is also expected to be influenced by the overlapping γ peak which is associated with aliphatic side chains [27]. PCI coal also shows a very sharp peak in this region which is expected, since aromaticity increases with coal rank [28]. Increased carbon aromaticity is linked with increased carbon ordering and true density and will negatively influence the reaction rate [26]. It is possible to split the first peak into symmetrical (002) and γ peaks, and subsequently integrate to calculate the degree of aromaticity, f_a with Eq. (3).

$$f_a = \frac{A_{(002)}}{A_{(002)} + A_\gamma} * 100\% \quad (3)$$

where A_{002} is the area under the (002) and A_γ is the area under the γ peak.

The resultant peak-fitting curves used in the calculation of the area can be found in Supporting information Fig. S3. For both char samples, two symmetrical peaks were able to match the original peak with an adjusted R^2 value above 0.998. The aromaticity of YC-1 and YC-2 chars were determined to be 67.8% and 82.8% respectively, further proving that the char aromaticity is increased in the case of YC-2 char.

Table 3 further summarizes the ash compositions (in its most stable oxide form) for the different sizes of YC-1 sample and ash fusion temperature. The most abundant element is Fe, followed by Mg and Ca, whereas the contents of alkali metals (Na and K) are extremely low. This is different from woody charcoal which is rich in alkali metals [11]. Due to the abundance of Fe and Mg, the ash melting temperature is also higher than 1550 °C. All these properties are superior over the bituminous coal with the abundance of silicon, aluminium, calcium, iron and even sodium in the ash. Due to the co-existence of these five elements, some of the bituminous coal ashes have a larger tendency to melt and cause fouling in the burner vicinity. Such problems would be

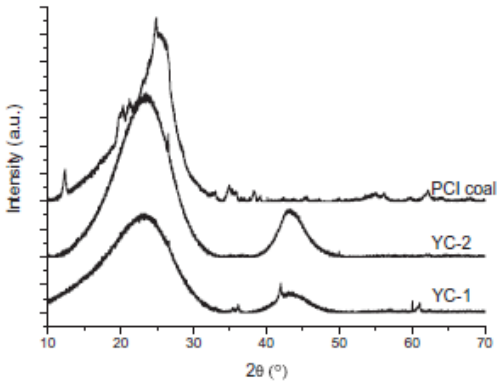

Fig. 3. XRD spectra for de-ashed YC-1 and YC-2 char samples as well as PCI coal.

Table 3
Size-dependent ash compositions of YC-1 sample and ash fusion temperatures.

	Char size, μm							
Element	>8000	4000–8000	1000–4000	600–1000	300–600	106–300	<106	PCI coal
SiO_2	2.9	2.1	2.9	3.4	2.6	3	3	42.5
Al_2O_3	0.8	1.7	1.4	1.4	1.3	1.4	1.3	27.6
Fe_2O_3	20.1	34.7	34.9	36	39	41	48.4	6.0
MgO	28.3	27.6	26.5	26.9	27.6	28.4	28.4	0.02
CaO	23.2	15.7	17.2	16.5	14.6	13.7	11.4	13.1
SO_3	22.2	16.5	15	14	13.6	11.5	6.7	6.6
K_2O	0.3	0.2	0.2	0.2	0.2	0.2	0.3	0.5
Na_2O	2.2	1.5	1.9	1.6	1.1	0.8	0.5	3.7

Ash fusion temperature, °C

	Reducing atmosphere	Oxidizing atmosphere
Deformation temperature	>1550	>1550
Hemispherical temperature	>1550	>1550
Spherical temperature	>1550	>1550
Flow temperature	>1550	>1550

obviously avoided in the case that the Yallourn char was used as the PCI fuel.

3.2. Reactivity and ignition in TGA

The results in Fig. 4 indicate that the ignition point of YC-1 is close to that of the PCI coal, although the volatile contents of YC-1 are less than that of its counterpart. YC-2 has an ignition point approximately 100 °C above that of YC-1. This should be attributed to a high volatile content for YC-1 char (as evident in Fig. 2) as well as an increased surface area of YC-1 char as evident in Table 2. Increasing particle size shows a marginal increase in the ignition temperature, further supporting the dominance of heterogeneous ignition mechanism for the Yallourn char.

Fig. 5 was plotted to compare the intrinsic char-O_2 reactivity of different samples. These reaction rates were plotted based on the kinetic parameters found by analysing the char mass loss curves (Fig. S4) using the previously described direct Arrhenius plot method (Fig. S5). The results show significantly higher reactivity for YC-1 samples, irrespective of its size. PCI coal showed lower reactivity than YC-1 char, while YC-2 char generally had the lowest reactivity below 800 °C. Above 800 °C, YC-2 shows a similar reactivity to PCI coal. This is expected, due to the increased pyrolysis time of YC-2, resulting in a lower surface area, higher true density (Table 2) and more ordered carbon structure (Fig. 3). The partially demineralised char samples were also analysed for their char-O_2 reactivity to discover whether the higher reactivity of YC-1 is partially attributed to its abundant ash-forming elements. As demonstrated in Fig. S6 in the SI, the results from the demineralised char samples were almost identical to the respective unwashed char, proving that differences in char-O_2 reactivity are purely due to the carbon structure.

In terms of particle size group, Fig. 5 also suggests that the smaller sizes showed increased reactivity, due to the larger specific surface area and the minimal/negligible diffusion control. Ground chars showed a comparable reactivity to that of samples of a similar size that were not ground. Clearly, the broad variation of the reactivity of char as a function of size should pose an effect on its combustibility. This will be examined by sensitivity analysis via CFD modelling later.

3.3. Ignition and burnout in DTF experiments

A CCD camera was used to capture the YC-1 particles ignition sequence after it was injected into the hot blast in the DTF at 1000 °C and an O_2/C ratio of 1.2, as shown in Fig. 6. Upon an exposure time of 0.25 s, the char particles sparkled individually, forming a long trajectory in the field of view (FOV) of the camera. Such an ignition should be mainly assigned to heterogeneous ignition of char surface, since the volatiles in this char are very lean. Otherwise, a large fireball formed upon the homogeneous firing of volatiles should be observed, as has been confirmed for raw brown coal combustion [29]. The char combustion was continued stably, radiating strong heat in the FOV of the camera in 0.5 s. In addition, it is noteworthy that, the heterogeneous sparkling of char particles observed here, due to the shortage of volatiles, is

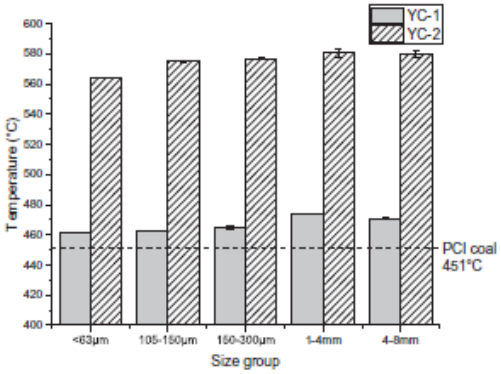

Fig. 4. Ignition temperatures for lignite char samples and PCI coal.

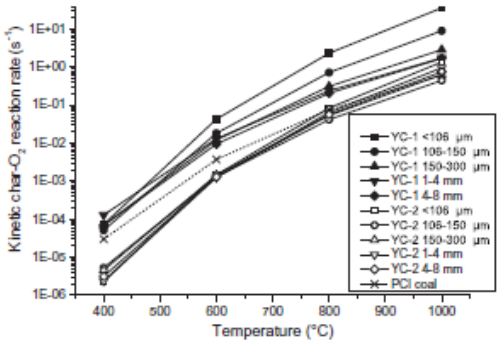

Fig. 5. Intrinsic char-O_2 reactivity of lignite char samples and PCI coal.

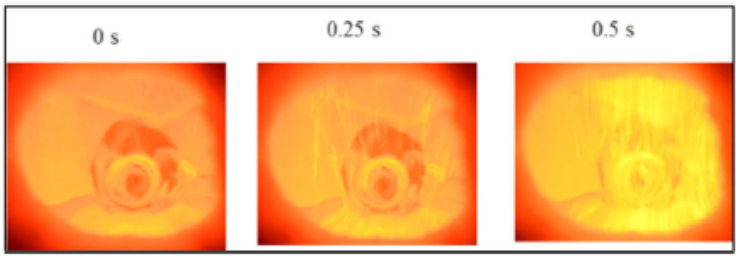

Fig. 6. Char ignition sequence of YC-1 < 106 μm at O_2/C = 1.2 and 1000 °C.

beneficial in providing a low pressure drop and hence a stable operation of the tuyere of the blast furnace [30].

The effects of char particle size and O_2/C molar ratio were tested for the burnout of YC-1 at three temperatures. Fig. 7(a) for YC-1 char shows that, irrespective of O_2/C ratio and reaction temperature, the particle size range of 106–150 μm only showed slightly decreased burnout compared to the smallest size < 106 μm for the same char, while the large size 150–300 μm show a much decreased burnout particularly at 800 °C and 900 °C. Such a decrease should be attributed to two reasons, one is the enlarged resistance against the internal diffusion of oxygen within char particle, and another one should be the decreased volatile matter content upon the increase of char particle size, as evident in Fig. 2. However, discrepancy between the three char sizes was narrowed considerably by increasing both the O_2/C molar ratio and furnace temperature. An increase in the O_2/C molar ratio is beneficial in reducing the resistance against the external diffusion of oxygen for larger particle sizes. The similar observation was confirmed for YC-2 with a much lower volatile content in panel b.

Fig. 8 further compares the burnout rate as a function of O_2/C molar ratio between two brown coal chars and the bituminous coal reference at 1000 °C, which is much closer to the temperature profile in the blowpipe in a real blast furnace. Note that, all the three samples are smaller than 106 μm in size. As can be seen, the commercial bituminous coal requires a minimum O_2/C molar ratio of 1.2 to reach its maximum possible burnout at 92.5 wt%. However, under such an excess O_2 condition, YC-1 sample reached a complete burnout, whereas YC-2 achieved around 95 wt% burnout, which is still higher than that of the commercial PCI coal. Apart from the high reactivity, the large porosity of Yallourn char is also another important variable affecting the necessary amount of oxygen for combustion. Compared to Yallourn char having a porosity of 52–63.1%, the bituminous coal tested here has a much smaller porosity of 12.3% which thus poses a larger resistance against the internal diffusion, in particular in the later stage of coal combustion where the oxygen in bulk gas is insufficient and its diffusion is thus critical.

Fig. 9 further substantiates the high burnout of Yallourn char and its distinct combustion mechanism at a fixed O_2/C molar ratio of 0.8–0.9 that is close to the stoichiometric ratio for the combustion. For the YC-1 char sample, increasing its particle size resulted in a decrease on the carbon burnout, substantiating the above hypothesis that the external diffusion of oxygen is the control step for the three blast temperatures tested here. Even so, the burnout for YC-1 is still very high, reaching a value of approximately 70 wt%-*daf* for its largest size that is close to the results for bituminous coal achieved at 1000 °C. With regard to the commercial bituminous coal, it is obvious that the external oxygen diffusion is insignificant at these three blast temperatures, as reflected by a rather comparable burnout between the three coal sizes at each temperature. To reiterate, the slow reaction rate and internal diffusion due to the small porosity are more important for bituminous coal combustion.

Finally, the burnout of brown coal char as a function of volatile matter was established in Fig. 10 at a fixed O_2/C molar ratio of 0.8–0.9 and 1000 °C. This is to assess the dependence of such a low-volatile char combustion on its volatile matter content, as well as to determine the minimum volatile content in the char to ensure a complete burnout. For the PCI coal application in the blast furnace, the volatile content is deemed as the most influential criteria for the coal selection [16]. Interestingly, a single linear trend line was not observed. Instead, the two char samples show rather different trend lines with different slopes. The YC-1 char has a smaller slope which is estimated to be around 0.68 for a volatile content down to 6 wt%. Such a slope was also much smaller than that has been established for commercial PCI coals in the literature [16]. However, for the YC-2 char produced with less volatiles under harsh conditions, a much steeper slope was found for its volatiles ranging from ~3 wt% to 6 wt%. By combining the trend lines for the two chars, it is obvious that ~6 wt% is the minimum volatile content requested for the prepared brown coal char, otherwise its burnout at 1000 °C and below would drop dramatically to a level that is even lower than the commercial PCI coal. Compared to the natural bituminous coal, the char tested here is a prepared material, and thus, change on its volatile content will lead to the change on the other properties including porosity, structure and reactivity of the remaining carbonaceous matrix. Since all these changes will interplay and affect the performance of the char combustion jointly, the results from CFD modelling in the next section will be further interpreted to appropriately address the combustion of Yallourn char under the simulated blast furnace conditions.

3.4. CFD modelling

3.4.1. Model validation

Apart from the previously described grid independence test and particle temperature measurements [17], the model for char burnout was further validated here by comparison of char burnout and outlet O_2 concentration in flue gas as obtained from the DTF experiments and as predicted by the CFD model. The comparison plots can be found in Fig. 11. A reasonable relationship is seen between the experimental and simulated results. Some variation is expected due to the sensitivity of DTF inputs and measurements.

3.4.2. CFD results interpretation

Fig. 12 first compares and predicts the effect of varying wall temperature, and subsequently the preheated gas temperature for the two Yallourn chars versus the reference coal, at a fixed O_2/C ratio of 1.0 (stoichiometric ratio) with a constant feeding rate and modified O_2 concentration. For the reference bituminous coal, its burnout profile shows a great dependence on the temperature. At 900 °C, it reaches a final burnout of only 60% at the exit of the whole reactor for a residence time of 1.8 s. The burnout profile consists of two steps, with the first step being finished in 0.2 s for the release and combustion of the volatiles, whereas the latter one for the heterogeneous oxidation of the char. Upon the rise of reaction temperature to 1100 °C, the two steps overlap considerably. This results in a relatively smooth burnout profile and the completion of the combustion in 1.4 s. Increasing the temperature to

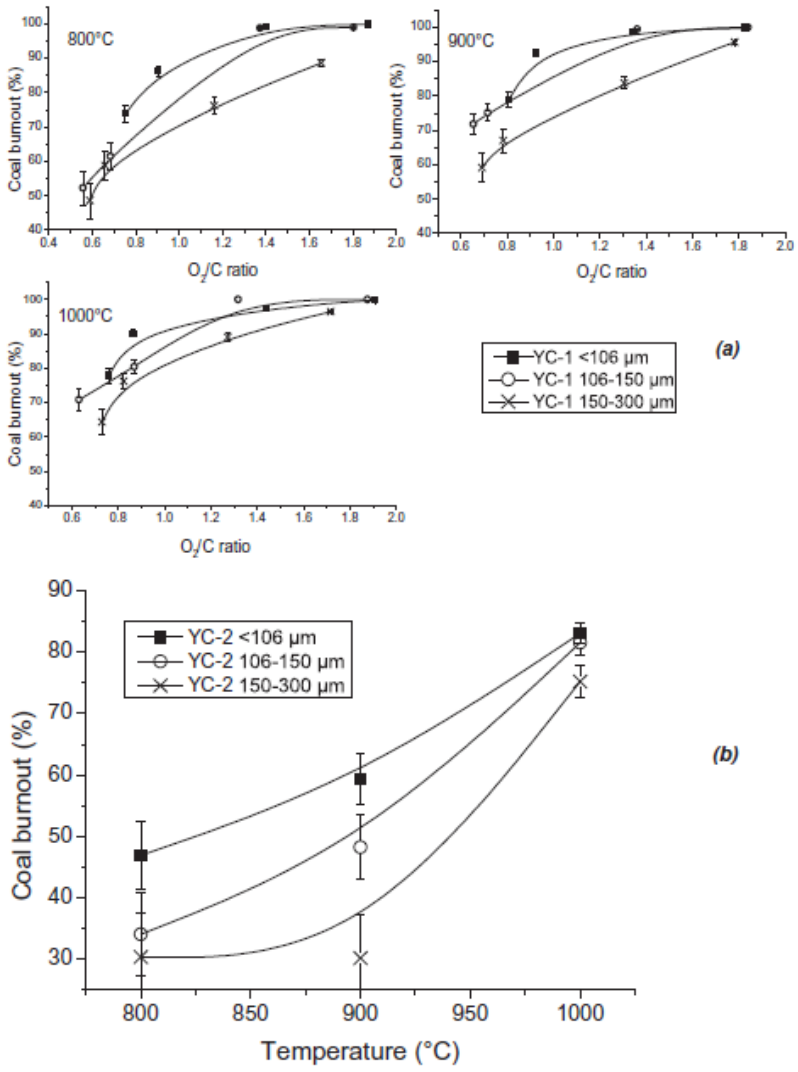

Fig. 7. Effect of particle size on burnout for (a) YC-1 at three O_2/C ratios and (b) YC-2 at a fixed O_2/C ratio of approximately 0.9.

1200 °C further enhanced the overlapping between different stages, and shortened the burnout time to about 1.0 s.

The YC-1 char combustion shows a less dependence on the temperature, even accomplishing its burnout in 1.6 s at 900 °C. Upon the rise of combustion temperature, the time to complete its burnout was further decreased to 1.0 s, 0.8 s and 0.7 s at 1000 °C, 1100 °C and 1200 °C, respectively. Moreover, the first step for YC-1 combustion, completed at around 0.3 s for 900 °C resulted in a loss of around 60 wt% of the char. By revisiting the visualized ignition sequence for this char in Fig. 6, one can clarify that the heterogeneous ignition occurred concurrently with the ignition of volatiles in such a short distance. The heterogeneous ignition even predominated since the volatiles only account for maximum 15 wt% (see Fig. 2) for YC-1 char. More interestingly, it is also referable from Fig. 12 that the two steps for YC-1 char are rather split at 1200 °C. The overall burnout profile at this temperature is also rather similar with that of the bituminous coal, suggesting the analogy of the combustion performance of these two fuels at the high furnace temperature. In other words, the properties of the original fuel are insignificant at high temperature. This could hold true, considering that the solid combustion generally shifts from reaction control to external diffusion control upon the elevation of the reaction temperature. The similar phenomena was also observed for another Yallourn char, YC-2.

Fig. 13 demonstrates the time-resolved particle temperature profile for bituminous coal versus YC-1 char at 1000 °C and 1200 °C at the stoichiometric O_2/C molar ratio of 1.0. According to panels (a) for bituminous coal, a particle was continuously heated until it reached a peak

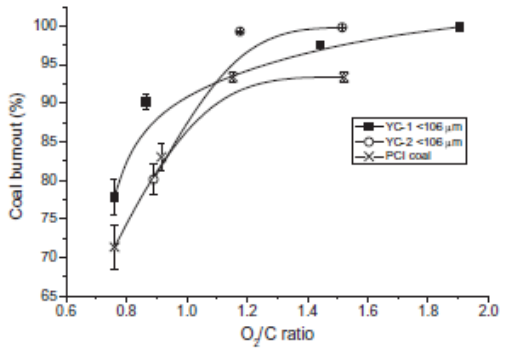

Fig. 8. Differences in reactivity between the two Yallourn char samples and PCI coal at 1000 °C.

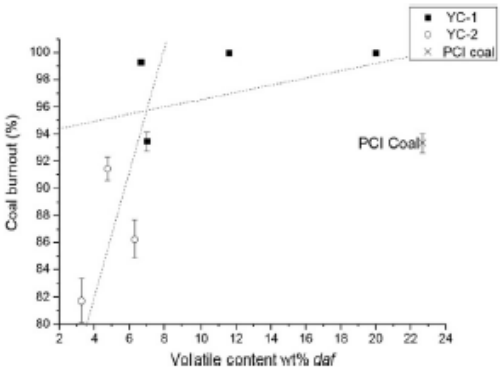

Fig. 10. Char burnout versus volatile content for two Yallourn chars at a fixed O_2/C ratio of 0.8–0.9 and 1000 °C.

temperature which was around 1300 °C and 1400 °C at the furnace temperature of 1000 °C and 1200 °C, respectively. This is due to the exothermic nature of the combustion providing heat feedback to the particle self. The respective first-order derivative in panel (a') further explored the existence of different combustion stages for bituminous coal. At 1000 °C, the initial peak for ignition was rather weak for bituminous coal, substantiating a slow release and ignition for the volatiles. A much stronger and broader peak at the residence time of 0.2 s was observed, reflecting the combustion of both the lagged volatiles and solid char at this stage. Increasing the furnace temperature to 1200 °C accelerated the volatile release rate, as echoed by a remarkable increase on the intensity of the first peak in panel (a'), and the second peak also shifted remarkably to a shorter residence which is around 0.1 s. Clearly, the PCI coal char reactivity holds a more sensitive variation than the volatiles upon the variation of the temperature. Since the distance between two stages was shortened at 1200 °C, the burnout profile in Fig. 12 is thus relatively smoother for the PCI coal at such a high furnace temperature.

The results of Fig. 13(b) for the time-resolved particle temperature of YC-1 are quite similar with the PCI coal in panel (a). However, the respective first-order derivative in panel (b') explored a rather distinct combustion behaviour for the Yallourn char. Even at the low furnace temperature of 1000 °C, the first peak for particle ignition is much stronger than that observed for the bituminous coal. Obviously, this peak should be partially attributed to the heterogeneous ignition of char particle, otherwise, less heat would be provided to heat up the particle rapidly. The amount of char participating in the first stage should also be considerable, thereby releasing sufficient heat feedback to heat up the particle at a peak rate of 2.4×10^4 °C/s, which is around four times of the particle heating rate observed for the bituminous coal. Consequently, around 60 wt% of the YC-1 was consumed at the first stage, as

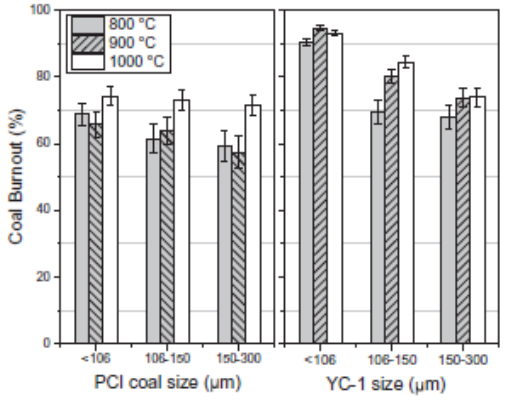

Fig. 9. Comparison of the burnout of differently sized YC-1 char (right) and commercial PCI coal (left) at an O_2/C molar ratio of 0.8–0.9.

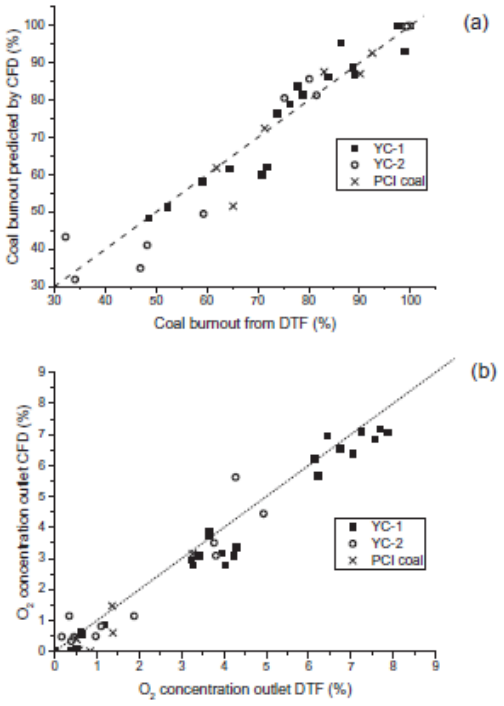

Fig. 11. Comparison of (a) burnout and (b) O_2 concentration in outlet between DTF and CFD model.

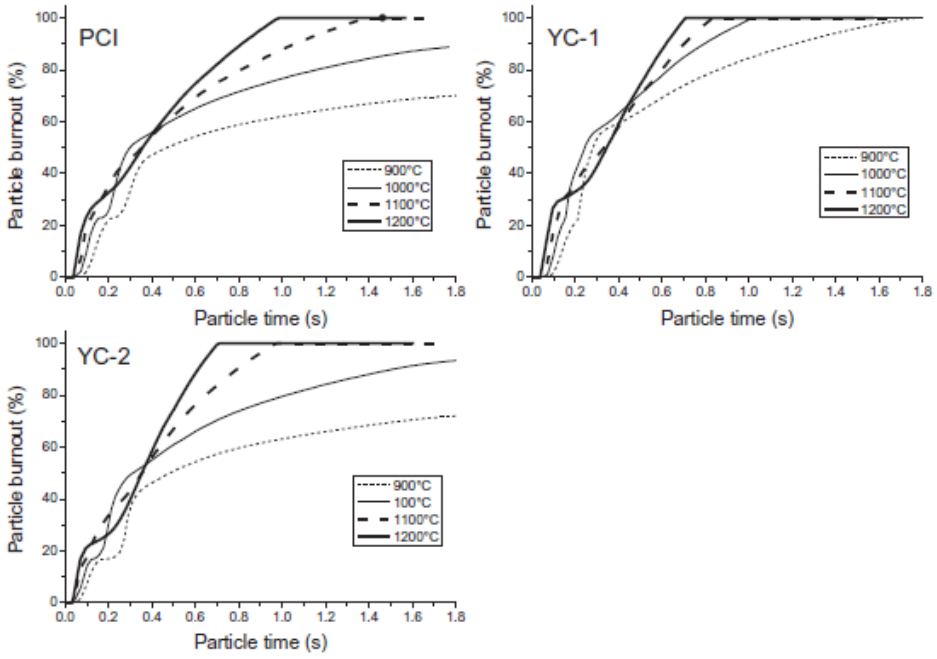

Fig. 12. Effect of temperature on particle burnout at $O_2/C = 1.0$.

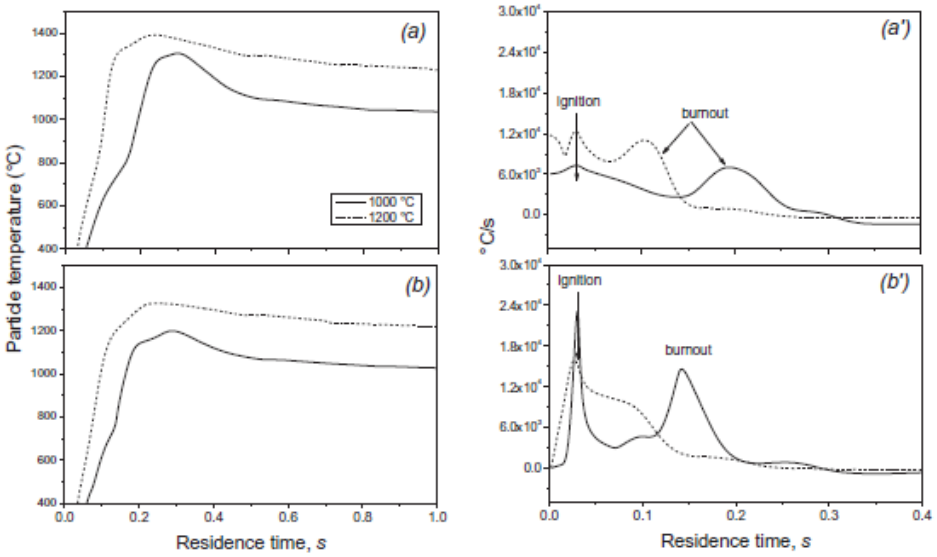

Fig. 13. Temperature distributions for PCI coal (a) and YC-1 char (b) near the injection zone with wall temperature (a) 1000 °C and (b) 1200 °C at $O_2/C = 1.0$. Panels (a') and (b') are the first-order derivative of panels (a) and (b), respectively.

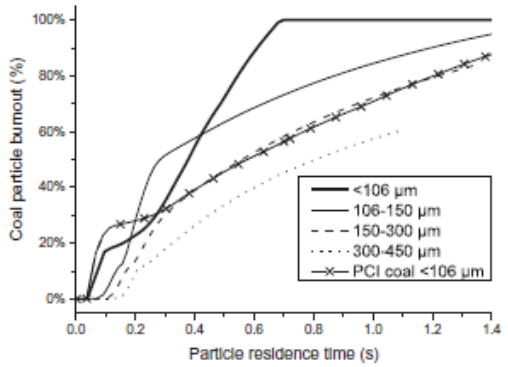

Fig. 14. Difference in burnout of YC-1 char with respect to particle size at 1200 °C and O_2/C = 1.0.

evident in Fig. 12. Regarding the temperature rise to 1200 °C, the left shift of the second peak for char burnout is not surprising, which can be fully assigned to the high reactivity of Yallourn char. However, it is more intriguing to observe a decreased intensity for the first peak when compared to 1000 °C. This explained the reduction on the mass loss at the first stage back to the burnout profile for YC-1 char in Fig. 12. It may also reveal a different reaction route for YC-1 char at such a high temperature. Since the radiative heat transfer from the furnace wall was enhanced upon the furnace temperature rise, it is very likely that the exothermic reaction such as C-CO_2 gasification has taken place at this stage. Otherwise, the particle would be heated up more quickly. As has been confirmed in a separate study [17], the gasification reaction contribution is remarkable for Victorian brown coal char. This should also be the case for the YC-1 and YC-2 char samples tested here, since they are also collected from the Latrobe valley.

Effort was further made by the CFD modelling to clarify the effect of particle size on the burnout of Yallourn char at 1200 °C for a stoichiometric oxygen to carbon molar ratio. As substantiated in Fig. 14, as particle size increased to a range of 150–300 μm, the burnout profile of YC-1 char is still comparable to PCI coal. The large specific surface area of woody charcoal was also proven accounting for its higher reactivity than the PCI coal [30]. Beyond that, the burnout for the particle of 300–450 μm dropped sharply due to the decreased surface area available and increased diffusional resistance. Clearly, irrespective of the pyrolysis conditions, the use of large size such as 300 μm for Yallourn char is viable, reaching a comparable burnout rate to the bituminous coal.

The last thing of interest to us is to validate the burnout of Yallourn char versus its volatile content, so as to elucidate the minimum volatile content that is a critical criteria for the selection of PCI coal. For this, CFD modelling was further conducted to extend the experimentally established results in Fig. 10 to three furnace temperatures, 800 °C, 1000 °C and 1200 °C, at a fixed O_2/C molar ratio of 1.0 and a fixed residence time, 0.7 s for the first two temperatures and 0.5 s for the last one. A residence time of 0.5 s rather than 0.7 s was chosen for 1200 °C, because both YC-1 and YC-2 char samples completed their burnout in 0.7 s at 1200 °C, as evident in Fig. 12. The different sizes of each char sample were reduced to the same particle size range (<106 μm) while keeping its reactivity unchanged. As illustrated in Fig. 15, the critical volatile content of 6 wt% was confirmed for 800 °C and 1000 °C, which agrees with the experimental observation as shown in Fig. 10. For YC-1 char with its volatile content varying from 6 wt% up to 20 wt%, it holds a clear upward trend for its burnout versus the volatile content. However, for the YC-2 char with a maximum 6 wt% volatile content, its broad scattering rather suggests that, for the char with extremely low volatile content, the higher heterogeneous

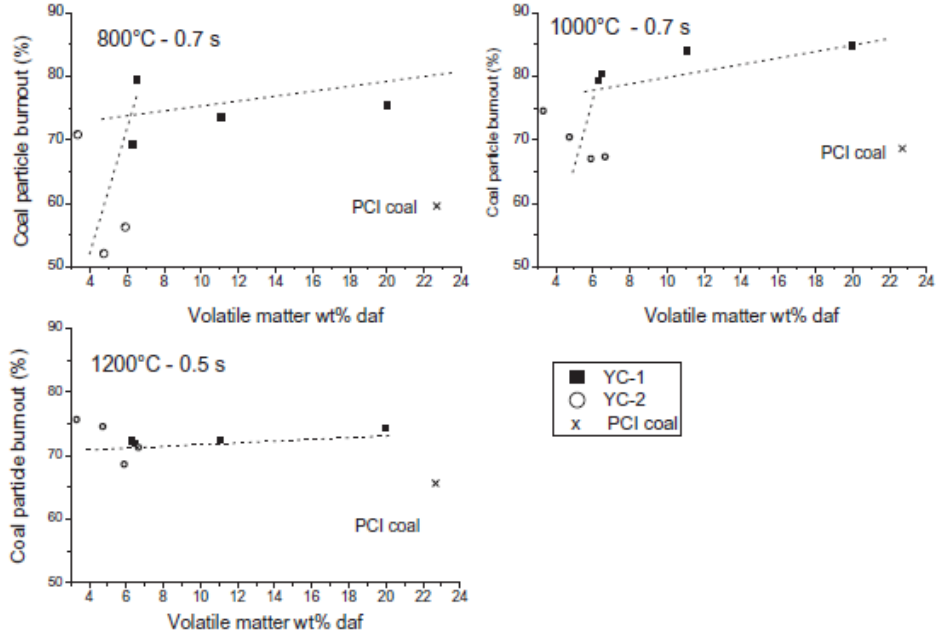

Fig. 15. Dependence of burnout on volatile matter predicted by CFD at 0.7 s (800 °C, 1000 °C) or 0.5 (1200 °C).

combustibility and larger porosity could outweigh the volatile content, enhancing the burnout rate of char via dominantly heterogeneous oxidation. Increasing the blast temperature to 1200 °C alleviates the dependence of brown coal char burnout on its volatile content, as evident by a rather flat slope for the trend line and insignificant variation of char burnout versus the volatile content. All the burnouts are also far higher than that of the PCI coal at this temperature, although its volatile content is high. Clearly, in an industrial blast furnace employing a hot blast temperature close to 1200 °C, the use of the lignite char tested here, irrespective of its preparation condition, is beneficial in offering a higher injection rate, thereby improving the coke replacement ratio and the productivity of the blast furnace.

4. Conclusion

In this paper, we have for the first time tried to establish the linkage between the brown coal pyrolysis condition and the end-use of the resultant char as a PCI fuel in the blast furnace. Efforts have been made to quantitatively examine the size-dependent properties of Yallourn char collected from an industry-scale shaft furnace, its potential and benefits for the replacement of commercial bituminous coal in the blast furnace. The major original findings from this study can be drawn as follows:

1. Irrespective of the pyrolysis condition, the char derived from Yallourn coal is suitable for the use as a top-grade PCI fuel in a blast furnace. Compared to the bituminous coal requiring a very fine size (e.g. <106 μm), excessive oxygen and high temperature (e.g. >1200 °C) for a complete burnout, the Yallourn char tested can achieve the comparable burnout rate under the rather mild conditions, e.g. 150–300 μm in size, stoichiometric O_2/C molar ratio of 1.0 and a furnace temperature as low as 1000 °C.
2. The homogeneous ignition of the remaining volatiles in Yallourn char is predominant at furnace temperatures of 1000 °C and below. Therefore, a minimum volatile content of 6 wt% in the prepared char is essential to ensure a stable ignition. The char structure is also influential in controlling the later heterogeneous char burnout. However, an elevation of the hot blast gas temperature to 1200 °C can compensate for the negative effect of volatile contents less than 6 wt% and the influence of char structure as well, due to the enhanced heterogeneous ignition and shift of the reaction to the diffusion control zone.
3. The larger porosity and specific surface area of Yallourn char are helpful for minimising the gas diffusion resistance, therefore, the coarse Yallourn char of 300 μm in size can burn efficiently under the stoichiometric O_2/C molar ratio at a high furnace temperature. Reducing the Yallourn char size is further beneficial in alleviating the external diffusion resistance to achieve a nearly complete burnout at 800 °C.

Acknowledgment

This work is supported by Brown Coal Innovation Australia (BCIA). Coal Energy Australia (CEA) is appreciated for providing the char samples.

Appendix A. Supplementary data

Supplementary data to this article can be found online at http://dx.doi.org/10.1016/j.fuproc.2016.10.028.

References

[1] P. Bennett, T. Fukushima, Impact of PCI coal quality on blast furnace operations, Proceedings of the 12th International Conference on Coal Science, 2003 (Cairns, Australia), http://www.coaltech.com.au/LinkedDocuments/Bennett_Fukushima.pdf.
[2] A.M. Carpenter, Use of PCI in Blast Furnaces, IEA Clean Coal Centre; London, 2006.
[3] H. Lüngen, A. Poos, Injection of coal into the blast furnace—ECSC synthesis report, Cokemaking International 8 (1996) 14–31.
[4] S. Zhang, Theoretical consideration of problems relating to high coal rate injection into blast furnaces, Ironmak. Steelmak. 30 (2003) 467–474.
[5] M.d.L.I. Gomes, E. Osório, A.C.F. Vilela, Thermal analysis evaluation of the reactivity of coal mixtures for injection in the blast furnace, Mater. Res. 9 (2006) 91–95.
[6] K. Ishii, Advanced Pulverized Coal Injection Technology and Blast Furnace Operation, Elsevier Science Ltd., Oxford, UK, 2000.
[7] R.G. Phillip, A. Bennet, Advantages of Low Volatile Coals for PCI, Report-Department of Mines and Energy-Q Therm Project, Brisbane QLD, 1997.
[8] Z. Wu, IEA Coal Research, Clean Coal Centre, Fundamentals of Pulverised Coal Combustion, International Energy Agency Coal Research, 2005.
[9] L. Lu, V. Sahajwalla, C. Kong, A. Mclean, Chemical structure of chars prepared under conditions prevailing in the blast furnace PCI operation, ISIJ Int. 42 (2002) 816–825.
[10] Y. Traa, Is a renaissance of coal imminent?—challenges for catalysis, Chem. Commun. 46 (2010) 2175–2187.
[11] K.W. Ng, L. Giroux, T. MacPhee, T. Todoschuk, Combustibility of charcoal for direct injection in blast furnace ironmaking, Iron and Steel Technology 9 (2012) 70.
[12] A. De Girolamo, A. Grufas, I. Lyamin, I. Nishio, Y. Ninomiya, L. Zhang, Ignitability and combustibility of Yallourn pyrolysis char blended with PCI coal under simulated blast furnace conditions, Energy Fuel 30 (2015) 1858–1868.
[13] C.Z. Li, Advances in the Science of Victorian Brown Coal, Elsevier Science, 2004.
[14] H.E. Kissinger, Reaction kinetics in differential thermal analysis, Anal. Chem. 29 (1957) 1702–1706.
[15] F. Low, A. De Girolamo, R.-Q. Dai, L. Zhang, Emission of organically bound elements during the pyrolysis and char oxidation of lignites in air and oxyfuel combustion mode, Energy Fuel 28 (2014) 4167–4176.
[16] H. Li, L. Elliott, H. Rogers, T. Wall, Comparative study on the combustion performance of coals on a pilot-scale test rig simulating blast furnace pulverized coal injection and a lab-scale drop-tube furnace, Energy Fuel 28 (2014) 363–368.
[17] J. Zhang, W. Prationo, L. Zhang, Z. Zhang, Computational fluid dynamics modeling on the air-firing and oxy-fuel combustion of dried Victorian Brown coal, Energy Fuel 27 (2013) 4258–4269.
[18] A.H. Al-Abbas, J. Naser, D. Dodds, CFD modelling of air-fired and oxy-fuel combustion of lignite in a 100 KW furnace, Fuel 90 (2011) 1778–1795.
[19] L. Ma, M. Gharebaghi, R. Porter, M. Pourkashanian, J.M. Jones, A. Williams, Modelling methods for co-fired pulverised fuel furnaces, Fuel 88 (2009) 2448–2454.
[20] T.F. Smith, Z.F. Shen, J.N. Friedman, Evaluation of coefficients for the weighted sum of gray gases model, J. Heat Transf. 104 (1982) 602–608.
[21] C.K. Westbrook, F.L. Dryer, Simplified reaction mechanisms for the oxidation of hydrocarbon fuels in flames, Combust. Sci. Technol. 27 (1981) 31–43.
[22] L. Chen, S.Z. Yong, A.F. Ghoniem, Oxy-fuel combustion of pulverized coal: characterization, fundamentals, stabilization and CFD modeling, Prog. Energy Combust. Sci. 38 (2012) 156–214.
[23] S. Badzioch, P.G. Hawksley, Kinetics of thermal decomposition of pulverized coal particles, Industrial & Engineering Chemistry Process Design and Development 9 (1970) 521–530.
[24] C. Standards, Specifications of Coal Used in Pulverized Coal Injection (PCI), 2008.
[25] J. Han, K. Cho, K.-H. Lee, H. Kim, Porous graphite matrix for chemical heat pumps, Carbon 36 (1998) 1801–1810.
[26] T.K. Gale, T.H. Fletcher, C.H. Bartholomew, Effects of pyrolysis conditions on internal surface areas and densities of coal chars prepared at high heating rates in reactive and nonreactive atmospheres, Energy Fuel 9 (1995) 513–524.
[27] T.F. Yen, J.G. Erdman, S.S. Pollack, Investigation of the structure of petroleum asphaltenes by X-ray diffraction, Anal. Chem. 33 (1961) 1587–1594.
[28] A.O. Odeh, Comparative study of the aromaticity of the coal structure during the char formation process under both conventional and advanced analytical techniques, Energy Fuel 29 (2015) 2676–2684.
[29] E. Binner, L. Zhang, C.-Z. Li, S. Bhattacharya, In-situ observation of the combustion of air-dried and wet Victorian brown coal, Proc. Combust. Inst. 33 (2011) 1739–1746.
[30] J.G. Mathieson, H. Rogers, M.A. Somerville, S. Jahanshahi, Reducing net CO_2 emissions using charcoal as a blast furnace tuyere injectant, ISIJ Int. 52 (2012) 1489–1496.

This page is intentionally left blank

Appendix C – Chapter 7 in publication form

This page is intentionally left blank

energy&fuels

Article

pubs.acs.org/EF

Ignitability and Combustibility of Yallourn Pyrolysis Char Blended with Pulverized Coal Injection Coal under Simulated Blast Furnace Conditions

Anthony De Girolamo,[†] Alexander Grufas,[†] Ilia Lyamin,[†] Iori Nishio,[‡] Yoshihiko Ninomiya,[‡] and Lian Zhang*[,†]

[†]Department of Chemical Engineering, Monash University, Clayton, Victoria 3800, Australia

[‡]Department of Applied Chemistry, Chubu University, Kasugai, Aichi 487-0027, Japan

ABSTRACT: Pulverized coal injection (PCI) is a widely used blast furnace technology aimed at reducing costs and increasing productivity. The prospect of blending PCI coal with a lower cost char, derived from Yallourn brown coal, is evaluated in this study by means of thermogravimetric analysis (TGA), flat-flame burner reactor, and drop-tube furnace experiments at four different blending ratios as well as computational fluid dynamics (CFD) modeling. Yallourn char has desirable properties compared to PCI coal, including a lower ash content and a higher heating value, although the reactivity is lower and the ignition temperature is higher. Because the combustion behavior of a blend is not always easily predicable based on the performance of the individual parent fuels, two Yallourn char samples (YC-1 and YC-2) are analyzed after blending with PCI coal at four ratios. According to the particle ignition time, a maximum of 40 wt % is allowable for YC-1 char which is comparably reactive with the commercial PCI coal. However, a maximum 20 wt % is only allowed for YC-2, which is less reactive. The negative heat sink effect of YC-2 char is influential, whereas the heterogeneous ignition of YC-1 overlapped considerably with the ignition of PCI coal, which is mainly in the homogeneous gas phase. In addition, it was found that the later char oxidation rate was accelerated greatly for the PCI coal blended with YC-1, irrespective of its blending ratio. In contrast, the heat sink effect is more obvious for the YC-2, the increase on the blending ratio of which greatly decreased the overall burnout rate, especially at low furnace temperatures (800 and 900 °C) and a shorter residence time, such as 0.8 s. For YC-1 char, its blending ratio is insignificant in the overall burnout. Increasing the furnace temperature to 1000 °C and the O_2/C ratio to 1.2 can assist in achieving a nearly complete burnout for all of its blends, even at a short residence time of 0.8 s. In contrast, for YC-2 char, a furnace temperature of 1200 °C and O_2/C ratio of 1.2 are essential to complete the burnout of all of its blends. The Yallourn pyrolysis conditions for the preparation of its char are critical. A good synergistic interaction between Yallourn char and commercial PCI in terms of reactivity is also essential for a broad blending ratio to be used in the blast furnace.

1. INTRODUCTION

Currently, 70% of iron production for steelmaking is attained through smelting iron ore by reduction with a carbon source (coke/coal) in a blast furnace.[1] To reduce the consumption of expensive coke and increase productivity, the pulverized coal injection (PCI) method is used to replace a portion of the coke used in the blast furnace.[2] This has been implemented in nearly all blast furnaces in China, Japan, Korea, and Taiwan and over half of those in North America, South America, and Europe.[3] As a result of this, the demand for coal suitable for PCI has been increasing steadily.[4]

Victorian brown coal (VBC) contains a relatively high amount of moisture and has a low ash yield. It is predominantly used for electricity generation at local power plants where it is inefficient and very carbon-intensive.[5] One of the promising applications for VBC is as a substitute for bituminous coals used in PCI in a blast furnace. Unprocessed brown coal is not suitable for blast furnace applications as a result of its high moisture content and low calorific value. Through a mild pyrolysis process, VBC could be upgraded to a higher value char, which is produced alongside other derivatives, coal gas and coal tar.[6] The VBC char could then be injected via the PCI method as a complete replacement for the commercial PCI coal or as a blend.

A previous study has confirmed the viability of a complete replacement of commercial PCI coal with two chars derived from Yallourn brown coal.[7,8] The char replacement has both advantages and disadvantages compared to the PCI coal. Yallourn char has a lower cost than the PCI coal and contains a higher calorific value, meaning that it can replace a greater portion of coke. It also has lower ash (<4 wt %) and moisture contents. On the other hand, the previous study showed that Yallourn char has a higher ignition temperature as a result of its lower volatile content, which, in turn, would cause a delay in the ignition and the formation of plenty of unburnt carbon entering the blast furnace.

Char can be blended with the normal PCI coal to balance these char characteristics; however, it is not always easily foreseeable how the created blend will behave as a result of

Special Issue: 5th Sino-Australian Symposium on Advanced Coal and Biomass Utilisation Technologies

Received: October 15, 2015
Revised: December 26, 2015
Published: December 27, 2015

DOI: 10.1021/acs.energyfuels.5b02425
Energy Fuels 2016, 30, 1858−1868

Table 1. Summary of Selected Works on Blending Combustion

purpose	testing method	findings	reference
investigate combustion characteristics of coal and pine sawdust blends	TGA	no synergistic effects observed	Gil et al., 2010[22]
investigate the combustion characteristic and kinetic behavior of microalgae/Yallourn brown coal blends	TGA	synergistic effect observed in reactivity and ignition	Tahmasebi et al., 2013[23]
investigate pyrolysis and combustion behavior of lignite/olive residue blends under air and oxy-fuel conditions	TGA/FTIR	experimental ignition temperature increased and burnout temperature is higher compared to a theoretical blend	Yuzbasi and Selçuk, 2011[24]
compare combustion characteristics of biomass/biochar blends	TGA	addition of biochar to biomass had similar combustibility up to a 30% blend	Yi et al., 2013[25]
assess whether the combustion behavior of blends could be predicted from that of the parent coals	IPFR	ash yield, proximate VM, LCV, char burnout, and true density are additive; VM yield in IPFR and apparent density not additive	Haas et al., 2001[10]
simulate flow and combustion of binary coal blends under BF conditions	BF CFD model	synergistic effect on the overall burnout observed	Shen et al., 2009[26]
investigate blending combustion performance of brown coal and char in a boiler	600 MW boiler CFD	50% blend ratio provided an optimum balance of moisture and combustibles	Zhang et al., 2015[27]
predict efficiency deviations in the combustion of coal blends in power plants	DTF	blended coals with large rank differences showed improved burnout compared to weighted average	Ullou et al., 2005[28]
evaluate the dependencies between the properties of coal blends and parent coals according to their mass contributions	EFR	some properties could be predicted (HGI and SO_2 emission), while others were specific for the blend (NO_x emission and burnout)	Maroń and Rybak, 2007[29]
test combustion behavior and flame structure of blends of biomass with coal of different ranks	TGA/slit burner	10% biomass addition could improve combustion efficiency of low-rank coal but had no apparent impact on high-rank coal	Moon et al., 2013[30]
study interaction of Ningxia coals of varying FC/VM ratios	TGA	ignition of blends is closer to that of the higher reactivity coal; additive behavior observed for similar ranks	Zhang et al., 2011[9]
blended combustion of high- and low-ash Indian coals	TGA/DTF	burnout of blends with 50% of high-ash coal showed better burnout than individual coals	Biswas et al., 2006[31]
evaluate performance of blending Brazilian sub-bituminous coal with imported PCI coal and wood charcoal	laboratory injection rig	blending of Brazilian coal with the imported coal led to a substantial increase in conversion; charcoal in blends increased conversion and reduced ash	Machado et al., 2010[32]
modeling the simultaneous injection of pulverized coal and charcoal into the blast furnace through the tuyeres with oxygen enrichment	BF CFD model	increase in productivity was observed with the addition of higher reactivity and higher VM charcoal	de Castro et al., 2013[33]
to verify combustion performance of biomass charcoal products was comparable to PCI coals	pilot-scale PCI rig	charcoal showed superior flame stability and combustion performance; burnout for blends could be adequately predicted by a weighted average	Mathieson et al., 2011[34]

DOI: 10.1021/acs.energyfuels.5b02405
Energy Fuels 2016, 30, 1858−1868

possible non-additive/synergistic interactions between different coals or chars.[9] Some properties of coals are always additive [C, H, O, N, and S analyses, moisture content, and lower calorific value (LCV)],[10] while others may be additive or non-additive depending upon the parent coals. Haas et al.[10] determined that non-additive effects were greater when parent coals had a larger difference in the coal rank. The stability of low-volatile coals could be enhanced by blending with a higher volatile coal (with the exception of low-rank coal), while burnout of blends will follow a linear trend,[11] with burnout being higher for coals with a larger volatile content.[12,13] Ignition temperatures of coal blends have been shown to decrease with an increased proportion of volatile matter (VM) in the blend; however, several studies have found the actual ignition temperature of blends to be lower than that predicted by a weighted average of the parent coals. Therefore, the ignition temperature will approach that of coal with a higher VM.[9,14,15]

Table 1 provides a summary of a number of studies that have been completed on blending combustion. Blend analysis by thermogravimetric analysis (TGA) has provided useful information about ignition and interactions between blends, although there is no clear consensus on whether a given blend will show non-additive behavior. Drop-tube furnace (DTF) and other lab-scale rigs provide heating rates that are much more applicable to those experienced by coal injection into a blast furnace and will allow for VM to potentially interact with fixed carbon. For industry-scale assessment, computational fluid dynamics (CFD) modeling has been favored as a result of the lower cost and ability to measure key performance parameters and modify input parameters with ease. However, the effect of the chemical interaction between blends may not be possible to fully take into account if only parent coal or char characteristics are considered. With this current state of research, it can only be assumed that the blend behavior will be expected to fall within or close to the constraints given by their parent fuels; therefore, analysis of each blending ratio should be examined prior to application in industry.

In this study, the properties, reactivity, and interaction of different mixtures of Yallourn char and a commercial PCI coal will be analyzed to determine an optimum ratio of blending. This research aims to clarify both ignition and burnout rate for coal−char blends, which are critical for the combustion of PCI coal in the tuyere/blowpipe of a blast furnace. Techniques used include TGA, ignition time measured in a flat-flame burner, DTF experiments, and CFD modeling. The DTF used is able to preheat the gas temperature up to 1000 °C, which can thus resemble an industrial blast furnace. It is of interest to maximize the replacement of PCI coal and, thus, have a greater content of Yallourn char in the blend to reduce fuel costs and ash burden. Additionally, if a Yallourn char blend is chosen with a higher calorific value than PCI coal, a higher coke replacement ratio would be achieved and, thus, additional cost savings in coke requirement would ensue. However, because these benefits could come at the cost of reduced reactivity and delayed ignition, it is pivotal to establish a blending ratio that balances the beneficial and detrimental effects. While it was established that both Yallourn char samples had a higher ignition temperature and larger ignition delay than the PCI coal (which was correlated with the higher volatile content of PCI coal), the blends containing Yallourn char with PCI coal will have a VM content higher than that of the individual Yallourn char samples. If the heterogeneous nature of the blend allows for PCI coal with a higher VM to ignite sooner, then the heat feedback from its VM combustion may, in turn, assist with the heterogeneous ignition and burnout of Yallourn char. In addition, the blending of char would increase the local O_2/C molar ratio for the PCI volatiles, thus promoting its ignition. However, if the reactivity of the char is very low and does not match the PCI, it could act as an "inert" species, causing heat sink near the igniting/burning PCI coal particles. This would, in turn, postpone the overall burnout. All of these hypotheses will be tested in this study, which is expected to ultimately diversify the use of Victorian brown coal by creation of a product that can be exported to the international market.

2. EXPERIMENTAL METHODOLOGIES

Yallourn char for this study is obtained by pyrolysis of raw wet Yallourn brown coal in a pilot-scale shaft furnace. As in the previous study,[7] two types of Yallourn char were produced under different conditions. These will be referred to as Yallourn char 1 (YC-1) and Yallourn char 2 (YC-2). The char is created under relatively mild conditions (around 800 °C), and YC-2 was pyrolyzed over a longer time period (~10 h) than YC-1 (~5 h). The most common size fraction was taken from each of these (1−4 mm), ground to a size of <106 μm, and mixed with a commercial PCI coal at four different ratios from 20 to 80% (mass fraction) char with the remaining PCI coal. The proximate and ultimate analyses of both fuels are shown in Table 2. Although Yallourn char samples have similar VM and fixed carbon contents, their physical properties vary considerably (Table 3).

Table 2. Proximate and Ultimate Analyses of Fuels

	YC-1	YC-2	PCI coal
Proximate Analysis			
moisture (%, ar)	10.2	1.2	1.9
ash (%, db)	7.4	5.2	8.7
VM (%, db)	6.5	4.5	20.7
fixed carbon (%, db)	86.1	90.3	70.6
Ultimate Analysis (%, db)			
carbon	87.10	93.22	80.84
hydrogen	1.20	0.49	3.90
oxygen[a]	3.31	0.00	4.89
nitrogen	0.66	0.76	1.20
sulfur	0.33	0.38	0.47

[a]By difference.

Table 3. True Density, Apparent Density, Calculated Porosity, and Higher Heating Value for Fuels

	YC-1	YC-2	PCI coal
true density (kg/m^3)	1863	2204	1441
apparent density (kg/m^3)	510.7	417.8	644.2
calculated porosity[a] (%)	72.6	81.0	55.3
higher heating value (MJ/kg)	27.2	32.3	30.5

[a]Porosity = (true density − apparent density)/true density × 100%.[35]

The kinetic parameter analysis (Table 4) showed a large variation in activation energy between YC-1 and YC-2 chars (103.0 and 151.6 kJ/

Table 4. Kinetic Parameters for Yallourn Char and PCI Coal

	pre-exponential constant (s^{-1})	activation energy (kJ/mol)	reaction rate at 800 °C (s^{-1})	reaction rate at 1000 °C (s^{-1})
YC-1	5.33×10^4	103.0	0.52	3.16
YC-2	3.90×10^6	151.6	0.16	2.35
PCI coal	8.20×10^5	129.0	0.43	4.19

DOI: 10.1021/acs.energyfuels.5b02425
Energy Fuels 2016, 30, 1858−1868

mol, respectively), although these two chars possess similar properties in terms of the content of remaining volatiles and ash. The method of determination of kinetic parameters is detailed in section 2.1. Likely, the pyrolysis condition is critical in affecting the char structure and its reactivity. In terms of the reaction rate at a high temperature, YC-1 shows higher reactivity, closer to the reactivity of PCI coal. The level of metal oxides in the ash of each fuel is shown in Table 5.

Table 5. Composition of Ash Weight Percent Oxides

metal oxide	YC-1	YC-2	PCI
SiO_2	1.79	1.58	40.46
Al_2O_3	2.41	3.82	27.61
Fe_2O_3	41.14	20.31	5.99
MgO	30.23	34.43	0.02
CaO	7.39	12.62	13.06
SO_3	8.99	13.16	6.57
K_2O	0.36	0.91	0.46
Na_2O	6.05	11.36	3.73

2.1. TGA. TGA (Shimadzu DTG-60H) was used to determine the ignition temperature of the coal−char blends, the intrinsic reactivity kinetic parameters for pure fuels (both activation energy and pre-exponential factors), and the ash content of the unburned residues collected after the DTF experiments.

A Kissinger plot was used to determine the activation energy and pre-exponential factor for the two Yallourn char samples and PCI coal. The Kissinger method considers the effect of the heating rate on the variation in the temperature at which the maximum reaction rate occurs.[16] Heating rates were varied between 4 and 10 °C/min to ensure that the temperature at the maximum rate was in the chemical kinetic control regime. The ignition temperature was defined as the temperature at which the combustion rate, for a certain heating rate, rises to 1 wt %/min of the current mass.[17]

2.2. Flat-Flame Burner Reactor (FFBR) Experiments. Ignition tests were also carried out in a FFBR to complement the TGA observation where ignition was measured at a slow heating rate. The FFBR was operated at atmospheric pressure with a measured flame temperature of approximately 1062 °C before the feeding of coal/char. A magnitude of 10^5 °C/s is expected for the heating of coal/char particles in the FFBR,[18] which is close to the industrial blast furnace heating rate.[3] The oxygen fraction was fixed at 0.21, and the O_2/C molar ratio was fixed at 2.5. The feed rate of coal/char to the burner is approximately 1 g/min, with deviations of up to 10% from this to maintain the correct O_2/C ratio for each sample. At least 100 images were captured with a Nikon P7000 charge-coupled device (CCD) camera and analyzed for each blend to quantify the ignition point of each sample as a distance from the burner base. A high-speed camera was used to measure particle velocity and, thus, calculate the ignition time. Further information about the FFBR can be found in a previous study.[18]

2.3. DTF Experiments. A 2 m high DTF was used to combust the coal and char samples, and a gas analyzer recorded the combustion gases exiting the furnace. A schematic drawing of the DTF setup can be found in a previous work.[19] The sample enters the DTF with a low-volume primary gas (1.0 L_{STD}/min), while a secondary gas (9.0 L_{STD}/min) is preheated to the furnace temperature and mixes with the coal or char at the injection point. Such a unique preheating system for the gas can resemble the blast furnace condition where coal is injected into a hot air stream. The coal/char feeding rate was approximately 0.7 g/min. Oxygen was added to the secondary gas to achieve the desired O_2/C ratio. The particle residence time was approximately 1.4 s in the furnace. The following parameters were varied in this study: blending ratio (with respect to Yallourn char content), 0, 20, 40, 60, 80, and 100%; furnace temperature, 800, 900, and 1000 °C; and O_2/C molar ratio, 0.7, 0.85, 1.0, and 1.3.

2.4. CFD Modeling. A three-dimensional (3D) CFD model of the DTF was used to gain a better understanding of the interactions of different blends. The mesh for this was taken from a previous study.[20] The model has been validated using particle temperature measurements, and a grid independence test was conducted to optimize the mesh cell number.[20] Blends were added to the model as two coal injections at the same inlet surface. This method may be used to study the interactions caused by differences in the volatile content and reactivity. This mesh was validated in a grid independence test as well as with measurements of the particle temperature. The models used in the simulation are summarized as follows: turbulence, $k-\varepsilon$ model; radiation, discrete ordinates (DO) model; radiation absorption, weighted sum of gray gases model (WSGGM); particle reactions, multiple surface reaction model; and gas reactions, Westbrook and Dryer mechanism.[21] The 3D double-precision pseudo-transient coupled solver was used with an initial pseudo-time step of 0.001 s for the first 30 iterations, followed by 0.1 s for the remainder of the calculation. Second-order discretization schemes were used for all equations apart from the discrete ordinates model, which remains as the default setting of first order. Relaxation factors are kept as the default settings, with the exception of the reduction of the species relaxation factor from 0.75 to 0.5 and the discrete particle phase relaxation factor from 0.5 to 0.25. The solver is set to run until all residuals were reduced below 10^{-7} to ensure that all variables monitored concurrently with the solution procedure, including temperature, velocity, and reaction rate variables were entirely stable and unchanging with further iterations. This overall strategy ensured that all cases could be solved with a steady reduction in residuals without divergence.

3. RESULTS AND DISCUSSION

3.1. Ignition Analysis. Figure 1 shows the TGA-measured ignition temperature as a function of the Yallourn char blending ratio at a heating rate of 10 °C/min. The ignition temperature generally increases with increasing Yallourn char content. This is due to the lower VM percent in the Yallourn char sample. However, the ignition temperature of blends increases nonlinearly with a reduced VM content in the coals. To some degree, this is to be expected and could be predicted on the basis of the burnout of the pure coal or char. If the parent fuels do not interact in the blend, the fuel with the lower ignition temperature will still have the opportunity to ignite independently. Therefore, this can be an advantage specific to heterogeneous fuels. Simulated curves are also shown in Figure 1 for ignition of the blends based on the weighted averaging of the burnout of the pure coal/char. These simulated curves predict the ignition point that would be measured if the blends do not interact in the TGA. Clearly, the experimental results show that, for both YC-1 and YC-2 blends, the predicted ignition temperature is lower than the simulated predictions.

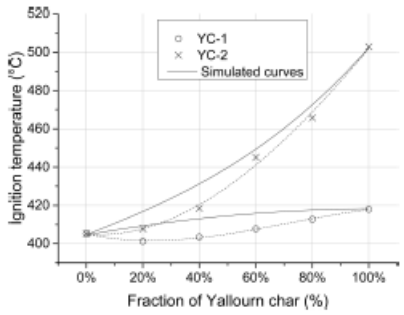

Figure 1. Ignition temperature of blends by TGA.

DOI: 10.1021/acs.energyfuels.5b02425
Energy Fuels 2016, 30, 1858−1868

Therefore, a weighted average of each respective coal ignition temperature is non-additive. A synergistic interaction could be due to the catalytic effect of minerals in Yallourn coal char, which is rich in Fe and alkaline earth metals. With respect to the difference between the two chars, it is obvious that the increase extent for the blending of YC-1 with PCI coal is much lower than that of YC-2, although they bear a similar volatile content, as evident in Table 2. For the use of YC-1 char, the ignition temperature was only increased by around 13 °C upon the shift from pure PCI coal to pure YC-1 char. The use of up to 40 wt % YC-1 caused little change on the ignition temperature. The physical properties of the two chars are not the affecting factors, because YC-2 char is indeed more porous than its counterpart, as evident in Table 3. It is most likely that YC-1 holds a distinct carbonaceous structure, which is clearly more reactive and prone to ignite heterogeneously. With regard to the use of YC-2 char, Figure 1 suggests that its blending ratio for YC-2 has to be limited to a maximum of 20 wt %; otherwise, the ignition for the coal−char blend would be delayed considerably, by a rise of the ignition temperature from 405 °C for pure PCI coal to 431 °C for 40 wt % YC-2 in the blend and as high as 503 °C for pure YC-2.

Figure 2 further plotted the correlation between the blend ignition temperature and its volatile content, which was

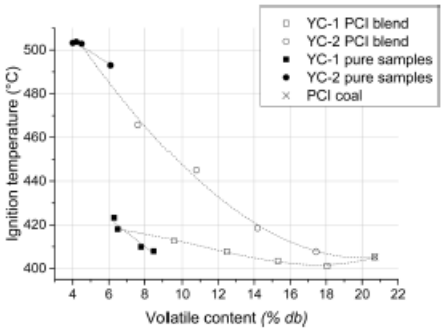

Figure 2. Effect of VM on the ignition temperature in TGA.

calculated by a linear combination of the volatile contents in the two pure fuels. It is evident that a nonlinear correlation exists between the ignition temperature and volatile content. In addition, the trend for YC-1 and YC-2 chars (from different size fraction groups) has their own dependencies of the ignition temperature on the volatile content. The degree to which the ignition temperature will depend upon the volatile content is greater for YC-1 than YC-2, indicated by the steeper curve. To reiterate, this supports the importance of the char structure on its reactivity.

The direct observation of coal/char ignition in the FFBR employing a very fast heating rate in Figure 3 shows an agreement with the ignition behavior for coal blends observed in TGA. That is, the ignition for coal−char blends was unaffected by blending at low ratios (up to 20%). A clear decrease on the ignition time is obvious upon increasing the char blending ratio. Although the coal/char particles are fed continuously into the FFBR, they are supposed to have little interparticle interaction. Similar to that observed in TGA employing a very slow heating rate and the use of preloaded

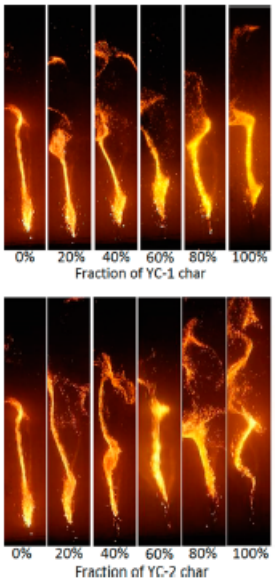

Figure 3. Effect of the blend ratio on the flame structure for YC-1 (top) and YC-2 (bottom).

samples with only a small amount, YC-2 blends show a larger ignition delay than for YC-1 blends. The flames for the blends using YC-2 char are discontinuous, indicative of the difficulty for their ignition. For YC-1, blends of 60% and below showed similar flame length and ignition points to those of PCI coal. In contrast, increasing the amount of YC-2 will drastically increase the ignition distance/time after 40% and increase the flame length.

Figure 4 further quantifies the ignition time as a function of the Yallourn char blending ratio. Clearly, the ignition delay for blending YC-1 with PCI coal is less obvious. The use of up to 40 wt % YC-1 char resulted in the same ignition time with the pure PCI coal. Such an observation is in line with the TGA

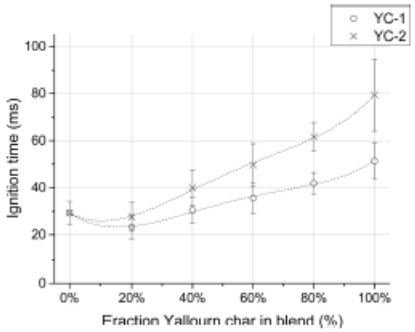

Figure 4. Ignition time for char blends as measured in the flat-flame burner.

DOI: 10.1021/acs.energyfuels.5b02425
Energy Fuels 2016, 30, 1858−1868

results (in Figure 1) using a very slow heating rate. On the other hand, the use of a maximum of 20 wt % is only allowed for the YC-2 char; otherwise, the ignition would be delayed considerably. Such a finding is also consistent with the TGA results in Figure 1. As was performed previously for the ignition temperature in TGA, the relationship between the ignition delay and volatile content is illustrated in Figure 5. Similarly,

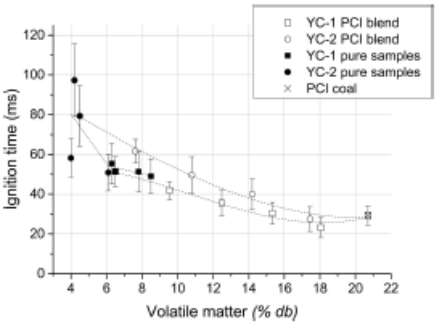

Figure 5. Effect of the VM content on the ignition delay in the flat-flame burner.

the ignition delay will decrease with the volatile content, although this relationship is not linear for blends. Moreover, by comparison of Figures 5 and 2, one can see that the discrepancy between the curves for the two chars in FFBR is rather narrow and their error bars even overlap one another. This is an indicator of the strong influence of the partide heating rate on its ignition. Upon a very fast heating rate in the FFBR, the heterogeneous ignition could occur once the char particles are injected into the hot gas stream. This is evident by the appearance of individual sparkling spots near the burner base in Figure 3. In other words, the influence of the carbonaceous structure on the coal−char blend ignition should be marginal in an industrial blast furnace. At least, its influence is less significant than the particle heating rate. In addition, from Figure 5, it can be seen that 14 wt % is the minimum volatile content in the coal−char blend, causing little change on the ignition time compared to the pure PCI coal. Such a volatile content corresponds to a maximum of ~40 wt % Yallourn char to be mixed with the PCI coal.

3.2. DTF Experimental Results. Figure 6 shows the burnout results for YC-1 char blended with PCI coal at six ratios, in different O_2/C ratios, 1000 °C, and a gas residence time of 1.4 s. As seen, although the blending of 20 wt % YC-1 lowered the burnout, irrespective of the O_2/C ratio, the blending ratio of 80 wt % YC-2 char clearly gave the best burnout at every O_2/C ratio. Such a finding is apparently contradictory to the ignition results discussed above. One probable reason is the large experimental error related to partide feeding in the DTF system. The YC-1 char was found to be strongly sticky and electrostatic, which largely slowed its feeding rate.

The results for YC-2 coal−char blends in Figure 7 are much more reasonable, showing a clearer trend for the burnout versus O_2/C ratio, furnace temperature, and char blending ratio as well. This is because the feeding problem does not exist for the YC-2 char, as observed during the experiments. Except 800 °C,

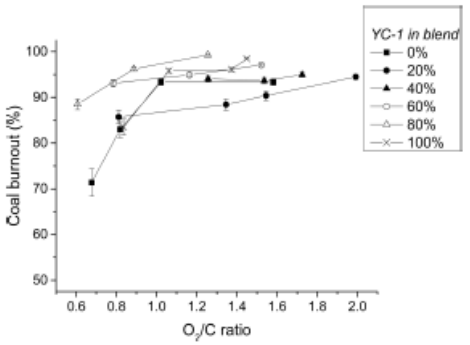

Figure 6. Burnout in the DTF for different blends for YC-1.

the blending ratio of YC-2 char is clearly less significant. At each temperature, the O_2/C ratio dependence trends for different blends overlap significantly. Back to the previous conclusion, for a maximum 40 wt % allowable blending ratio for YC-2 char in terms of ignition, it is apparent that the later char oxidation step for the blended combustion, irrespective of the char blending ratio, was occurring faster than the single PCI coal char. One reason could still be the interparticle heat feedback between char and PCI coal particles. The fast ignition of PCI volatiles induced the heating and heterogeneous ignition/oxidation of char, which, in turn, released more heat (as a result of its larger calorific value) to accelerate the oxidation of PCI char. For these two temperatures, increasing the O_2/C molar ratio above 1.2 is clearly beneficial in promoting the burnout dose to completion. With regard to the lowest temperature examined here, 800 °C, the combustion rate, irrespective of the blending ratio, is very low, thereby requiring an O_2/C ratio above 1.6 to achieve a close-to-completion burnout. Interestingly, the 20 wt % ratio for YC-2 shows the least burnout, even at an O_2/C ratio as high as 1.6, whereas the use of 60 wt % YC-2 char was even able to achieve a burnout close to 95 wt % at the same O_2/C ratio. This indicates that the ignition delay is insignificant in affecting the final burnout rate for the coal−char blends. One reason could be due to the relatively long residence time (1.4 s) used here.

3.3. CFD Modeling Prediction. *3.3.1. Influences of the O_2/C Ratio, Blending Ratio, and Furnace Temperature.* Because the experimental conditions in the DTF are difficult to control, in most cases, changing only one variable was unavailable for the DTF system. For instance, the calibration curve between the coal feeding rate and the voltage for the piezoelectric feeder varies broadly for different blends, and hence, the influence of individual parameters is difficult to be assessed. In this sense, CFD modeling has been conducted to manipulate the experimental conditions to assess the influence of individual variables. The use of this model was validated by comparison of burnout and exit O_2 percent in flue gas with the respective values predicted by the CFD model. Figure 8 shows a reasonable agreement between these values given the variable nature of the DTF.

Figure 9 shows the effect of the temperature on the burnout for both Yallourn char samples at three O_2/C ratios. At the lowest O_2/C ratio of 0.85, in which O_2 is insufficient, YC-1 blends show more comparable burnout for different blending

DOI: 10.1021/acs.energyfuels.5b02425
Energy Fuels 2016, 30, 1858−1868

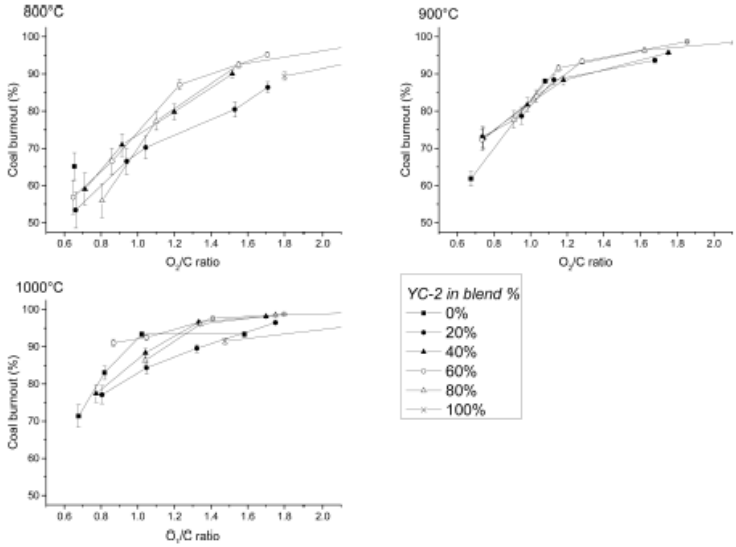

Figure 7. Burnout in the DTF for different blends for YC-2.

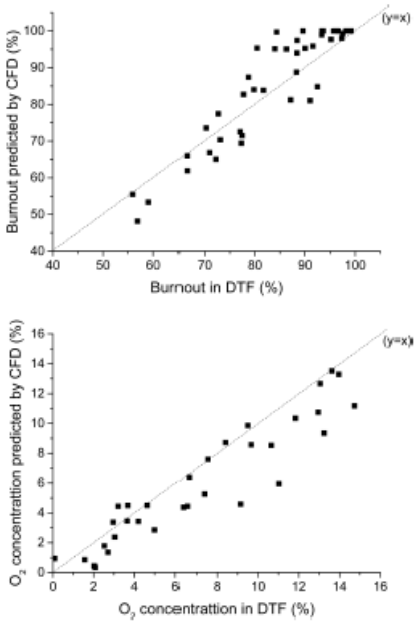

Figure 8. Experimental validation by comparing DTF experimental burnout and O_2 outlet concentration to CFD prediction.

ratios, especially at the temperatures of 900 °C and above. At 800 °C, the burnout was slightly decreased from the blending ratio of 40 wt % for YC-1. In combination with the ignition results, it is evident that the overall burnout was slightly negated by the initial ignition delay. However, such a delay is trivial and even negligible, which indicates the comparable/similar reaction rate for YC-1 char with the PCI coal at such a low furnace temperature. Consequently, these two fuels burned rather concurrently in the furnace. Upon increasing the furnace temperature to 900 and 1000 °C that is identical with the FFBR temperature, the initial ignition delay, as observed in Figures 1−5, was non-influential in the final burnout rate. Again, this should be due to the interparticle heat feedback that accelerated the YC-1 char ignition and oxidation rate. In other words, the heterogeneous oxidation of YC-1 should overlap greatly with the initial ignition stage rather than in a consecutive mode. In contrast, the results observed for the YC-2 char showed a stronger dependence of burnout upon the blending ratio at 800 and even 900 °C. This further supports a lower reactivity for YC-2 char than the PCI coal. Therefore, blending YC-2 char into the PCI coal provided a heat sink effect on the ignition and burnout. A maximum blending ratio of 20 wt % was further confirmed for the YC-2 char at 800 °C, which is consistent with the ignition results discussed above.

The results observed at a stoichiometric O_2/C molar ratio of 1.0 show a similar trend for both chars with their respective results at the lowest O_2/C molar ratio of 0.85. The effect of the blending ratio is much weaker for YC-1 char, even at 800 °C. This further substantiates a strong overlapping between different steps for the combustion of YC-1 char and PCI coal blends, particularly at the temperatures from 900 °C onward. In contrast, the different steps took place rather consecutively at 800 °C. This is particularly the case for YC-2 char, which has a slower ignition and also a lower reactivity. Therefore, its heat sink effect is stronger. The 800 °C results for YC-2 char blends are rather linear versus the blending ratio.

DOI: 10.1021/acs.energyfuels.5b02405
Energy Fuels 2016, 30, 1858−1868

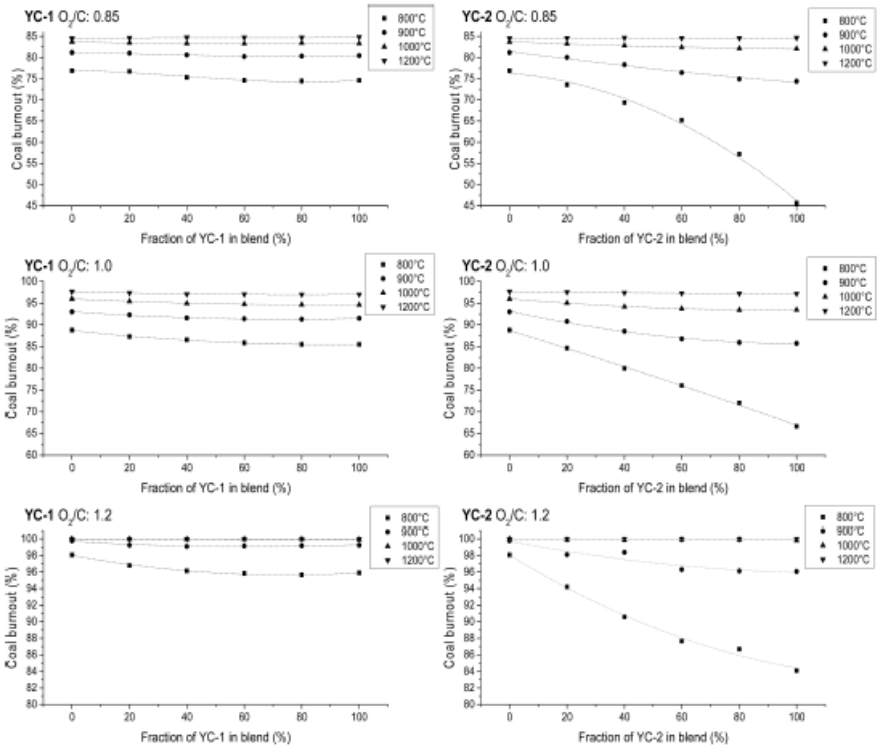

Figure 9. Effect of the blend ratio and temperature on the burnout at three O_2/C ratios for YC-1 (left) and YC-2 (right).

Increasing the O_2/C ratio to 1.2 closed the discrepancy in the burnout between blends and pure PCI coal from 900 °C and above for YC-1 char and 1000 °C and above for YC-2 char. At 800 °C, the burnout of the blends still depended upon the blending ratio, even for YC-1 char. This is due to the reaction control for the combustion at such a low temperature. The inherent reactivity (or the nature) of the fuel is more important than the O_2 partial pressure in the furnace. Upon the increase in the furnace temperature, the overall burnout gradually moves to the diffusion control regime; therefore, the nature of the blends is insignificant. In other words, using a higher O_2/C ratio for oxygen-enriched combustion and a blast temperature above 1000 °C can eliminate the dependence of the overall burnout upon the char blending ratio.

3.3.2. Influence of the Gas Residence Time. Because the residence time in a blast furnace is very short, effort was further made by evaluating the burnout at a shorter residence time in the DTF, 0.8 s. The results are shown in Figure 10 for three O_2/C molar ratios for two chars at varying blending ratios. For comparison, the respective results for the residence time of 1.4 s were also included here. With respect to YC-1 char at the lowest O_2/C ratio of 0.85, its results observed at 0.8 s are very similar to the longer residence time of 1.4 s, except for a dearer decrease on the overall burnout upon increasing the char blending ratio at 1000 °C. The decrease on the burnout is more obvious upon the blending of YC-2 at 1000 °C and 0.8 s. Such a descending trend also reflects the ignition results observed in Figures 1−5, further proving our previously mentioned hypothesis that the ignition delay mainly exerted its effect on the initial stage, whereas the later char oxidation stage was accelerated upon the blending of char and PCI coal. For the YC-2 char, its negative effect on the overall burnout is even discernible at 1200 °C in 0.8 s. This substantiates the strong heat sink impact of YC-2 char, which has a much lower reactivity and, thus, failed to synchronize with PCI coal in terms of combustion.

Similar phenomena were observed for the two chars at the stoichiometric O_2/C ratio of 1.0. In particular, the use of a furnace temperature of 1200 °C is essential to eliminate the negative heat sink effect of YC-2 char at a short residence time of 0.8 s. Such a conclusion is further strengthened at the excessive O_2/C molar ratio of 1.2.

3.4. Particle Temperature Profile. The temperature contours in Figure 11 show how the temperature shifts along the reactor from the injection point as the blend ratio increases for both YC-1 and YC-2 for a fixed condition, furnace temperature of 1000 °C, and O_2/C ratio of 1.0. The heat sink effect of YC-1 char, although it is not very strong, is still influential at the initial particle heating and volatile ignition stage. That is, upon the blending of char, the total volatile

DOI: 10.1021/acs.energyfuels.5b02425
Energy Fuels 2016, 30, 1858−1868

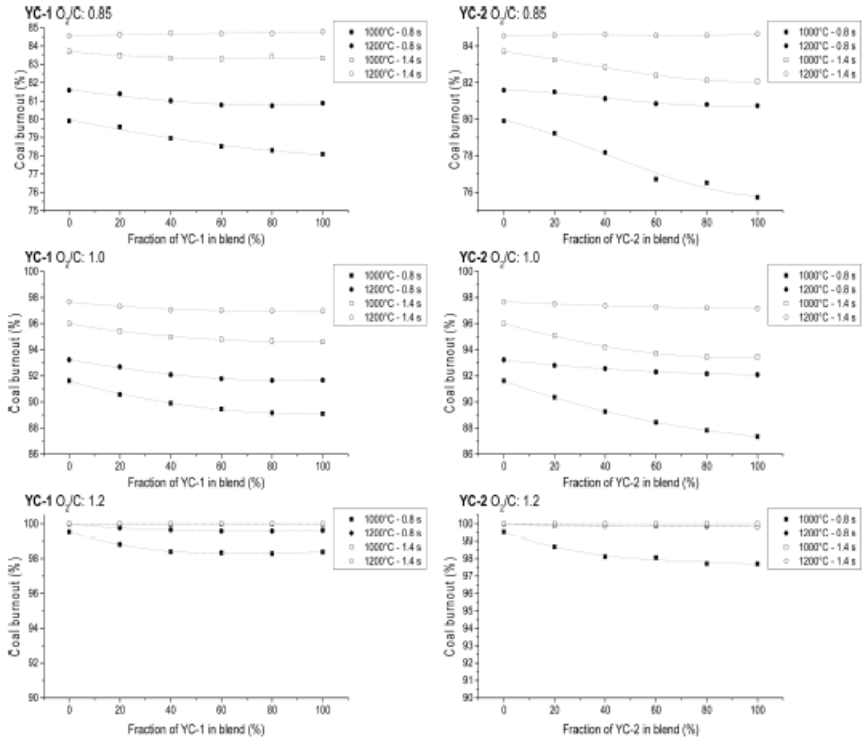

Figure 10. Effect of the blend ratio and residence time on the burnout at three oxygen/carbon ratios for YC-1 (left) and YC-2 (right).

concentration will be lower. Consequently, the particles remain hot and glowing, whereas their ignition was delayed. This is supported by the ignition flame in Figure 3 and a gradual decrease on the ignition position in the CFD temperature contour in Figure 11. Similar results were predicted for the YC-2 char. Its dilution effect (for heat sink) is more obvious, leading to a greater decrease on the flame front position and the intensity of flame as well. Also, similar to the ignition results in Figure 3, for both char blends, the delay in the flame position shifts gradually with increasing the char content at low blend ratios while having a more noticeable delay in ignition above a 60% blend.

Figure 12 further illustrates the average temperature for each distance away from the injector of the reactor for YC-1 and YC-2 chars under the same condition. For either YC-1 or YC-2 char, increasing its blending ratio leads to a gradual decrease in the particle temperature before 0.15 m, which refers to the particle heating and ignition stage. The peak temperature was decreased considerably at the distance of 0.15−0.2 m for the flame propagation regime. All of the blends with YC-1 char produced a marginal drop within 20 °C, while for YC-2, increasing to only a 60% blending ratio will decrease the temperature by the same amount. Such a temperature gap should be mainly caused by the heat sink effect of YC-2 char, which is difficult to ignite and burn. Above an 80% blend for YC-2, there is a slight increase in the peak temperature because the char will combust in the same location further from the injector than for PCI coal. The distance to the peak temperature confirms a rather close relationship for all of the YC-1 blends, varying only 0.04 m between pure PCI coal and pure YC-1 (denoting the heterogeneous char oxidation stage) onward. This is strong evidence of the comparable reactivity of PCI char and YC-1 char and their concurrent oxidation. On the contrary, the peak gas temperature varies broadly with the YC-2 blending ratio, extending the distance to the peak temperature by 0.06 m, further indicating its strong dilution and heat sink effect. This further suggests that optimizing the brown coal pyrolysis conditions is critical in maximizing the blending performance of the resultant char under the blast furnace combustion conditions.

4. CONCLUSION

Through the joint efforts on experimental investigation and CFD modeling, the combustion performance of two Yallourn chars, produced under different pyrolysis conditions, has been evaluated by blending it with a commercial PCI coal under different ratios. The influences of the furnace temperature and O_2/C molar ratio were also assessed. The ignition of coal−char blends at both slow and fast heating rates were also diagnosed. The major conclusions can be drawn as follows: (1) According to the particle ignition time, a maximum of 40 wt % is allowable for YC-1 char, which is comparably reactive with the

DOI: 10.1021/acs.energyfuels.5b02425
Energy Fuels 2016, 30, 1858−1868

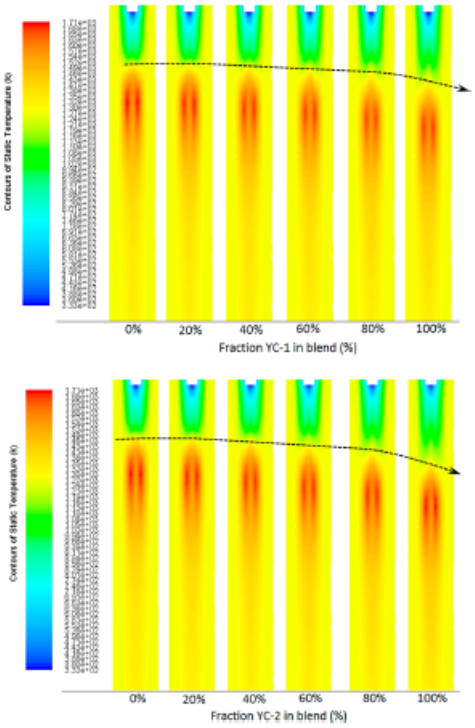

Figure 11. Contours of temperature for YC-1 (top) and YC-2 (bottom) blends at 1000 °C and O_2/C ratio of 1.0.

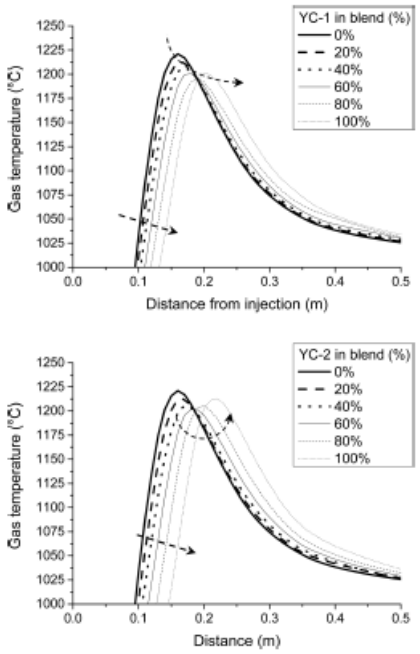

Figure 12. Effect of the blend ratio on the gas temperature profile for YC-1 (top) and YC-2 (bottom) blends at 1000 °C and O_2/C ratio of 1.0.

commercial PCI coal. However, a maximum of 20 wt % is only allowed for YC-2, which is less reactive. The negative heat sink effect of YC-2 char is influential, whereas the heterogeneous ignition of YC-1 overlapped considerably with the ignition of PCI coal, which is mainly in the homogeneous gas phase. (2) According to the burnout rate observed by DTF experiments and CFD modeling, the later char oxidation rate was accelerated greatly for the PCI coal blended with YC-1, irrespective of its blending ratio. In contrast, the heat sink effect is more obvious for YC-2, the increase on the blending ratio of which greatly decreased the overall burnout rate, especially at low furnace temperatures (800 and 900 °C) and a shorter residence time, such as 0.8 s. (3) For YC-1 char, its blending ratio is insignificant in the overall burnout. Increasing the furnace temperature to 1000 °C and the O_2/C ratio to 1.2 can assist in achieving a nearly complete burnout for all of its blends, even at a short residence time of 0.8 s. In contrast, for YC-2 char, a furnace temperature of 1200 °C and O_2/C ratio of 1.2 are essential to complete the burnout of all of its blends. (4) The Yallourn pyrolysis conditions for the preparation of its char are critical. A good synergistic interaction between Yallourn char and commercial PCI coal in terms of reactivity is also essential for a broad blending ratio to be used in the blast furnace.

AUTHOR INFORMATION

Corresponding Author

*Telephone: +61-3-9905-2592. E-mail: lian.zhang@monash.edu.

Notes

The authors declare no competing financial interest.

ACKNOWLEDGMENTS

This work is supported by Coal Energy Australia (CEA) and Brown Coal Innovation Australia (BCIA). Iori Nishio is grateful to the Japan Society for the Promotion of Science (JSPS) for the support to his stay in Monash, through the Joint Partnership program between JSPS and Australian Academy of Technological Science and Engineering (ATSE). This research was also supported in part by the Monash e-Research Centre and eSolutions–Research Support Services through the use of the Monash Campus High-Performance Computing (HPC) Cluster.

REFERENCES

(1) World Coal Association (WCA). *Coal & Steel Statistics*; WCA: London, U.K., 2014.

(2) Ishii, K. *Advanced Pulverized Coal Injection Technology and Blast Furnace Operation*; Elsevier Science, Ltd.: Oxford, U.K., 2000.

(3) Carpenter, A. M. *Use of PCI in Blast Furnaces*; International Energy Agency (IEA) Clean Coal Centre: London, U.K., 2006.

DOI: 10.1021/acs.energyfuels.5b02405
Energy Fuels 2016, 30, 1858−1868

(4) International Energy Agency (IEA). *Coal Information 2005 with 2004 Data*; Organisation for Economic Co-operation and Development (OECD)/IEA: Paris, France, 2005; p 498.
(5) Traa, Y. Is a renaissance of coal imminent?—challenges for catalysis. *Chem. Commun.* **2010**, *46* (13), 2175−2187.
(6) Clarke, M. C. *Low Rank Coal/Lignite Upgrading Technologies*; M.E.T.T.S. Pty Ltd: Helensvale, Queensland, Australia, 2014.
(7) De Girolamo, A.; Lameu, N. K.; Zhang, L.; Ninomiya, Y. Ignitibility and Combustibility of Lignite Pyrolysis Char under Simulated Blast Furnace Conditions. *Fuel* **2016**, submitted.
(8) De Girolamo, A.; Lameu, N. K.; Zhang, L.; Ninomiya, Y. Ignitibility and Combustibility of Lignite Pyrolysis Char under Simulated Blast Furnace Conditions. *Proceedings of the 8th International Symposium on Coal Combustion*; Beijing, China, July 19−22, 2015.
(9) Zhang, X.; Liu, Y.; Wang, C. a.; Che, D. Experimental study on interaction and kinetic characteristics during combustion of blended coals. *J. Therm. Anal. Calorim.* **2012**, *107* (3), 935−942.
(10) Haas, J.; Tamura, M.; Weber, R. Characterisation of coal blends for pulverised fuel combustion. *Fuel* **2001**, *80* (9), 1317−1323.
(11) Su, S.; Pohl, J. H.; Holcombe, D.; Hart, J. A. Techniques to determine ignition, flame stability and burnout of blended coals in p.f. power station boilers. *Prog. Energy Combust. Sci.* **2001**, *27* (1), 75−98.
(12) Zhang, S. Theoretical consideration of problems relating to high coal rate injection into blast furnaces. *Ironmaking Steelmaking* **2003**, *30* (6), 467−474.
(13) Ariyama, T. *Combustion Behavior of PC Particle Group*; Elsevier Science: Oxford, U.K., 2000.
(14) Gao, Y. H.; Bian, L. T. A Evaluation on Pulverized Coal Combustion Properties Using a Thermogravimetric Analyze Method. *Appl. Mech. Mater.* **2013**, *423*−*426*, 609−613.
(15) Qiu, J.; Li, F.; Zeng, H.; Yao, B.; Ma, Y. Determination of optimum blending ratio during coal blends combustion. *Combust. Sci. Technol.* **2000**, *157* (1), 167−184.
(16) Kissinger, H. E. Reaction Kinetics in Differential Thermal Analysis. *Anal. Chem.* **1957**, *29* (11), 1702−1706.
(17) Wang, C. a.; Liu, Y.; Zhang, X.; Che, D. A study on coal properties and combustion characteristics of blended coals in Northwestern China. *Energy Fuels* **2011**, *25* (8), 3634−3645.
(18) Prationo, W.; Zhang, J.; Abbas, H. A. A.; Wu, X.; Chen, X.; Zhang, L. Influence of External Clay and Inherent Minerals on Lignite Optical Ignition and Volatile Flame Propagation in Air-Firing and Oxy-Firing. *Ind. Eng. Chem. Res.* **2014**, *53* (7), 2594−2604.
(19) Low, F.; De Girolamo, A.; Dai, B.-Q.; Zhang, L. Emission of Organically Bound Elements during the Pyrolysis and Char Oxidation of Lignites in Air and Oxyfuel Combustion Mode. *Energy Fuels* **2014**, *28* (6), 4167−4176.
(20) Zhang, J.; Prationo, W.; Zhang, L.; Zhang, Z. Computational Fluid Dynamics Modeling on the Air-Firing and Oxy-fuel Combustion of Dried Victorian Brown Coal. *Energy Fuels* **2013**, *27* (8), 4258−4269.
(21) Westbrook, C. K.; Dryer, F. L. Simplified Reaction Mechanisms for the Oxidation of Hydrocarbon Fuels in Flames. *Combust. Sci. Technol.* **1981**, *27* (1−2), 31−43.
(22) Gil, M. V.; Casal, D.; Pevida, C.; Pis, J. J.; Rubiera, F. Thermal behaviour and kinetics of coal/biomass blends during co-combustion. *Bioresour. Technol.* **2010**, *101* (14), 5601−5608.
(23) Tahmasebi, A.; Kassim, M. A.; Yu, J.; Bhattacharya, S. Thermogravimetric study of the combustion of Tetraselmis suecica microalgae and its blend with a Victorian brown coal in O_2/N_2 and O_2/CO_2 atm. *Bioresour. Technol.* **2013**, *150*, 15−27.
(24) Yuzbasi, N. S.; Selçuk, N. Air and oxy-fuel combustion characteristics of biomass/lignite blends in TGA-FTIR. *Fuel Process. Technol.* **2011**, *92* (5), 1101−1108.
(25) Yi, Q.; Qi, F.; Cheng, G.; Zhang, Y.; Xiao, B.; Hu, Z.; Liu, S.; Cai, H.; Xu, S. Thermogravimetric analysis of co-combustion of biomass and biochar. *J. Therm. Anal. Calorim.* **2013**, *112* (3), 1475−1479.
(26) Shen, Y.; Guo, B.; Yu, A.; Zulli, P. A three-dimensional numerical study of the combustion of coal blends in blast furnace. *Fuel* **2009**, *88* (2), 255−263.
(27) Zhang, J.; Wang, Q.; Wei, Y.; Zhang, L. Numerical Modeling and Experimental Investigation on the Use of Brown Coal and Its Beneficiated Semicoke for Coal Blending Combustion in a 600 MW_e Utility Furnace. *Energy Fuels* **2015**, *29* (2), 1196−1209.
(28) Ulloa, C.; Borrego, A. G.; Helle, S.; Gordon, A. L.; García, X. Char characterization and DTF assays as tools to predict burnout of coal blends in power plants. *Fuel* **2005**, *84* (2−3), 247−257.
(29) Moroń, W.; Rybak, W. Combustion characteristics of blended coals. *Proceedings of the 3rd European Combustion Meeting*; Crete, Greece, April 11−13, 2007.
(30) Moon, C.; Sung, Y.; Ahn, S.; Kim, T.; Choi, G.; Kim, D. Effect of blending ratio on combustion performance in blends of biomass and coals of different ranks. *Exp. Therm. Fluid Sci.* **2013**, *47*, 232−240.
(31) Biswas, S.; Choudhury, N.; Sarkar, P.; Mukherjee, A.; Sahu, S. G.; Boral, P.; Choudhury, A. Studies on the combustion behaviour of blends of Indian coals by TGA and Drop Tube Furnace. *Fuel Process. Technol.* **2006**, *87* (3), 191−199.
(32) Machado, J. G. M. S.; Osório, E.; Vilela, A. C. F.; Babich, A.; Senk, D.; Gudenau, H. W. Reactivity and Conversion Behaviour of Brazilian and Imported Coals, Charcoal and Blends in view of their Injection into Blast Furnaces. *Steel Res. Int.* **2010**, *81* (1), 9−16.
(33) de Castro, J. A.; Araújo, G. d. M.; da Mota, I. d. O.; Sasaki, Y.; Yagi, J.-i. Analysis of the combined injection of pulverized coal and charcoal into large blast furnaces. *J. Mater. Res. Technol.* **2013**, *2* (4), 308−314.
(34) Mathieson, J. G.; Rogers, H.; Somerville, M. A.; Jahanshahi, S.; Ridgeway, P. Potential for the use of biomass in the iron and steel industry. *Proceedings of Chemeca 2011*; Sydney, New South Wales, Australia, Sept 18−21, 2011.
(35) Xie, K. C. *Structure and Reactivity of Coal: A Survey of Selected Chinese Coals*; Springer: Berlin, Germany, 2015.

DOI: 10.1021/acs.energyfuels.5b02425
Energy Fuels 2016, 30, 1858−1868